Author:
Lamb, Rachel A

Title:
Synthesis of Phosphine Glycoconjugates for Radiochemical Applications

Synthesis of Phosphine Glycoconjugates for Radiochemical Applications

Rachel A. Lamb

October 2021

A thesis submitted to the University of Bristol in accordance with the requirements for award of the degree of Doctor of Philosophy in the Faculty of Science

Abstract

Several examples of phosphine glycoconjugate ligands, whereby a carbohydrate is covalently bonded to a phosphine moiety, have previously been reported but they have been used exclusively for catalytic applications. In this thesis, the synthesis of phosphine glycoconjugates has been investigated with a view to their use in medical imaging applications. Incorporation of a carbohydrate was explored to target cancerous cells, which exhibit increased glucose avidity compared with normal cells.

A variety of methods for the synthesis of monophosphine glycoconjugates with alkyl linkers have been investigated: Lewis acid catalysed glycosylation chemistry, hydrophosphination chemistry, lithium phosphide chemistry, quaternisation chemistry and amide coupling chemistry. Generally, these methods were incompatible with the phosphine moiety. However, we have demonstrated that amide coupling is a promising method by synthesising phosphine glycoconjugate **2.21**, where D-glucose is conjugated to a PPh_2 moiety *via* an alkyl linker (Figure I). The Re coordination chemistry of **2.20** (the peracetylated analogue of **2.21**) was investigated and this informed the subsequent ^{99m}Tc radiolabelling study. High quality results for the ^{99m}Tc radiolabelling of **2.21** was observed. However, poor serum stability of the ^{99m}Tc complex of **2.21** precluded *in vivo* testing.

In 1999, Beller *et al.* reported a method to prepare ligands **3.1** and **3.7** (Figure I), where D-glucose and D-galactose, respectively, were conjugated to a PPh_2 moiety via an aryl linker, and their use in biphasic catalysis was investigated. Using this method, a small library of related monophosphine glycoconjugates was synthesised. The phosphine moiety (PR_2 = PPh_2, P(*o*-tol)$_2$, P(*p*-tol)$_2$, PCy_2) and carbohydrate moiety (Glc, Gal, Lac) were varied and the Re coordination chemistry of these ligands was investigated. All examples, except where PR_2 = P(*o*-tol)$_2$, formed a Re(I) complex and consequently, the ^{99m}Tc radiolabelling of these ligands was studied; these results reflect those of the Re(I) coordination study. Additionally, Re(I) uptake studies (in HeLa, HDF and EA.hy926) were performed for several of the complexes. Key findings include: (i) the introduction of a carbohydrate led to greater uptake in cells, compared with incorporation of a non-glycoconjugate phosphine ligand and (ii) cell lines could distinguish between Gal and Glc moieties.

The final Chapter presents the routes towards diphosphine glycoconjugate ligands that have been explored. Attempts to synthesise a bidentate glycoconjugate containing N-diphosphinomethyl groups (**4.29,** Figure I) have been shown to be promising, but its purity was insufficient to justify radiolabelling. A 1,1-diphosphine moiety was conjugated to D-glucose via amide coupling to give ligand **4.36** (Figure I) and consequently, the Re(V) coordination studies were performed. However, ^{99m}Tc radiolabelling of **4.36** was unsuccessful.

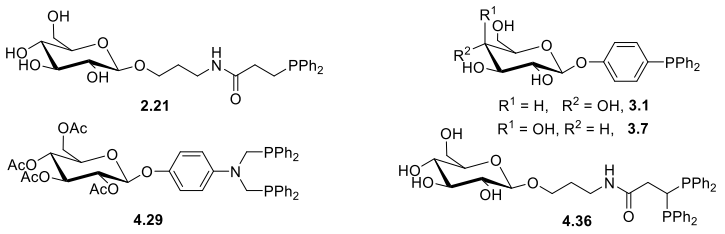

Figure I Structures of phosphine glycoconjugates referred to above.

Declaration

I declare that the work in this dissertation was carried out in accordance with the requirements of the University's *Regulations and Code of Practice for Research Degree Programmes* and that it has not been submitted for any other academic award. Except where indicated by specific reference in the text, the work is the candidate's own work. Work done in collaboration with, or with the assistance of, others, is indicated as such. Any views expressed in the dissertation are those of the author.

Rachel A. Lamb

University of Bristol

October 2021

Acknowledgements

First, I must thank Paul. His support and guidance though-out this project has been brilliant and without it my PhD would not have been the same. I will miss our weekly catch-up meetings and his endless supply of hilarious anecdotes! I also must extend these thanks to my second supervisor, Professor Carmen Galan, for teaching me everything I know about carbohydrate chemistry and biochemistry, and for her continued support, and Dr Michelle Ma, without whom I would not have had the chance to learn about radiochemistry. I am forever grateful for all these opportunities my supervisors have given me, and the time and support they have shown me throughout this project.

Thanks to all the people who have contributed to this research, in particular, Dr Radhe Shyam, who performed all biological studies in this project (and answered all of my ridiculous questions about cell testing with a straight face!), those at the London Metallomics Facility (Dr Theodora Stewart, Alex Griffiths and Maral Amrahli) with whom we collaborated to perform ICP-MS analysis on cellular samples, and to IB for making me feel welcome when I arrived at St Thomas's Hospital and who, alongside Michelle, taught me how to work with radioisotopes!

I would also like to thank the brilliant technical staff including, Paul Lawrence in NMR, Hazel Sparks and Natalie Pridmore in X-ray Crystallography and Paul Gates and Sam Ferrins in Mass Spectrometry. Thank you also to Tony Rodgers for his technical support and keeping the lab functioning!

My time at the University of Bristol would not have been the same without past and present members of the Pringle and Galan groups, and my CDT cohort. In particular, thank you to the following Pringles: Dr's Branfoot, Chadwick, Gorman, Meissel, Miles-Hobbs, Wise and King (honorary Pringle), Derek Durand, Daniel Good and especially Rachel Nuttall and Sarah Williams. Rach and Sarah, my fellow Pringals, I will miss seeing you every day! Your friendship, advice and support has kept me going through many a crisis! During my time in the group we have had so many fantastic memories and I will miss the crazy fancy-dress themed Christmas parties, the karaoke, the conference trips together and the usual pub/Royal Fort sessions!

To all the staff who were involved in the re-opening of the Chemistry department during the COVID-19 pandemic, in particular Paul Pringle, Nick Norman, Simon Osborne, and Tony Rogers, thank you for providing a sense of normality at a very strange time, and for enabling research to continue.

Thank you to my parents, you have always supported me and for that I am ever thankful, and to my friends for keeping me smiling! Lastly, thank you Chris for your skills as a proof-reader and agreeing to move to Bristol without seeing the city! But seriously, I could not have done this without you - your patience, love and support are unmatched.

Collaborator Acknowledgments

The work in Chapters 2 and 4 is unpublished and was carried out by the author, with radiolabelling performed by the author, in collaboration with Dr Michelle Ma at King's College London.

Chapter 3 contains compounds that were synthesised by the author and cellular testing which was performed by Dr Radhe Shyam at the University of Bristol. Inductively coupled plasma mass spectrometry (ICP-MS) was performed by Alex Griffiths, Maral Amrahli and Dr Theadora Stewart at the London Metallomics Facility, whilst collaboration with Dr Michelle Ma, at King's College London, enabled radiolabelling studies to be performed.

Chapter 6 describes the experimental and supporting information for Chapters 2-4, whilst Chapter 7 is the appendix and contains details of the ICP-MS studies and the calculations that were performed for Chapter 3.

Contents

Table of Contents

Abbreviations

General			
AIBN	azobisisobutyronitrile	**LMF**	London Metallomics Facility
Ar	aryl	**MBq**	megabecquerel
ATP	adenosine triphosphate	**MeCN**	acetonitrile
BBB	blood-brain barrier	**MeOH**	methanol
Bn	benzyl	**min**	minute(s)
BTEAB	benzyl triethyl ammonium bromide	**mmol**	millimole(s)
CAGR	compound annual growth rate	**mol**	mole(s)
COD	cyclooctadiene	**nBu**	normal-butyl
Cy	cyclohexyl	**NIR**	near infra-red
d	day(s)	***o***	ortho
DCM	dichloromethane	**OAc**	acetyl
DIPEA	N,N-diisopropylethylamine	**OTf**	trifluoromethylsulfonyl
DMAP	4-dimethylaminopyridine	**p**	para
DMSO	dimethyl sulfoxide	**PET**	positron emission tomography
dppbz	bis(diphenylphosphino)benzene	**Ph**	phenyl
dppm	bis(diphenylphosphino)methane	**PKM1**	pyruvate kinase M1 isoform
dppp	bis(diphenylphosphino)propane	**PKM2**	pyruvate kinase M2 isoform
DVT	deep vein thrombosis	**PSMA**	prostate specific membrane antigen
EDC-HCl	N-'ethylcarbodiimide hydrochloride	**R**	aryl or alkyl group
ee	enantiomeric excess	**SPECT**	single-photo emission tomography
eq.	equivalents	**$t_{1/2}$**	half-life
Et	ethyl	**TBAHS**	tertbutyl ammonium hydrogen sulphate
EtOH	ethanol	**tBu**	tert-Butyl
FDA	Food and Drug Administration	**THF**	tetrahydrofuran
FDG	flurodeoxyglucose	**TMS**	trimethylsilyl
g	gram(s)	**Tol**	toluene
GLUT	glucose transporter	**TPPO**	triphenylphosphine oxide
GPIIb/IIIa	glycoprotein IIb/IIIa	**WHO**	World Health Association
h	hour(s)	**α**	alpha
HATU	1-[Bis(dimethylamino)methylene]-1H-1,2,3-triazolo[4,5-b]pyridinium 3-oxide hexafluorophosphat	**β**	beta
HK	hexokinase	**β+**	positron
HOBt	Hydroxybenzotriazole	**γ**	gamma
KCL	King's College London	**μmol**	micromole(s)
L	ligand	**μg**	microgram(s)
LDH-A	lactose dehydrogenase-A	**μL**	microlitre(s)

Spectroscopic			
{1H}	proton decoupled	**LC-MS**	liquid chromatography mass spectroscopy
app.	apparent	**m**	multiplet
br	broad	**m/z**	mass/charge
C	Celcius	**M+**	molecular ion
d	doublet	**NMR**	nucleur magnetic resonance
dd	doublet of doublets	**ppm**	parts per million
dt	doublet of triplet	**q**	quartet
ESI	electrospray ionisation	**quart.**	quartet
HPLC	high performance liquid chromatography	**s**	singlet
HR-MS	high resolution mass spectrometry	**t**	triplet
Hz	Hertz	δ	chemical shift
ICP-MS	Inductively coupled plasma mass spectrometry		
J	coupling constant		

Chapter 1 : Introduction

The focus of the project has been development of ^{99m}Tc complexes that contain phosphine glycoconjugate ligands. The examples given in Chapters 2-4 are the first such ^{99m}Tc complexes to be reported. A variety of concepts will therefore be introduced in this Chapter to put this work into context. First, the general subject of nuclear medicine will be introduced before a more detailed review of ^{99m}Tc imaging agents, in particular *Myoview* which is the only example of a P(III)-based radiopharmaceutical that is used clinically. The biological relevance of carbohydrates is discussed as it is relevant to the central theme of using carbohydrate-phosphine ligands to target cancerous cells. This is possible as cancerous cells experience a switch in metabolic mechanism (the Warburg Effect, Section 1.3.2), thereby increasing their D-glucose avidity compared with healthy cells. Finally, an overview of glycoconjugate examples that have informed the design of carbohydrate-phosphine ligands in this project is discussed.

1.1. Nuclear Medicine: A Brief Background

The global nuclear medicine market is experiencing a compound annual growth rate (CAGR) of almost 7.5% (forecasted for 2021-2026) as a consequence of its increasing importance in modern medicine.[1] Nuclear medicine is concerned with the incorporation of radioisotopes into small molecules, or bio-molecules, to achieve therapeutic or diagnostic effects.[2] The therapeutic nature of radioisotopes that emit either non-penetrating alpha- (α) or high-energy beta-particles (β^-), can be exploited due to the cytotoxic behaviour of these particles. Additionally, decaying radioisotopes that release penetrating gamma-rays (γ-rays) – which can be generated by nuclear decay or positron (β^+) annihilation – can be used for diagnostic purposes. [3] Incorporating the radioisotope into a small molecule (or biomolecule) can affect the bio-distribution and clearance of the radiopharmaceutical from the body. It is crucial that the radioisotope is strongly chelated to prevent unwanted accumulation of the radionucleotide within biological tissue.[4]

de Hevesy is widely considered to be the progenitor of nuclear medicine, and was awarded the 1943 Nobel Prize in Chemistry for his contributions to developing the concept of radiotracers.[5] This award stems from research he performed at the Niels Bohr Institute in 1934, regarding the incorporation of phosphorus-32 (^{32}P) in molecules, and the uptake of this radioisotope within the skeletons of mice.[6] Hamilton and Soley further developed the field of nuclear medicine in 1938, by reporting the uptake of iodine-131 (^{131}I) in human thyroid glands.[7] This is still relevant in medicine today, with the continued use of ^{131}I for the detection and treatment of thyroid cancer.

According to a report by the World Health Organisation (WHO), cancer is now the second leading cause of death globally and was responsible for approx. 9.0 million deaths in 2018.[8] Early detection of the disease has been shown to significantly increase the chances of survival for cancer patients, and therefore the development of radiopharmaceuticals to detect tumours, or metastases, is more relevant than ever. Furthermore, the WHO have reported that cardiovascular diseases, which can be diagnosed by radiopharmaceuticals such as *Myoview* (see Section 1.2.3), now account for 17.9 million deaths annually worldwide, making it the leading cause of death. These statistics by the WHO explain the large CAGR attributed to the global nuclear medicine market.

1.2. SPECT Imaging

Single photon emission computed tomography (SPECT) is a two-dimensional imaging technique that is routinely used in hospitals to determine the localisation of a radioisotope within a patient.[5] The patient is first injected with a γ-emitting radiopharmaceutical that will accumulate in the organ(s) or tissue of interest. The SPECT scanner is equipped with a γ-camera to detect the photons that are emitted by the radioisotope as it undergoes radioactive decay. Each image that is collected provides two-dimensional information on the bio-distribution of the radioisotope. As the SPECT camera rotates, multiple images are collected before a tomographic algorithm is applied to combine the images to generate a three-dimensional image showing the radioisotope distribution (Figure 1.1).[9] Elements including indium-111 (^{111}In), thallium-201 (^{201}Th) and technetium-99m (^{99m}Tc) are commonly detected *via* SPECT imaging, and will be discussed in more detail in Section 1.2.1.[10]

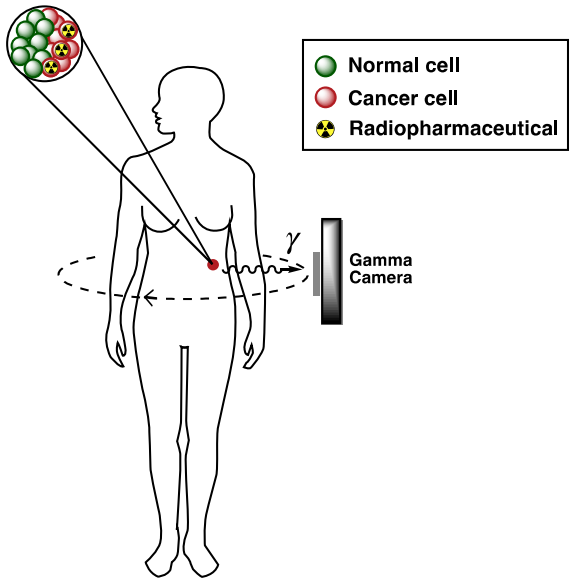

Figure 1.1 Diagram illustrating the SPECT imaging process.

Positron (β^+) emission tomography (PET) imaging also determines the localisation of a radiotracer by detection of γ-rays. However, these γ-rays are produced indirectly by a β^+-emitting radiotracer. β^+ particles are annihilated by collision with electrons to generate two γ-rays that travel in opposite directions. PET imaging produces images of a higher-quality than SPECT imaging, but SPECT is a more widespread technique in hospitals because γ-emitting radioisotopes generally have longer half-lives than β^+-emitting isotopes, and SPECT scans are less expensive to perform.[11] This is because the cameras required for SPECT imaging are significantly cheaper than those required for PET imaging.[12]

1.2.1. Indium and thallium radiopharmaceuticals

^{111}In ($t_{1/2}$ = 67.3 h) was the first clinically approved radionucleotide for γ-imaging.[3] The development of ^{111}In chemistry coincided with a surge of interest in monoclonal antibodies and ^{111}In imaging agents were primarily employed for their radio-labelling.[13] The ^{111}In-labelled Satumomab pendetide (*OncoSint*) was the first example of a radiolabelled antibody that was FDA-approved. It was used to target TAG-72 - a glycoprotein found on the surface of colorectal and ovarian cancer cells.[14] Although no longer commercially available, *OncoSint* consisted of a monoclonal antibody (B72.3) that was conjugated to the pendetide molecule in order to facilitate the radiolabelling of B72.3 (Figure 1.2).[15] Because monoclonal antibodies possess slow pharmacokinetics (*i.e.* slow clearance from the blood and accumulation in tumours), the imaging had to be carried out over a period of 24-72 h; the long half-life of ^{111}In therefore made it useful for such applications.[3]

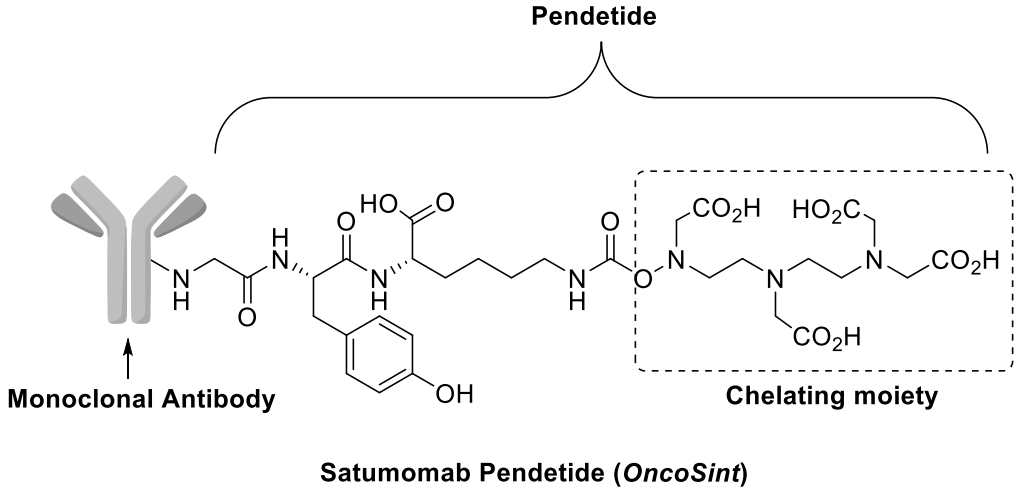

Figure 1.2 Representations of the active species in *OncoSint*. The pendetide moiety drawn in full, a cartoon IgG molecule represents B27.3, and the region of pendetide that chelates to ^{111}In is highlighted.

^{201}Tl ($t_{1/2}$ = 73 hr), in the form of thallium(I) chloride, was the original imaging agent for myocardial perfusion imaging. Uptake in the myocardium is proposed to be due to Tl^+ acting as a K^+ mimic, and being transported into the myocardium by potassium ATPase. Despite ^{201}Tl possessing a low γ-yield (10%), it was widely used clinically until the development of ^{99m}Tc myocardial imaging agents.

Today, much of the chemistry performed by ^{111}In and ^{201}Tl has been replaced by ^{99m}Tc.[3]

1.2.2. Technetium-99m radiopharmaceuticals (First and Second Generation)

Technetium-99m (^{99m}Tc) is a γ-emitting, metastable radioisotope, which is used in >80% of all nuclear imaging tests. Despite there being no stable isotopes of Tc, its chemistry is well-developed because of its importance in diagnostic medicine. The widespread use of ^{99m}Tc in hospitals is due to: (i) the extensive coordination chemistry of Tc in a range of oxidation states (+7 to -1) which has allowed the development of targeted radiopharmaceuticals; (ii) the convenient nuclear properties of ^{99m}Tc; (iii) the ready availability of ^{99m}Tc and its ease of nuclear synthesis.[16,17]

Fission of ^{235}U, results in the formation of radioactive ^{99}Mo ($t_{1/2}$ = 66.0 h), which decays to ^{99m}Tc (84%, $t_{1/2}$ = 6.02 h) (Scheme 1.1). This metastable technetium nucleus relaxes relatively slowly, by emission of a γ-photon to its ground state (^{99}Tc, $t_{1/2}$ = 2.12x10^5 y) because this process is nuclear-spin-forbidden. The γ-rays that are emitted by ^{99m}Tc are relatively low in energy, measuring 141 keV. These photons therefore have enough energy to be penetrating to tissue and organs without causing significant cell-damage.[16] In addition, ^{99m}Tc imaging is technologically advantageous because commercially available γ-cameras detect rays with an energy of 100-200 keV.[18]

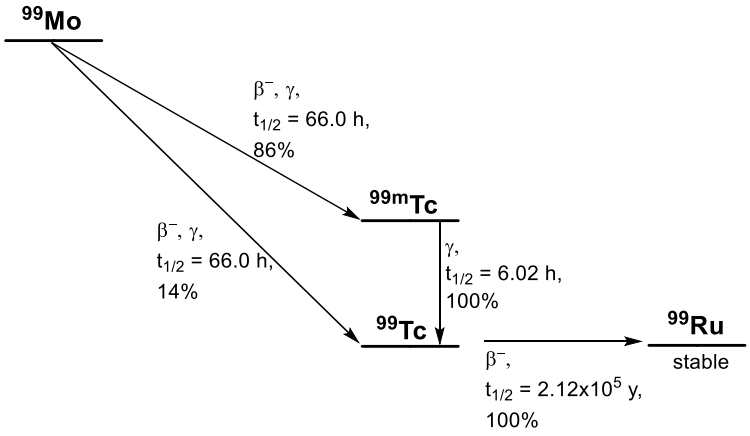

Scheme 1.1 Decay pathway for ^{99}Mo *via* ^{99m}Tc.[16]

Due to the development of the $^{99}Mo/^{99m}Tc$ generator in the late 1950's, daily production of ^{99m}Tc in hospitals is now commonplace. ^{99m}Tc is delivered in the form of its parent radioisotope as molybdate ($[^{99}MoO_4]^{2-}$) on an alumina stationary phase. Potential problems associated with the short half-life of ^{99m}Tc ($t_{1/2}$ = 6 h) are overcome as follows.[19] $[^{99}MoO_4]^{2-}$ decays to pertechnetate ($[TcO_4]^-$), and using a saline solution, $[TcO_4]^-$ can be selectively eluted from the column due to the difference in overall charge of the two anionic species. $[TcO_4]^-$ is added to lyophilised 'kits' for immediate use within the hospital. These kits contain all the necessary reagents to form the ^{99m}Tc radiopharmaceutical except for the radio-metal, including the ligand, buffer, and reducing agent necessary to reduce the pertecnetate(VII). The kits generate ^{99m}Tc radiopharmaceuticals in high yield, which can be delivered to the patient within 30 minutes; this is important due to the relatively short half-life of ^{99m}Tc.[2,20]

Although originally developed more than 50 years ago, many first-generation ^{99m}Tc complex are still used in the clinic. These include $[^{99m}TcO_4]^-$, ^{99m}Tc-MDP, ^{99m}Tc-DTPA and ^{99m}Tc-HIDA that are used for thyroid, bone, renal and liver scintigraphy, respectively. The chemistry of these complexes (except $[^{99m}TcO_4]^-$) has been little studied and the structures of the Tc complexes of the ligands shown in Figure 1.3 are yet to be fully characterised. The uptake of the first-generation radiopharmaceuticals is likely based on their physical properties such as size, charge, lipophilicity and metabolism.[20]

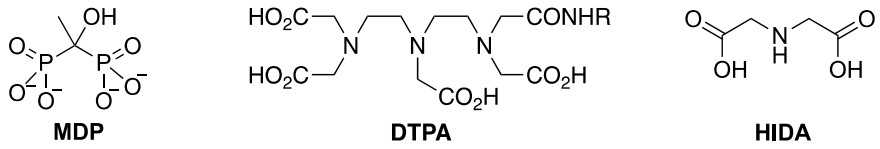

Figure 1.3 Examples of ligands used in 'first-generation' ^{99m}Tc imaging agents.

In contrast with the 'first-generation' ^{99m}Tc complexes, the structures of 'second-generation' complexes are well understood. Researchers in the 1980's developed structure-activity relationships for ^{99m}Tc complexes by designing specific cores that could be modified to effect the bio-distribution and localisation of the radiopharmaceuticals within the body.[21] A number of these cores are still in use, and are discussed below.

Tc(I)-hexakis(isonitrile) and Tc(I)-tricarbonyl (**1.2**, Figure 1.4) are both examples of Tc(I) cores. ^{99m}Tc-sestamibi (**1.1**, Figure 1.4), where R = $CH_2C(Me)_2(OMe)$, is an example of an FDA-approved Tc complex based on a Tc(I)-hexakis(isonitrile) core. ^{99m}Tc-sestamibi is used for myocardial perfusion imaging and breast tumour imaging under the names of *Cardiolite* and *Miraluma*, respectively.[20] There are no examples of FDA-approved radiopharmaceuticals containing the Tc(I) tricarbonyl core. However, since its development by Alberto *et al.*, it has been favoured for research due to its ease of synthesis, ease of ligand

substitution in water, and its chemical stability.[22,23] Consequently, the Tc(I)-tricarbonyl core is the focus of research in Chapter 3.

The technetium-oxo core ($[TcO]^{3+}$) is an example of a Tc(V) core. Using a mercaptoacetyltriglycine chelator gave the ^{99m}Tc complex MAG_3 (**1.3**, Figure 1.4). MAG_3 has undergone FDA-approval and is used to identify renal failure, congenital abnormalities or urinary tract obstruction. This chelator is useful for conjugation of biomolecules, but *syn* and *anti* isomers can be formed. This can be unfavourable if the isomers display different bio-accumation.[24,25]

The Tc-HYNIC core (**1.4** and **1.5**, Figure 1.4) and Tc(V)-dioxo core (**1.6**, Figure 1.4) are both examples of Tc(V) cores. Structure **1.4** or **1.5** (Figure 1.4) can be formed by the HYNIC ligand, as it can occupy one or two coordination sites, respectively. Development of **1.4** and **1.5** has been important in the development of ^{99m}Tc-radiolabelled bioconjugates and will be referred to in Section 1.2.5. The Tc(V)-dioxo core (**1.6**) has become one of the most frequently used ^{99m}Tc cores in research, in part, due to its ease of handling and preparation. **1.6** used in the clinically approved imaging agent *Myoview* (Section 1.2.3), and will also be discussed in Chapters 2 and 4.

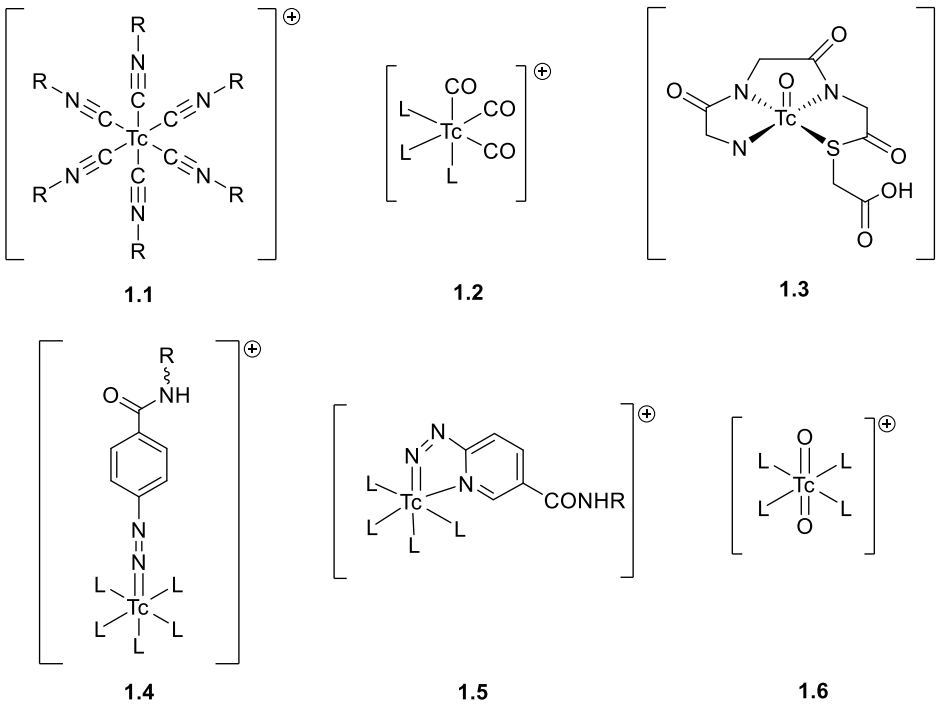

Figure 1.4 Examples of ^{99m}Tc complexes and cores used in radiopharmaceuticals: Tc(I)-hexakis(isonitrile) (**1.1**), Tc(I)-tricarbonyl (**1.2**), $TcMAG_3$ (**1.3**), Tc(V)-η_1-(HYNIC) (**1.4**), Tc(V)-η_2-(HYNIC) (**1.5**) and Tc(V)-dioxo (**1.6**).

1.2.2.1. Myoview

Initially developed in 1993, *Myoview* remains an important 'second-generation' ^{99m}Tc agent, which accumulates in myocardial cells.[18] This radiopharmaceutical consists of a Tc(V)-dioxo core ($[TcO_2]^+$) that is ligated by two tetrofosmin ligands, making it the only FDA-approved imaging agent that utilises a P(III) diphosphine ligand to control its biodistribution.[26] As shown in Scheme 1.2, the ligand is synthesised by an azobisisobutyrontrile (AIBN) catalysed hydrophosphination reaction between 1,2-bis(phosphino)ethane and four equivalents of ethyl vinyl ether *Myoview* (Scheme 1.2) is of particular interest in this project, as its use of P(III) ligands has inspired us to develop new phosphine ligands aimed at alternative imaging applications.

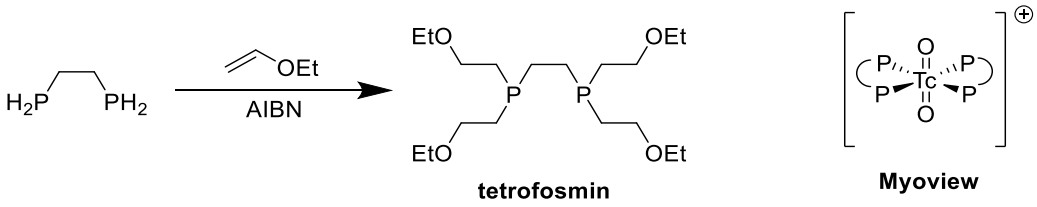

Scheme 1.2 Synthesis of the ligand tetrofosmin, that is used in the imaging agent, *Myoview*.

The distribution of *Myoview* within the heart is proportional to the rate of blood-flow there, and whilst it clears rapidly from the bloodstream and non-target tissue – a property attributed to the ether groups – it is cleared slowly from the myocardial tissue.[18] The rapid clearance from the bloodstream/non-target tissue means that myocardial perfusing imaging (whereby coronary heart disease can be detected) can be performed just 15 min after injection of *Myoview* into the patient. [27,28]

Myoview is delivered to patients in hospitals across the world using a pre-formulated "kit", which contains tetrofosmin, the diphos ligand; stannous chloride, to reduce the pertechnetate to a Tc(V) species; sodium gluconate, to stabilise Tc(V) intermediates; sodium bicarbonate, to act as a pH buffer; and disodium sulphosalicylate. Addition of $[TcO_4]^-$ to the kit gives the desired radiopharmaceutical that can then be administered to the patient. The development of such kits will be discussed further in Chapters 2 and 4.

1.2.3. 3rd Generation Technetium-99m radiopharmaceuticals

The biodistribution of many ^{99m}Tc imaging agents are controlled by their physical properties *i.e.* size, charge and lipophilicity. However, a shift in research perspective has led to the development of 'third-generation' ^{99m}Tc radiopharmaceuticals in which incorporation of biomolecules is used to direct the Tc to specific bio-receptors, with the aim of producing a more targeted approach to treatment. Typically, these biomolecules are either peptides capable of binding to a particular receptor, or antibodies, which can target specific

antigens.[20] When incorporating a radioisotope into a biomolecule, it is vital that any changes to the structure, as a result of Tc binding, do not significantly affect the motif responsible for biotargeting.

1.2.3.1. Peptide-based Technetium-99m Radiopharmaceuticals

Many ^{99m}Tc imaging agents that have peptides incorporated in their structure have been developed.

The first peptide-based ^{99m}Tc radiopharmaceutical to be clinically approved, ^{99m}Tc-P246 (*AcuTect*, Figure 1.5), was developed for the detection of deep vein thrombosis (DVT).[29] *AcuTect* was generated by adding [$^{99m}TcO_4^-$] to a kit containing the peptide biapcitide (P280), stannous chloride dihydrate, sodium glucoheptonate and a pH buffer. The peptide P280 is an ether linked dimer of the peptide apcitide (P246). Crucially, P246 binds to the glycoprotein IIb/IIIa (GPIIb/IIIa) receptor that is expressed on the surface of activated platelets which are integral to thrombosis formation.[29] By binding selectively to GPIIb/IIIa, *AcuTect* enables the diagnosis of DVT. Although *AcuTect* is available for DVT diagnosis, routine identification of this condition is now performed by either ultrasonography or a blood test.

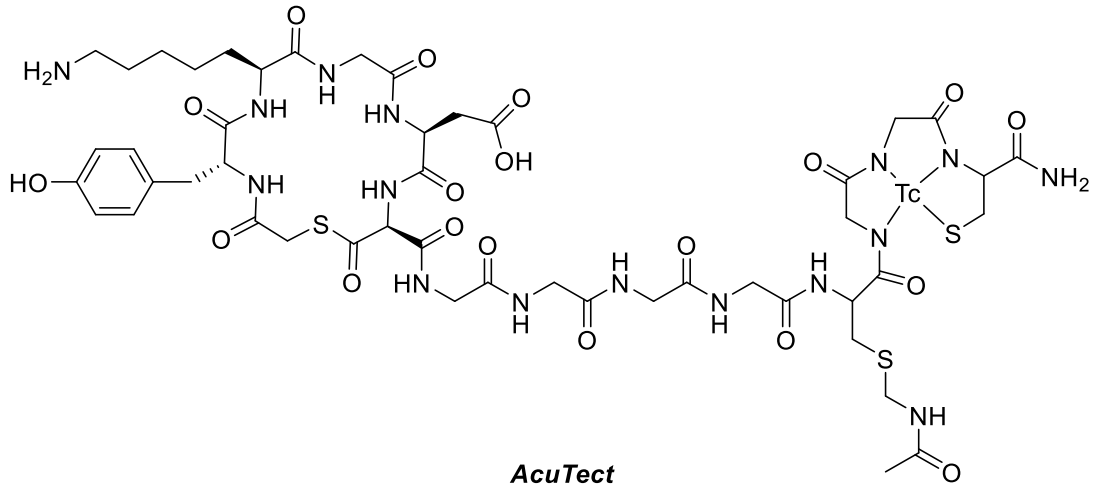

Figure 1.5 Structure of *AcuTect* (^{99m}Tc-P246).

Subsequently, the development of agents based on cores such as ^{99m}Tc(HYNIC) (Figure 1.4, **1.4-1.5**) - where the carboxylic acid group is used for peptide conjugation - has since led to a dramatic growth in the number of peptide-based ^{99m}Tc imaging agents.[30] Although none have yet achieved widespread clinical usage, this is expected to change with the development of several prostate-specific membrane antigen (PSMA) targeted ^{99m}Tc imaging agents. PSMA is located on the surface of prostate cancer cells, and therefore PSMA-targeted compounds enable their imaging or treatment.

[^{99m}Tc(CO)$_3$(MIP-1404)]$^+$ and [^{99m}Tc(CO)$_3$(MIP-1427)]$^+$ (Figure 1.6) both contain PSMA targeting peptides (PSMAt), which are conjugated to a tridentate chelator that contains an amine and two imidazole groups. These radiopharmaceuticals require two separate kits. The first is to generate the [Tc(CO)$_3$]$^+$ core and the second generates the MIP-species. Despite this inconvenience, [^{99m}Tc(CO)$_3$(MIP-1404)]$^+$ has recently passed phase three clinical trials and is a promising compound for measuring both the treatment response, and staging for prostate cancer.[30] Staging is the process of establishing how large a tumour is and whether it has spread to any other organs.[31]

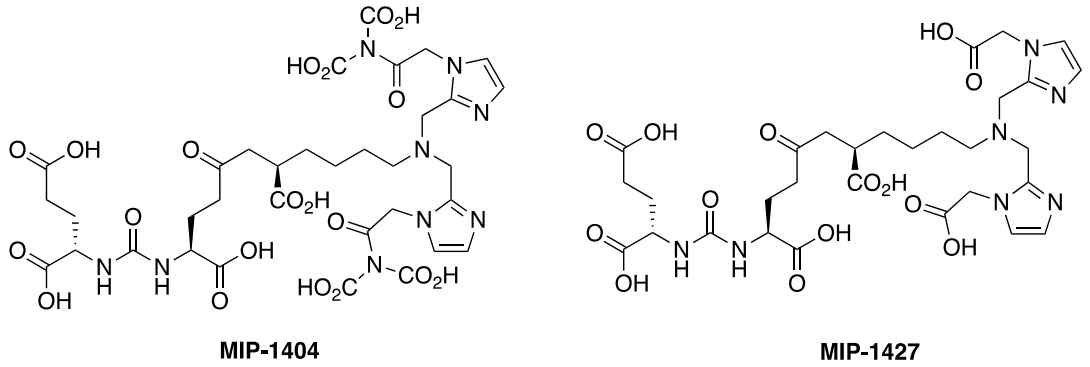

Figure 1.6 Structure of MIP-1404 and MIP-1427 ligands.

The Tc(V) radiopharmaceutical [^{99m}TcO(mas$_3$-PSMAt)] (commonly referred to as Tc-PSMA-I&S, Figure 1.7) can be prepared from a single kit.[30] The kit contains a mercaptoacetyl-D-Ser-D-Ser-D-Ser sequence, which is conjugated to the PSMAt moiety, to produce the ^{99m}Tc radiolabelling of this pharmacophore. These three serine residues were incorporated to improve the metabolic stability of the radiotracer.[32] In the clinic, Tc-PSMA-I&S is being used in the SPECT imaging of prostate cancer, and in radio-guided surgery. In this case, it is administered to a patient 24 h before surgery to enable the detection of metastases with a gamma-camera, and so increase the efficiency of their removal.[30,32]

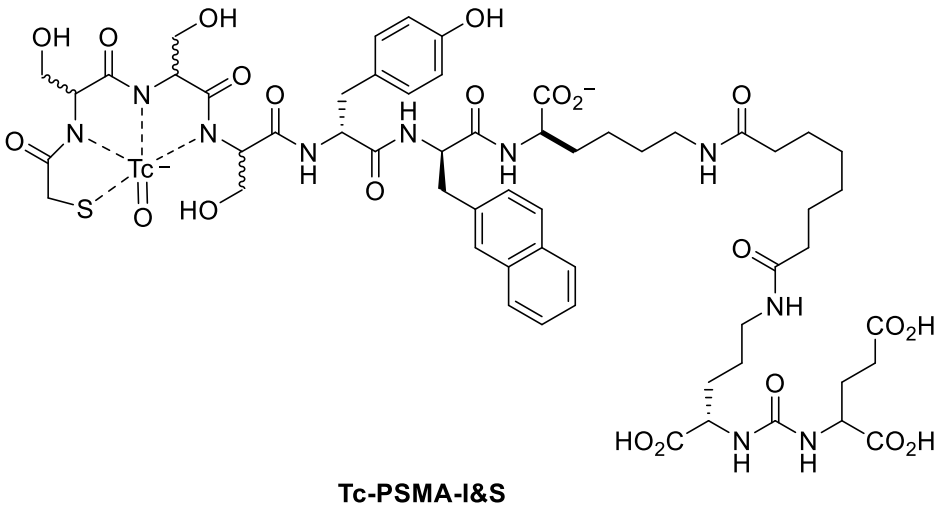

Figure 1.7 Structure of imaging agent ^{99m}Tc-PSMA-I&S.

From these examples, it is clear that peptide-based ^{99m}Tc radiopharmaceuticals are giving promising results by targeting peptide-specific receptors. In this project, we aim to use carbohydrates as the targeting vector and generate ^{99m}Tc agents that are selective towards cancer cells. Consequently, carbohydrate metabolism is discussed below as this project looks at their incorporation into phosphine ligands.

1.3. Carbohydrate Metabolism

Carbohydrates are involved in many processes that are necessary for life to exist, including: cell signalling, molecular recognition, foetus development and production of adenosine triphosphate (ATP).[33] ATP is considered to be the biomolecular unit of currency, and provides the energy for most cellular functions and processes to happen within living species.[33] Production of ATP occurs though glycolysis, the Krebs cycle and oxidative phosphorylation, and is initiated by the consumption of D-glucose.[25]

1.3.1. Glucose Metabolism in Normal Cells

In normal cells, aerobic glycolysis is the initial process by which ATP can be produced. In this process, a single molecule of D-glucose is broken down to produce two units of pyruvate and two units of ATP (Figure 1.8(a)). The pyruvate is typically converted to Acetyl-CoA, which is used in the Krebs cycle, where NADH is produced. NADH is required for the process of oxidative phosphorylation, which involves both the Krebs cycle and electron transport chain. Oxidative phosphorylation generates an additional 36 units of ATP, therefore aerobic respiration in the mitochondrion results in an 18-fold increase in ATP/energy production.[25,33] Because oxidative phosphorylation is a significantly more efficient method of producing ATP, normal cells exclusively use glycolysis under anaerobic conditions, *i.e.* during heavy exercise. In this case, the pyruvate is converted into lactate and

then hydrolysed to lactic acid, which accounts for the 'muscle burn' experienced after intensive exercise. [34]

1.3.2. Glucose Metabolism in Cancer Cells and The Warburg Effect

Often cancerous cells exhibit a dramatic decrease in the process of oxidative phosphorylation, and consequently an increase in the glycolysis pathway, when their metabolism is compared with normal cells. Hence, the glycolytic pathway is often favoured in cancerous cells, even in the presence of oxygen (Figure 1.8(b)). This change in mitochondrial metabolism is referred to as the Warburg Effect, after first being noted by Otto Warburg almost 100 years ago, and is a hallmark of almost all cancerous cells.[25,33,35]

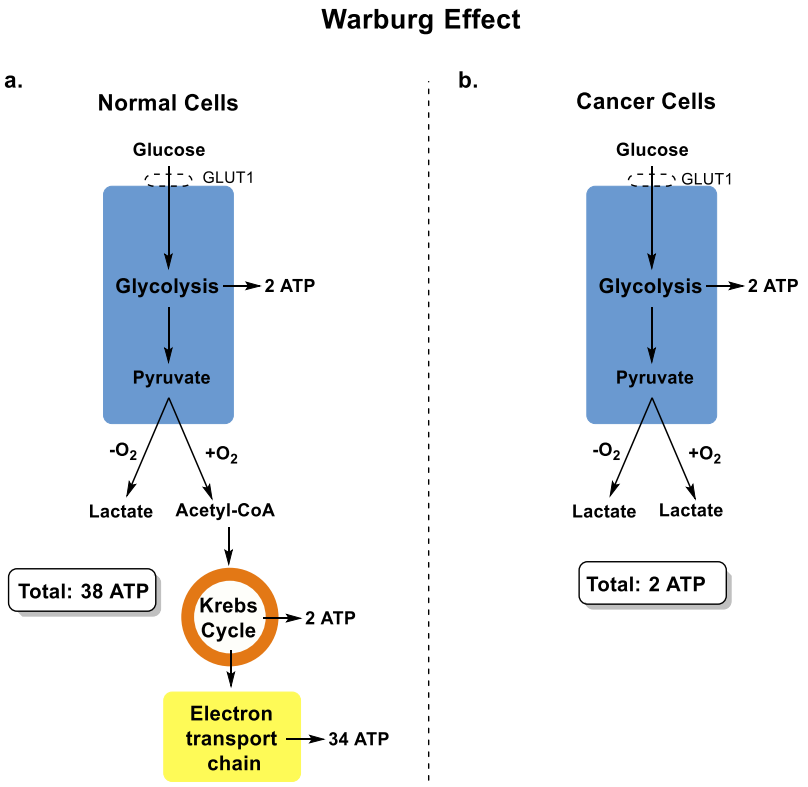

Figure 1.8 Diagram demonstrating the metabolism of D-Glucose in (a) normal and (b) cancer cells, and the Warburg Effect.

The Warburg Effect has two main features: (i) ATP production is now considerably less economical per molecule of glucose (2 *versus* 38 units of ATP), and (ii) the uptake of glucose is accelerated considerably when compared with that in normal cells.[35] Because of this second outcome, where the glucose metabolism *via* aerobic glycolysis is between 10-100 times faster than oxidative phosphorylation, it is possible to exploit the Warburg Effect. Glucose can be utilised as a targeting molecule for the diagnosis and treatment of cancer cells because they have a much greater avidity for glucose; they must generate enough ATP to enable rapid cell proliferation.[35] Whilst the consequences of the Warburg Effect are well-

understood, establishing why this occurs in cancerous cells, or whether it is essential for their growth, remains unresolved.

A 2006 study on lactate dehydrogenase-A (LDH-A) expression by Leder *et al.* revealed that the previous commonly held hypothesis, where the Warburg Effect was attributed to a mitochondrial defect – which therefore blocked the oxidative phosphorylation pathway – was unlikely.[36] Subsequently, in 2008, Cantley and co-workers showed that cancerous cells exclusively express the M2 isoform of pyruvate kinase (PKM2). Pyruvate kinase regulates the final step in the glycolysis process, with the M1 isoform (PKM1) of the enzyme being found in normal cells.[37] By disabling the PKM2 enzyme in a H1299 (lung cancer) cell line, and expressing the PKM1 enzyme instead, they were able to reverse the Warburg Effect. This was evidenced by a decrease in lactate production and an increase in oxygen consumption. Additionally, Cantley *et al.* demonstrated that cancer cells that contain the PKM1 enzyme exhibit a great decrease in both ATP production and the rate of cell proliferation when compared to those containing the PKM2 enzyme.[37] Consequently, it is now understood that the PKM2 enzyme enables cancer cells to consume glucose at an accelerated rate, and also dramatically increases the rate of the final step in glycolysis, which is rate-limiting. Whilst these results have increased our understanding of how glucose uptake is accelerated in cancer cells, due to the Warburg Effect, it still does not establish why this phenomenon arises.

The Warburg Effect is often thought to exist due to its ability to promote anabolic metabolism (the building of large complex molecules from smaller simple building blocks). However, this process must be indirect because the lactate generated by aerobic glycolysis is ejected from the cell. Therefore, it does not lead to carbon production for biosynthetic pathways. As a result of this finding, a more recent theory suggests that the Warburg Effect arises in cancerous cells because it enables these cells to maintain large pools of glycolytic intermediates. These intermediates feed several non-mitochondrial pathways including the pentose-phosphate pathway; this favours the generation of lipids and nucleic acids, which are important for rapid cell growth and is particularly important in rapidly dividing cancerous cells.[34] This is an interesting idea but further work is required to fully establish the origins of the Warburg Effect.

1.3.3. Glucose Transporters (GLUTs)

Glucose transporters (GLUTs) are transmembrane proteins that facilitate the efficient transport of hydrophilic carbohydrates across lipophilic cell membranes. There are 14 isoforms of GLUTs (GLUT-1–14) known in humans, ranging in size from 45-60 kDa (492-

524 amino acids) and these enable the transport of glucose and/or other sugars across the cell membrane depending on the specific receptor.[33,38,39]

GLUT-1 is the most studied of these 14 receptors, and is found in almost all foetal tissues, and in numerous adult tissues too.[38] Particularly high levels of GLUT-1 receptors are found in erythrocyte cells, in barrier tissues (*i.e.* blood-brain barrier (BBB) and epithelial tissue), and in a majority of cancerous cells.[39] Because the quantity of any given GLUT receptor within a cell membrane depends upon the energy/carbohydrate requirement of that cell, it is therefore reasoned that over-expression of GLUT-1 receptors occurs in most cancerous cells, as a consequence of their high glucose requirement (which arises from the Warburg Effect).[40]

High substrate specificity is typically observed for each of the GLUTs, for example, the GLUT-2 receptor exhibits a low affinity for D-glucose but a high affinity for D-glucosamine.[39] Perhaps more subtly, the GLUT-1 receptor has been found to possess a high affinity for D-glucose, but very poor affinity for its enantiomer, L-glucose.[41] It is the GLUT-1 receptor that we initially aimed to target in our research. Despite such strong substrate specificity, conjugation of a specific carbohydrate (*i.e* D-glucose) can enable transport of a non-natural species into a cell *via* the corresponding receptor (*i.e* GLUT-1). Examples of this being used in research and medical science will be discussed in Section 1.4.

It is important to note, that whilst the GLUT-1 receptor is efficient at transporting D-glucose across any cell membrane equipped with this receptor, it also has affinity for D-mannose, D-galactose and D-glucosamine.[35,39]

1.3.4. Hexokinase

The phosphorylation of glucose to glucose-6-phosphate is performed by the hexokinase (HK) enzyme. This is the first step in the glycolytic pathway because once the carbohydrate has been transported into the cell *via* a GLUT receptor, phosphorylation ensures that the carbohydrate is trapped inside the cell. This is because glucose-6-phosphate is anionic at physiological pH, which prevents its transport across the cell membrane.[42]

In order to manage the enhanced glucose avidity and increased number of GLUT receptors on the surface of cancerous cells, HK is often over expressed within these neoplastic cells. There are four different isoforms of HK, each of which measure approximately 100 kDa and consist of two domains with the enzymatic active site located in the cleft between the domains (Figure 1.9).[43,44] Binding of both the substrate (*i.e.* D-glucose) and ATP in the cleft causes the two domains to rotate, thereby narrowing the gap in the cleft and promoting the transfer of a phosphate group from ATP to the substrate. The phosphorylated substrate (*i.e.*

glucose-6-phosphate) and a molecule of ADP is then released. This is the first of ten steps in the glycolysis process, which leads to the formation of pyruvate.[42]

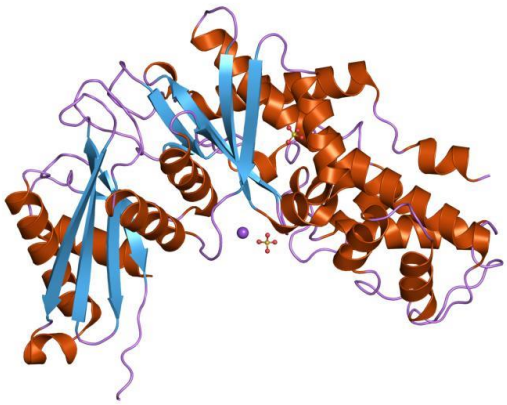

Figure 1.9 Crystal Structure of HKI with the different domains highlighted in blue and orange. Image source https://pfam.xfam.org/family/PF00349

Because HK is responsible for preventing the transport of carbohydrates back out of cells *via* a GLUT receptor, it would be advantageous for any ligands designed as part of this project to react with HK. This would prevent removal of the imaging agent from the target cells, and instead lead to their accumulation inside of such cells.

1.4. Glycoconjugates in medical imaging

Glycoconjugates are defined as compounds where a carbohydrate is covalently linked to another molecule (such as a lipid, peptide, protein or other compound).[45] There are numerous examples of glycoconjugates reported in the literature and their applications are wide ranging and include use in drug-delivery systems, vaccines and in biphasic or asymmetric catalysis.

In this project, we have focused on the synthesis of phosphine glycoconjugates, whereby a carbohydrate has been appended to a phosphine moiety. Phosphines ligands that are simply based on the structure of carbohydrates (where a portion of the native carbohydrate motif has been removed to enable phosphine incorporation, see Figure 1.10) will not be discussed, as they are not suitable for biorecognition - particularly given that many examples also contain protecting groups in their final structure.[46,47].

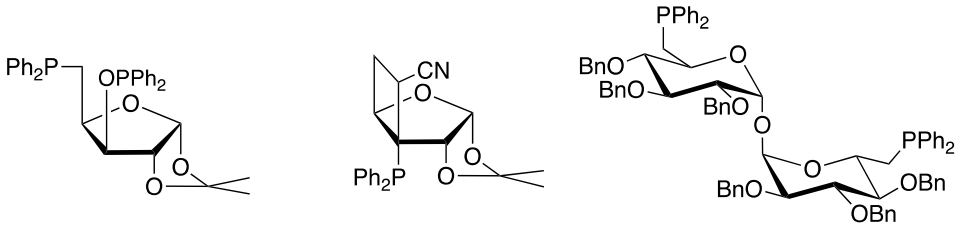

Figure 1.10 Examples of carbohydrate-based phosphine ligands, as opposed to P-glycoconjugates.[46]

Here the focus will be restricted to D-glucose-based glycoconjugates (and complexes) that have an application in medical imaging (Section 1.4.1-1.4.3), and phosphine glycoconjugates (Section 1.4.4), as these are pertinent to this project.

1.4.1. Metal-Free D-Glucose-Based Glycoconjugates for Medical Imaging

As noted in Section 1.3.3, GLUTs typically exhibit strong substrate specificity. However, conjugation of the correct carbohydrate moiety (*e.g.* D-glucose) to a non-natural substrate can facilitate its transport into the cell (*e.g. via* GLUT-1). This method has been employed in literature to enable the imaging of cancer cells, often by designing fluorophore-based glycoconjugates. For a comprehensive review of fluorescent glycoconjugates see the work of Vidal *et al*.[48] In this project, we aim to use radioactive ^{99m}Tc to image the cells rather than a fluorophore, but the principles when designing a useful glycoconjugate remain the same. Several key examples will be discussed as they have influenced the design of phosphine-carbohydrate ligands in this project.

The first example is the earliest case of a fluorescent tagged bioprobe, which was reported by Kutchai *et al.* in 1985. It consists of 7-nitrobenz-2-oxa-1,3-diazol (NBD) conjugated to D-glucose at the C-6 position to form 6-NBDG (Figure 1.11).[49] The uptake of 6-NBDG was studied in red blood cells and was seen to be inversely proportional to D-glucose concentration. Additionally, the uptake of 6-NBDG was also reduced in the presence of cytochalasin B (a mycotoxin), which is a high affinity GLUT-inhibitor. These two results confirm that 6-NBDG is transported into cells *via* GLUT receptors. However, as the carbohydrate was conjugated to the fluorophore at the C-6 position, the glycoconjugate was not able to interact with HK. Moreover, the uptake of 6-NBDG was comparatively slow when compared to other monosaccharide species.

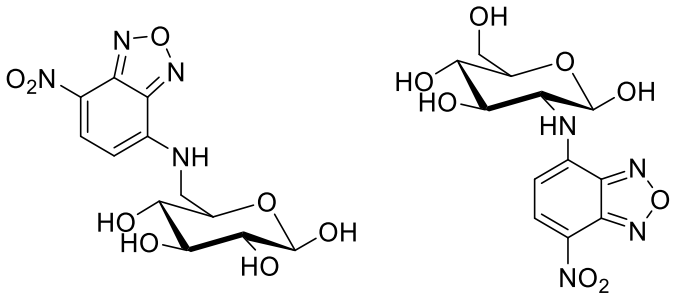

Figure 1.11 Structures of 6- and 2-NBDG, reported by Kutchai and Matsuoka et al.[49,50]

Consequently, Matsuoka and co-workers synthesised 2-NBDG in 1996 (Figure 1.11).[50] As the conjugate was formed at the C-2 position of D-glucose, this glycoconjugate could undergo phosphorylation by HK. Therefore, 2-NBDG can accumulate inside live cells and so provide information about cellular metabolic activity. Because 2-NBDG remains fluorescent once phosphorylated, but then degrades to non-fluorescent components during glycolysis, 2-NBDG has been used to study the cellular glucose uptake rate and metabolism in biological systems (*i.e.* demonstrating the Warburg Effect in cancer cells).[51]

The next pertinent example is Pyro-2DG (Figure 1.12). This example, published by Zheng *et al.* in 2003, demonstrates that considerably more bulky species, such as porphyrin, can be transported *via* GLUTs.[52]

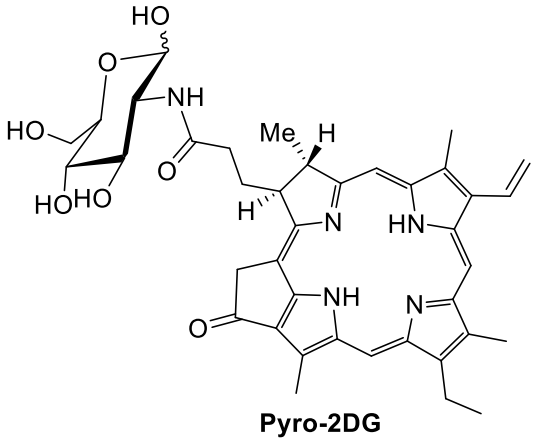

Figure 1.12 Structure of the glycoconjugate Pyro-2DG.[52]

In Pyro-2DG, porphyrin is conjugated to D-glucosamine at the C-2 position, to give a glycoconjugate that is capable of accumulating in cancerous cells. Pyro-2DG works as a near-infrared (NIR) dye, so is used for imaging the cancer cells through the detection of this compound's fluorescence at 720 nm. Additionally, this glycoconjugate has the potential to be used in photodynamic therapy (PDT); irradiation of cancerous cells after uptake of Pyro-2DG has been found to result in damage to their mitochondria, leading to cell damage and

ultimately cell death.[52] Zheng *et al.* have proposed that the accumulation of Pyro-2DG in cancerous cells occurs by GLUT transport, as uptake is inhibited by large quantities of D-glucose. Confocal fluorescence microscopy show that there is no back-transfer of Pyro-2DG once it has localised inside the cells, and hence it can be inferred that the compound must be reacting with hexokinase (HK) once inside the cell.[52] Notably, Pyro-2DG uses a 3-carbon flexible linker to conjugate the porphyrin and carbohydrate because generally, glycoconjugates with very short, and inflexible linkers are unable to transport bulky fluorophores *via* GLUT receptors. Therefore, to prevent poor cellular uptake when using a short linker comparatively low molecular weight fluorophores have been used, such as those examples reported by Park *et al*.[53]

In 2018 Park *et al.* developed new NIR glycoconjugate tracers based on rhodamine (Figure 1.13).[53] Rhodamine derivatives typically fluoresce at ~ 570 nm, outside of the NIR range, but Park and co-workers hypothesised the emission wavelength would be shifted towards the NIR region (>680 nm) if the oxygen atom in the fluorophore was replaced with a silicon atom. Two glycoconjugates were designed: neutral Glc-SiR-CO_2H and cationic Glc-SiR-Me (Figure 1.13). Both exhibited near identical photophysical properties, but Glc-SiR-CO_2H displayed superior cell uptake.[53] This was attributed to it being a neutral species overall. Park *et al.* studied the GLUT transport of Glc-SiR-CO_2H by incubating the fluorophore (10 μM) with varying concentrations of L- and D-glucose (0-55 mM) in with HeLa cells for 1 h. It was found that uptake of Glc-SiR-CO_2H was independent of L-glucose concentration but inhibited with increasing D-glucose concentration. This implies there is GLUT mediated transport of the glycoconjugate; tests with additional cell lines suggest that it is both the GLUT-1 and GLUT-4 receptors that promote the transport of this fluorophore. LC-MS analysis of the lysates (after incubation of Glc-SiR-CO_2H with HeLa cells) revealed that the compound was phosphorylated (presumably by hexokinase).[53] The NIR dye therefore has the potential to be used for the imaging of cells, but *in vivo* studies are yet to be reported.

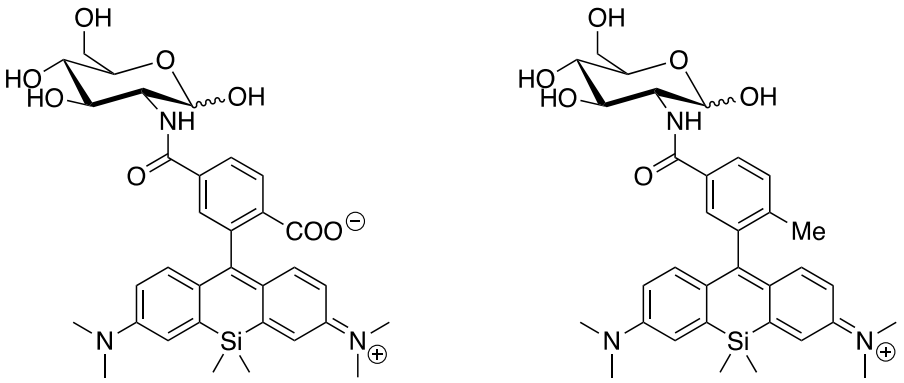

Figure 1.13 Structures of rhodamine-based glycoconjugates.[53]

Despite previous results that have suggested a longer linker between the carbohydrate and conjugated molecule is required for receptor recognition, Li and co-workers have shown that this is not always necessary. In 2020, Li *et al.* developed Glu-1-O-DCSN (Figure 1.14), which incorporates a dicyanoisophorone-based dye.[54] A D-glucose competition experiment demonstrated that the uptake of Glu-1-O-DCSN was significantly inhibited by this carbohydrate, suggesting GLUT-1 transport. Although L-glucose competition tests were not performed, the uptake of Glu-1-O-DCSN was also studied in normal (NE1) and cancer (HeLa and KYSE150) cell lines. Greater uptake was observed in the cancer cell lines, again indicating GLUT-1 transport of the red-emitting dye (λ_{em} = 654 nm). *In vivo* studies demonstrated the gradual accumulation of Glu-1-O-DCSN in the tumours of tumour-bearing mice (uptake peaks at 23 h), and in the liver, kidneys and brain of normal mice. [54] This positive result provides further evidence of GLUT-1 transport, as GLUT-1 receptors are found localised at the blood brain–barrier (BBB) and enable the uptake of D-glucose in the brain.

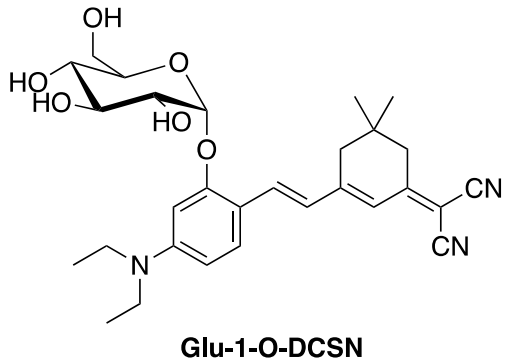

Figure 1.14 Structure of glycoconjugate Glu-1-O-DCSN.[55]

1.4.2. Fluorodeoxyglucose (^{18}FDG)

Kutchai, Matsuoka, Zheng, Park and Li *et al.* have all developed red- or NIR-emitting glycoconjugates for the imaging of cancerous cells. These examples have shown that conjugation at the C-1 and C-2 position is preferable (*versus* C-6), the species should be neutral, and both long and short linkers can enable GLUT transport. However, developing fluorophores with λ_{em} capable of deep tissue penetration remains an issue. This can be overcome by the incorporation of radioisotopes (*i.e.* ^{18}F, ^{99m}Tc).

Fluorodeoxyglucose (FDG, Figure 1.15) remains the most routinely used compound for the diagnosis of cancer, because it is one of the simplest bioconjugates; the hydroxy group at the C2 of D-glucose is replaced by the PET radioisotope, fluorine-18 (^{18}F, $t_{1/2}$ = 110 min). FDG is transported *via* GLUT-1 receptors, where it is phosphorylated by HK to form FDG-6-phosphate, thereby trapping the PET-imaging agent within the target tissue. FDG uptake is maximised in cells with the greatest number of GLUT-1 receptors and HK activity – these are predominantly cancer cells.[25]

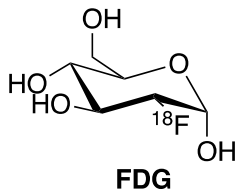

Figure 1.15 Structure of ^{18}F-fluorodeoxyglucose (FDG).

Although FDG is extremely successful, there are a several drawbacks linked to this radioisotope: (i) ^{18}F has a very short half-life ($t_{1/2}$ = 110 min) which presents challenges for the preparation of the imaging agents; (ii) ^{18}F is prepared in a cyclotron so its production is expensive and its use in hospitals can be geographically limited with respect the location of the cyclotron.[25] For these reasons, it has become attractive to research analogues that make use of SPECT isotopes (*e.g.* ^{99m}Tc) instead.

1.4.3. Technetium 99m Glycoconjugates

So far, only one ^{99m}Tc glycoconjugate imaging agent has achieved FDA-approval. This radiopharmaceutical is referred to as *Lymphoseek* and is used to identify the sentinel lymph nodes in cancer patients. These are the lymph nodes to which cancer is most likely to spread first. The structure of *Lymphoseek* is extremely complex and the glycoconjugate ligand contains a dextran backbone made up of 60 glucose units. Four molecules of DTPA and 55 units of mannose are conjugated to the dextran backbone, with the DTPA molecules used for chelation to ^{99m}Tc(IV), whilst the mannose molecules bind to the protein on the surface of endothelial cells found within the lymph node.

In this project, only Tc(V) and Tc(I) cores have been considered due to the ease of synthesis of Tc(V) complexes, and because of the stability associated with the Tc(I) core. Consequently, whilst a comprehensive review into ^{99m}Tc glycoconjugates has been published by Orvig *et al.*, only examples relating to Tc(V) and Tc(I) species will be discussed below.[56] None of these examples contain phosphine glycoconjugates, but they do demonstrate the complexity involved when attempting to synthesise a ^{99m}Tc glycoconjugate for applications in medical imaging.

1.4.3.1. Technetium(V)-99m D-Glucose-based Glycoconjugates

Although technically not a glycoconjugate, the first Tc(V) complex involving a carbohydrate molecule was prepared from 5-thio-D-glucose (Figure 1.16) in 1999.[57] As with many older ^{99m}Tc-labelled species, characterisation data were not reported. Unfortunately, the resultant species did not behave like D-glucose, and no interaction with the GLUTs or HK were detected. Because the ^{99m}Tc complexes are generally prepared in dilute aqueous conditions, the weakly coordinating -OH groups of the carbohydrate are not particularly suitable for direct coordination to the radiometal. Instead, conjugation of the carbohydrate to a binding moiety with a higher affinity for ^{99m}Tc is necessary.

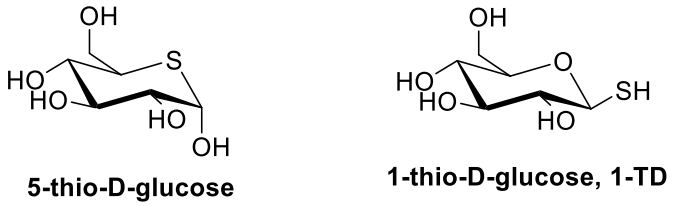

Figure 1.16 Structures of 5- and 1-thio-D-glucose.

This led to a more recent study involving the isomeric glycoconjugate, 1-thio-β-D-glucose (1-TD, Figure 1.16). However, the HPLC traces recorded for the ^{99m}Tc(V) complex of 1-TD were found to vary with ligand concentration and pH, suggesting that a number of species were formed.[58] When the ^{99m}Tc species was synthesised at pH 7 (near physiological pH), it exhibited poor stability and did not remain intact after 2 h. Additionally, attempts to form the analogous Re(V)-1-TG complexes were unsuccessful and so further studies were not performed. Characterisation of ^{99m}Tc complexes are typically performed by preparing the non-radioactive Re complex. This is because the handling of non-radioactive complexes is simpler, and specialist facilities are necessary to work with radioisotopes.[25] Re is a suitable model because it is the heavier congener of Tc, and therefore possess similar coordination chemistry and reactivity. The similarities and differences between Re and Tc complexes will be discussed in more detail in Chapter 2.

In contrast to the examples above, the ^{99m}Tc-ECDG glycoconjugate developed by Podoloff *et al.* is more complete in its characterisation.[59] The glycoconjugate ligand, ethylenedicysteindeoxyglucosamine (ECDG, Figure 1.17), was synthesised by amide coupling between two D-glucosamine units and an ethylenedicystein (EC) moiety. The EC backbone has an N_2S_2 binding sphere, which enabled efficient coordination of the ligand to the radiometal. This meant the complex, ^{99m}Tc(V)-ECDG, was formed from $[TcO_4]^-$ in 94% radiochemical yield.[60] Podoloff *et al.* performed L- and D-glucose competition assays to confirm transport of the complex *via* GLUT receptors. These results were supported by *in vivo* studies, where the uptake of ^{99m}Tc-ECDG was upregulated in the tumours of rats that had been pre-treated with insulin *versus* those that were not.[60] Although not stated in the paper, this would suggest transport of ^{99m}Tc-ECDG *via* GLUT-4 receptors, as they are insulin dependent, whilst GLUT-1 receptors are insulin independent. Podoloff *et al.* repeated the *in vivo* studies with ^{99m}Tc-EC, and showed that without the carbohydrate, this species does not accumulate in tumours, but instead in organs involved in excretion. Despite the authors claims that ^{99m}Tc-ECDG is phosphorylated by HK, the evidence for this is weak, and the activity measured in the blood during *in vivo* testing is twice that found inside the tumours.[25,60] This could suggest that HK-mediated phosphorylation does not occur, and therefore the ^{99m}Tc species can be transported out of the cells.

These complexes appear to exhibit reasonable levels of stability as no activity was detected in the thyroid. This is significant because if a ^{99m}Tc complex is unstable *in vivo*, it will be re-oxidised to $[TcO_4]^-$ which is known to accumulate in the thyroid. Currently, ^{99m}Tc-ECDG is undergoing a 154-person Phase 3 clinical trial investigating its application in the diagnosis of lung cancer. This study is due to be completed in March 2023.[61] Further Tc(V) complexes of tetradentate ligands have been reported by Liu *et al.*, but these Tc(V) glycoconjugates have often exhibited poor stability *in vivo*.[62]

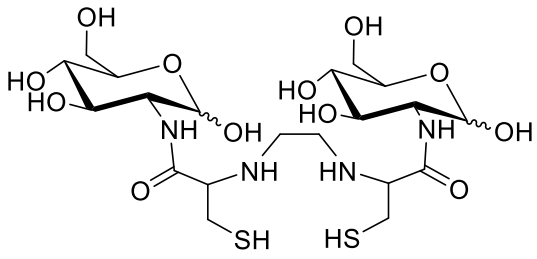

ECDG

Figure 1.17 Structure of ECDG ligand.

In 2015, Porcal *et al.* reported the synthesis of the *bis*-Tc(V) complex ^{99m}Tc-AADG, (Figure 1.18).[63] ^{99m}Tc-AADG is structurally similar to ^{99m}Tc-ECDC (which was undergoing Phase 2 clinical trials at this time). However, ^{99m}Tc-AADG has a bidentate chelator, whilst ^{99m}Tc-

ECDC used a tetradentate chelator.[64] The AADG ligand was prepared by amide coupling of D-glucosamine hydrochloride and ethyl-bromoacetate. Radiolabelling of AADG with $[TcO_4]^-$ (in the presence of $SnCl_2$) gave the ^{99m}Tc-AADG complex in 98% radiochemical yield. This complex also exhibited good stability (>80%) after 5 h, although whether this was performed *in vitro* or *in vivo* remains unclear.[63] *In vitro* D-Glucose competition studies showed no evidence for GLUT transport, and *in vivo* localisation studies did not demonstrate a greater accumulation of ^{99m}Tc-AADG in tissue that consumes larger quantities of D-glucose (such as the brain, heart and muscle). Most disappointingly, whilst high uptake was observed for ^{99m}Tc-AADG in B16 murine melanoma cells, this result was the same for the for the carbohydrate-free analogue, ^{99m}Tc-AA, indicating that the carbohydrate has no influence on uptake in this system.

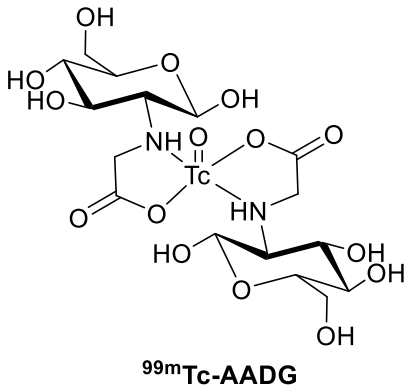

Figure 1.18 Structure of imaging agent ^{99m}Tc-AADG.[63]

1.4.3.2. Technetium(I)-99m Tricarbonyl Glycoconjugates

As mentioned in section 1.2.2, Alberto and co-workers developed the technetium(I) tricarbonyl core. This is often favoured for biological applications due its size, stability towards oxidation and ability to coordinate a wide variety of chelating ligands.[25] The synthesis of $[Tc(CO)_3]^+$ complexes will be further discussed in Chapter 3, where this core has been employed.

One of the first examples of a ^{99m}Tc(I) glycoconjugate was developed in the Orvig group. The ligand used for this complex contained a 2-hydroxybenzyl moiety that was conjugated at the C-2 position of D-glucosamine (Figure 1.19). Despite expectations that the ligand would coordinate in bidentate fashion *via* the amine and phenolic-OH groups, ^{1}H NMR spectroscopy revealed a downfield shift (7.4 ppm) of the C-3 proton when recording the NMR spectrum of the 'cold' (non-radioactive) Re complex. This suggested that the OH group at the C-3 position was additionally involved in binding to the metal centre. Therefore, the glycoconjugate ligand was likely coordinating to Tc in a tridentate fashion (Figure 1.19). Orvig *et al.* hypothesised that because of this, the Re complex, and its ^{99m}Tc

derivative, would not be recognised biologically and therefore no further work was carried out on this system.[65]

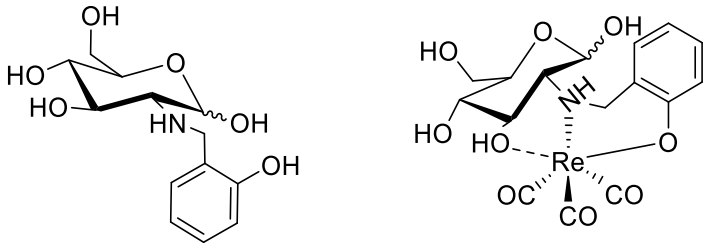

Figure 1.19 Structure of a glycoconjugate ligand and its $Re(CO)_3$ complex, by Orvig *et al.*[25]

Consequently, the Orvig group designed a series of 3-hydroxy-pyridone glycoconjugates.[66] Here, the distance and rigidity between the carbohydrate moiety and binding site was increased to ensure that the carbohydrate could not participate in binding to the Re/Tc centre, as seen in the previous example. A series of five ligands were designed and a variety of linker lengths, conjugation methods, and conjugation positions (C-1, C-3 and C-6) were investigated. These included examples containing an ether linkage at the C-1 position of D-glucose (Figure 1.20(a)), an amide linkage at the C-2 position of D-glucosamine (Figure 1.20(b)) and an amide linkage at the C-6 position of D-glucose (Figure 1.20(c)).

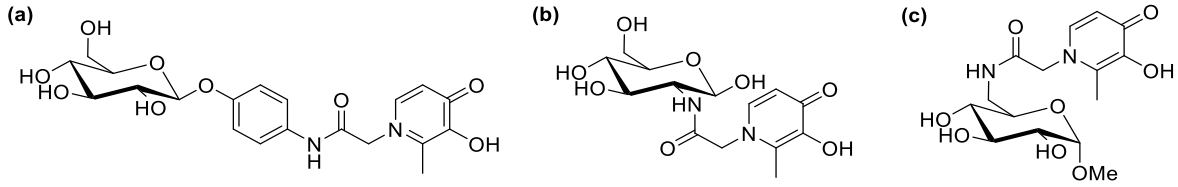

Figure 1.20 Examples of 3-hydroxy-pyridone glycoconjugate conjugated at the (a) C-1, (b) C-2 and (c) C-6 positions.[66]

These ligands formed complexes with 'cold' Re and radioactive ^{186}Re and ^{99m}Tc sources. The ^{99m}Tc complexes were found to exhibit excellent stability in solutions of cysteine and histidine after 4 h, and although some degradation was noted after 24 h, this was not considered a significant issue as this exceeded the half-life of ^{99m}Tc.[66] Analysis of the ^{99m}Tc complexes after 24 h was still possible as the samples had not exceeded HPLC detection limits. However, the Tc(I) complexes did not undergo phosphorylation by HK and in the concluding remarks of the paper, it was acknowledged that competitive uptake experiments with D-glucose (and/or L-glucose) were not performed.[66] As the GLUT recognition of these compounds is unknown and the results of the HK assay were not promising, it is possible that recognition of these molecules by GLUT receptors may be poor. Orvig and co-workers noted that if receptor mediated transport was facilitated then these compounds could be medically relevant and consequently, further studies including a D-glucose competition

experiment would be performed in the future. To date, no follow up paper has been published. It is therefore possible that the linker may be too bulky and/or rigid to allow the complex to behave as a D-glucose analogue. A more flexible alkyl chain may have yielded more promising results.

In 2007, Gottschaldt and Yano *et al.* synthesised a Tc(I) glycoconjugate in 95% radiochemical yield. The bidentate glycoconjugate ligand consisted of a 2,2'-bipy moiety for radiometal coordination. Two D-glucose molecules were incorporated into the bipy-chelator *via* flexible thioether linkages and the 'cold' Re complex was synthesised to enable full characterisation of the ^{99m}Tc(I) complex. The N,N-ligand was found to coordinate in a *cis*-fashion, whilst a chloride ligand coordinated *trans* to the glycoconjugate ligand. The chloride ligand is denoted by a 'L' in the Tc(I) complex, as at higher levels of dilution this can exchange for an aqua ligand, Figure 1.21.[67] Good stability was observed for the ^{99m}Tc(I) complex after 4 h incubation in histadine, but after 24 h significant degradation was noted by HPLC analysis. It was expected that the degraded product would be $[^{99m}Tc(His)(CO)_3]^+$, where complete ligand exchange has taken place. However, when Gottschaldt *et al.* synthesised and analysed this compound ($[^{99m}Tc(His)(CO)_3]^+$), they discovered that this was not the case. They therefore hypothesised displacement of a ligand by histidine was only occurring at the labile site on the Tc(I) core (L=H_2O or Cl). This has been seen previously for $[Tc(CO)_3]^+$ species that contain pyridine or imidazole ligands.[67] Accordingly, HK and GLUT assays were not performed due to this lack of stability.

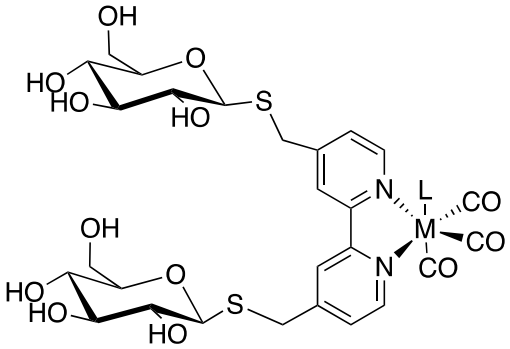

Figure 1.21 Tricarbonyl complex (M = Re or ^{99m}Tc) with a 2,2'-bipy-based glycoconjugate ligand.[67]

The labile site (L), generated by coordination of a bidentate ligand to the $[Tc(CO)_3]^+$ core, can often cause issues *in vivo*. It has been postulated that a protein can bind to the metal centre at this 'vacant' site. Over time, this often leads to complete displacement of the bidentate ligand. Use of tridentate ligands should therefore overcome stability issues within Tc(I) complexes - although examples of complexes of tridentates by the Orvig[25], Schibli[50] and Zubieta[51] groups still demonstrated poor stability *in vivo*. Despite these results, in 2014,

Gottschaldt *et al.* demonstrated that it is possible to generate stable [$Tc(CO)_3$] species using bidentate ligands. A series of pyridyltriazole ligands were designed where copper(I)-mediated 'click chemistry' was used to conjugate the following carbohydrates: D-glucose (Figure 1.22), D-galactose, D-mannose, D-xylose or D-maltose.[70] ^{99m}Tc(I) radiolabelling of the D-glucose glycoconjugate proceeded in high radiochemical yield and the product was found to be was stable in histidine for 24 h, with no changes seen in the HPLC trace. This contrasted with the cold Re analogue, that only demonstrated stability in histidine up to 4.5 h. Cell testing was performed with the Re(I) analogue, as it is not possible to test ^{99m}Tc complexes over such time frames (0-96 h). The Re(I) species was found to exhibit no cytotoxicity towards HepG2 cells (liver cancer cells), which makes the Tc(I) complex a potential candidate for testing *in vivo*.[70]

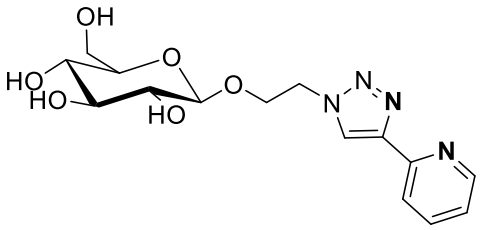

Figure 1.22 Glycoconjugate ligand synthesised by 'click-chemistry' (where bolded atoms denote those that coordinate to $^{99m}TcCO_3$ core).

1.4.4. Phosphine Glycoconjugates

Despite reports of a number of N-, S- and O-based glycoconjugates, there are very few examples reported for P-based glycoconjugates. Prior to the results reported in this thesis (Chapters 2-4), there have been no reports of ^{99m}Tc complexes featuring phosphine glycoconjugates, to the best of our knowledge.

Phosphine glycoconjugates were first reported during the 1990's, and they were aimed at being used as water-soluble ligands for applications in biphasic catalysis. Biphasic catalysis, where the catalyst is more soluble in the aqueous phase than the organic phase, is considered advantageous as the separation and recovery of catalysts from organic products is often a challenge.[71,72] Catalyst separation is often costly, and is a particular problem during the development of pharmaceuticals, where trace levels of transition metals (<100 ppm) in final products remains an issue.[73]

The first route to a C1-linked phosphine glycoconjugate was published by Beller *et al.* in 1997 (Scheme 1.3) and used sodium hydroxide to promote the glycosylation of 4-hydroxyphenyldiphenylphosphine and a halopyranose carbohydrate, under biphasic conditions. D-glucosamine, D-galactose and D-glucose phosphine glycoconjugates were prepared, but this method was low yielding (33-50%, dependent on the carbohydrate).

However, more traditional methods of glycosylation (*e.g.* Lewis acid catalysed glycosylation) gave even poorer yields (2-14%).[71]

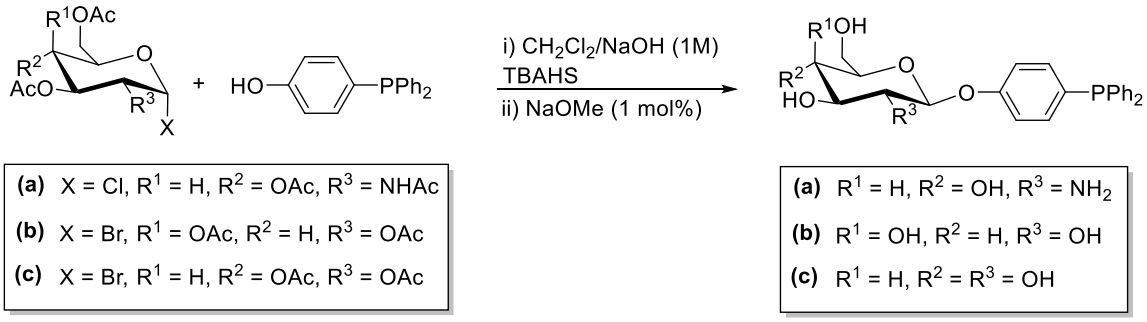

Scheme 1.3 1997 route by Beller *et al.* for the synthesis of phosphine glycoconjugates.[71]

In 1999 a second route to these molecules was disclosed by Beller *et al.*[72] Here, Pd-cross coupling was used to add $HPPh_2$ (or H_2PPh) to 4-iodophenyl-pyranose derivatives (Scheme 1.4). This method gave improved yields to the same targets as above (85% *versus* 50% for the galactose-containing glycoconjugate). The yield for the synthesis of the D-glucose-based glycoconjugate *via* the 1999 method was not reported.[72]

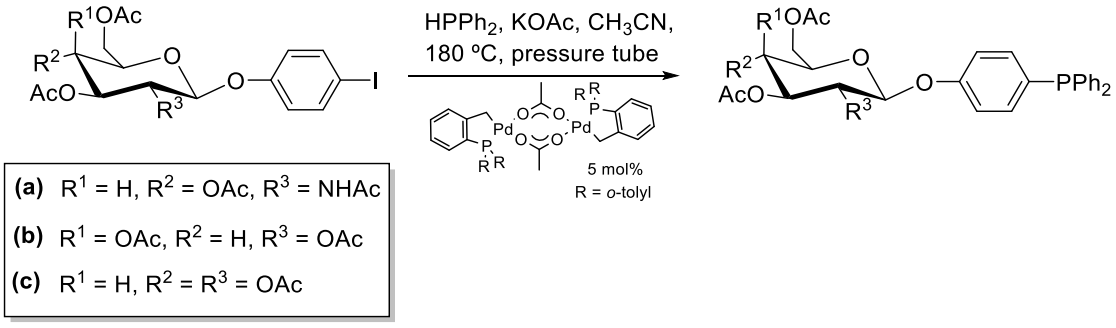

Scheme 1.4 General scheme of the alternative route to P-glycoconjugates, by Beller *et al.*[72]

Measuring the Nernst partition coefficient at various temperatures meant that Beller *et al.* could demonstrate that catalysts with the glycoconjugate ligands were capable of thermoreversible solvation. This means that at higher temperatures the hydrophilic catalyst can expel its hydrate shell and become more lipophilic. Analogous Pd-catalysts with TPPTS ligands do not do this. Therefore, the glycoconjugate-based catalysts were expected to exhibit greater activity when tested in biphasic catalytic applications. In 'two-phase' Heck and Suzuki cross coupling reactions, the Pd catalysts with phosphine glycoconjugates ligands were found to give better yields and higher activities that those with TPPTS ligands.[71] Both catalysts were tested under the same conditions, with the two-phase system being a 2:1:3 mixture of ethanol, water and di-*n*-butyl ether. Additionally, Beller *et al.* investigated the use of phosphine glycoconjugate ligands in the two-phase hydroformylation

of 1-octene. This reaction was performed in a water/toluene mixture, but catalyst recovery was not quantitative because of the catalyst's property of partitioning between the two phases at any given temperature. This reaction was of particular interest, as industrially 1-butanal is prepared from the two-phase hydroformylation of propene, using a Rh-TPPTS catalytic system (Ruhrchemie/Rhone-Poulenc process).[72]

Although the Beller group thoroughly researched the applications of phosphine glycoconjugate ligands, they were not the first group to develop such molecules. Earlier, in 1992, Heesche-Wagner and Mitchell synthesised the first examples of phosphine glycoconjugates, with conjugation at the C-1 (fructose and mannose), C-3 (glucose) and C-6 (galactose) positions. By adding an allyl group at the C-1, C-3 or C-6 positions, it was shown that hydrophosphination could be used to introduce the phosphine moiety (Scheme 1.5). Unfortunately, removal of the acetonide protecting groups led to the cleavage the propyl linker between the phosphine and carbohydrate, in all cases except the D-glucose derivative (Scheme 1.5).[74]

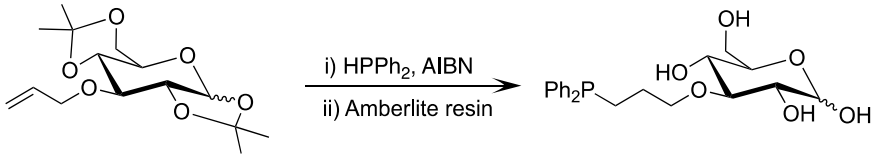

Scheme 1.5 Synthesis and deprotection phosphine glycoconjugate ligand by Heesche-Wagner *et al.*[74]

More recently, Sinou *et al.* reported phosphine glycoconjugates **1.7** and **1.8** (Figure 1.23). These ligands were prepared by amide coupling of a COOH-functionalised phosphine and D-glucosamine.[75] Although **1.7** and **1.8** exhibited no catalytic activity when peracetylated, once deprotected they became efficient ligands for 'biphasic' (3:2:2, Tol:EtOH:H_2O) Suzuki cross-coupling. A 1 mol% catalyst loading was required for the reaction to reach completion in 2 h, but this could be reduced to 0.1 mol% if the reaction time was extended.[75]

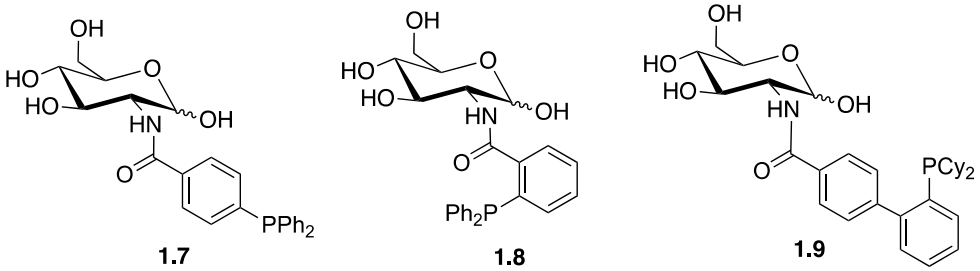

1.7 **1.8** **1.9**

Figure 1.23 Structures of C2-based phosphine glycoconjugates.[75,76]

Subsequently, Sinou *et al.* also published the synthesis of compound **1.9** (Figure 1.23). This ligand enabled the substrate scope of the biphasic Suzuki coupling reaction to be extended from Ar-Br and Ar-I species, to Ar-Cl species too. However, Sinou *et al.* admitted that this reaction was not truly biphasic (3:2:2, Tol:EtOH:H_2O), and stated that further work must be done to improve the ligands' water solubility to perform the reaction in a two-solvent biphasic system.[76]

Additionally, Sinou and co-workers have compared their system involving ligand **1.9**, with that designed by Miyuara *et al.* (Figure 1.24), as both groups' glycoconjugate ligands give complexes with similar catalytic activity.[77] Whilst Sinou and co-workers synthesised their ligands by reacting a COOH-functionalised phosphine with a NH_2-functionalised carbohydrate, the Miyuara group have swapped this functionality.[76] Miyuara and co-workers have used D-gluco-1,5-lactone as there carbohydrate moiety. This is hydrolysed in water to the ring-opened form, D-gluconic acid, which can then undergo amide coupling with an NH_2-functionalised phosphine.[77] Consequently, extending their system to di- or oligosaccharides may be more difficult than simply selecting one of the many naturally occurring amino-carbohydrates. Consequently, Sinou and co-workers believe their system allows for easier screening of alternative carbohydrates, which is desirable for improving the activity and recyclability of the catalyst.

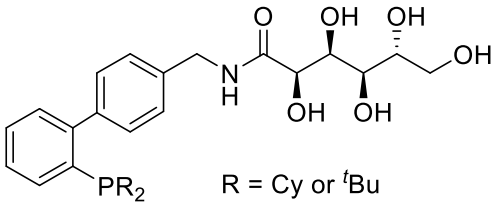

Figure 1.24 Structure of a D-gluco-1,5-lactone containing P glycoconjugate synthesised by Miyuara *et al.*[77]

In 2007, Sinou and co-workers researched the applications of phosphine glycoconjugates in alternative Pd catalysed reactions. They discovered that the peracetylated derivative of **1.7** (Figure 1.23) could be used as an efficient ligand in catalytic asymmetric methylation. By varying the group at the C-1 position of **1.7**, it was established that high ee's (85%) could only be achieved with a β-OAc occupying the C1 position. All other groups that were tested at this position (α-OAc, α/β-OMe, and α/β-OBn) gave significantly decreased ee values (0-30%).[78] Despite these interesting results, the Trost ligand remains a better ligand for catalytic asymmetric methylation. Consequently, in 2011, a glycoconjugate based on Trosts' privileged ligand was synthesised by Ruffo *et al.* (Figure 1.25), and will be discussed further in Chapter 4.[79]

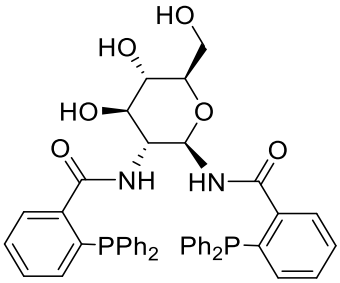

Figure 1.25 Structure of a diphosphine glycoconjugate, by Ruffo *et al.*[79]

Lastly, there are a few examples of phosphine glycoconjugates whereby a β-cyclodextrin, rather than a monosaccharide, has been used to introduce carbohydrate functionality to a P(III)-species. These include examples by Waldvogel, and Rudolf *et al*., but these will not be discussed here.[80,81]

1.4.5. Positional isomers of Glycoconjugates

D-glucose is highly functionalised and can be conjugated at a variety of positions (C1-6), but information is limited regarding the optimal position for modification. A 2016 study by Lippard *et al.* tried to address this issue by synthesising all possible positional isomers (C-1α, -1β, -2, -3, -4 and -6) of a D-glucose-based Pt drug (Figure 1.26).[41]

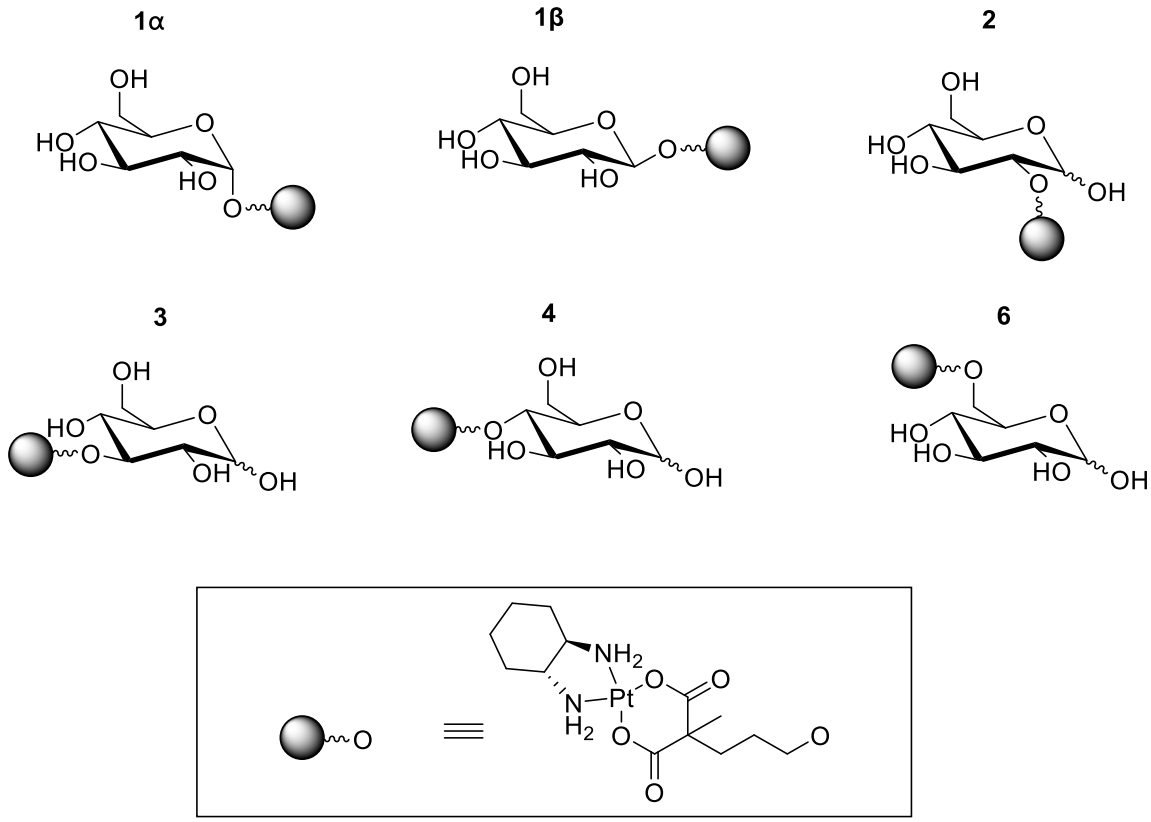

Figure 1.26 Series of positionally isomeric Pt-based glycoconjugate ligands, by Lippard *et al.*[41]

The C2-posistional isomer was identified as most potent in terms of cytotoxicity towards DU145 (prostate) cancer cells (2 ≥ 1α = 1β ≥ 4 = 6 ≥ 3), although the C1 isomers (α/β) showed very similar activity. The C3 species was the least potent of the isomers. In terms of cellular uptake, the C2-isomer again gave the best results. Uptake inhibition tests were performed by treating the cells with a GLUT-1 inhibitor (Cytochalasin B). Here, the uptake was most inhibited for the C2-isomer, followed by the C1-isomers (2 > 1α ≥ 1β > 3 = 4 = 6), suggesting that the GLUT-1 receptor has the greatest affinity for the C2-isomer. Overall, the C2 isomer performed the best, whilst the C1 isomers performed relatively well and the C3 isomer performed the worst.[41]

In this project, modifications have focused on the C1 position, due to the enhanced reactivity at this position of D-glucose when compared to the C2-6 positions. Despite the C1α-anomer performing better than the C1β-anomer in the publication by Lippard *et al.*, the glycoconjugates formed in this project are the C1β-anomer. This is a consequence of using acetyl protecting groups - which generally favour β-selectivity through an anchimeric effect - when forming phosphine glycoconjugates. Removal of protecting groups in the presence of a phosphine is non-trivial, and as the conditions for acetyl deprotection are compatible with

the phosphine, this has been our preferred protecting group. It should be noted that the paper by Lippard *et al.*[41] is a single result and consequently it may not be representative of all glycoconjugate-containing metal complexes.

1.5. Radiotherapy

Although our primary objective is to use phosphine glycoconjugate ligands in imaging applications - by radiolabelling with ^{99m}Tc – it is possible that these ligands could be used in radiotherapy too.[4] Typically high energy β^--emitting radioisotopes are used for therapeutic purposes, as the ejected β^--particles release energy when they collide with molecules in the body. This causes DNA damage within cells, resulting in cell death.[2]

Rhenium has two β^--emitting radioisotopes – rhenium-186 (^{186}Re) and rhenium-188 (^{188}Re) – and is the radiotherapeutic "matched pair" for diagnostic ^{99m}Tc as both metals are isoelectronic and produce essentially isostructural complexes for a given ligand set. This has led to the idea of developing 'theragnostic' agents; a single ligand with directed uptake could be used for both diagnostic and therapeutic purposes by simply changing the choice of radiometal.[82] Despite this potential application, radiolabelling with rhenium-186 or -188 has not been investigated in this project, because of the lack of its availability. Therefore, only non-radioactive Re complexes will be detailed in this thesis.

1.6. Summary and Objectives

1.6.1. Summary of literature survey

Several projects within the Ma and Pringle group have previously investigated the incorporation of peptides into ^{99m}Tc and ^{64}Cu imaging agents.[83,84] However, this thesis will focus on the incorporation of carbohydrates *via* a number of routes, to develop novel phosphine glycoconjugates as ligands for ^{99m}Tc radio-imaging.

Whilst many examples of ^{99m}Tc-glycoconjugate complexes have been reported (Section 1.4.3), none of these use phosphine glycoconjugate ligands. Few examples of phosphine glycoconjugates ligands are reported in the literature, and all examples have been designed for biphasic catalysis rather than bioimaging applications. Consequently, several fluorophore-based glycoconjugates have also been discussed in this Chapter (Section 1.4.1). This is because the principles required when designing a glycoconjugate species that is capable of imaging cells are valid regardless of whether it is a fluorophore or radioactive moiety that is performing the imaging.

The ^{99m}Tc glycoconjugate results were varied (Section 1.4.3). However, from the literature survey above (primarily Section 1.4.1) we can make the following key generalisations about glycoconjugate species:

- Carbohydrate conjugation should be performed at the C-1 or C-2 position if we aim to see an interaction with GLUT receptors and the enzyme HK. Evidence for this is the synthesis of 2-NBDG[49] *versus* 6-NBDG,[49] and the Pt(II) study where all positional isomers of a glycoconjugate ligand were synthesised (C-1α-, -1β, -2, -3, -4 and -6, see Section 1.4.5).[41]

- Incorporation of bulky species does not necessary inhibit GLUT transport, as demonstrated by the chemistry of Pyro-2DG.[52]

- A species with no overall charge is likely to have better cellular uptake, as shown by Park *et al.* preparing neutral Glc-SiR-CO_2H and cationic Glc-SiR-Me.[53]

- The linker between the carbohydrate and imaging moiety can be longer and more flexible (see example by Park *et al.*)[53] or shorter and more rigid (see example by Li *et al.*),[54] but this individually does not dictate whether the molecule will undergo GLUT transport.

1.6.2. Objectives

The aims of the research described in this thesis were:

- To explore methods for the conjugation of phosphines and carbohydrate molecules, in order to access phosphine glycoconjugate ligands that may be capable of biorecognition.

- To investigate the rhenium coordination chemistry of all phosphine glycoconjugate ligands prepared in this project as a model for ^{99m}Tc radiolabelling.

- To investigate the ability of phosphine glycoconjugate ligands to undergo radiolabelling with ^{99m}Tc, either using a kits-based approach based on that used for Myoview for Tc(V) radiolabelling, or a tricarbonyl-kit for Tc(I) radiolabelling.

- To evaluate the toxicity and uptake of non-radioactive Re complexes of phosphine glycoconjugates in various cell lines.

- To expand the current scope of P(III)-based phosphine glycoconjugates from mono- to diphosphine glycoconjugates.

1.7. References

1 Grand View Research, *Nuclear Medicine Market Size, Share & Trends Analysis Report By Product (Diagnostics (SPECT, PET), Therapeutics (Alpha Emitters, Beta Emitters, Brachytherapy)), By Application, By Region, And Segment Forecasts, 2020 - 2027*, 2020.

2 P. J. Blower, *Dalton Trans.*, 2006, **14**, 1705–1711.

3 P. J. Blower, *Dalton Trans.*, 2015, **44**, 4819–4844.

4 V. Carroll, D. W. Demoin, T. Hoffman and S. S. Jurisson, *Radiochim. Acta.*, 2012, **100**, 653–667.

5 L. S. Zuckier, *Principles and Advanced Methods In Medical Imaging and Image Analysis*, World Scientific Publishing Co. Pte. Ltd., Singapore, 2008.

6 H. Levi, *J. Nucl. Med.*, 1976, **1**, 3–10.

7 J. G. Hamilton and M. H. Soley, *Proc. N. A. S*, 1940, **26**, 483–489.

8 World Health Organisation, *World Health Statistics 2018 - Monitoring Health for the SDGs*, Luxembourg, 2018.

9 P. P. Bruyant, *J. Nucl. Med.*, 2002, **43**, 1343–58.

10 J. S. Lewis and K. R. Keshari, Eds., *Imaging and Metabolism*, Springer, New York, 2018.

11 E. E. van der Wall, *Netherlands Hear. J.*, 2014, **22**, 257–258.

12 J. E. Stirrup and S. R. Underwood, *J. Nucl. Cardiol.*, 2017, **24**, 1960–1964.

13 G. H. Hinkle, J. A. Loesch, T. L. Hill, S. R. Lefevre and J. Olsen, *J. Nucl. Med. Technol.*, 1990, **18**, 16-28.

14 P. J. Bohdiewicz, *J. Nucl. Med. Technol.*, 1998, **26**, 155–63.

15 Satumomab Pendetive Overview, Creative Biolabs, https://www.creativebiolabs.net/satumomab-pendetide-overview.htm, (accessed 13 May 2020).

16 U. Abram and R. Alberto, *J. Braz. Chem. Soc.*, 2006, **17**, 1486–1500.

17 M. Ono, R. Ikeoka, H. Watanabe, H. Kimura, T. Fuchigami, M. Haratake, H. Saji and M. Nakayama, *Bioorganic Med. Chem. Lett.*, 2010, **20**, 5743–5748.

18 S. Jones and R. C. Hendel, *J Nucl Med*, 1993, **21**, 191–195.

19 M. D. Bartholoma, A. S. Louie, J. F. Valliant and J. Zubieta, *Chem. Rev.*, 2010, **110**, 2903–2920.

20 *Technical Reports Series No. 466; Technetium-99m Radiopharmaceuticals: Manufacture of Kits*, 2008.

21 S. Jürgens, W. A. Herrmann and F. E. Kühn, *J. Organomet. Chem.*, 2014, **751**, 83–89.

22 S. Shi, L. Yao, L. Li, Z. Wu, Z. Zha, H. F. Kung, L. Zhu and D.-C. Fang, *R. Soc. Open Sci.*, 2019, **6**, 191247.

23 Ca Pat., WO 98/48848, 1998.

24 R. J. Kowalsky, *Radiopharmaceuticals in nuclear pharmacy and nuclear medicine*, 3rd edn., 2012, vol. 46.

25 M. L. Bowen and C. Orvig, *Chem. Commun.*, 2008, 5077–91.

26 Cardinal Health, *FDA-approved radiopharmaceuticals*, Dublin, Ohio, 2016.

27 J. D. Kelly, M. Forster, B. Higley, C. M. Archer, F. S. Booker, L. R. Canning, K. W. Chiu, B. Edwards, H. K. Gill and M. McPartlin, *J. Nucl. Med.*, 1993, **34**, 222–227.

28 K. Schomacker and H. Schicha, *Eur. J. Nucl. Med.*, 2000, **27**, 1845–1863.

29 L. C. Francesconi, Y. Zheng, J. Bartis, M. Blumenstein, C. Costello and M. A. De Rosch, *Inorg. Chem.*, 2004, **43**, 2867–2875.

30 J. A. Jackson, I. N. Hungnes, M. T. Ma and C. Rivas, *Bioconjug. Chem.*, 2020, **31**, 483–491.

31 NHS Website, https://www.nhs.uk/common-health-questions/operations-tests-and-procedures/what-do-cancer-stages-and-grades-mean/, (accessed 5 August 2021).

32 S. Robu, M. Schottelius, M. Eiber, T. Maurer, J. Gschwend, M. Schwaiger and H.-J. Wester, *J. Nucl. Med.*, 2017, **58**, 235–242.

33 T. M. Devlin, Ed., *Textbook of Biochemistry*, John Wiley & Sons, United States of America, 7th edn., 2011.

34 T. Hitosugi and J. Chen, *Oncogene*, 2014, **33**, 4279–4285.

35 E. C. Calvaresi and P. J. Hergenrother, *Chem. Sci.*, 2013, **4**, 2319.

36 V. R. Fantin, J. St-Pierre and P. Leder, *Cancer Cell*, 2006, **9**, 425–434.

37 H. R. Christofk, M. G. Vander Heiden, N. Wu, J. M. Asara and L. C. Cantley, *Nature*, 2008, **452**, 181–186.

38 R. A. Simmons, *Fetal and Neonatal Physiology*, Elsevier, 2017, **1**, 428–435.

39 M. Mueckler and B. Thorens, *Mol. Aspects Med.*, 2013, **34**, 121–138.

40 J. Ma, Q. Wang, X. Yang, W. Hao, Z. Huang, J. Zhang, X. Wang and P. G. Wang, *Dalton Trans.*, 2016, **45**, 11830–11838.

41 M. Patra, S. G. Awuah and S. J. Lippard, *J. Am. Chem. Soc.*, 2016, **138**, 12541–12551.

42 X. Li, J. Gu and Q. Zhou, *Thorac. Cancer*, 2015, **6**, 17–24.

43 S. P. Mathupala, Y. H. Ko and P. L. Pedersen, *Oncogene*, 2006, **25**, 4777–4786.

44 A. E. Aleshin, C. Zeng, G. P. Bourenkov, H. D. Bartunik, H. J. Fromm and R. B. Honzatko, *Structure*, 1998, **6**, 39–50.

45 Nature Journal Website, https://www.nature.com/subjects/glycoconjugates, (accessed 22 May 2020).

46 M. Diëguez, O. Pàmies and C. Claver, *Chem. Rev.*, 2004, **104**, 3189–3215.

47 S. Castillón, C. Claver and Y. Díaz, *Chem. Soc. Rev.*, 2005, **34**, 702–713.

48 B. Thomas, K. C. Yan, X. Le Hu, M. Donnier-Maréchal, G. R. Chen, X. P. He and S. Vidal, *Chem. Soc. Rev.*, 2020, **49**, 593–641.

49 L. Speizer, R. Haugland and H. Kutchai, *Biochim. Biophys. Acta - Gen. Subj.*, 1985, **815**, 75–84.

50 K. Yoshioka, H. Takahashi, T. Homma, M. Saito, K. B. Oh, Y. Nemoto and H. Matsuoka, *Biochim. Biophys. Acta - Gen. Subj.*, 1996, **1289**, 5–9.

51 S. N. Rampersad, *Sensors (Switzerland)*, 2012, **12**, 12347–12360.

52 M. Zhang, Z. Zhang, D. Blessington, H. Li, T. M. Busch, V. Madrak, J. Miles, B. Chance, J. D. Glickson and G. Zheng, *Bioconjug.Chem.*, 2003, **14**, 709–714.

53 A. Jo, J. Sung, S. Lee, H. Nam, H. W. Lee, J. Park, H. M. Kim, E. Kim and S. B. Park, *Bioconjug. Chem.*, 2018, **29**, 3394–3401.

54 Y. Cheng, G. Shabir, X. Li, L. Fang, L. Xu, H. Zhang and E. Li, *Chem. Commun.*,

2020, **56**, 1070.

55 N. A. Lodhi, J. Y. Park, K. Kim, M. K. Hong, Y. J. Kim, Y.-S. Lee, G. J. Cheon, K. W. Kang and J. M. Jeong, *Inorganics*, 2020, **8**, 1–19.

56 M. L. Bowen and C. Orvig, *Chem. Commun.*, 2008, **41**, 5077–5091.

57 K. Ozker, B. D. Collier, D. J. Lindner, L. Kabasakal, Y. Liu, A. Z. Krasnow, R. S. Hellman, S. D. Edwards, C. R. Bourque and P. D. Crane, *Nucl. Med. Commun.*, 1999, **20**, 1055–1058.

58 S. Jun Oh, J.-S. Ryu, E.-J. Yoon, M. Sun Bae, S. Joo Choi, K. Bae Park and D. Hyuk Moon, *Appl. Radiat. Isot.*, 2006, **64**, 207–215.

59 D. J. Yang, C.-G. Kim, N. R. Schechter, A. Azhdarinia, D.-F. Yu, C.-S. Oh, J. L. Bryant, J.-J. Won, E. E. Kim and D. A. Podoloff, *Radiology*, 2003, **226**, 465–473.

60 D. J. Yang, C. Kim, N. R. Schechter, A. Azhdarinia, D. Yu, J. L. Bryant, J. Won, E. E. Kim and D. A. Podoloff, *Radiology*, 2003, **226**, 465–473.

61 US National Library of Medicine - Clinical Trials, https://clinicaltrials.gov/ct2/show/NCT01394679, (accessed 23 July 2021).

62 X. Chen, L. Li, F. Liu and B. Liu, *Bioorg. Med. Chem. Lett.*, 2006, **16**, 5503–5506.

63 R. Dapueto, R. B. Aguiar, M. Moreno, C. M. L. Machado, F. L. N. Marques, J. P. Gambini, R. Chammas, P. Cabral and W. Porcal, *Bioorg. Med. Chem. Lett.*, 2015, **25**, 4254–4259.

64 U.S. National Library of Medicine, https://clinicaltrials.gov/ct2/show/NCT01899833, (accessed 23 July 2021).

65 S. R. Bayly, C. L. Fisher, T. Storr, M. J. Adam and C. Orvig, *Bioconjug. Chem.*, 2004, **15**, 923–926.

66 C. L. Ferreira, S. R. Bayly, D. E. Green, T. Storr, C. A. Barta, J. Steele, M. J. Adam and C. Orvig, *Bioconjug. Chem.*, 2006, **17**, 1321–1329.

67 M. Gottschaldt, D. Koth, D. Müller, I. Klette, S. Rau, H. Görls, B. Schäfer, R. P. Baum and S. Yano, *Chem. Eur. J.*, 2007, **13**, 10273–10280.

68 R. Schibli, J. Petrig, L. Spadola, L. Scapozza, E. Garcia-Garayoa and P. A. Schubiger, *Bioconjug. Chem.*, 2005, **16**, 105–112.

69 N. Lazarova, S. James, J. Babich and J. Zubieta, *Inorg. Chem. Commun.*, 2004, **7**,

1023–1026.

70 J. A. Czaplewska, F. Theil, E. Altuntas, T. Niksch, M. Freesmeyer, B. Happ, D. Pretzel, H. Schäfer, M. Obata, S. Yano, U. S. Schubert and M. Gottschaldt, *Eur. J. Inorg. Chem.*, 2014, **2014**, 6290–6297.

71 M. Beller, J. G. E. Krauter and A. Zapf, *Angew. Chem. Int. Ed. Eng.*, 1997, **36**, 772–774.

72 M. Beller, J. G. E. Krauter, A. Zapf and S. Bogdanovic, *Catal. Today*, 1999, **48**, 279–290.

73 D. R. Abernethy, A. J. Destefano, T. L. Cecil, K. Zaidi and R. L. Williams, *Pharm. Res.*, 2010, **27**, 750–755.

74 T. N. Mitchell and K. Heesche-Wagner, *J. Organomet. Chem.*, 1992, **436**, 43–53.

75 S. Parisot, R. Kolodziuk, C. Goux-Henry, A. Iourtchenko and D. Sinou, *Tetrahedron Lett.*, 2002, **43**, 7397–7400.

76 A. Konovets, A. Penciu, E. Framery, N. Percina, C. Goux-Henry and D. Sinou, *Tetrahedron Lett.*, 2005, **46**, 3205–3208.

77 M. Nishimura, M. Ueda and N. Miyaura, *Tetrahedron*, 2002, **58**, 5779–5787.

78 K. Glegoła, E. Framery, C. Goux-Henry, K. Michał Pietrusiewicz and D. Sinou, *Tetrahedron*, 2007, **63**, 7133–7141.

79 V. Benessere, A. De Roma, R. Del Litto, M. Lega and F. Ruffo, *Eur. J. Org. Chem.*, 2011, 5779–5782.

80 M. T. Reetz and S. R. Waldvogel, *Angew. Chem. Int. Ed. Engl.*, 1997, **36**, 865–867.

81 M. T. Reetz and J. Rudolph, *Tetrahedron: Asymmetry*, 1993, **4**, 2405–2406.

82 A. J. North, J. A. Karas, M. T. Ma, P. J. Blower, U. Ackermann, J. M. White and P. S. Donnelly, *Inorg. Chem.*, 2017, **56**, 9725–9741.

83 A. Chadwick, PhD Thesis, University of Bristol, 2019.

84 I. N. Hungnes, PhD Thesis, King's College London, 2021.

Chapter 2 Alkyl Linked Monophosphine Glycoconjugates

2.1. Introduction

2.1.1. Carbohydrates: Key Terminology and Reactivity

This project concerns exclusively *O*-glycosides, *i.e.* glycosides linked *via* an oxygen atom. Glycosidic links are formed by reaction of a glycosyl donor with a glycosyl acceptor. When synthesising glycoconjugate species, the glycosyl donor is a carbohydrate, whilst the glycosyl acceptor is a non-carbohydrate species (*e.g.* a phosphine).

The newly formed glycosidic linkage can be described as either an α- or β-linkage. This descriptor (α/β) refers to the configurational relationship between the anomeric carbon (C-1) and the anomeric reference atom (*e.g.* C-5 for hexapyranose molecules). An *anti* relationship between these atoms gives an α-glycoside, whilst a *syn* relationship gives a β-glycoside (Scheme 2.1).

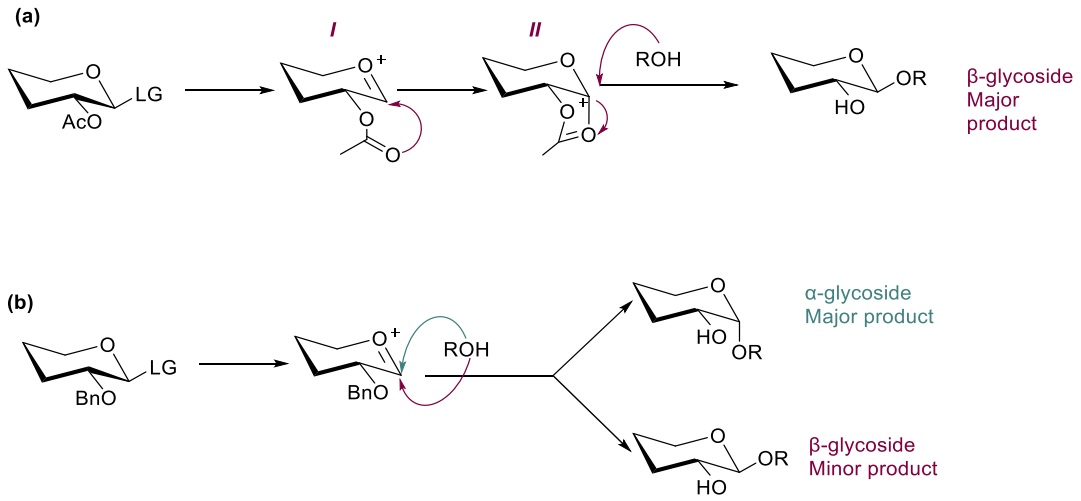

Scheme 2.1 Formation of α and β glycosides, where ROH can denote a carbohydrate or non-carbohydrate species. Protecting groups at the C-3 to C-6 positions have been omitted for clarity.

When forming new glycosides and glycoconjugates, it is typically the C-2 centre that imparts the greatest influence on the stereochemical outcome of the reaction. Participating groups, such as *O*-acetyl and *O*-benzoyl groups, assist in the stereoselective formation of β-linked glycosides.[1] This is often referred to as anchimeric assistance, or neighbouring group participation. It is widely accepted that participating groups aid the formation of a bicyclic intermediate (***II***), which forms to stabilise the glycosyl oxocarbenium species (***I***) (Scheme 2.1(a)). This bicyclic intermediate forms on the bottom face of the carbohydrate, thereby forcing the glycosyl donor to approach from the top face.[2] This results in selective formation of the β-linked product.

Non-participating groups, such as *O*-benzyl groups, often lead to the formation of the α-linked species as this is thermodynamically favoured due to the anomeric effect (Scheme 2.1(b)). Non-participating groups do not lead to exclusive formation of the α-product, and varying amounts of the β-product can also be formed.[2]

Protecting groups can influence the activity of the glycosyl donor. Electron-rich protecting groups (e.g. *O*-benzyl groups) are referred to as 'arming' groups, whilst electron-withdrawing groups (e.g *O*-acetyl groups) are described as 'disarming' groups.[3] 'Disarming' groups disfavour the formation of the carbocationic oxocarbenium species, and therefore disfavour glycosylation reactions, compared with 'arming' groups.

These terms and concepts discussed above will be highlighted in several of the glycoconjugation reactions discussed within this Chapter.

2.1.2. Binding to Tc(V)

Widespread clinical use of ^{99m}Tc-labelled radiopharmaceuticals has been achieved, in part, due to the ease of their preparation. This is a consequence of the development of kit-based ^{99m}Tc cores (Figure 2.1) during the 1980s, which has resulted in numerous clinically approved ^{99m}Tc imaging agents.[4] The lyophilised kits contain all of the reagents required to prepare the active compound (chelating ligand, reducing agent, buffer and weak chelator), bar the radiometal itself.[5] This is added to the kit as a saline solution of pertechnetate ($[^{99m}TcO_4]^-$). After leaving this mixture to stand for a short period of time to allow for complexation (15-30 min), the radiopharmaceutical can then be administered to a patient, where SPECT imaging is used to detect its localisation. The development of kits is therefore a vital step towards the usage of any ^{99m}Tc complex in the clinic, so has been explored for several of the ligands developed within this project, and will be discussed in Section 2.6.5 of this Chapter.

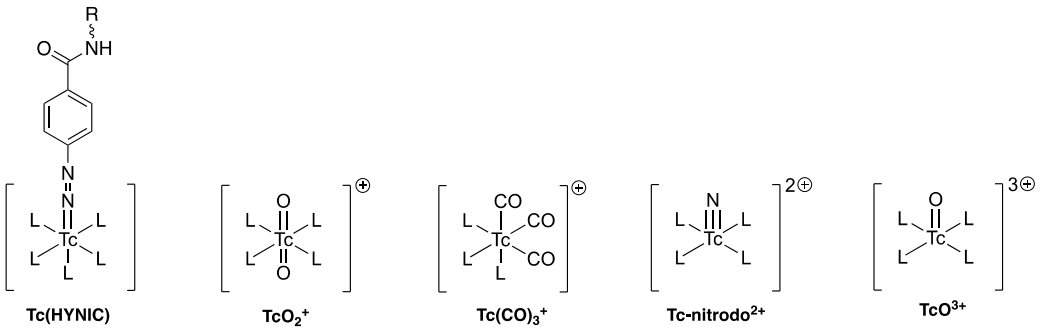

Figure 2.1 A variety of kit-based cores utilised in the synthesis of ^{99m}Tc radiopharmaceuticals.

Although nitrogen- and phosphorus(V)-based ^{99m}Tc imaging agents have achieved widespread clinical usage, only one phosphorus(III)-based ^{99m}Tc species has this status.[6–8] Structurally, *Myoview* consists of a dioxo-Tc(V) core ($[^{99m}TcO_2]^+$) and two tetrofosmin ligands (Figure 2.2). The lipophilicity of these phosphine ligands, and the positive charge on the complex facilitate its localisation within myocardial cells leading to its application in myocardial perfusion imaging.[6] More information regarding *Myoview* can be found in Chapter 1 (Section 1.2.3).

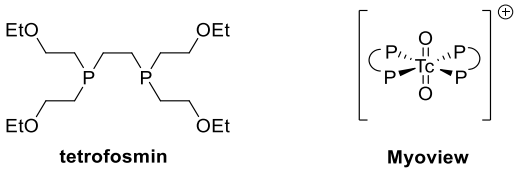

Figure 2.2 Structure of radiopharmaceutical *Myoview* and tetrofosmin ligand.

2.1.3. Glycoconjugation Methods

Instead of attempting to control biodistribution through changes to an imaging agent's charge, size or lipophilicity, a more predicatable and targeted approach is favoured. The aim of this project was therefore to develop new phosphine ligands that incorporate monosaccharides into the ligand structure, so that the bio-distribution would be based on the location of carbohydrate receptors. Cancerous cells often (i) over-express glucose receptors, and (ii) have an increased uptake of glucose – both results of the Warburg Effect - thereby making them a valuable target.[10]

Inspired by the phosphine glycoconjugate ligands synthesised by Beller *et al.*, initial work focused on exploring their method, originally published in 1997 (Scheme 2.2).[11] While it was possible to reproduce the synthesis of this molecule, albeit after a longer reaction time (40 hours), potential issues regarding the short and inflexible linker between the carbohydrate and phosphine were identified.

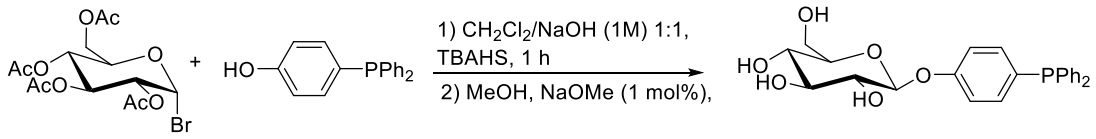

Scheme 2.2 Route to the synthesis of phosphine glycoconjugates, published by Beller *et al.* in 1997.

The groups of Schibli and Orvig reported that the molecules in Figure 2.3(a) do not have the necessary GLUT-1 transport to become useful compounds for cellular imaging. Orvig and co-workers have hypothesised in both cases that the lack of GLUT-1 receptor recognition is due to the proximity of the carbohydrate to the rest of the molecule.[12] These results led us to focus on generating phosphine glycoconjugates with a longer linker between the carbohydrate moiety and ^{99m}Tc-binding site.[12]

More recently, research published by Li and co-workers (2020) has shown that in some cases, a longer linker between the carbohydrate and conjugated molecule may not be necessary for receptor recognition, as evidenced by the compound shown in Figure 2.3(b). This molecule has exhibited successful transport *via* GLUT receptors (likely the GLUT-1 receptor), despite the relatively inflexible fluorophore being bound directly to the glucose moiety.[13] As results by Li *et al.* were published after the work in this Chapter was carried out, this will not be reflected in this work, but will be taken into account in the subsequent Chapters (3 and 4).

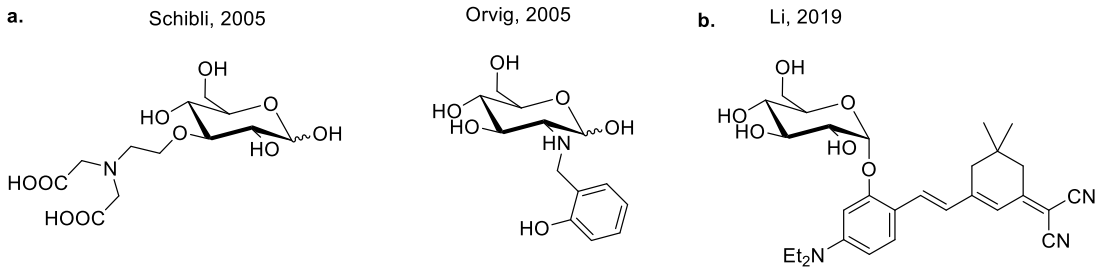

Figure 2.3 Glycoconjugates reported by (a) the Schibli and Orvig group and (b) the Li group.

2.2. Ligand Synthesis

Herein, four unsuccessful routes to phosphine glycoconjugates will first be discussed. Initially, Lewis acid catalysed glycosylation chemistry was investigated as a route to P(III)-containing glycoconjugates, before more traditional methods for the synthesis of P(III) molecules were explored: hydrophosphination chemistry, lithium phosphide chemistry and quaternisation chemistry. A variety of problems were encountered with these methods, and

this will be discussed in detail below (Section 2.2.1-2.2.4). Amide coupling chemistry was the final route considered for the synthesis of a phosphine glycoconjugate (Section 2.2.5). This led to the successful synthesis of a novel phosphine glycoconjugate, which was radiolabelled with ^{99m}Tc to form the first ^{99m}Tc-labelled phosphine glycoconjugate (to the best of our knowledge).

2.2.1. Glycosylation Chemistry

2.2.1.1 Lewis-acidic Glycosylation Reactions with Unprotected Phosphines

To address the structural concerns (Section 2.1.3) that were noted at the outset of this project, 2-(diphenylphosphino)ethan-1-ol was prepared, as reported by Sulzbach *et al.* (Scheme 2.3)[14].

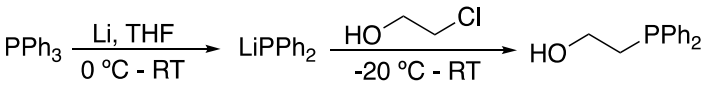

Scheme 2.3 Synthesis of (diphenylphosphino)ethan-1-ol, as published by Sulzbach *et al.*[14]

Attempts to conjugate this primary alcohol with acetobromo-α-D-glucose (Scheme 2.4) following the originally reported route by Beller *et al.* (Scheme 2.2) were unsuccessful. Only phosphino-starting material was recovered after 24 h. It is therefore likely that the initial productive step in this reaction is the deprotonation of the hydroxyl group. Whilst deprotonation of a phenolic species with sodium hydroxide is possible, the pK_a of a typical alcohol (~15 *versus* ~10 for phenols) is such that it cannot be significantly deprotonated by a 1M solution of this base. This therefore inhibited the anticipated glycosylation reaction.[15]

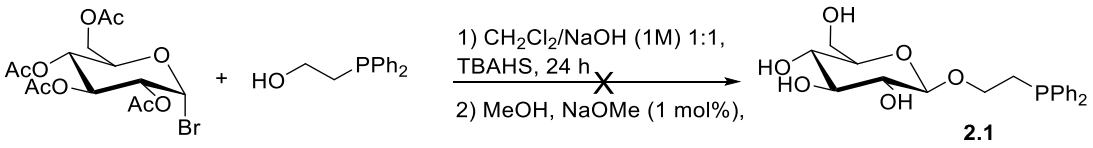

Scheme 2.4 Unsuccessful route to synthesise **2.1**.

As Beller's method proved unproductive for the coupling of alcohols (as opposed to phenols) with carbohydrates, Lewis acid promoted glycosylation reactions were investigated.

In literature reports, and in unpublished research carried out in the Galan group, $BF_3.OEt_2$ is routinely used for the coupling of alcohols with acetyl-protected carbohydrates.[16,17,18] It was therefore hypothesised that the reaction of 2-(diphenylphosphino)ethan-1-ol at -40 °C with peracetylated glucose in the presence of $BF_3.OEt_2$ would lead to the formation of **2.2** (Scheme 2.5(a)). Disappointingly, despite the successful analogous reaction between

peracetylated glucose and 2-bromoethan-1-ol, no reaction was detected when 2-(diphenylphosphino)ethan-1-ol was the acceptor; only starting materials were observed after stirring for a period of 48 h.

$BF_3.OEt_2$ was therefore replaced with a more reactive Lewis acid: freshly-distilled trimethylsilyl trifluoromethanesulfonate (TMSOTf) (Scheme 2.5(b)). This however, resulted in partial oxidation of 2-(diphenylphosphino)ethan-1-ol as shown by ^{31}P NMR spectroscopy, and ^{1}H NMR and MS analysis confirmed that no coupling reaction took place.

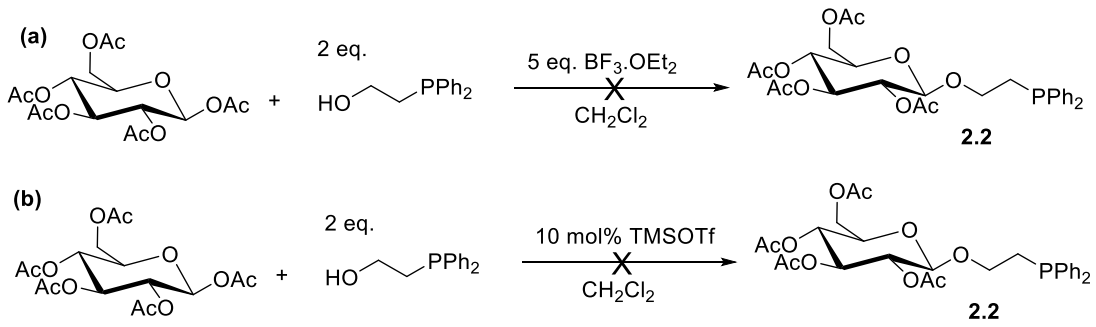

Scheme 2.5 Unproductive routes to **2.2** using Lewis acidic $BF_3.OEt_2$ and TMSOTf.

As trichloroacetimidate groups are much more efficient glycosyl donors than acetyl groups, this was next investigated. Incorporation of a trichloroacetimidate group will result in the anomeric position being more greatly activated and should lead to enhanced reactivity. The glycosyl trichloroacetimidate, **2.4**, can be prepared from peracetylated glucose by several routes, but there, just two were investigated: a literature one-pot method without isolation of **2.3** (31% yield)[19] and the equivalent two-step method, with isolation and purification of **2.3** (52% yield overall). The second of these routes was therefore favoured for the synthesis of **2.4** (Scheme 2.6).

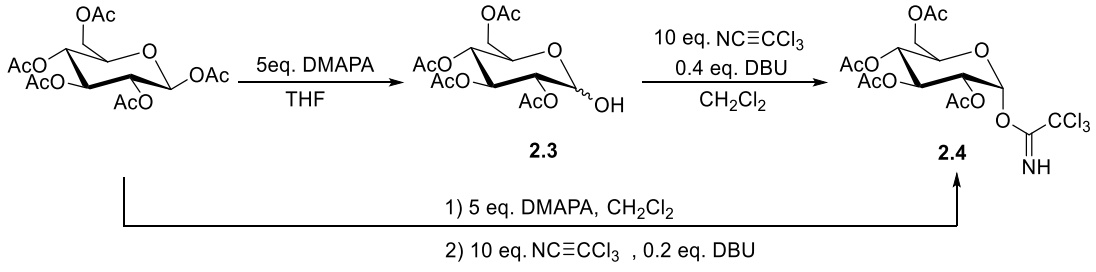

Scheme 2.6 Synthesis of 2,3,4,6-Tetra-O-acetyl-α-D-glucopyranosyl trichloroacetimidate, **2.4**.

Reacting 2-(diphenylphosphino)ethan-1-ol (δ_P -23.6 ppm) and **2.4** in the presence of TMSOTf (10 mol%) resulted in partial oxidation of 2-(diphenylphosphino)ethan-1-ol (δ_P

27.7 ppm). No evidence of coupling products was identified, but a second species was seen in the $^{31}P\{^{1}H\}$ NMR spectrum at 74.0 ppm, (Figure 2.4). This suggests that a chlorophosphine or aminophosphine species is being formed.[20,21] Repetition of this reaction in the absence of the carbohydrate resulted again in the oxidation of 2-(diphenylphosphino)ethan-1-ol upon addition of TMSOTf. As this Lewis acid was therefore found to be incompatible with the phosphine, borane protection of the P(III) species was investigated next.

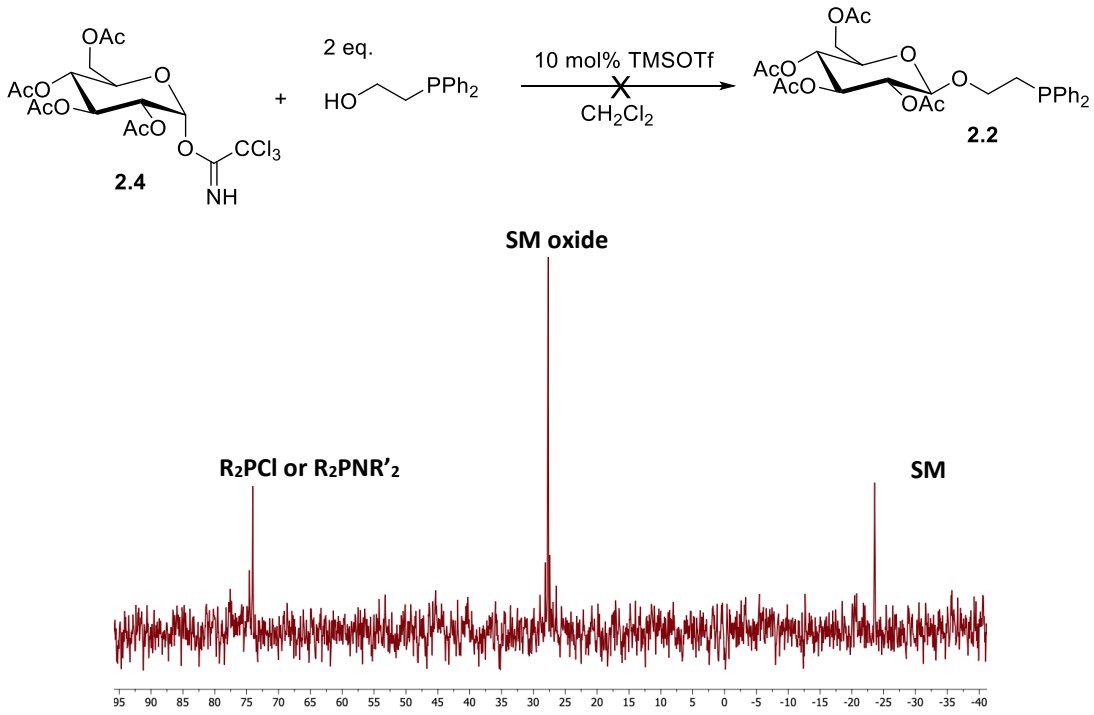

Figure 2.4 $^{31}P\{^{1}H\}$ NMR (121 MHz, $CDCl_3$) showing the product mixture formed by the above reaction of 2-(diphenylphosphino)ethan-1-ol, **2.4** and TMSOTf (10 mol%).

2.2.1.1. Lewis-acid Promoted Glycosylations with Borane-protected Phosphines

Radical catalysed hydrophosphination by diphenylphosphine ($HPPh_2$) of allyl alcohol, using azobisisobutyronitrile (AIBN) as the radical initiator, was used to synthesise 3-(diphenylphosphino)propan-1-ol, **2.5** (Scheme 2.7). Borane protection of **2.5** with $BH_3.SMe_2$ was employed to give **2.6** in an attempt to prevent oxidation of the phosphine during subsequent glycosylation reactions.

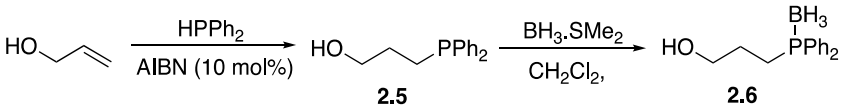

Scheme 2.7 Radical catalysed hydrophosphination and borane protection to give **2.6**.

Borane protected **2.6** was reacted with the glucopyranosyl trichloroacetimidate (**2.4**) and TMSOTf (10 mol%). After 16 h, primarily glucose tetraacetate and unreacted **2.6** were isolated following aqueous work-up under inert conditions. Evidence of the desired glycoconjugate product, **2.7**, could not be established by NMR spectrometry or HR-MS (Scheme 2.8).

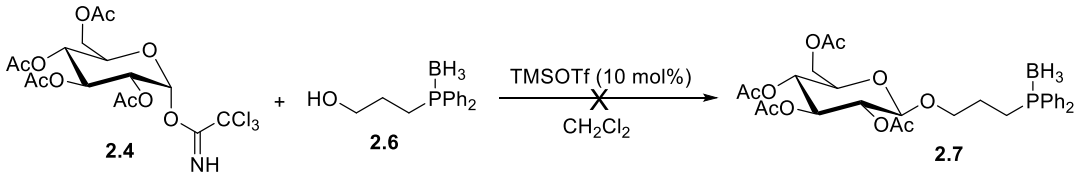

Scheme 2.8 Unproductive route to **2.7** using Lewis acidic TMSOTf.

O-Acetyl groups are 'disarming' groups and therefore poorly activating of the trichloroacetimidate leaving group. Carbohydrates **2.8** and **2.9** were therefore investigated as they contain 'arming' groups, so are consequently better glycosyl donors (Figure 2.5). By incorporating more electron-rich benzyl groups instead of acetyl groups, the reactivity of the glycosyl trichloroacetimidate group is increased. This should enable greater reactivity at the anomeric position and better stabilisation of intermediates in the reaction. The subsequent reactions of carbohydrates **2.8** and **2.9** with phosphine **2.6** followed the same procedure and reaction scale as before.

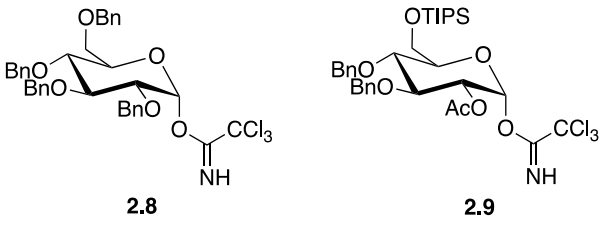

Figure 2.5 Structure of carbohydrates **2.8** and **2.9**.

Reacting **2.6** with **2.8** (Scheme 2.9) produced a mixture containing five different species, as identified by thin-layer chromatography (TLC). Gradient column chromatography (EtOAc:Hexane, 10:90 to 100:0) was employed to isolate each of these species, and $^{31}P\{^{1}H\}$ NMR spectroscopy then used to determine which of these contained phosphorus. Only two such species were identified; the first being unreacted **2.6** (δ_P 15.3 ppm), whilst the second

was confirmed by ^{1}H and ^{11}B NMR, and HR-MS, as the configurationally impure glycosylation product, **2.10** (Scheme 2.9). Unfortunately, just 4.5 mg of **2.10** was isolated, and as a result, subsequent deprotection of the benzyl groups, removal of the borane or separation of the two anomers was not attempted. As a yield of just 6% was recorded for this step, and several other side-products were also formed, this method was not considered as an appropriate route to form target phosphine glycoconjugates for medical applications.

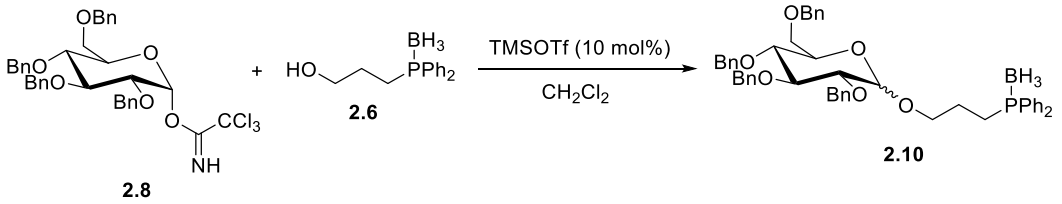

Scheme 2.9 Carbohydrate **2.10** formed as a mixture of anomers.

Compound **2.10** was formed as a 1.8:1 α:β mixture as neighbouring group participation was not possible due to the benzyl ether at the C-2 atom. Reaction of **2.9** with **2.6** was therefore investigated, as acetyl protection of the 2-hydroxyl group enables its anchimeric assistance (Scheme 2.10).[22] This should ensure that only a single anomer can be formed. Disappointingly, no evidence of formation of the desired phosphine glycoconjugate was observed. This has been attributed to less electron-rich groups occupying the C-2 and -6 positions of carbohydrate **2.9**, when compared with the perbenzylated **2.8**.

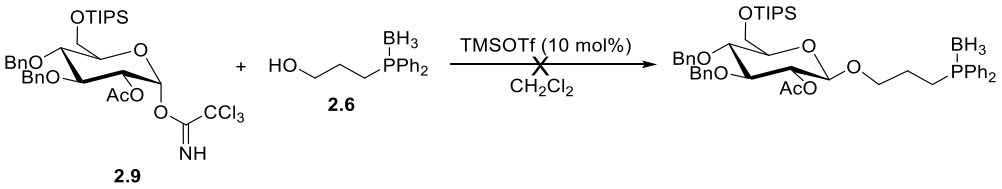

Scheme 2.10 Unproductive route from reacting **2.9** with **2.6** in the presence of TMSOTf.

N.B. **2.9** was provided R. Williams (Galan Group), and therefore TIPS protection of the C-6 hydroxy group is an artefact of his research.

2.2.1.2. Metal-Catalysed Glycosylations

Many traditional promotors for glycosylation reactions ($BF_3.OEt_2$, TMSOTf, *p*-TsOH, AgOTf *etc.*) are organic Lewis acids that typically require stochiometric quantities and low temperatures for the reaction to proceed.[23,24] Therefore, in recent years, much effort has focussed on the development of more efficient and milder glycosylation methodologies.[25–27] One such method has been the development of $AuCl_3$-promoted glycosylation using glycosyl trichloroacetimidates and alcohol-based acceptors.[28] These reactions typically occur

at room temperature and with <1 h reaction times, especially in the presence of phenylacetylene (Scheme 2.11).

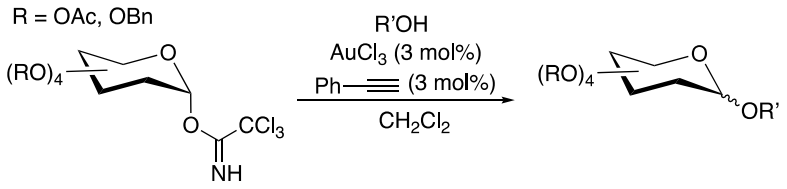

Scheme 2.11 Gold(III) trichrichloride promoted glycosylation reported by Vankar *et al.*[28]

The $AuCl_3$-phenylacetylene promoted glycosylation reaction has been reported for carbohydrates **2.4** (R=OAc) and **2.8** (R=OBn), but this method is non-stereoselective so an α:β mixture is formed when using **2.8** as the donor.[28] Therefore, this route was only investigated for the coupling of **2.4** with phosphine **2.5** to give the corresponding glycoconjugate product, **2.11** (Figure 2.6).

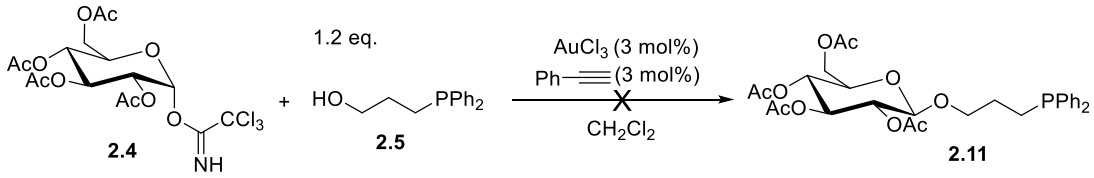

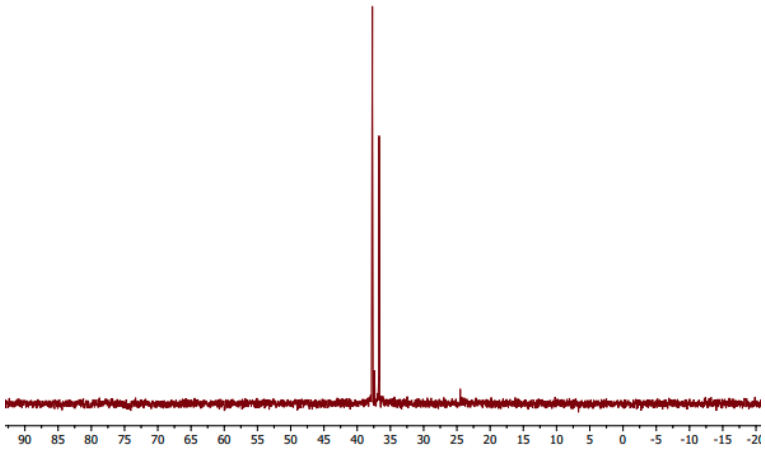

Figure 2.6 $^{31}P\{^{1}H\}$ NMR spectra (121 MHz, CD_3OD) showing a mixture of P(V) containing species, including oxidised **2.5** and **2.11**, as a consequence of the attempted reaction shown above.

After 30 min, the starting materials were fully consumed as confirmed by TLC analysis, and the reaction was quenched by addition of water. Two major singlets were observed in the 'oxide region' of the $^{31}P\{^{1}H\}$ NMR spectrum, at 37.7 and 36.7 ppm (Figure 2.6). HR-MS confirmed the mixture of species were likely to be oxidised **2.11** (*m/z* calcd. $C_{29}H_{36}O_{11}P$

([M+O]$^+$) = 591.1995; obs. = 591.2008) and oxidised **2.5** (*m/z* calcd. $C_{15}H_{18}O_2P$ ([M+O]$^+$) = 261.1004; obs. = 261.1053). Gold(III) compounds often have high oxidation potentials, and are therefore rapidly reduced.[29] This is likely to be at the expense of P(III) species in this reaction, which can undergo oxidation to a P(V) species. Consequently, this reaction was repeated with the borane protected phosphine, **2.6** (Scheme 2.12).

Reacting carbohydrate **2.4** with borane protected **2.6** under the same conditions as before, was expected to give glycoconjugate **2.7** (Scheme 2.12) as the product. Disappointingly, in this case only starting materials were recovered after 2 h, and hence the borane protecting group appears to inhibit the expected reactivity. Consequently, subsequent work did not employ classical glycosylation methods but instead focused on methods such a hydrophosphination, which are more commonly utilised in the synthesis of novel phosphine ligands.

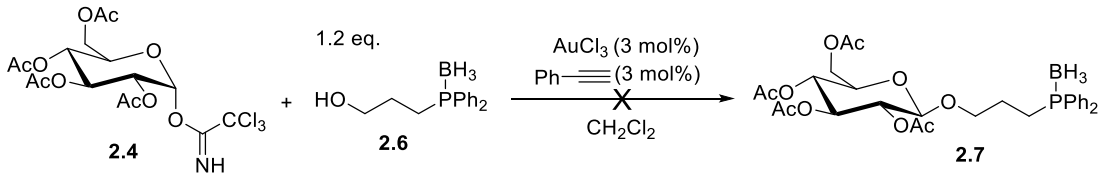

Scheme 2.12 Attempted synthesis of **2.7**.

2.2.2. Attempted Hydrophosphination Routes to Glycoconjugates

As traditional glycosylation methods were unsuccessful, hydrophosphination was investigated as a means of coupling secondary phosphines and carbohydrates. The development of hydrophosphination chemistry has been the focus of a number of projects within the Pringle group,[30,31] with a particular drive to understand the scope and mechanism by which Michael-accepting alkenes can react with phenyl- and diphenylphosphine when employing platinum(0) catalysis.

Hydrophosphination was also exploited by Heesche-Wagner and co-workers in the late 1990's, to prepare C-3 coupled phosphine glycoconjugates for a variety of carbohydrates: glucose (Scheme 2.13), fructose, mannose, and galactose.[32] Heesche-Wager *et al.* found that removal of the acetonide groups was problematic for all but the glucose-based glycoconjugate, and hence a decision was made to focus on benzyl protecting groups which appeared the most promising for the formation of phosphine glycoconjugates, based on our findings in Section 2.2.1. Key differences between this work, and that performed by Heesche-Wager *et al.* include the choice in protecting groups (benzyl *versus* acetonide) and position of allyl conjugation (C-1 *versus* C-3).

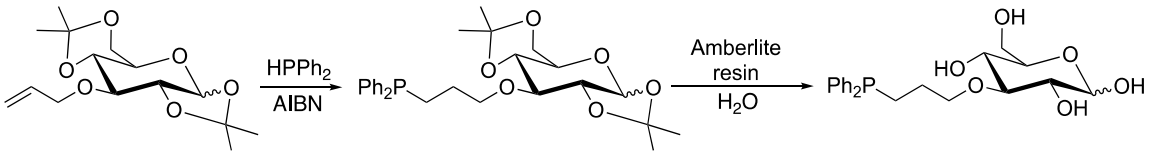

Scheme 2.13 Synthesis of a phosphine glycoconjugate reported by Heesche-Wagner *et al.*[32]

Carbohydrate **2.13** was synthesised in good yield (83%), by modifying a procedure previously reported in the literature. The method used $BF_3.OEt_2$ to promote the glycosylation of allyl alcohol with **2.12** (Scheme 2.14).

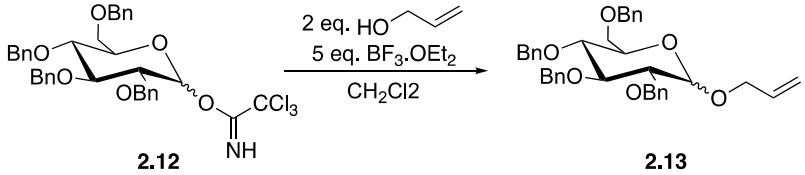

Scheme 2.14 Preparation of carbohydrate **2.13**.

A condition screen is reported for the coupling of $HPPh_2$ and **2.13** and the results are reported in Table 2.1, but no successful conditions were found.[17]

Table 2.1 Reaction conditions tested for the attempted hydrophosphination reaction of $HPPh_2$ and **2.13**.

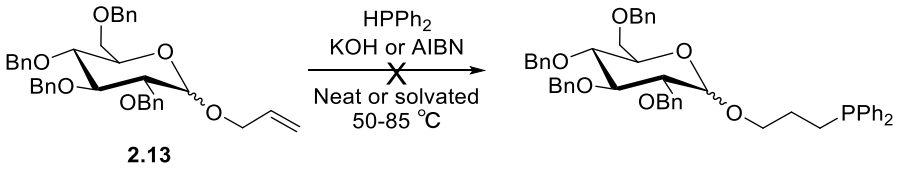

Entry	Method	Solvent	Temp/ ºC	Time/hr
1	AIBN (10 mol%)	None	70	18
2	AIBN (10 mol%)	Toluene	70	48
3	AIBN (10 mol%)	Hex:Tol (3:1)	70	18
4	AIBN (10 mol%)	MeCN	70	18
5	KOH	MeCN	50	24
6	KOH	MeCN	85	96

Radical catalysed reactions often proceed with fewer side products when no solvent was added (as was the case when synthesising phosphine **2.5**, Scheme 2.7, Section 2.2.1.2). However, using no solvent was impracticable in this case as the quantity of $HPPh_2$ was insufficient to dissolve solid **2.13**, even when performed in a crystallisation tube. Consequently, only starting material was observed after 18 h (Entry 1). This reaction was repeated using both polar (acetonitrile) and non-polar (hexane, toluene) solvents (Entries 2-4). Several species were seen in the P(V) regions by $^{31}P\{1H\}$ NMR spectroscopy in all cases, but no significant signals were observed in the P(III) region (-10- to -20 ppm), which would be characteristic of the expected products. Base-catalysed hydrophosphination was therefore tested at 50 °C, and at reflux (Entries 5 & 6), but neither of these conditions gave rise to expected products (Figure 2.7).

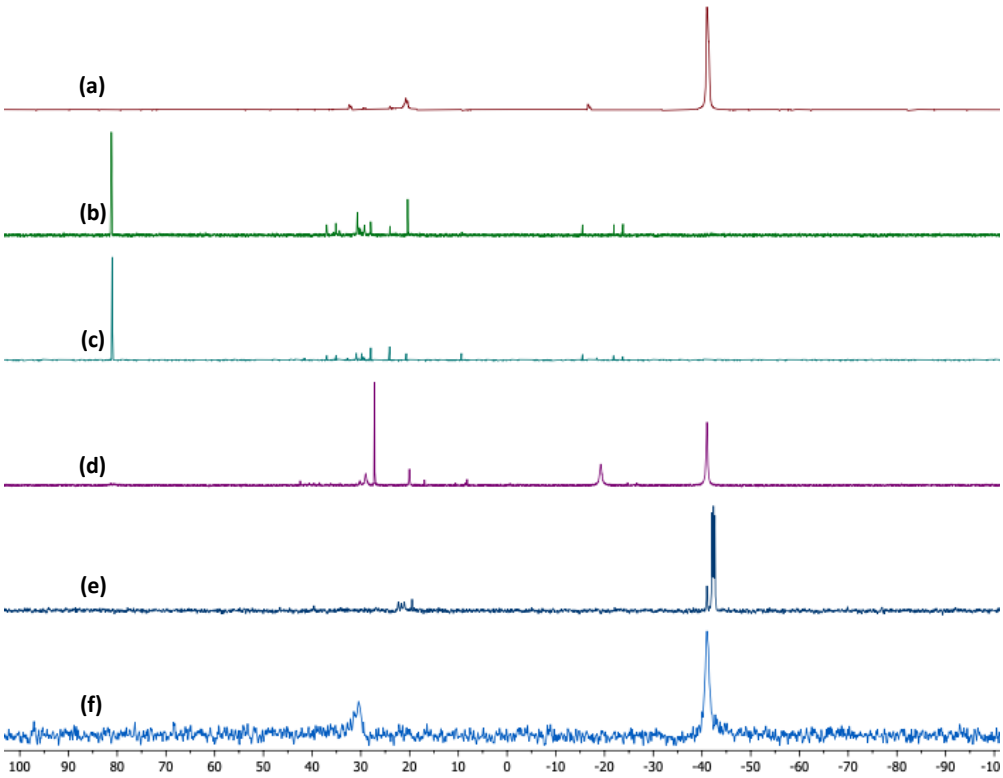

Figure 2.7 $^{31}P\{^{1}H\}$ NMR spectra (121 MHz, $CDCl_3$) of the product mixtures from (a) Entry 1, (b) Entry 2, (c) Entry 3, (d) Entry 4, (e) Entry 5 and (f) Entry 6.

Subsequent research from Heesche-Wagner *et al.* and within the Pringle Group (R. Nuttall, unpublished results) have revealed that there is a significant positional dependence regarding the hydrophosphination of phosphines with alkene-containing carbohydrates.[32,33] In particular, Nuttall has shown that hydrophosphination of diphenyl(2-diphosphinoethyl)phosphine proceeds under radical (AIBN) catalysed conditions for a tetra-benzyl-glucopyranoside with an allyl group at the C-6 position (Scheme 2.15). This is in

contrast to the lack of radical catalysed activity observed for **2.13** and $HPPh_2$, where the allyl group is incorporated at the C-1 position of a structurally-isomeric carbohydrate.

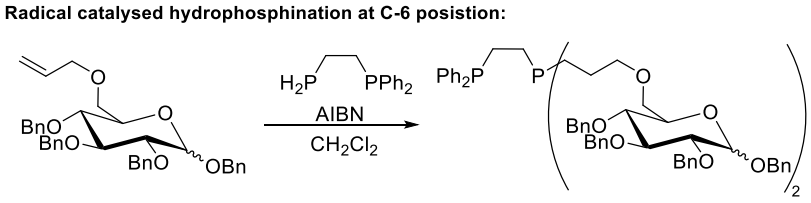

Scheme 2.15 Hydrophosphination to give phosphine glycoconjugates (Nuttall, unpublished results).

2.2.3. Attempted Phosphide Route to Glycoconjugates

Lithium phosphides are often reacted with haloalkyl or haloaryl species to prepare novel tertiary phosphines. This method was therefore explored using the bromoalkyl derivate **2.14** which was prepared using a modified literature procedure (Scheme 2.16).[34] Compound **2.14** was isolated in 91% yield as a mixture of anomers with an α:β ratio of 1.2:1.[17] Benzyl protecting groups were employed due to their stability towards a wide range of conditions, although α-lithiation of benzyl ethers can occur under certain conditions.[35] *n*-Butyllithium was reacted with $HPPh_2$ to form lithium diphenylphosphide, and **2.14** was then added to the phosphide.

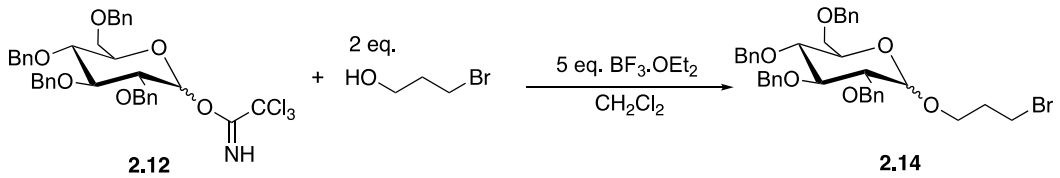

Scheme 2.16 Synthesis of carbohydrate **2.14**, in 91% yield with an α:β ratio of 1.2:1.

Using the conditions outlined in Figure 2.8, a singlet at -15.5 ppm was observed by *in situ* $^{31}P\{^{1}H\}$ NMR spectroscopy. Several resonances, corresponding to P(V) species, were observed between 36.4 and 23.1 ppm (Figure 2.8(a)). Analysis of the mixture by ^{1}H NMR spectroscopy and mass spectrometry were inconclusive. The ^{1}H NMR spectrum contained signals that supported the formation of the expected product, but other overlapping resonances in the alkyl region of this spectrum suggested that by-products have also formed. Masses corresponding to oxidised **2.15** (*m/z* calcd. $C_{49}H_{52}NO_7P$ ($[M+O+H]^+$) = 783.9; obs. = 783.4) and tetraphenyldiphosphine (Ph_2P-PPh_2, *m/z* calcd. $C_{24}H_{21}P_2$ ($[M+H]^+$) = 370.4; obs. 370.4) were detected by MS. These data were concerning given that the chemical shift for Ph_2P-PPh_2 measures -14.5 ppm (in $CDCl_3$), and is a common by-product of phosphino-

lithium exchange chemistry.[36] Attempts to purify this compound by crystallisation and column chromatography proved unsuccessful.

Addition of $[PtCl_2(COD)]$ to the crude product produced the $^{31}P\{^1H\}$ NMR spectrum in Figure 2.8(b), containing a singlet at 68.5 ppm with ^{195}Pt satellites ($J_{P\text{-}Pt}$ = 4035 Hz). This indicates that the desired compound **2.15** was formed during the lithium-exchange reaction.

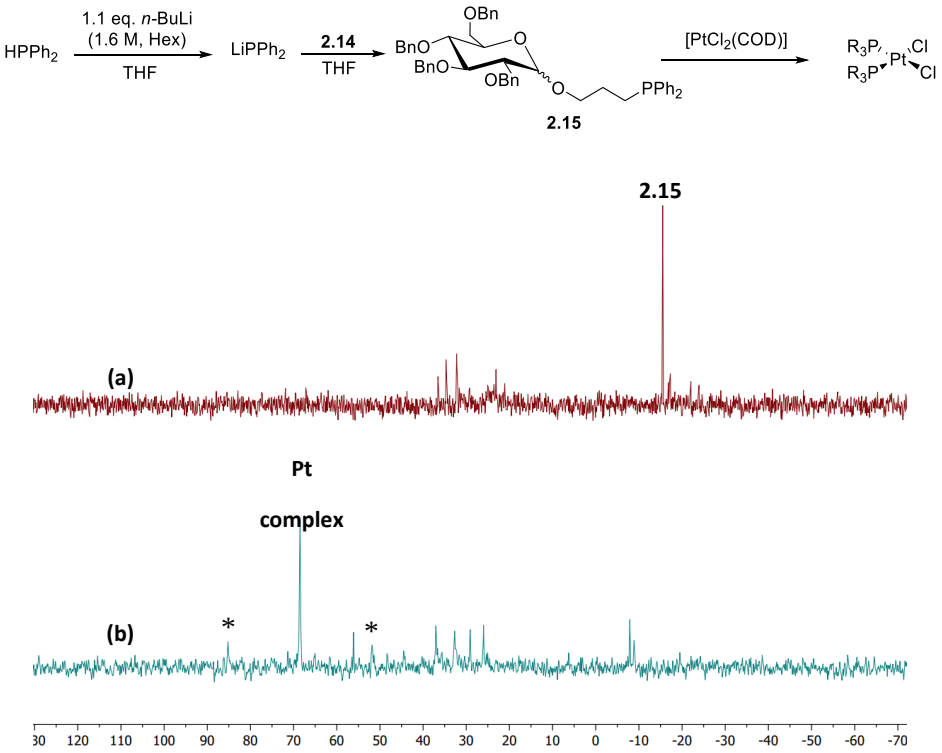

Figure 2.8 $^{31}P\{^1H\}$ NMR spectra (121 MHz, $CDCl_3$) of (a) the product mixture from reaction $LiPPh_2$ and **2.15,** which is shown schematically above the spectrum, and (b) after addition of $[PtCl_2(COD)]$. Asterix (*) mark the ^{195}Pt-^{31}P satellites.

In an attempt to form **2.15** with improved purity, a number of conditions were altered but to no avail (see Table 2.2). Running the reaction are greater dilution (Entry 2 *versus* 1) and changing the order of addition (Entry 3 *versus* 2) had no significant impact on the outcome of the reaction. Additionally, altering the work-up conditions (Entry 3 *versus* entries 4 and 5) led to further reduction in the purity of the final product and consequently, further work on this system was not continued.

Table 2.2 Reaction conditions tested for the attempted reaction of $LiPPh_2$ and **2.14**.

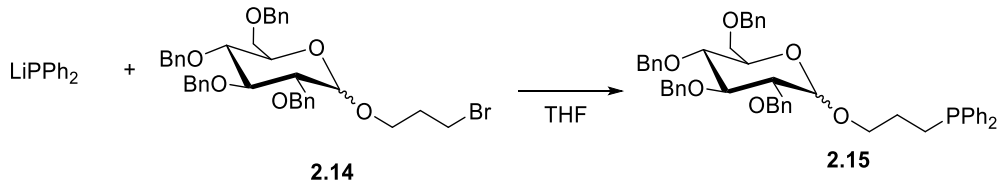

2.14 **2.15**

Entry	Eq. *n*BuLi	[2.14] in THF /M	Order of addition	Work Up Method
1	1.1	0.050	**2.14** to $LiPPh_2$	Aqueous
2	1.1	0.025	**2.14** to $LiPPh_2$	Aqueous
3	1.1	0.025	$LiPPh_2$ to **2.14**	Aqueous
4	1.0	0.025	**2.14** to $LiPPh_2$	Dissolved in CH_2Cl_2 and filtered
5	1.0	0.029	**2.14** to $LiPPh_2$	Dissolved in Tol and filtered

2.2.4. Attempted Quaternisation Route to Glycoconjugates

Quaternisation of phosphines can be used generate a phosphonium salt; if a secondary phosphine is used for this reaction, subsequent deprotonation will give a tertiary phosphine of the form of R_2PR'. This method was therefore investigated as an alternative route to access phosphine glycoconjugates. Phosphine quaternisation requires an electrophile with a good leaving group, such as a halide. Phosphine nucleophilicity is greatest for trialkylphosphines, and decreases with the number of aryl groups.[37] Initial studies therefore focused on the quaternisation of dicyclohexylphosphine ($HPCy_2$) with carbohydrate **2.16** (Scheme 2.17), which has a substituent with a potentially labile C-Br bond.

Carbohydrate **2.16** is structurally analogous to **2.15**, and was prepared using the same method. However, it utilises acetyl protecting groups so is formed solely as the β-anomer (Scheme 2.17). Acetyl groups should pose no issue in terms of stability during this procedure and notably, their removal is significantly more compatible with phosphines than the removal of benzyl ethers.

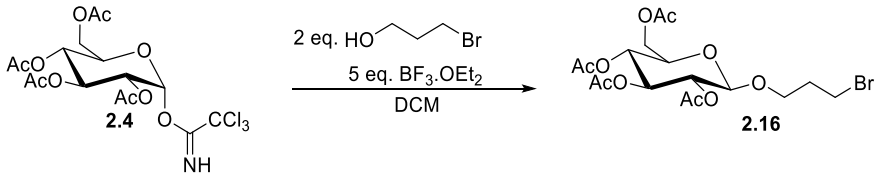

Scheme 2.17 Synthesis of carbohydrate **2.16** from the trichloroimidate **2.4**.

Quaternisation of $HPCy_2$ with **2.16** was therefore attempted by heating them together at 50 °C in acetonitrile or in acetone, but no conversion to **2.17** was observed by $^{31}P\{^{1}H\}$ NMR spectroscopy after 7 days; the major species observed by NMR spectroscopy was the dicyclohexylphosphine oxide (49.0 ppm) (Figure 2.9(a)).[38] Repeating this reaction in acetonitrile under reflux (90 °C, Figure 2.9(b)) afforded several products, including a major species at 23.2 ppm after heating for just 72 h. The proton-coupled ^{31}P NMR spectrum exhibits a doublet with $J_{P\text{-}H}$ = 421 Hz. This region is characteristic of a quaternised species, and the observed P-H coupling suggests that the proton is bound directly to the phosphorus atom, as would be expected in **2.17**.

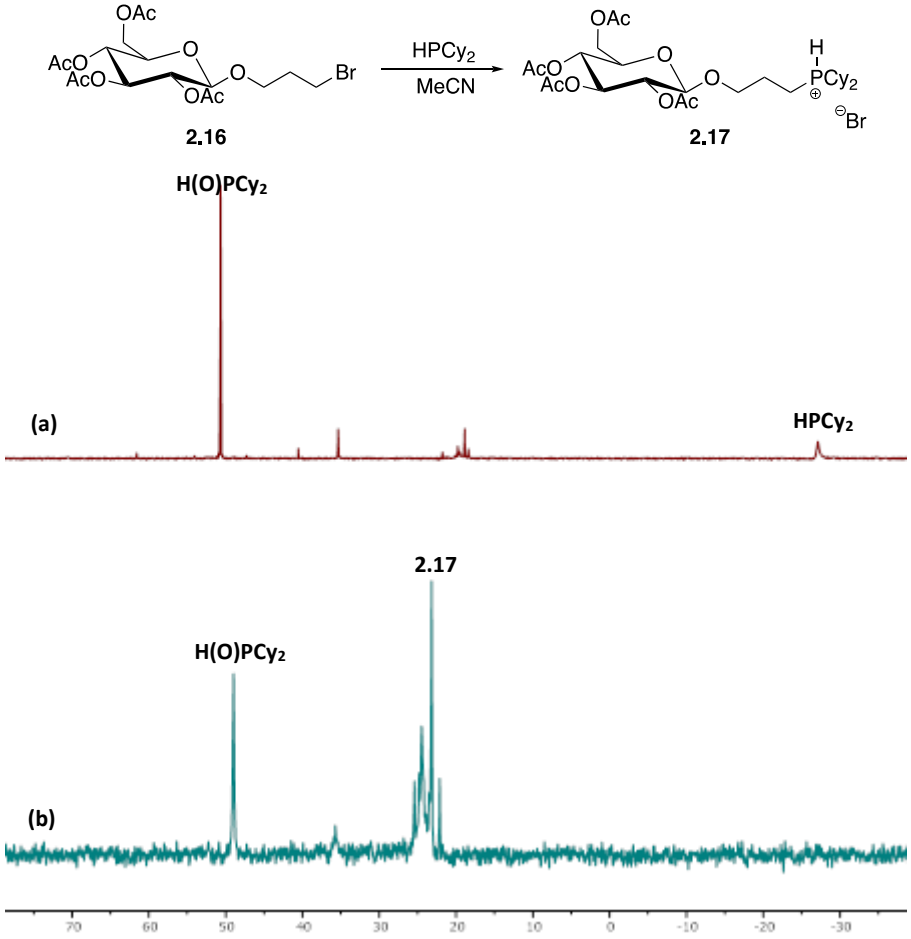

Figure 2.9 Figure showing the general conditions for the quaternisation reaction in MeCN and the $^{31}P\{^{1}H\}$ NMR spectra (121 MHz, $CDCl_3$) of this reaction at (a) 50 °C and (b) 90 °C.

For **2.17** to be a suitable phosphine glycoconjugate for radiolabelling it must be capable of loss of a proton and coordinating to rhenium. Rhenium coordination can be used as measure of the ligand's ability to be radiolabelled with ^{99m}Tc and will be discussed in more detail in Section 2.3.

In the literature, deprotonation of a dicyclohexylphosphonium salt was achieved by reaction with potassium bis(trimethylsilyl)amide (KHMDS) (Scheme 2.18).[39] These conditions were applied to our system, but despite addition of KHMDS at both -78 °C and at room temperature, deprotonation of **2.17** did not appear to occur. Increased $HPCy_2$ (-27.4 ppm) and a number of other species, were formed instead (Figure 2.10(b)).[10,24] Using a weaker base (Et_3N) also did not lead to the deprotonation of **2.17**.

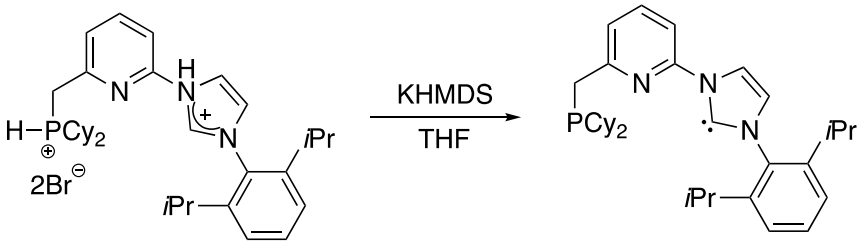

Scheme 2.18 Literature deprotonation of phosphonium species to give a P(III) ligand.

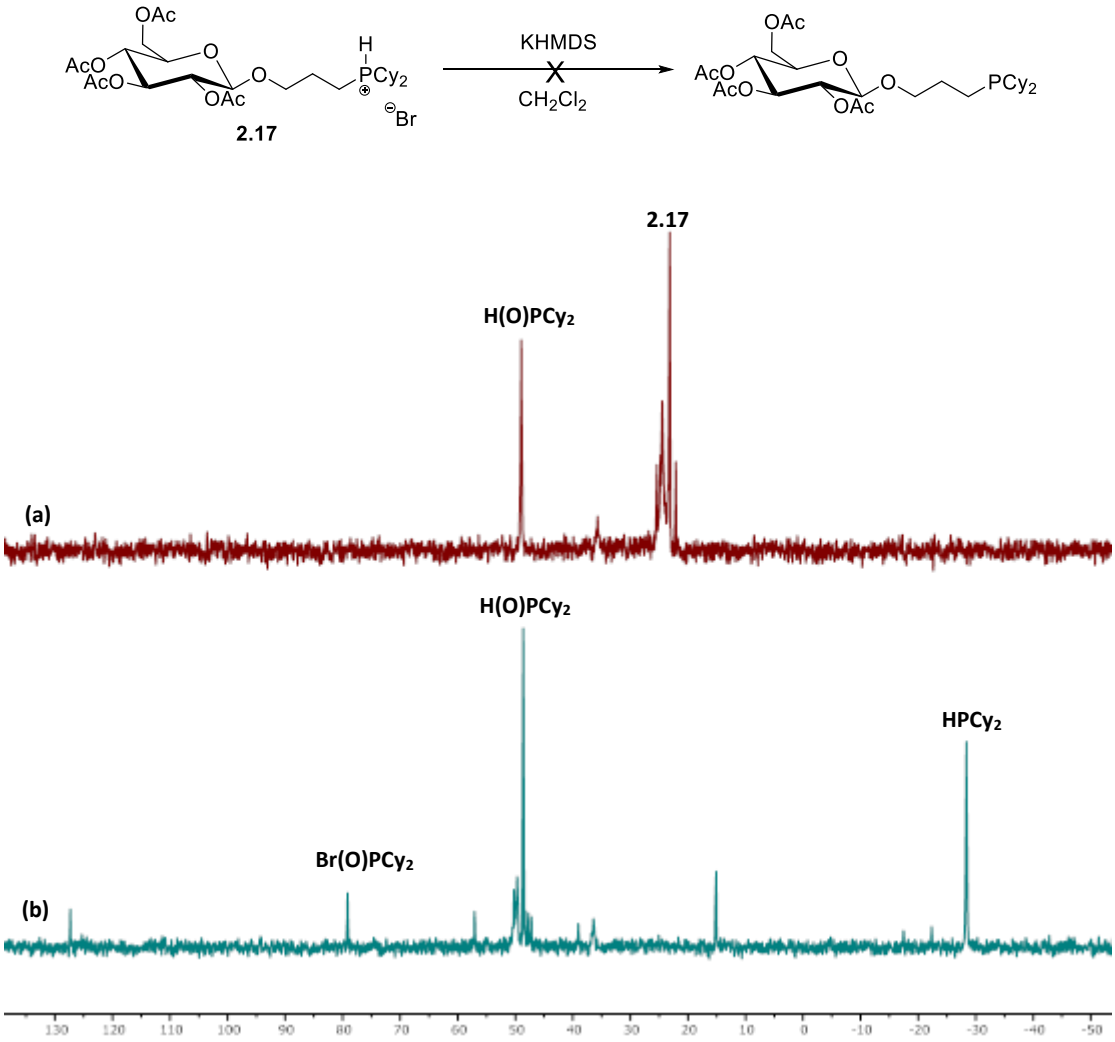

Figure 2.10 Scheme showing the unsuccessful deprotonation of **2.17** and the $^{31}P\{^{1}H\}$ NMR spectra (121 MHz, $CDCl_3$) of this reaction at (a) before and (b) after treatment with KHMDS.

It was hypothesised that although $HPPh_2$ is a less nucleophilic phosphine, which may inhibit quaternisation, the salt would be less acidic and so deprotonation should be facile. Disappointingly, quaternisation of $HPPh_2$ with **2.16** did not transpire despite heating the mixture under reflux for two weeks.

2.2.5. Amide Coupling as a Route to Glycoconjugates

2.2.5.1. Synthesis of ligand and precursors

An approach involving amide coupling chemistry, was investigated as a route to alkyl linked monophosphine glycoconjugates. As discussed in Chapter 1, the bifunctional chelation approach often utilises amide coupling chemistry to form a bioconjugate.[12] Here, this method inspired the synthesis of compound **2.21** (Figure 2.11). The monophosphine glycoconjugate was synthesised in several steps; by synthesising an amino-functionalised

carbohydrate and a carboxylic acid-containing phosphine before conjugating them *via* formation of an amide bond.

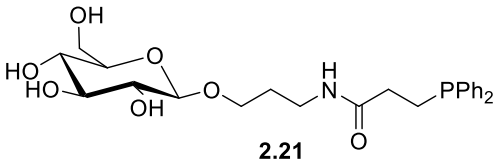

2.21

Figure 2.11 Structure of phosphine glycoconjugate **2.21**.

Carbohydrate **2.18** was designed to have a 3-carbon linker, with a terminal amine and was synthesised in six steps from D-glucose, as shown in Scheme 2.19. Whilst the synthesis of **2.18** has been previously reported in the literature, full characterisation of this compound has not been published, and this carbohydrate is typically used without purification.[17,40,41]

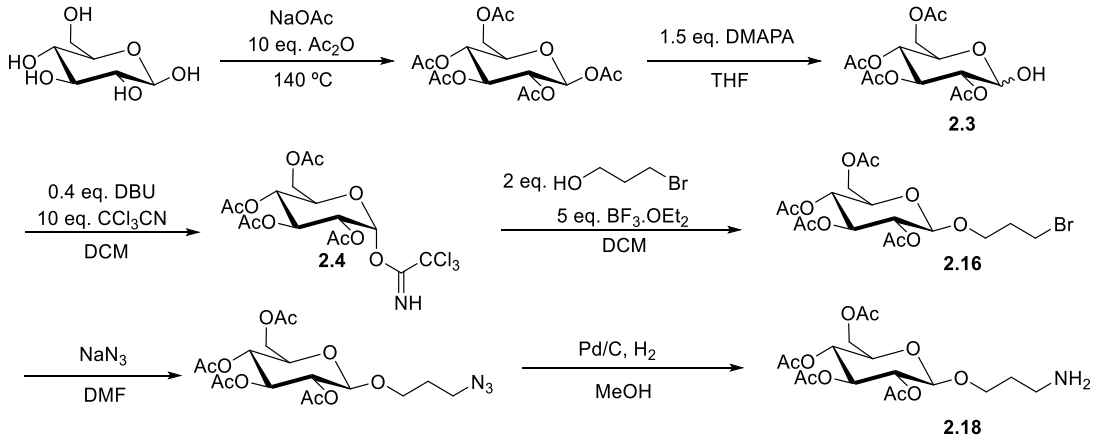

Scheme 2.19 Synthesis of **2.18** in 6 steps from D-glucose.

A carboxylic acid functionalised phosphine, **2.19**, was prepared using hydrophosphination chemistry, previously developed in the group by Dr A. Chadwick, and base catalysed ester hydrolysis previously reported by Myers *et al.* (Scheme 2.20).[42,43]

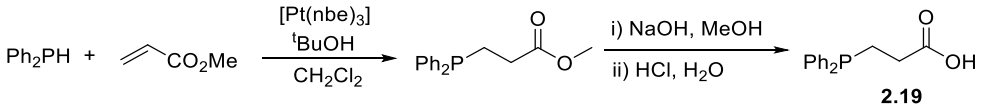

Scheme 2.20 Synthesis of carboxylic acid functionalised phosphine **2.19**.[42,43]

A variety of amide coupling conditions were initially tested (Table 2.3). Use of EDC-HCl as the carbodiimide, and DMAP as the base, proved the most successful method. The conjugated product, **2.20**, was purified by column chromatography. To our surprise this could be performed in air without oxidation.

Table 2.3 Reaction conditions tested for the amide coupling of **2.18** and **2.19**.

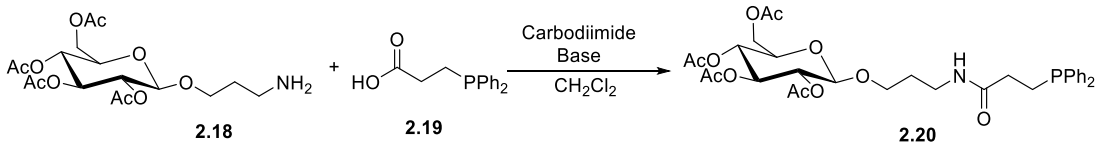

Entry	Carbodiimide	Base	Analysis of Crude
1	EDC-HCl	DMAP	63% pure by 31P
2	HATU	DIPEA	42% pure by 31P
3	EDC-HCl	HOBt	41% pure by 31P

Acetyl deprotection of **2.20** in MeOH gave compound **2.21**, but deprotection was found to be significantly slower (24 h) than typically reported for acetyl protected carbohydrates (30 min). Pleasingly, no hydrolysis of the amide bond was observed under the acetyl deprotection conditions (Scheme 2.21). Production of **2.21** was confirmed by HR-MS (*m/z* calcd. $C_{24}H_{32}NO_7PNa$ ($[M+Na]^+$) = 500.1814; obs. = 500.1825) and ^{13}C NMR where the amide carbonyl resonance was observed at 173.7 ppm. Despite an overall yield of just 1.5% for the 10-step synthesis of **2.21**, this ligand can be prepared on a 50 mg scale, which is sufficient radiolabelling applications. For full characterisation of **2.20** and **2.21**, see Chapter 6.

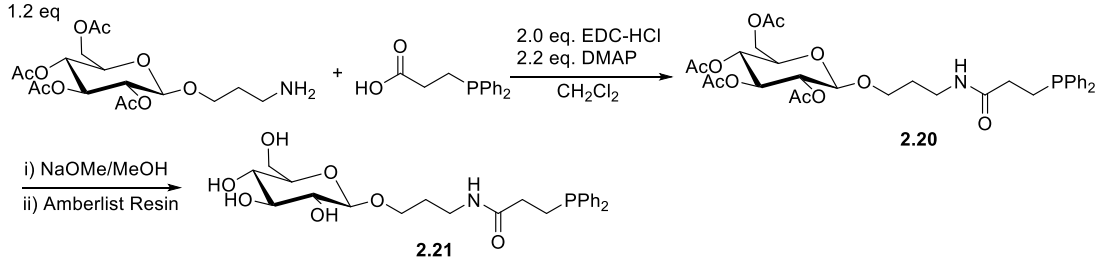

Scheme 2.21 Penultimate and final steps for the synthesis of monophosphine glycoconjugate **2.21** (of 10 steps overall from starting materials D-glucose & methyl acrylate).

2.3. Rhenium Coordination Chemistry

Rhenium and technetium are considered to be a 'matched pair' in the radiopharmaceutical sector.[44] This is due to Re and Tc being valence isoelectronic, and because complexes for a given oxidation state are often isostructural. Advantageously, rhenium also possesses a non-

radioactive isotope unlike its lighter congener technetium; so rhenium is often used as a model for ^{99m}Tc radiolabelling.

Chemically, differences in the rate of substitution and redox chemistry exist between the two elements, with Tc favouring lower oxidation states and faster ligand substitution, when compared with Re.[45] However, given the limited difference in physical characteristics between Re and Tc compounds, biological systems often cannot distinguish between them. This has enabled us to use rhenium as a model to understand the ^{99m}Tc coordination chemistry of any phosphine glycoconjugates at the University of Bristol, prior to radiolabelling these compounds at St Thomas's Hospital in a radiochemistry laboratory. For the purposes of this project, rhenium will only be considered a model for ^{99m}Tc radiolabelling, and not used to develop ^{188}Re radiolabelling; however, this would be of interest in the future (Section 2.6).

Within this project, two alternative cores will be considered for radiolabelling purposes: (1) a ^{99m}Tc(I) tricarbonyl core and (2) a ^{99m}Tc(V) dioxo core. The tricarbonyl core often exhibits greater stability under biological conditions so will be the core of choice initially. In cases where this proves not to be suitable, the dioxo core will also be investigated. Both of these Tc cores have Re analogues.

To investigate whether **2.20** and **2.21** were promising ligands for radiolabelling, the Re coordination chemistry of these molecules were probed.

2.3.1. Rhenium(I) Coordination Chemistry of 2.20

The coordination chemistry of peracetylated **2.20** was initially investigated due its ease of handling and characterisation when compared with **2.21**. 2 equivalents of **2.20** in CH_2Cl_2 were added to $[Re(CO)_3(H_2O)_3]Br$ in methanol. After 30 min, a new species was observed by $^{31}P\{^1H\}$ NMR spectroscopy with a chemical shift of 7.1 ppm; a coordination shift of $\Delta\delta$ = 22 ppm compared with free ligand **2.20**. This complex has been attributed to the expected complex **2.22** (Figure 2.12). Over time, the intensity of this signal decreased and formation of a second species with a chemical shift of -10.2 ppm was observed. This second signal in the $^{31}P\{^1H\}$ NMR spectrum has since been identified as complex **2.23** (Figure 2.12) which is formed by cleavage of the amide bond.

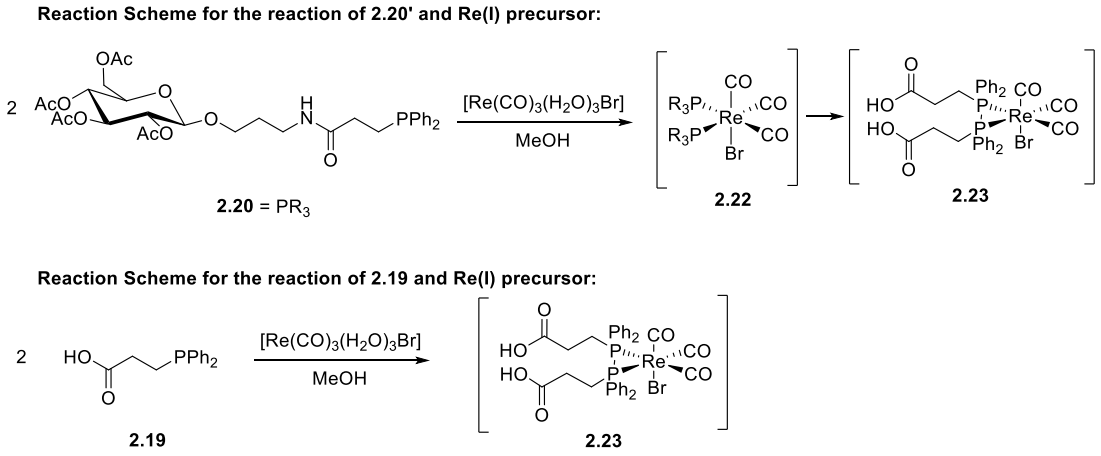

Figure 2.12 This figure includes the reaction schemes for the reaction of ligand **2.20** with the Re(I) precursor, and reaction of carboxylic acid phosphine **2.19** with Re(I) precursor. Below these schemes are the associated $^{31}P\{^{1}H\}$ NMR spectra (121 MHz, CD_3OD) which show the outcome of the reactions between ligand **2.20** and $[Re(CO)_3(H_2O)_3]Br$ after (a) 1 h and (b) 16 h, and (c) **2.19** and $[Re(CO)_3(H_2O)_3]Br$ at 1 h.

^{1}H NMR spectroscopy showed, amongst other changes, loss of the amide proton at 5.93 ppm in complex **2.22**, and formation of new signal at 1.63 ppm after 16 hours. This new signal appears in the range associated with amine protons and suggests that the amide bond is cleaved when **2.20** is bound to Re(I). Hydrolysis of the amide bond in **2.22** could be promoted by aqua ligands either on the Re centre, or in solution. Both mechanisms have been reported for Co-, Cu- and Ni-aqua complexes, although accounts of this occurring on Re are so-far unreported.[46] Based on the literature mechanisms for Co-, Cu- and Ni-aqua

complexes, and the likelihood that an intramolecular pathway would be favoured the following hypothetical mechanism for formation of **2.23** has been proposed in Figure 2.13.

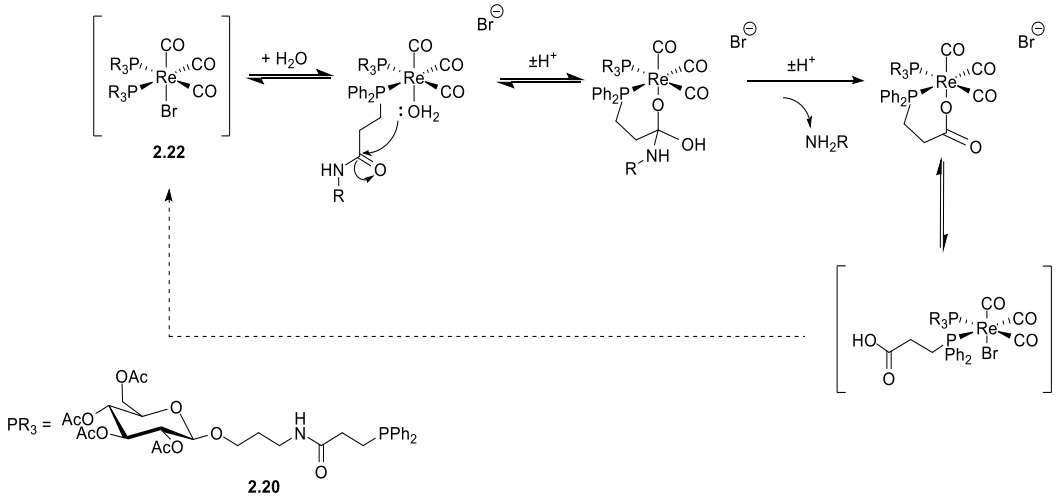

Figure 2.13 Hypothetical mechanism for the hydrolysis of **2.22** to **2.23**. This process must occur twice to hydrolyse both ligands when PR_3 = **2.20**. This proposed mechanism is based on a similar cycle that occurs on a Co-di(aqua) complex.[46]

MS analysis of **2.22** was carried out by repeating the reaction, and isolating **2.22** as a solid after 30 min; the $[M+2H]^+$ species was stored at -20 °C prior to identification (*m/z* calcd. $C_{67}H_{82}N_2O_{25}P_2ReBr$ ($[M+2H]^+$) = 1643.3; obs. = 1643.3). Further NMR analysis to fully characterise **2.22** was not possible as decomposition to **2.23** occurs in solution.

The amide hydrolysis was further evidenced, by reacting two equivalents of 3-(diphenylphosphino)propanoic acid, **2.19**, with $[Re(CO)_3(H_2O)_3]Br$, to give **2.23** (Figure 2.12) evidenced by a singlet at -10.4 ppm in the ^{31}P NMR spectrum. Crystals suitable for X-ray diffraction were grown in MeOH by slow evaporation of the solvent (Figure 2.14). When crystalline, the coordinated phosphine ligand is the methyl ester of **2.23** showing that esterification had taken place in MeOH.

The crystal structure confirms that the two phosphorus ligands are coordinated in a *cis* fashion, with a bond angle of 96.14(2)° for P1-Re-P2 in the solid state. The bromide counter ion has displaced an aqua ligand at an axial site, resulting in the bromide ligand being *cis* to the phosphine ligands and *trans* to one of the CO ligands. The angle, C34-Re-Br, measures 178.67(9)° so is close to a perfect 180° angle. The Re-C bond for the carbonyl that is *trans* to the bromide (Re-C34, 1.913(4) Å) is marginally shorter than the Re-C bonds of the CO ligands *cis* to the bromide ligand (Re-C35, 1.954(3) and Re-C33, 1.940(2) Å). This difference is minor and can be simply be attributed to the trans influence.

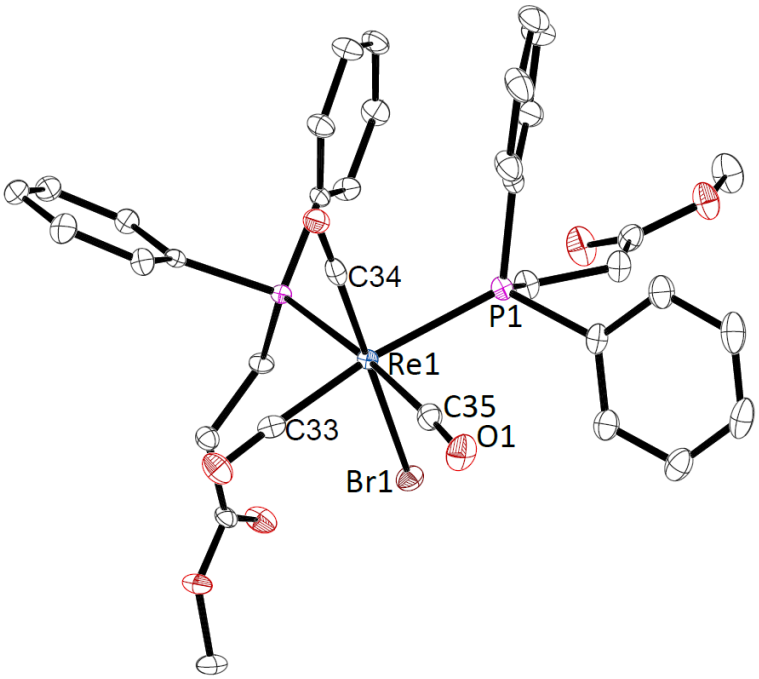

Figure 2.14 Crystal structure of **2.23**: Re-Br 2.6399(5) Å, Re-P1 2.4857(8) Å, Re-P2 2.4955(6) Å, Re-C35 1.954(3), Re-C34 1.913(4), Re-C33 1.940(2) Å, P1-Re-P2 96.14(2)°, C34-Re-Br 178.67(9)°.

2.3.2. Rhenium(V) Coordination Chemistry of 2.20 and 2.21

Coordination of **2.20** to a dioxo-Re(V) core ($[ReO_2]^+$) was investigated, using commercially available $[ReO_2I(PPh_3)_2]$ as an alternative to the previously studied Re(I) core ($[Re(CO)_3]^+$). This Re(V) core is used as a model for the dioxo-Tc(V) ($[TcO_2]^+$) core, which has shown to be successful in a number of imaging agents, including *Myoview*.

$[ReO_2I(PPh_3)_2]$ and two equivalents of **2.20** were reacted to form complex **2.24** (Scheme 2.21). The $^{31}P\{^1H\}$ NMR spectrum shows a singlet a -0.3 ppm and a coordination shift of $\Delta\delta$ 14.6 ppm, with a second signal for the displaced PPh_3 found at -6.1 ppm. Repeated washing of this complex with ice-cold ether removed the majority of the PPh_3 and pleasingly, **2.24** was found to be stable in H_2O over a period of at least 3 days. As no cleavage of the amide bond was observed once the ligand complexed to Re(V), the next was to investigate the coordination of **2.21**, the deprotected phosphine glycoconjugate ligand, with $[ReO_2I(PPh_3)_2]$.

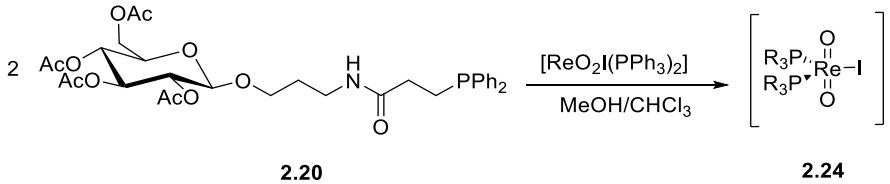

2.20 **2.24**

Scheme 2.21 Synthesis of the Re(V) complex **2.24**.

Attempts to form the Re(V) complex of **2.21** were carried out in a similar fashion; however, the ^{31}P NMR spectrum showed only two signals - PPh_3 and $O{=}PPh_3$ (TPPO) (Figure 2.15(b)) - both *in situ* and after isolation. No other signals were observed, and HR-MS was inconclusive regarding the identity of any other species formed. To confirm that the oxide was TPPO and not oxide of **2.21**, TPPO (10 mg) was added to this sample. This resulted in displacement of **2.21**, as TPPO is capable of acting as a ligand for Re(V) centres.[47] This was observed by new signals appearing in the $^{31}P\{^1H\}$ NMR spectrum, which correspond to **2.21** (-15.3 ppm) and to its oxide (37.0 ppm) (Figure 2.15(c)). One explanation for this observation is that the signal for complex **2.24** is broadened to the extent that is cannot be observed by $^{31}P\{^1H\}$ NMR spectroscopy. Low temperature NMR spectroscopy could be used to provided further insight on this. Additionally, whilst the route by which oxidation of PPh_3 and **2.21** occurs is unknown, it is plausible that an oxygen atom could be abstracted from the Re(V)-dioxo complex by the P(III) ligands.[48]

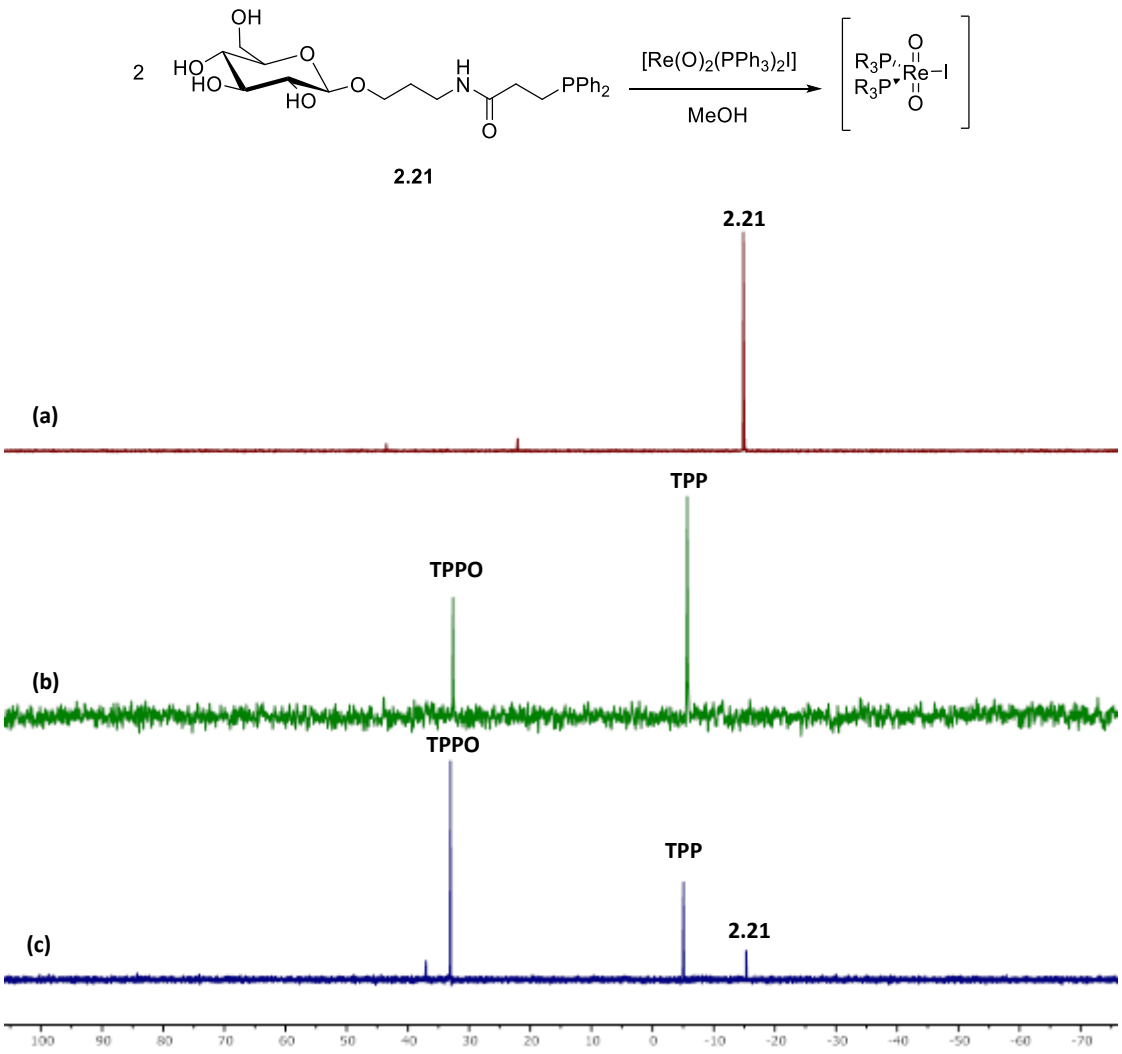

Figure 2.15 Scheme showing the attempted coordination reaction of **2.21** and Re(V) precursor and the $^{31}P\{^1H\}$ NMR spectra (162 MHz, CD_3OD) showing (a) uncoordinated

ligand **2.21** and (b) the mixture which forms from reaction of **2.21** and $[Re(CO)_3(H_2O)_3]Br$ and (c) this mixture after addition of TPPO.

2.4. Radiolabelling & Stability Study

The results of the Re coordination chemistry influenced the choice in Tc core (Tc(I) *versus* Tc(V)) when performing radiolabelling studies. Due to the poor stability observed for the peracetylated glycoconjugate, **2.20**, when coordinated to Re(I), radiolabelling with Tc(V) only was investigated. It should be noted that the radiolabelling of **2.21** only was considered, despite the peracetylated analogue, **2.20**, producing a better result upon coordination with the Re(V) core. This is because radiolabelling must be performed at least partially in water ($[TcO_4]^-$ is supplied in saline) and **2.21** showed significantly better solubility than **2.20**.

Typically, the preparation of Tc(V) radiopharmaceuticals with dioxo-cores are often favoured within hospitals as they are prepared in a single step; those with a Tc(I) tricarbonyl core require a two-step preparation. Tc(V) radiopharmaceuticals are typically prepared from a kit containing the ligand, a reducing agent (stannous chloride), a buffer (sodium hydrogen carbonate) and weak chelator for stabilisation of intermediates (sodium tartrate). These kits are freeze-dried so they can be stored in hospitals for a period of months, before a clinician adds the pertechnetate ($[TcO_4]^-$) and administers the radiopharmaceutical to a patient. In this project, the Tc(V) kits have been based on those used for *Myoview*, but the diphosphine tetrofosmin has been replaced with monophosphine **2.21**. (Table 2.4). All radiolabelling and stability studies were performed in duplicate, or triplicate, with full details given in the Chapter 6.

Table 2.4 Kit preparation for radiolabelling of monophosphine ligand **2.21**, shown in **Scheme 2.22**.

Kit	Ligand (μmol)	$SnCl_2.2H_2O$ (μmol)	Sodium tartrate dihydrate (μmol)	$NaHCO_3$ (μmol)
1	1.05	0.52	0.52	0.42
2	1.05	0.26	0.52	0.42
3	1.05	0.26	0.26	0.42
4	2.10	1.04	1.04	0.8

It was anticipated that addition of $[TcO_4]^-$ to kits containing **2.21** would form a complex with either two (**2.25**) or four (**2.26**) ligands bound to the Tc centre (Scheme 2.22).

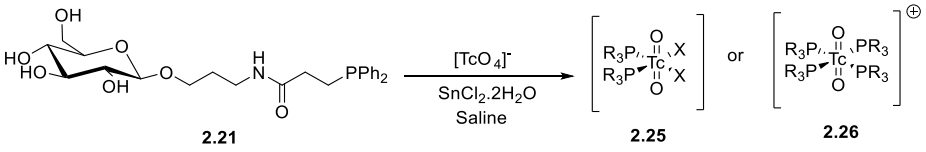

Scheme 2.22 Radiolabelling of monophosphine glycoconjugate **2.21**, with both possible products shown (**2.25** and **2.26**). 'X' is assumed to be a chloride or aqua ligand.

Kit 1 (Table 2.4) that contained 0.5 equivalents of both the reductant ($SnCl_2.2H_2O$) and weak chelator (Na_2tatrate.$2H_2O$), with respect to **2.21**, was found to give the best results after heating with $[TcO_4]^-$ in saline for 30 min at 50 ºC. The radio-HPLC chromatogram for this kit shows a single major peak with a retention time of 11.5 min (Figure 2.16). This peak shows a shoulder suggesting small quantities of another species may also be formed. Although a small amount of $[TcO_4]^-$ is still observed (retention time 2 min by HPLC), this is very minor when compared to the product peak showing that 2.21 can effectively be radiolabelled using a Tc(V) kit.

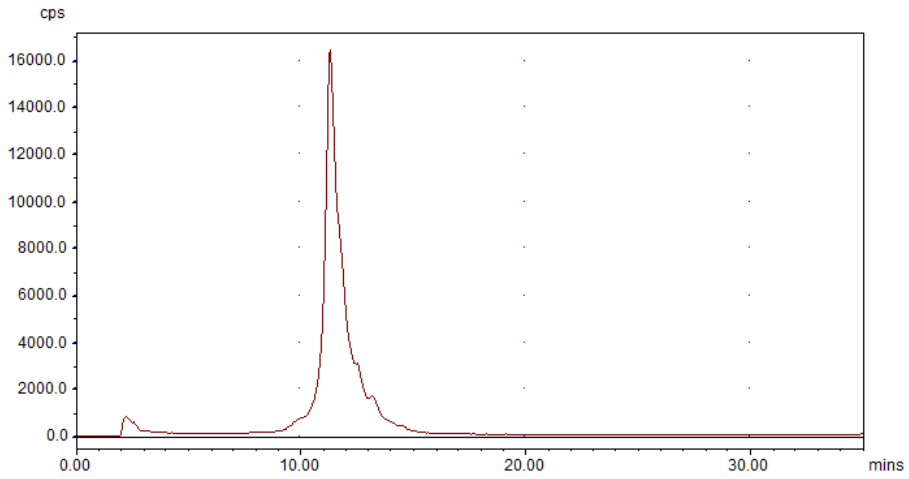

Figure 2.16 HPLC chromatogram of the radiolabelling of Kit 1 with $[^{99m}TcO_4]^-$.

Very similar radio-HPLC traces were observed for Kits 2 and 3. However, decreasing the amount of stannous chloride resulted in unligated $[TcO_4]^-$ (Kit 2), and decreasing the amount of tartrate in the kit resulted in an increase in the tailing of the major peak, which suggested that more unwanted species were being formed (Kit 3).

This work was repeated with Kit 4 (twice the scale of Kit 1), but spiked with ^{99}Tc ($t_{1/2}$ = $2x10^5$ y) as well as ^{99m}Tc($t_{1/2}$ = 6 h), so MS analysis could be employed to determine the identity of the Tc(V) complex. The MS data indicated formation of complex **2.25** (Scheme 2.22), with two ligands coordinated to the dioxo-Tc core rather than four (ESI+ calc. for $C_{48}H_{62}N_2O_{16}$TcNa.2HCOOH ($[M+2HCOOH+Na]^+$ = 1200.01; obs. = 1200.26). The identity

of the other two ligands (denoted 'X' in Scheme 2.22) on the centre were not elucidated by ESI, although mass spectrometry suggests the coordination of formic acid in these sites. This is likely to originate from the LC-MS mobile phase, which contained 0.1% formic acid. It is therefore likely that these ligands were aqua or chloride ligands prior to analysis, due to the media used during radiolabelling.

Unfortunately, **2.25** was found to exhibit very poor stability when incubated with mouse serum at 37.5 ºC. After just 1 h, a significant reduction in the peak corresponding to **2.25** (11.5 min) was noted, and a new peak with a retention time of approx. 5 min was observed instead. After 2 h, the species at 11.5 min could no longer be seen (Figure 2.17) in the HPLC trace. Based on the change in retention time, and the structure of **2.25**, it is probable that a protein in the mouse serum binds more favourably to the [TcO_2] core than our ligand. This effect has been previously reported in the literature.[12] As a consequence of this disappointing result, toxicity testing and *in vivo* imaging studies were not performed. MS analysis confirmed that the compound at 5 min does not correspond to the complex that would have been formed from amide bond hydrolysis of **2.25**. Further identification of this new species has not been carried out.

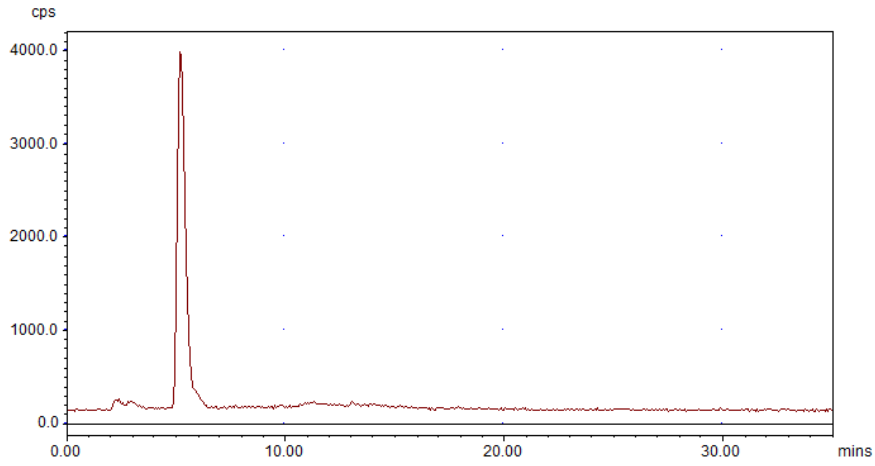

Figure 2.17 HPLC chromatogram from the stability study of **2.25** incubated in serum (37.5 °C, 2 hrs).

2.5. Conclusions

Several unproductive routes for the formation of phosphine glycoconjugates with an alkyl linker have been described which illustrates some of the challenges that are faced in conjugating phosphines with carbohydrates. The routes attempted include Lewis acid catalysed glycosylation chemistry, hydrophosphination chemistry, lithium phosphide chemistry and quaternisation chemistry. A variety of problems were encountered with these methods, one of which is the incompatibility of the reagents with the P(III) reactant.

Additionally, we have reported the first example of a ^{99m}Tc-labelled phosphino-glycoconjugate (to the best of our knowledge). A multi-atom alkyl linker was incorporated due to results published by Orvig *et al.* and Schibli *et al.* (Section 2.1), which indicated that poor cellular transport was observed for their ^{99m}Tc-amino glycoconjugates. This was attributed to too short a linker between the carbohydrate moiety and the rest of the molecule. This amide containing phosphine glycoconjugate, **2.20**, was prepared by amide coupling (using EDC-HCl and DIPEA) of an aminopropanol conjugated glucopyranose, **2.18**, and a carboxylic acid-based phosphine **2.19**. The synthesis of the novel peracetyled phosphine glycoconjugate, **2.20**, required 10 steps from D-glycose and allyl alcohol, with an overall yield of 2.5%. The amide bond was stable to deprotection conditions, and no hydrolysis was observed when forming **2.21**.

The Re(I) and Re(V) coordination chemistry of the acetyl protected analogue (**2.20**) was investigated to determine which ^{99m}Tc cores would be suitable for radiolabelling. Results showed that stability of the Re(I)-water complex was poor and hydrolysis of the amide bond was observed. Pleasingly, good stability was observed for the Re(V) complex with **2.20** and radiolabelling studies therefore focused on the Tc(V) analogue. The ^{99m}Tc(V) radiolabelling of **2.21** was very promising, but the stability of the Tc(V) complex in mouse serum was poor, hence this compound did not undergo further testing (*i.e.* cell toxicity testing or *in-vivo* imaging studies). Despite this result, this complex could have applications in intracellular protein labelling if stability is sufficient to be transported into cells.

2.6. Future Work

To address the lack of stability provided by **2.21** (Figure 2.17) for the ^{99m}Tc(V) complex in mouse serum, subsequently work has focused on the synthesis of diphosphine analogues, which are reported in Chapter 4. Additionally, the hydrophosphination and lithium phosphide methods could be reinvestigated in the future.

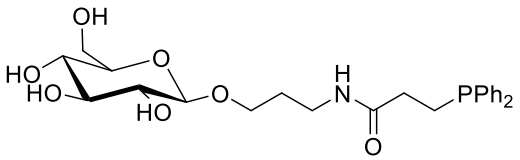

2.21

Figure 2.17 Structure of phosphine glycoconjugate **2.21**.

Research in the Pringle group (unpublished results by R.Nuttall, Scheme 2.13, Section 2.2.2), and by Heesche-Wagner, has shown that hydrophosphination occurs readily at the C-3 and C-6 positions of *O*-glycoconjugates for glycosyl donors containing an allyl and

acryloyl groups; this does not take place at the C-1 position when using an allyl group. Pt(0)-catalysed hydrophosphination chemistry was not considered within this project as this would require the alkene to be a Michael acceptor. Installation of an acryloyl group instead of an allyl group at the C-1 could therefore be investigated in the future (Scheme 2.23). Pt(0) catalysed hydrophosphination may not exhibit the same positional dependence as radical (AIBN) and base (KOH) catalysed hydrophosphination.

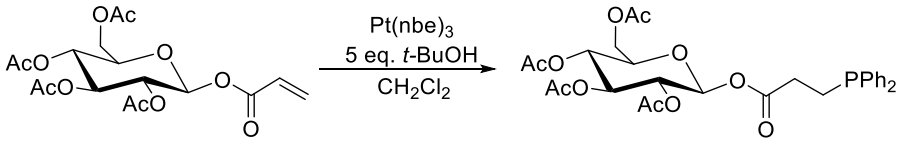

Scheme 2.23 Plausible route to a phosphine glycoconjugate using Pt(0)-catalysed hydrophosphination chemistry.

Lithium-phosphide chemistry was evaluated, but unfortunately, the reaction between **2.14** (Figure 2.18) and $HPPh_2$ proceeded with less efficacy than expected, and a number of side products were formed. Isolation of the desired product also proved to be a challenge, with reactions appearing cleaner *in-situ*. Future work could therefore incorporate repeating this work, with BH_3-protected $HPPh_2$. This could address the issues noted during synthesis and work-up.

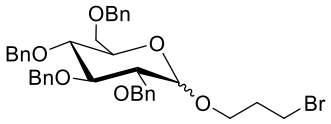

2.14

Figure 2.18 Structure of compound **2.14**.

2.7. References

1 J. Guo and X.-S. Ye, *Molecules*, 2010, **15**, 7235–7265.

2 A. V. Demchenko, *Synlett*, 2003, 1225–1240.

3 D. R. Mootoo, P. Konradsson, U. Udodong and B. Fraser-Reid, *J. Am. Chem. Soc.*, 1988, **110**, 5583–5584.

4 S. Jürgens, W. A. Herrmann and F. E. Kühn, *J. Organomet. Chem.*, 2014, **751**, 83–89.

5 *Technetium-99m Radiopharmaceuticals: Manufacture of Kits*, International Atomic Energy Agency, Vienna, 2008.

6 A. Boschi, L. Uccelli and P. Martini, *Appl. Sci.*, 2019, **9**, 1–16.

7 O. O. Sogbein, A. E. C. Green, P. Schaffer, R. Chankalal, E. Lee, B. D. Healy, P. Morel and J. F. Valliant, *Inorg. Chem.*, 2005, **44**, 9574–9584.

8 J. D. Kelly, M. Forster, B. Higley, C. M. Archer, F. S. Booker, L. R. Canning, K. W. Chiu, B. Edwards, H. K. Gill and M. McPartlin, *J. Nucl. Med.*, 1993, **34**, 222–227.

9 S. Jones and R. C. Hendel, *J. Nucl. Med.*, 1993, **21**, 191–195.

10 E. C. Calvaresi and P. J. Hergenrother, *Chem. Sci.*, 2013, **4**, 2319.

11 M. Beller, J. G. E. Krauter and A. Zapf, *Angew. Chemie Int. Ed. Eng.*, 1997, **36**, 772–774.

12 M. L. Bowen and C. Orvig, *Chem. Commun.*, 2008, 5077–5091.

13 Y. Cheng, G. Shabir, X. Li, L. Fang, L. Xu, H. Zhang and E. Li, *Chem. Commun.*, 2020, **56**, 1070.

14 J. Ipaktschi and W. Sulzbach, *J. Organomet. Chem.*, 1992, **434**, 287–302.

15 J. Clayden, N. Greeves and S. Warren, *Organic Chemistry*, Oxford University Press, New York, 2nd edn., 2001.

16 G. R. Morais, R. A. Falconer and I. Santos, *Eur. J. Org. Chem.*, 2013, 1401–1414.

17 J. Ma, Q. Wang, X. Yang, W. Hao, Z. Huang, J. Zhang, X. Wang and P. G. Wang, *Dalton Trans.*, 2016, **45**, 11830–11838.

18 R. Williams and M. C. Galan, *Eur. J. Org. Chem.*, 2017, **2017**, 6247–6264.

19 S. Meng Anderson, M. Heuckendorff and H. H. Jensen, *Org. Lett.*, 2015, **17**, 944–947.

20 L. M. Broomfield, Y. Wu, E. Martin and A. Shafir, *Adv. Synth. Catal.*, 2015, **357**, 3538–3548.

21 J. Q. Zhang, S. Yang and L. B. Han, *Tetrahedron Lett.*, 2020, **61**, 151556.

22 J. Clayden, N. Greeves and S. Warren, *Organic Chemistry*, Oxford University Press,

New York, 2nd edn., 2001.

23 D. Benito-Alifonso and M. C. Galan, in *Selective Glycosylations: Synthetic Methods and Catalysts*, 2017, pp. 155–172.

24 C. S. Bennett and M. C. Galan, *Chem. Rev.*, 2018, **118**, 7931–7985.

25 R. Williams, PhD Thesis, University of Bristol, 2019.

26 R. Williams and M. C. Galan, *Eur. J. Org. Chem.*, 2017, **2017**, 6247–6264.

27 X. Li and J. Zhu, *Eur. J. Org. Chem.*, 2016, **2016**, 4724–4767.

28 R. Roy, A. K. Palanivel, A. Mallick and Y. D. Vankar, *European J. Org. Chem.*, 2015, **2015**, 4000–4005.

29 B. F. Straub, *Chem. Commun.*, 2004, **10**, 1726–1728.

30 E. Costa, P. G. Pringle and K. Worboys, *Chem. Commun.*, 1998, **3**, 49–50.

31 A. C. Chadwick, M. A. Heckenast, J. J. Race, P. G. Pringle and H. A. Sparkes, *Organometallics*, 2019, **38**, 3871–3879.

32 Heesche-W, K. Agner and T. N. Mitchell, *J. Organomet. Chem.*, 1994, **468**, 99–106.

33 R. Nuttall, First Year Report, University of Bristol, 2020.

34 R. Williams, PhD Thesis, University of Bristol, 2019.

35 M. L. Raposo, F. Fernández-Nieto, L. Garcia-Rio, P. Rodríguez-Dafonte, M. R. Paleo and F. J. Sardina, *Chem. Eur. J.*, 2013, **19**, 9677–9685.

36 M. S. S. Adam, A. D. Mohamad, P. G. Jones, M. K. Kindermann and J. W. Heinicke, *Polyhedron*, 2013, **50**, 101–111.

37 J. L. Methot and W. R. Roush, *Adv. Synth. Catal.*, 2004, **346**, 1035–1050.

38 K. Yu, X. Liu, Q. Zeng, M. Yang, J. Ouyang, X. Wang and Y. Tao, *Angew. Chemie Int. Ed.*, 2013, **52**, 11034–11039.

39 T. Simler, A. A. Danopoulos and P. Braunstein, *Chem. Commun.*, 2015, **51**, 10699–10702.

40 J. Ma, X. Yang, W. Hao, Z. Huang, X. Wang and P. G. Wang, *Eur. J. Med. Chem.*, 2017, **128**, 45–55.

41 K. Huang, F. Parmeggiani, H. Ledru, K. Hollingsworth, J. Mas Pons, A. Marchesi, P. Both, A. P. Mattey, E. Pallister, G. S. Bulmer, J. M. Van Munster, W. B. Turnbull, M. C. Galan and S. L. Flitsch, *Org. Biomol. Chem.*, 2019, **17**, 5920–5924.

42 A. Chadwick, PhD Thesis, University of Bristol, 2017.

43 E. L. Myers and R. T. Raines, *Angew. Chem. Int. Ed.*, 2009, **48**, 2359–2363.

44 V. Carroll, D. W. Demoin, T. J. Hoffman and S. S. Jurisson, *Radiochim. Acta*, 2012, **100**, 653–667.

45 E. Deutsch, K. Libson, J. L. Vanderheyden, A. R. Ketring and H. R. Maxon, *Int. J. Radiat. Appl. Instrum.*, 1986, **13**, 465–477.

46 K. Mrejen, Masters Thesis, McGill University, 1991.

47 J. C. Bryan, M. C. Perry and J. B. Arterburn, *Acta Crystallogr. Sect. C Cryst. Struct. Commun.*, 1998, **54**, 1607–1608.

48 J. M. Hoffman, A. G. Oliver and S. N. Brown, *J. Am. Chem. Soc.*, 2017, **139**, 4521–4531.

Chapter 3 : Aryl Linked Monophosphine Glycoconjugates

3.1. Introduction

Numerous examples of nitrogen-based glycoconjugates are known,[1–3] but few examples of phosphine glycoconjugates have been reported,[4–6] particularly those involving the C-1 functionalisation of glucose; an example of such a phosphine was originally published by Beller *et al.* in 1997 (Figure 3.1).[4]

This ligand was applied in biphasic catalytic applications, but no research into the pharmacological applications of this ligand has been reported. This publication therefore partly inspired this project, with initial developments focussing on whether this ligand could be utilised for radio-imaging. The rhenium coordination chemistry, ^{99m}Tc radiolabelling and kit preparation of this ligand is discussed in this Chapter, along with a variety of analogues that we have synthesised.

These analogues were prepared by modifying the phosphine donor (where PR_2 = P(*o*-Tol)$_2$, P(*p*-Tol)$_2$ or PCy_2) or carbohydrate moiety of the ligand shown in Figure 3.1, and the rhenium coordination chemistry and ^{99m}Tc radiolabelling of these analogues was investigated. Additionally, cellular testing was performed for complexes involving some of these phosphine carbohydrate ligands and this work will be discussed in Section 3.4.

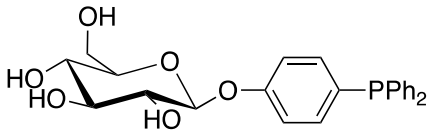

Figure 3.1 Structure of a C-1 functionalised phosphine glycoconjugate synthesised by Beller *et al.*[4]

Chapter 2 focused on the synthesis of phosphine glycoconjugates with an alkyl chain as the linker between the carbohydrate and the phosphine moiety, whilst in this Chapter the focus is on phosphine glycoconjugates with aryl linkers. This work was inspired by research published in 2020 by Li and co-workers, where they showed that in some cases, a longer linker between the carbohydrate and conjugated molecule may not be necessary for receptor recognition, as evidenced by the glycoconjugate in Figure 3.2.[7] This molecule exhibited successful transport *via* GLUT receptors (likely the GLUT-1 receptor), despite the relatively inflexible fluorophore being bound directly to the glucose moiety.[7] This result therefore led us to investigate the molecule synthesised by Beller *et al.* (Figure 3.1) and go on to produce a small library of analogues where either the phosphine or carbohydrate moiety was modified.

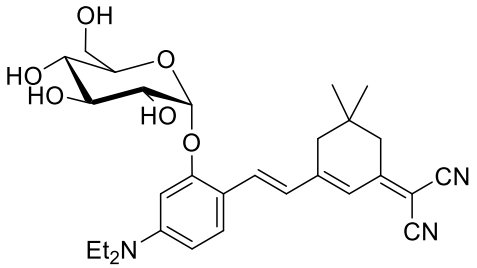

Figure 3.2 Structure of a C-1 functionalised glycoconjugate ligand designed by Li *et al*.[7]

3.1.1. Technetium(I) Core

As discussed in Chapter 1, many different technetium cores exist.[8,9] The two cores of most interest for this project are the Tc(I)-tricarbonyl and Tc(V)-dioxo cores' (Figure 3.3). Radiopharmaceuticals with different cores are prepared using different kits and methods, yet all use pertechnetate ($[TcO_4]^-$) as their precursor. Whilst the preparation of Tc(V) radiopharmaceuticals with a dioxo-core is often favoured within hospitals as they are synthesised *via* a single step, those with a tricarbonyl core often exhibit greater stability but require a two-step preparation.[10]

$[Tc(CO)_3(H_2O)_3]^+$ was first made by Alberto in 1998, and the preparation of this species has since been patented.[11,12] The $[Tc(CO)_3(H_2O)_3]^+$ species is synthesised by adding $[TcO_4]^-$ to commercially available tricarbonyl kits from the Paul Scherrer Institute (Centre for Radiopharmaceutical Sciences). The kit itself contains sodium tartrate (a stabilising ligand), sodium tetraborate (a reductant), sodium carbonate (a base) and sodium boranocarbonate (the carbon monoxide source).[13] The sodium tetraborate reduces $[TcO_4]^-$ from Tc(VII) to Tc(I), whilst the sodium boranocarbonate undergoes hydrolysis and subsequent release of CO to enable the formation of the $[Tc(CO)_3(H_2O)_3]^+$ complex.[14] Once this species has been prepared, the ligand (L) can then be added to give the desired $[Tc(CO)_3(L)_n]^+$ compound. The radiolabelling of aryl-linked phosphine glycoconjugate ligands to generate novel ^{99m}Tc(I)-tricarbonyl complexes is the focus of this Chapter.

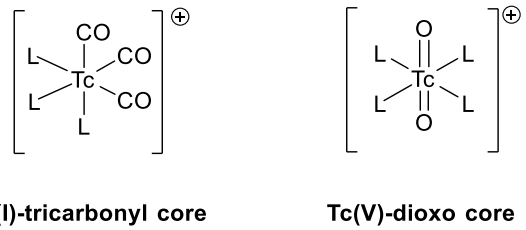

Figure 3.3 Tc(I)-tricarbonyl and Tc(V)-dioxo cores.

3.2. Ligand Synthesis

3.2.1. Investigation of two routes to a glucose-containing phosphine glycoconjugate

As highlighted in Section 3.1, Beller and co-workers originally published the synthesis of a glucose-containing phosphine glycoconjugate, **3.1**, in 1997 (Scheme 3.1) then subsequently improved the synthesis of this compound in 1999 (Scheme 3.2).[4,15]

The method reported in 1997 used basic glycosylation chemistry to conjugate (4-hydroxyphenyl)diphenylphosphine to acetobromo-α-D-glucose; this route, although successful, could only be reproduced with significantly longer reaction times (24 h *versus* 4 h) and was relatively low yielding (14% *versus* 33% in the literature).[4] 2,3,4,6-tetra-O-acetyl-D-glucose, and partially deprotected analogues of this carbohydrate are believed to be the major by-products of this reaction. Note that here, the deprotection step was performed *in situ*. Additionally, Beller *et al.* used 5 eq. of the carbohydrate in this reaction which is extremely inefficient. We have since found this can be reduced to 2.5 eq. without any decrease in yield. As an excess of sugar must be used, this route requires column chromatography to isolate pure material.

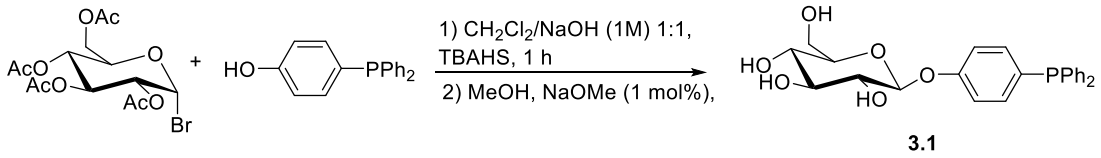

Scheme 3.1 The 1997 method, published by Beller *et al.*, for the synthesis of **3.1.**

By contrast, the method reported in 1999, and shown in Scheme 3.2, uses Pd-catalysed cross-coupling to introduce the phosphine moiety in the form of $HPPh_2$.[15]

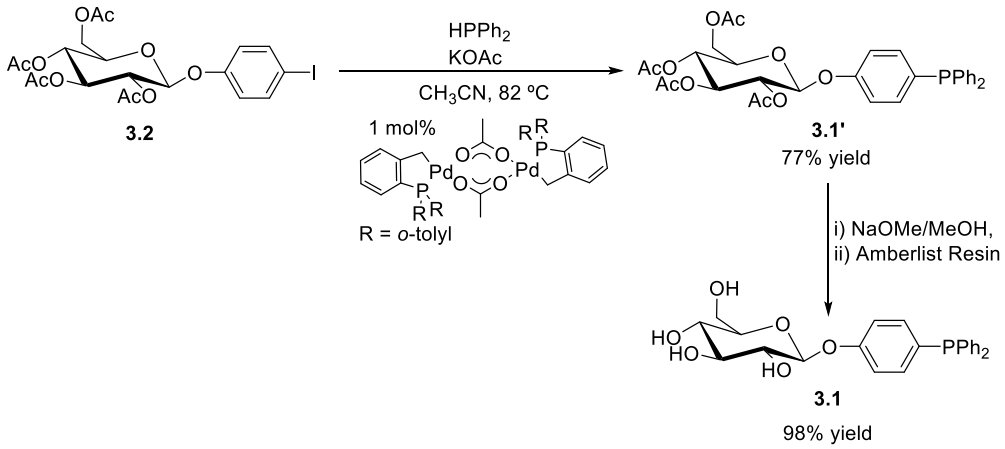

Scheme 3.2 The 1999 method, published by Beller *et al.*, for the synthesis of **3.1.** For phosphine glycoconjugate ligands, and their complexes, prime symbols will be used to

denote those which are peracetylated (such as **3.1′**) whilst the absence of a prime will refer to the deprotected analogue (such as **3.1**).

1-(4-iodophenoxy)-2,3,4,6-acetoxyglucopyranose (**3.2**) can be prepared in three sequential steps: acetylation, anomeric bromination and then glycosylation with 4-iodophenol; the overall yield from D-glucose was 27% (Scheme 3.3).

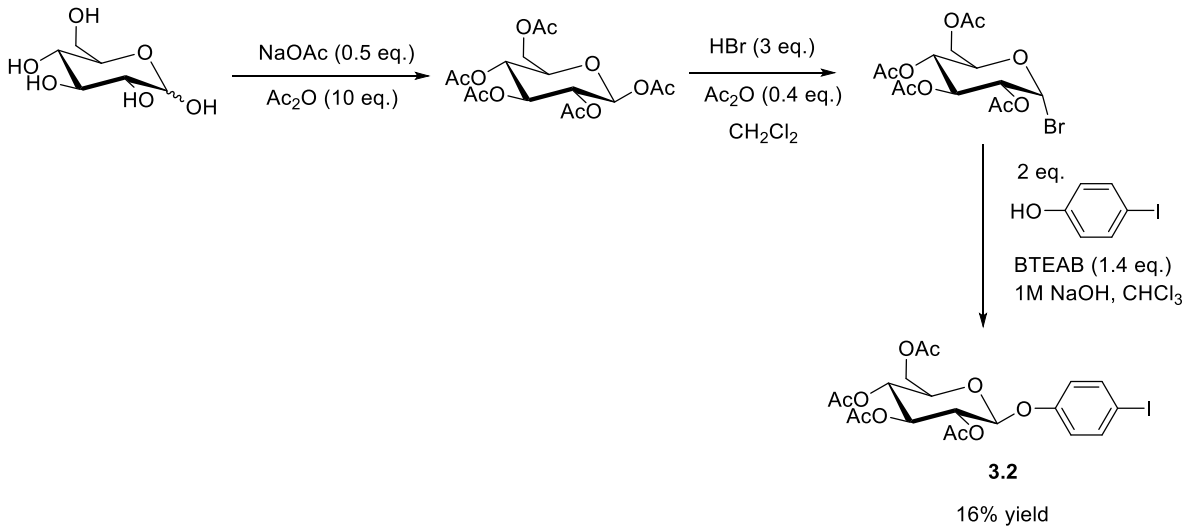

Scheme 3.3 Three step route to known carbohydrate, (4-iodophenol)-2,3,4,6-acetoxyglucopyranose, **3.2**, from D-Glucose.

The Pd-catalysed cross-coupling method for synthesis of **3.1** (Scheme 3.2) is more efficient as only 1 eq. of carbohydrate is required, and the reaction is significantly higher yielding (74% based on carbohydrate **3.2**). We have since modified the work-up conditions reported by Beller *et al.* and found that an aqueous work-up in CH_2Cl_2 and short silica plug achieves the same result as column chromatography. This ease in purification is particularly important when making derivatives that are sensitive to oxygen. Additionally, removing the acetoxy groups in a 1:1 mixture of ethyl acetate and methanol gives better product solubility and results in none of the partially deprotected compound being isolated. This was a problem when performing the deprotection in methanol only. Deprotection of the acetyl groups is necessary for adequate radiolabelling as it is performed under aqueous conditions.

After investigating both routes published by Beller *et al.*, it was decided that the Pd-catalysed cross-coupling method should be favoured for the synthesis of all derivatives where possible. This was due to the ease of purification, the greater atom efficiency of this reaction, and higher overall yield. This is relevant given the commercial value of (4-hydroxphenyl)diphenylphosphine (£331/g, *versus* £5.30/g for $HPPh_2$).[16]

3.2.2. Modification of the phosphine moiety

Derivatives of ligand **3.1** were prepared by varying the R groups of the PR_3 moiety. This was expected to affect the coordination chemistry, radiolabelling and biological features of the molecule because varying the PR_3 groups should alter the lipophilicity of the ligand. Such effects have previously been investigated in unpublished work performed as part of a collaboration between the Ma and Pringle group (Figure 3.4). *In vivo* testing revealed that the ^{64}Cu complex was cleared *via* the kidneys of a mouse when R = Cy, and *via* the bladder when R = Ph.[17,18]

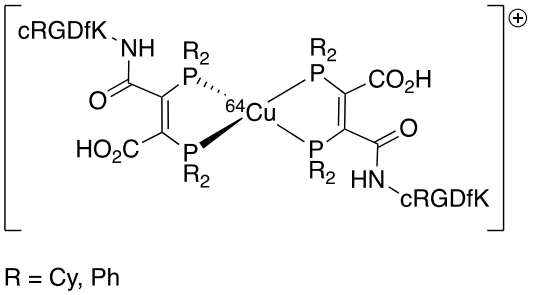

R = Cy, Ph

Figure 3.4 Structure of ^{64}Cu complex, which is cleared *via* the kidneys when R = Cy, and *via* the bladder of a mouse when R = Ph, during *in vivo* testing.

3.2.2.1. P(o-Tol)$_2$ analogue

To explore the effect of substituents on radiolabelling, the first analogue, **3.3′** (where PR_2 = P(*o*-Tol)$_2$), was prepared by reacting HP(*o*-Tol)$_2$ with an equimolar quantity of carbohydrate **3.2** in the presence of a palladacycle catalyst (1 mol%) and KOAc (Scheme 3.4). Compound **3.3′** was prepared by heating the reaction mixture to reflux overnight, although it was subsequently shown that the reaction proceeds to completion within 5 h. This reaction is slower than the analogous reaction with $HPPh_2$ to form **3.1′**, which reaches completion in 3 h. Additionally, the yield for the synthesis of **3.3′** is lower compared to that of **3.1′** (67% for **3.3′** *versus* 77% for **3.1′**), which could be attributed to the increase in steric bulk of the secondary phosphine. For **3.1′**, δ_P = -6.5 ppm, whereas for **3.3′** δ_P = -21.9 ppm, and this high field shift is characteristic of a tertiary RP(*o*-Tol)$_2$ species.

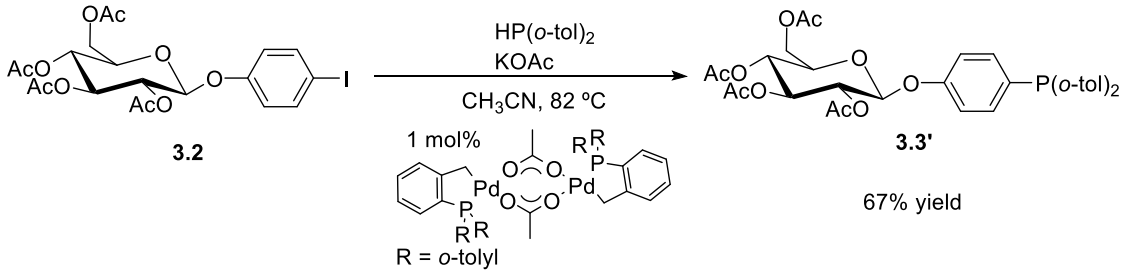

Scheme 3.4 Synthesis of ligand **3.3′**, from carbohydrate **3.2** and HP(*o*-Tol)$_2$.

Compound **3.3′** was then deprotected to give **3.3** (78% yield), which resulted in a chemical shift difference of $\Delta\delta$ = 1.0 ppm, with a new singlet at δ_P = -22.9 ppm seen for **3.3** (Scheme 3.5). Glycan deprotection results in a marginally more shielded phosphorus environment. For full characterisation of **3.3′** and **3.3**, see Chapter 6.

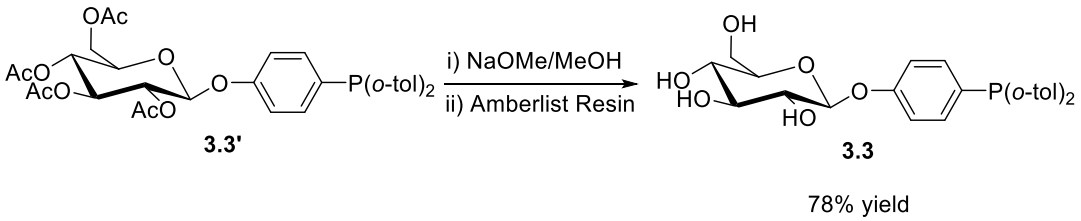

Scheme 3.5 Deprotection of ligand **3.3′**, to give **3.3**, where PR_2 = P(*o*-tolyl)$_2$.

The coordination chemistry of **3.3′** will be discussed in Section 3.3.1, but difficulties encountered when attempting to form a Re complex led us to synthesise ligands **3.4′/3.4** (see below).

3.2.2.2. P(p-Tol)$_2$ analogue

Compound **3.4′** was prepared with HP(*p*-Tol)$_2$ in good yield (73%) using the same method as outlined above for **3.3′**. As HP(*p*-Tol)$_2$ is not commercially available, it was prepared by $LiAlH_4$ reduction of the chlorophosphine, ClP(*p*-Tol)$_2$. The reaction to synthesise **3.4′** takes place on a similar timescale (6 h) as the *o*-tolyl analogue, (Scheme 3.6). The ^{31}P NMR shift for **3.4′** is -7.9 ppm, which is *cf.* for **3.1′** (δ_P = -6.5 ppm).

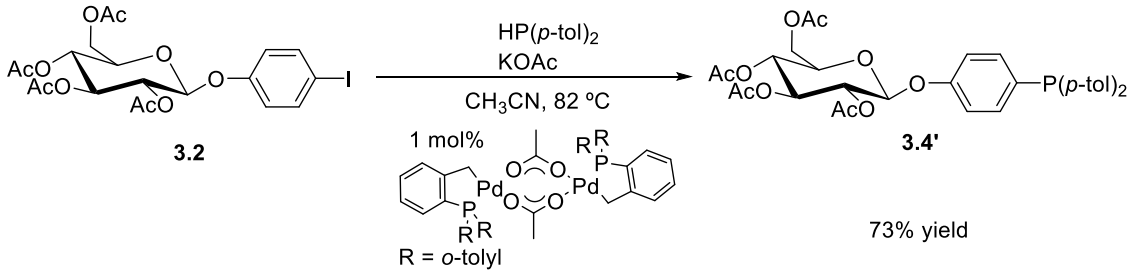

Scheme 3.6 Synthesis of ligand **3.4′**, from carbohydrate **3.2** and HP(*p*-Tol)$_2$.

Compound **3.4′** was deprotected to give **3.4** (δ_P = -8.3 ppm, 84% yield, Scheme 3.7). For full characterisation of **3.4′** and **3.4**, see Chapter 6.

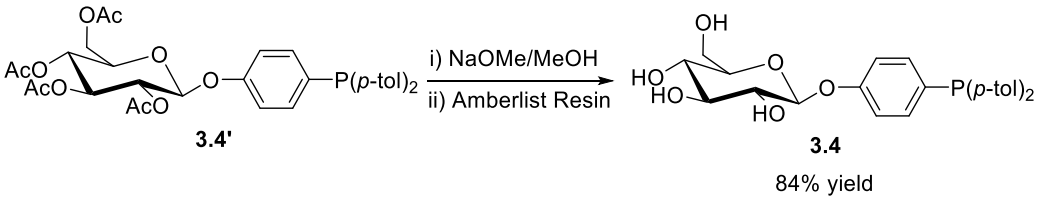

Scheme 3.7 Deprotection of ligand **3.4′**, to give **3.4**, where PR_2 = P(*p*-Tol)$_2$.

3.2.2.3. PCy_2 analogue

To explore the effect of alkyl *versus* aromatic groups on the phosphine moiety, the synthesis of **3.5′/3.5** was investigated. The synthesis of this ligand was significantly slower than for the aromatic analogues, with the reaction to form **3.5′** taking 5 d to reach completion (Scheme 3.8).

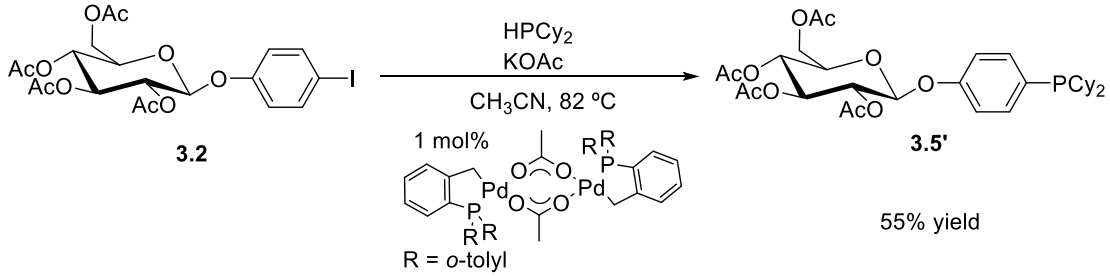

Scheme 3.8 Synthesis of ligand **3.5′**, from carbohydrate **3.2** and $HPCy_2$.

The reaction was carried out with an excess of phosphine ($HPCy_2$) and monitored by ^1H NMR spectroscopy to determine complete consumption of **3.2**. This was possible because the phenylene linker has two characteristic doublets that each shift by 0.2 ppm in the ^1H NMR spectrum upon exchange of the -I atom for a -PCy_2 moiety. The excess of $HPCy_2$ is readily removed at the end of the reaction by partitioning the crude material between MeCN and hexane and then extracting the unreacted $HPCy_2$ into the non-polar phase. A 55% yield was achieved for synthesis of **3.5′**, which has δ_P = -2.2 ppm. Introduction of a PCy_2 moiety has resulted in an increase in steric bulk compared with a PPh_2 moiety.

Despite the increased reaction time to form **3.5′**, the deprotection reaction took place on the same timescale (1 h) as with all other ligands in this series to give **3.5** (Scheme 3.9). A shift difference $\Delta\delta$ = 0.3 ppm was observed upon removal of the protecting groups, with a new signal at δ_P = 1.9 ppm seen for **3.5**, which was prepared in 90% yield. For full characterisation of **3.5′** and **3.5**, see Chapter 6.

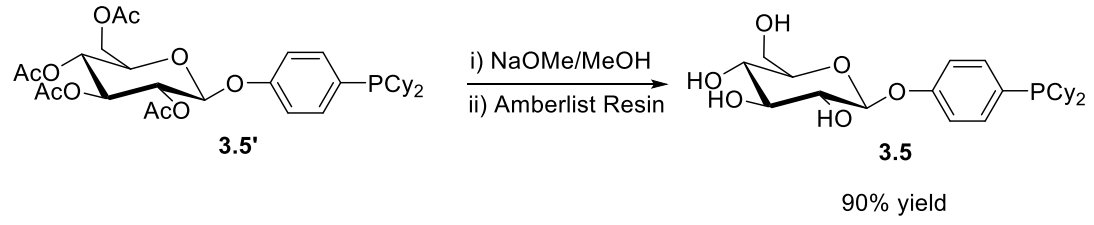

Scheme 3.9 Deprotection of ligand **3.5′**, to give **3.5**, where PR_2 = PCy_2.

3.2.3. Modification of the carbohydrate moiety

As discussed in the introduction, glycoside conjugates are commonly used to increase cancer cell uptake *via* the Warburg Effect. To evaluate whether glucose is required in our system or whether other sugars can be used — such as galactose, which bears an axial OH at C-4 as opposed to an equatorial OH in glucose, or disaccharides such as lactose — we decided to target ligands with varying carbohydrate moieties. Whilst this should not significantly affect the coordination chemistry or radiolabelling of the molecule, it should influence the cellular uptake. In the case of the disaccharide analogue, the water solubility of the ligand and associated complex will be affected. To confirm whether we could modify the carbohydrate to tune the cellular uptake, without affecting the radiochemistry, we prepared galactose and lactose analogues of **3.1**. Galan *et al*. have previously demonstrated that the type of glycan on a given probe can affect cellular targeting.[19]

3.2.3.1. Galactose analogue

The galactose ligand, **3.7′** and its deprotected analogue, **3.7** were — like **3.1′** and **3.1** — published by Beller *et al.* using both methods discussed in Section 3.2.1.

Compound **3.7′** can be synthesised in good yield (69% yield) by reacting $HPPh_2$ with carbohydrate **3.6** in the presence of a palladacycle catalyst (Scheme 3.10). This reaction goes to completion within several hours, although the final product is stable to overnight reflux too. A lower yield is observed for the synthesis of **3.7′** when compared with **3.1′** (69% *versus* 77% yield). The δ_P for **3.7′** is -6.3 ppm, which is similar to that of **3.1′** (δ_P -6.5 ppm), confirming the expectation that the remote carbohydrate has little influence on the phosphorus centre.

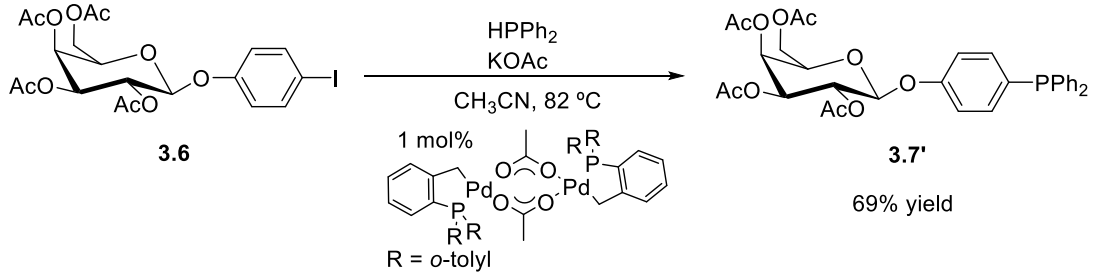

Scheme 3.10 Synthesis of ligand **3.7′**, from carbohydrate **3.6** and $HPPh_2$.

Deprotection of **3.7′**, to give **3.7**, occurs within just 30 min in a yield of 96%. The removal of the acetyl groups results in a shift difference of $\Delta\delta$ = 1.6 ppm (Scheme 3.11); this is the largest shift difference noted in any of the carbohydrate phosphines upon deprotection. Therefore, **3.7** can be prepared in two-steps with an overall yield of 66%, compared to the 50% yield reported by Beller *et al.*[15]

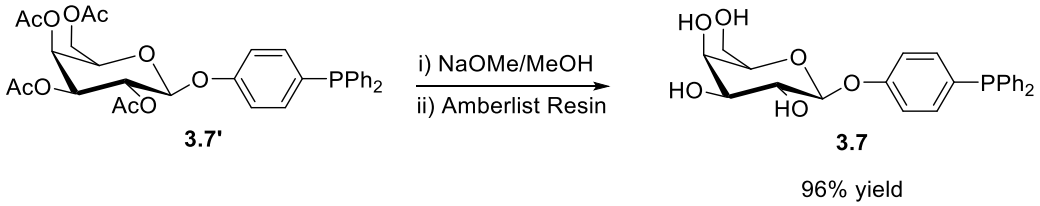

Scheme 3.11 Deprotection of ligand **3.7′**, to give **3.7**, where the carbohydrate is Galactose.

3.2.3.2. Lactose analogue

Incorporation of a disaccharide (such as lactose) was expected to generate a significantly more water-soluble ligand. Improving solubility is desirable, as evidenced by the fact that up to 37% DMSO had to be added to milliQ water to fully solubilise some of the carbohydrate phosphines during radiolabelling (Section 3.5.1), and EtOH had to be added to the Re(I) samples during cell testing.

To prepare the lactosyl phosphine glycoconjugate, the iodophenol-conjugated carbohydrate, **3.9**, first had to be prepared (Scheme 3.12). This was done in three steps from lactose with an overall yield of 10%. The final step produced significantly more species compared with the glucose (**3.2**, 16% yield) and galactose (**3.6**, 8% yield) analogues, and these could not be purified by recrystallisation. Despite this, **3.9** was isolated in a yield of 11% after purification by column chromatography.

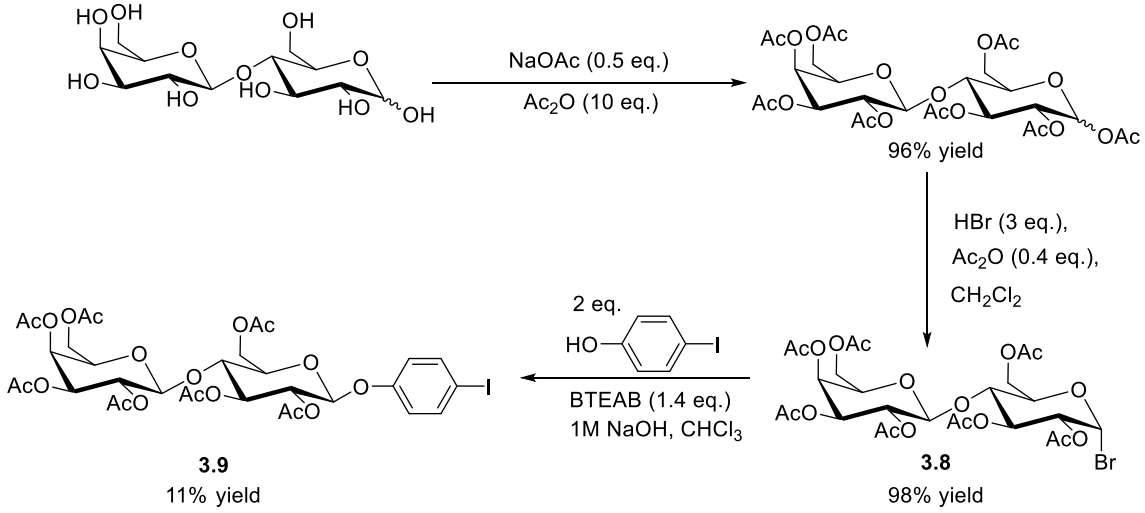

Scheme 3.12 Route to lactosyl precursor, **3.9**, *via* acetobromo-α-D-lactose, **3.8**.

It was expected that reaction of **3.9** and $HPPh_2$ in the presence of the palladacycle catalyst (1 mol%) would smoothly lead to the synthesis of **3.10′** (Table 3.1). However, several unwanted by-products were observed when synthesising **3.10′**; the expected product only accounted for 48% of the species according to ^{31}P NMR spectroscopy. For other carbohydrate phosphines reported above, this method leads to the formation of the desired

product in yields of >90%, as measured by *in-situ* $^{31}P\{^{1}H\}$ NMR spectroscopy. The other species formed during Entry 1 (Table 3.1 and Figure 3.5(a)) included $Ph_2(O=)P\text{-}PPh_2$ (13%), $H(O=)PPh_2$ (25%), and the oxide of **3.10′** (13%). Repetition of this reaction (Entry 2**,** Table 3.1 and Figure 3.5(b)) using solvent that was carefully deoxygenated resulted in only limited improvement.

Doubling the catalyst and base loading (Entry 3, Table 3.1 and Figure 3.5(c)) to try and ensure the phosphine reacted completely with **3.9**, led to a more significant improvement. In this case, **3.10′** accounted for 72% of the species according to ^{31}P NMR spectroscopy. The oxides were removed by passing the crude mixture through a silica plug. However, ^{1}H NMR and HR-MS analysis revealed that only 50% of the carbohydrate starting material (**3.9**) had reacted and hence a 50:50 mixture of **3.9** and **3.10′** was isolated. Column chromatography under nitrogen was ineffective at separating these products due to their near-identical R_f values. Furthermore, only 50% conversion of **3.9** was observed when doubling the equivalents of $HPPh_2$ (Entry 4, Table 3.1 and Figure 3.5(d)). Instead, sequential addition of $HPPh_2$ was investigated, with the first equivalent added at the start of the reaction, and the second equivalent added after leaving the reaction overnight. Again only 50% conversion of **3.9** was observed by ^{1}H NMR (Entry 5, Table 3.1 and Figure 3.5(e)).

Table 3.1 Reaction conditions tested for the attempted synthesis of ligand **3.10′**, from carbohydrate **3.9** and $HPPh_2$.

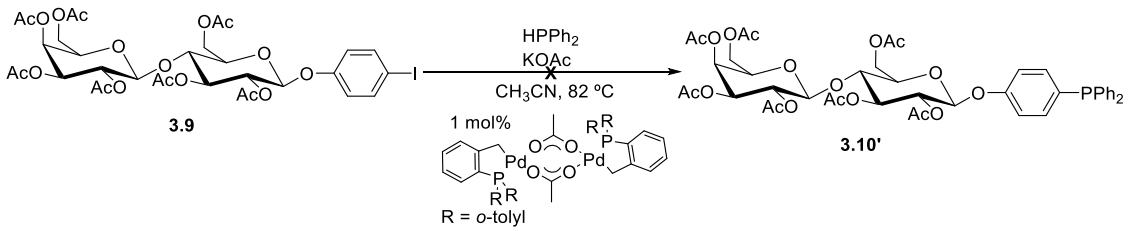

Entry	Catalyst Loading	Base (Equivalents)	$HPPh_2$ (Equivalents)	% of 3.10′ by ^{31}P NMR
1	1 mol%	1.2	1	48%
2	1 mol%	1.2	1	49%
3	2 mol%	2.4	1	68%
4	2 mol%	2.4	2	35%
5	2 mol%	2.4	2	17%

Whilst the Pd catalysed method proved a good route to **3.1′**, **3.3′ -3.5′** and **3.7′**, it did not lead to the clean synthesis of **3.10′**. Instead, we reverted to the method published by Beller *et al*. in 1997 to synthesise **3.10′**.

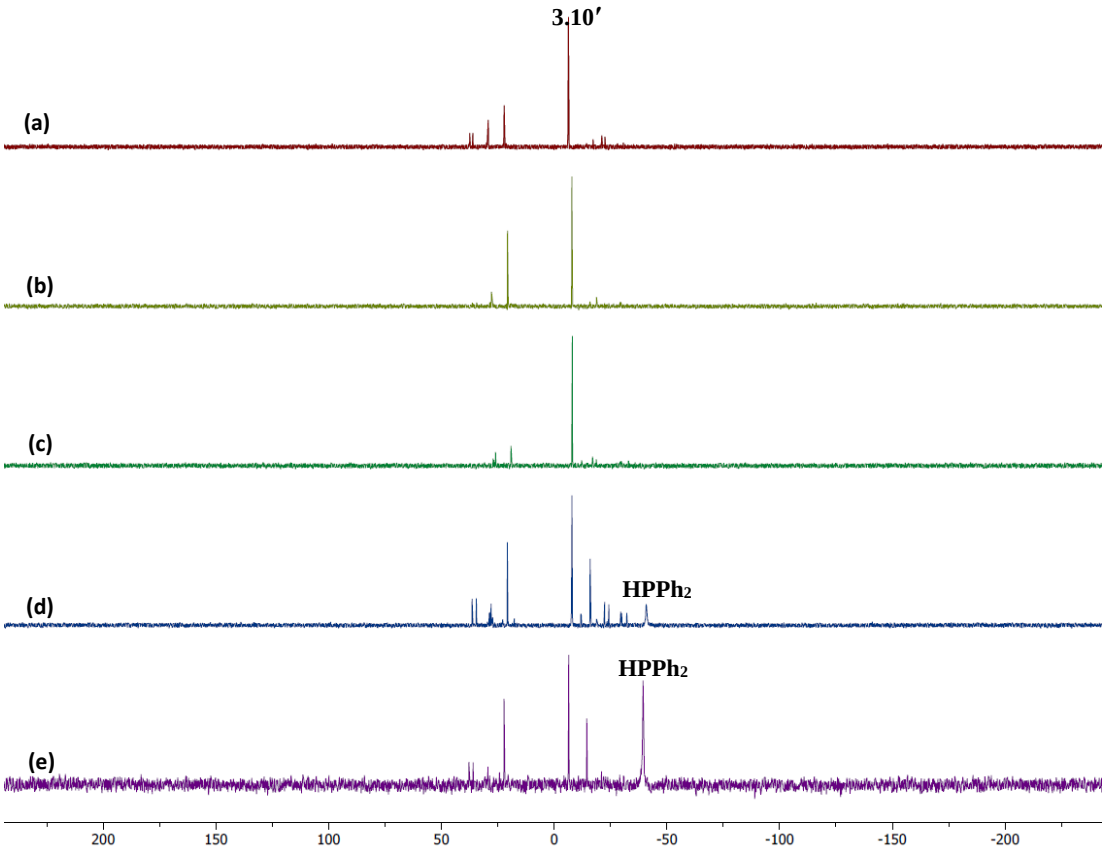

Figure 3.5 $^{31}P\{^{1}H\}$ NMR spectra (121 MHz, $CDCl_3$) of the product mixtures from (a) Entry 1, (b) Entry 2, (c) Entry 3, (d) Entry 4 and (e) Entry 5.

The biphasic route to **3.10′** (Scheme 3.13) requires an excess of bromide **3.8** (3 eq.) and hence column chromatography, under an inert atmosphere, was employed for purification of the crude product. Pleasingly, the excess of carbohydrate (which is likely the hydrolysed hemi-acetal of **3.8**) and **3.10′** were separated on the column enabling **3.10′** to be isolated as a single species, albeit in a low yield (9%). The δ_P of **3.10′** (δ_P = -6.3 ppm) again confirmed that the carbohydrate has a minimal effect on the electronics at the P-centre (for **3.1′**, δ_P = -6.5 ppm). Attempts to reduce the number of equivalents of **3.8** used in this reaction have been unsuccessful, resulting in incomplete conversion of the (4-hydrophenyl)diphenylphosphine.

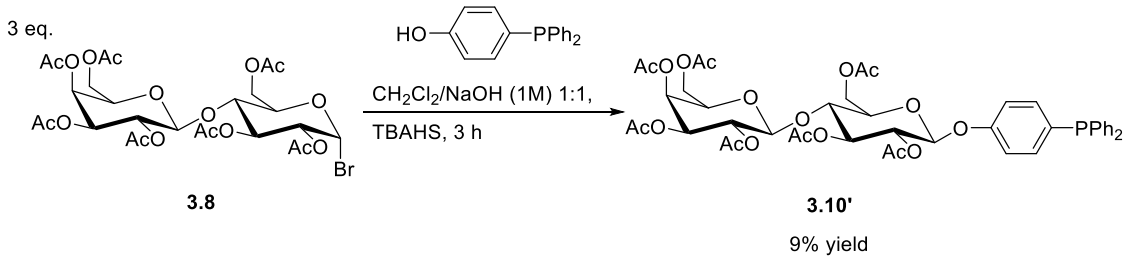

Scheme 3.13 Synthesis of **3.10'**, from carbohydrate **3.8** and (4-hydroxphenyl)diphenylphosphine.

Deprotection of **3.10′** to **3.10** gave a yield of 64% within 2 h in the presence of an NaOMe catalyst. The removal of the acetyl groups from **3.10′** results in a shift difference of just 0.3 ppm (Scheme 3.14), as **3.10** has a δ_P of -6.6 ppm. It was expected that this shift difference may be greater, due to the removal of almost twice an many acetoxy groups as the other analogues. For full characterisation of **3.10′** and **3.10**, see Chapter 6.

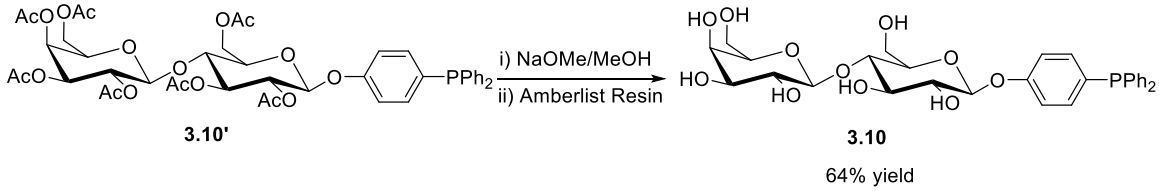

Scheme 3.14 Deprotection of ligand 3.10′, to give 3.10.

3.3. Coordination Chemistry

As discussed in Chapter 2, Re and Tc are one of the few diagnostic/therapeutic 'matched pairs'.[20] This behaviour arises as a result of Re and Tc being valence isoelectronic and isostructural for a given oxidation state. Therefore, ligands that coordinate to Re are expected to give a structurally analogous complex with Tc, and so providing access to a theragnostic system.

Additionally, Re possesses a non-radioactive isotope that can be used as a model for ^{99m}Tc ($t_{1/2}$ = 6 h) radiolabelling. This has been particularly useful within this project, as ligand synthesis was carried out at the University of Bristol, whilst all radiochemistry was performed at St Thomas's Hospital, where specialist facilities for the handling of radioactive compounds are located.

Chemically, there are differences in the rate of substitution and redox chemistry for the two elements; Tc favours lower oxidation states and exhibits faster ligand substitution.[21] However, as the physical characteristics between Re and Tc compounds do not vary significantly, biological systems cannot distinguish between them, thereby making 'cold' Re

a good model for ^{99m}Tc (and ^{188}Re) compounds. Consequently, 'cold' Re complexes were synthesised at the University of Bristol to act as a model for any radiolabelling with ^{99m}Tc.

3.3.1. Synthesis of the Re(I) precursor, [Re(CO)$_3$(H$_2$O)$_3$]Br

The coordination chemistry of the phosphine glycoconjugates described in Section 3.2 was investigated with the Re(CO)$_3$ core using [Re(CO)$_3$(H$_2$O)$_3$]Br as the precursor; this was prepared by heating [Re(CO)$_5$Br] in deoxygenated H$_2$O (Scheme 3.15) at reflux for 24 h to ensure that the thermodynamic product, [Re(CO)$_3$(H$_2$O)$_3$]Br, is exclusively formed. Rhenium complexes containing fewer aqua ligands (< 3) may obtained if the reaction time is shorter. The tricarbonyl core was selected as the Tc analogue ([Tc(CO)$_3$]) is considered particularly stable to oxidation in radio-imaging applications. A discussion of the preparation of the [Tc(CO)$_3$] core can be found in Section 3.5.

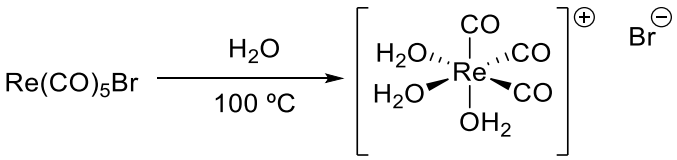

Scheme 3.15 Synthesis of [Re(CO)$_3$(H$_2$O)$_3$]Br.

3.3.2. Coordination of 3.1′ and 3.1

Addition of two equivalents of **3.1**′ to [Re(CO)$_3$(H$_2$O)$_3$]Br resulted in formation of the neutral complex [Re(CO)$_3$(**3.1′**)$_2$Br] (**3.11′**, Scheme 3.16) in 88% yield. The composition of **3.11′** has been confirmed by HR-MS (*m/z* [M+Na]$^+$ = 1589.2109, obs. = 1589.2076). The ^{31}P{^{1}H} NMR spectrum shows a singlet at -1.9 ppm (despite the P atoms being diastereotopic, see below), with a small coordination shift of $\Delta\delta$ = +4.6 ppm. Despite recording the ^{31}P{^{1}H} NMR spectrum at high field (202 MHz), no AB splitting pattern was observed for this complex, therefore the phosphorus atoms appear accidentally equivalent by NMR spectroscopy. Addition of three equivalents of **3.1′** to [Re(CO)$_3$(H$_2$O)$_3$]Br does not lead to displacement of all three aqua ligands to form the +1 charged complex, [Re(CO)$_3$(**3.1′**)$_3$]Br.

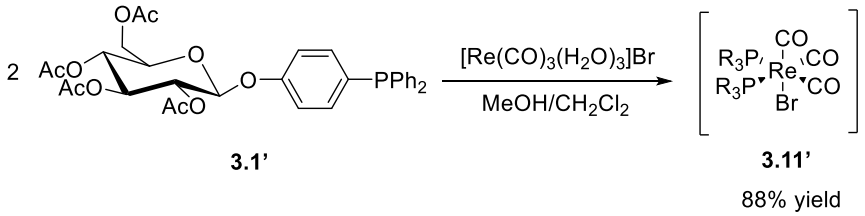

Scheme 3.16 Synthesis of the Re(I) complex 3.11′.

Deprotection of **3.11′** using a NaOMe solution in methanol gave complex **3.11** (Figure 3.6) in good yield (93%). This was confirmed by HR-MS (*m/z* calcd. for $C_{51}H_{50}O_{15}P_2BrReNa$

([M+Na]$^+$) = 1253.1264; obs. = 1253.1240), ^{1}H NMR spectroscopy, and a coordination shift in the ^{31}P{^{1}H} NMR spectrum measuring $\Delta\delta$ = +0.7 ppm (see Chapter 6 for full details). An AB splitting pattern was observed at -1.1 ppm (J_{PP} = 29.2 Hz) and -1.3 ppm (J_{PP} = 29.2 Hz) in the ^{31}P{^{1}H} NMR spectrum (spectrum was measured at 162 MHz, Figure 3.6). This is observed because the two phosphorus atoms are diastereotopic (the complex has C_1 symmetry), but this shift difference is very small and can only be discerned at high fields.

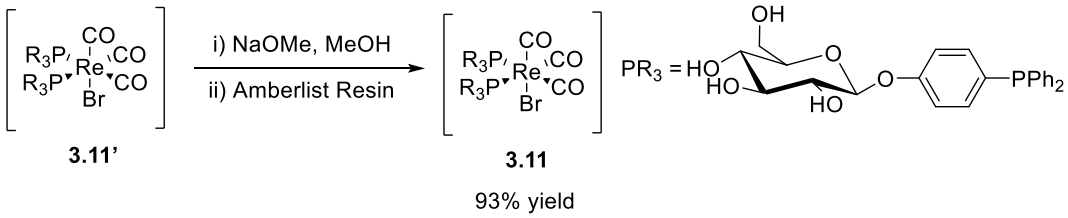

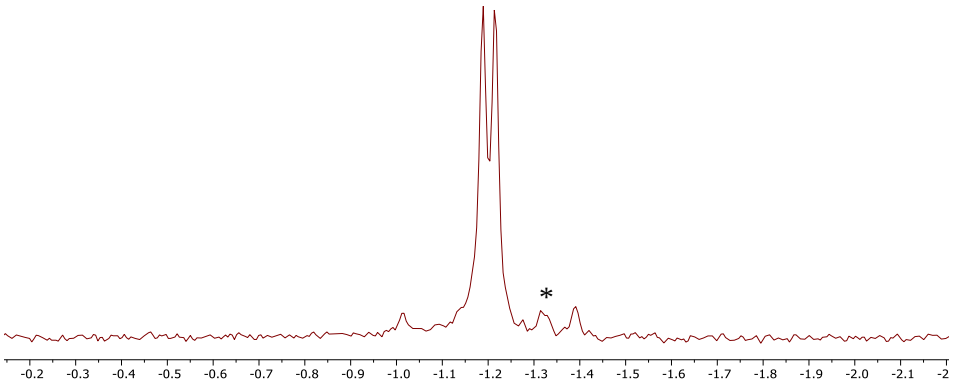

Figure 3.6 Synthesis of the Re(I) complex **3.11,** and ^{31}P{^{1}H} NMR spectrum (CD_3OD, 162 MHz) between *ca*. 0 and -2 ppm, with an impurity at -1.3 ppm (*). See Chapter 6 for full details.

The above route to **3.11** was developed because adding two eq. of the deprotected ligand, **3.1**, to [Re(CO)$_3$(H$_2$O)$_3$]Br gave a different complex, **3.12**, which gave an apparent singlet at δ_P = +9.1 ppm in the ^{31}P{^{1}H} NMR spectrum. HR-MS analysis was unable to confirm the identity of the ligand denoted 'X' in Scheme 3.17 (*m/z* calc. $C_{51}H_{50}O_{15}P_2Re$ [M-X]$^+$) = 1151.2182; obs. = 1151.2178). The difference in phosphorus chemical shift for **3.11** (-1.9 ppm, where X = Br) and **3.12** (9.1 ppm) can therefore be attributed to the different identity of ligand 'X'. For cell testing, it is important to know the coordination sphere, and hence the Re(I) complexes were first formed with peracetylated ligands and then deprotected once coordinated to Re(I), to access the Re(I) complexes with unprotected glycoconjugate ligands.

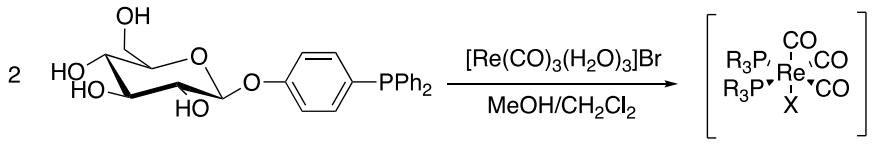

3.1 **3.12**

Scheme 3.17 Synthesis of the Re(I) complex **3.12**, where 'X' denotes an unidentified ligand.

3.3.3. Coordination of di-*o*-tolylphosphino-glucose conjugates 3.3′ and 3.3

Ligand **3.3′** was added to $[Re(CO)_3(H_2O)_3]Br$, but no reaction was observed after 18 h. This difference in reactivity between **3.3′** and **3.1′** is attributed to the greater steric bulk of P(*o*-Tol)$_2$ compared to PPh_2 inhibiting reaction with Re. Furthermore, heating the reaction mixture to reflux in DCE for 16 h (Figure 3.7) led to the formation of many species according to $^{31}P\{^1H\}$ NMR spectroscopy and although the expected complex was detected by HR-MS, the signal was very weak. Based on structurally similar complexes, the peak at -1.8 ppm in the $^{31}P\{^1H\}$ NMR has tentatively been assigned to the expected product, $[Re(CO)_3(\mathbf{3.3'})_2Br]$. However, this species accounts for only 4% of the mixture based on integration of the $^{31}P\{^1H\}$ NMR signals (Figure 3.7). Broad signals at δ_P = -21.7 ppm and δ_P = +36.7 ppm account for 80% of the mixture and suggests that a fluctional monophosphine species (δ_P = +36.7 ppm) is being formed, where the free ligand (δ_P = -21.7 ppm) is undergoing rapid ligand exchange. Low temperature $^{31}P\{^1H\}$ NMR spectroscopy should provide further information about this system and this could be investigated in the future.

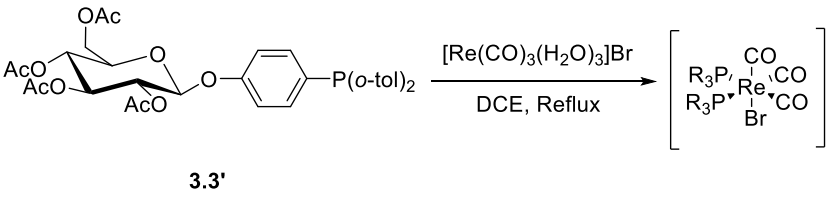

3.3'

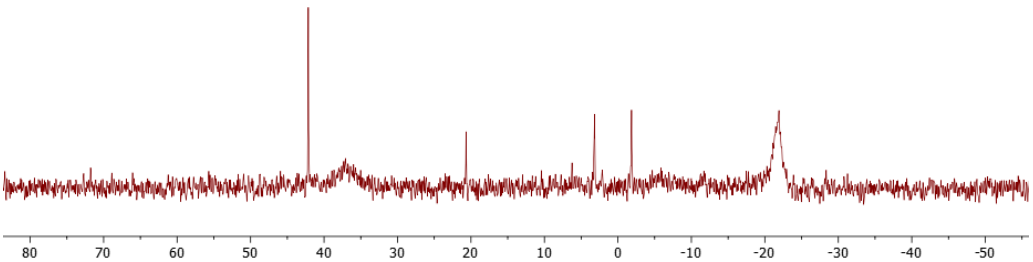

Figure 3.7 $^{31}P\{^1H\}$ NMR spectrum (CD_3OD, 121 MHz) produced by heating the above reaction to reflux for 18 h.

To further investigate the coordination chemistry of **3.3′**, 1 eq. of the ligand was reacted with $[AuCl(SMe_2)]$ (Scheme 3.18). A new singlet was seen in the $^{31}P\{^1H\}$ NMR spectrum at 14.6 ppm, and the reaction reached completion in 30 min. The complex is assigned the structure of **3.13′**, on the basis of HR-MS (*m/z* calcd. for $C_{34}H_{37}O_{10}PClAuNa$ ($[M+Na]^+$) = 891.1376;

obs. = 891.1365), a large coordination shift of $\Delta\delta_P$ = +37.4 ppm and ^{1}H NMR spectroscopy (see Chapter 6 for the data); **3.13′** was isolated in 73% yield.

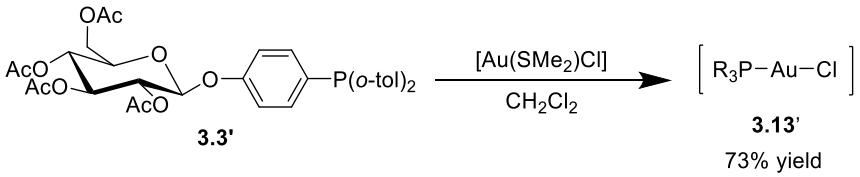

Scheme 3.18 Reaction of **3.3′** with [Au(SMe$_2$)Cl] to form complex **3.13′**.

When 2 eq. of **3.3′** were added to *cis*-[PtCl$_2$(COD)] no reaction was observed (Scheme 3.19(a)). However, when this rection was repeated with *trans*-[PtCl$_2$(NC^{t}Bu)$_2$], complex **3.14′** was isolated in 67% yield (Scheme 3.19(b)). Coordination of **3.3′** to give complex **3.14′** resulted as indicated by a singlet in the ^{31}P{^{1}H} NMR spectrum at 15.0 ppm with platinum satellites and a $J_{P\text{-}Pt}$ value (2583 Hz), which is characteristic of a *trans*-PtP$_2$ complex. The formation of the *trans* complex is consistent with the large steric bulk of ligand **3.3'**.

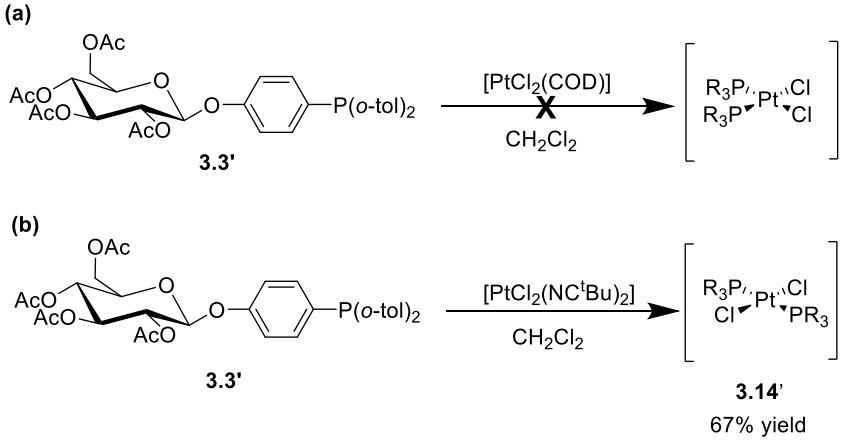

Scheme 3.19 Reaction of **3.3′** with (a) *cis*-[PtCl$_2$(COD)] and (b) *trans*-[PtCl$_2$(NC^{t}Bu)$_2$].

This preference for *trans* complex formation has previously been observed by Pringle and Wingad with tris(*o*-tolyl)phosphine.[22] Our attempts to form the *cis*-Pt complex (from [PtCl$_2$(COD)] and tris(*o*-tolyl)phosphine) have been unsuccessful (Scheme 3.20). This result confirms that the formation of *cis*-MP$_2$ complexes are inhibited by P(*o*-Tol)$_2$ groups.

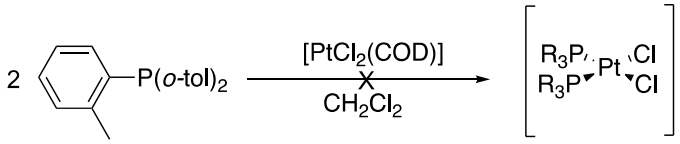

Scheme 3.20 Unsuccessful reaction of tris(*o*-tolyl)phosphine and [PtCl$_2$(COD)].

3.3.4. Coordination of di-*p*-tolylphosphino-glucose conjugates 3.4′ and 3.4

In contrast to the lack of reactivity observed between **3.3′** and $[Re(CO)_3(H_2O)_3]Br$, the *para*-isomer **3.4′** reacted with the Re(I) precursor within 2 h to give **3.15′** (Scheme 3.21) in 88% yield. As the complex has C_1 symmetry, the phosphine atoms are inequivalent so an AB splitting pattern should be observed by $^{31}P\{^1H\}$ NMR spectroscopy, but even at high field (202 MHz) a singlet is observed for **3.15′** (δ_P = -1.9 ppm). HR-MS confirmed the presence of the Br ligand in the neutral complex, **3.15′** (*m/z* calcd. for $C_{71}H_{74}O_{23}P_2BrReNa$ ($[M+Na]^+$) = 1645.2735; obs. = 1645.2715).

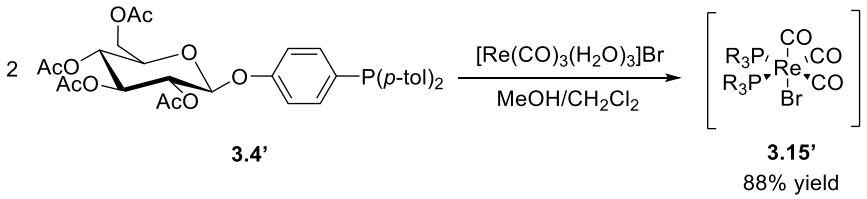

Scheme 3.21 Synthesis of the Re(I) complex 3.15′.

Deprotection of this species using NaOMe in MeOH gave complex **3.15** in an 83% yield, as confirmed by ^1H NMR spectroscopy and HR-MS (*m/z* calcd. for $C_{55}H_{58}O_{15}P_2BrReNa$ ($[M+Na]^+$) = 1309.1890; obs. = 1309.1879, see Chapter 6). Complex **3.15** showed an AB splitting pattern at -3.0 ppm (J_{PP} = 28.3 Hz) and -3.2 ppm (J_{PP} = 28.3 Hz) in the $^{31}P\{^1H\}$ NMR spectrum (recorded at 202 MHz, Figure 3.8).

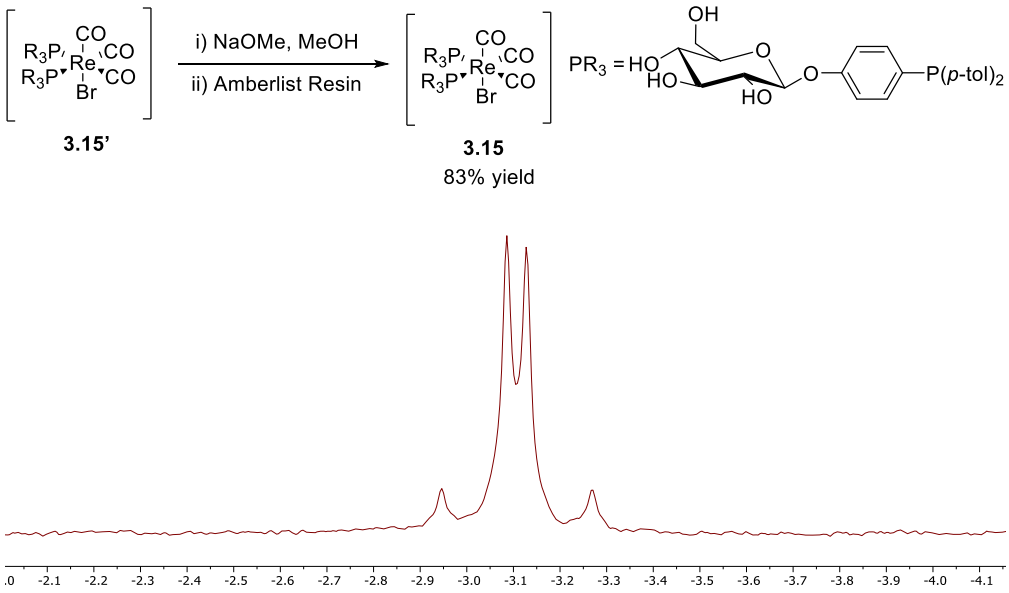

Figure 3.8 Synthesis of the Re(I) complex **3.15**, and $^{31}P\{^1H\}$ NMR spectrum (CD_3OD, 202 MHz) between *ca*. -2 and -4 ppm. See Chapter 6 for full details.

3.3.5. Coordination of dicyclohexylphosphino-glucose conjugates 3.5′ and 3.5

Complex **3.16′** was formed in 88% yield within 2 h, by reacting two equivalents of **3.5′** with $[Re(CO)_3(H_2O)_3]Br$. The $^{31}P\{^1H\}$ NMR spectrum showed a well resolved doublet at -2.7

ppm, with a J_{PP} coupling of 22.4 Hz, and a broad singlet at -5.3 ppm (Figure 3.9(a)). It is likely that the broad signal is in fact an unresolved doublet. Additionally, the ^{1}H NMR spectrum exhibited twice as many aromatic signals as expected (Figure 3.9(b)), in agreement with the two P-ligands being inequivalent. The coordination of the bromide ligand is supported by the HR-MS (*m/z* calcd. for $C_{67}H_{90}O_{23}P_2BrReNa$ ($[M+Na]^+$) = 1613.3956; obs. = 1613.3987). Despite repeating this reaction under various conditions, the product **3.16′** was not obtained in pure form (see Figure 3.9(a)).

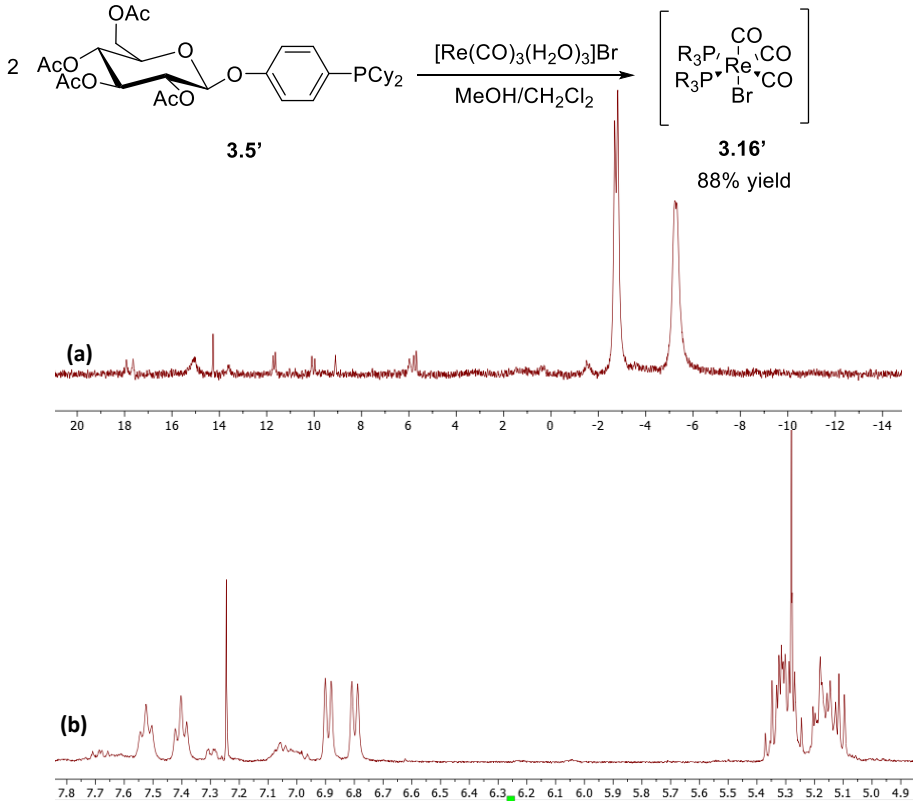

Figure 3.9 (a) The $^{31}P\{^{1}H\}$ NMR spectrum ($CDCl_3$, 202 MHz) and (b) partial ^{1}H NMR spectrum ($CDCl_3$, 400 MHz, 7.8-4.9 ppm) of the reaction shown schematically.

Upon deprotection of **3.16′** with a NaOMe catalyst to form **3.16**, a singlet was observed in the $^{31}P\{^{1}H\}$ NMR spectrum at 1.4 ppm (Figure 3.10). An AB splitting pattern should have been observed by $^{31}P\{^{1}H\}$ NMR spectroscopy, but the two phosphorus atoms appear equivalent even at high field (202 MHz). The expected complex, **3.16**, was only formed with *ca.* 55% purity by $^{31}P\{^{1}H\}$ NMR spectroscopy, and the HR-MS spectrum did not show peaks associated with M^+. Consequently, **3.16** has not undergone toxicity testing as it has not been obtained in pure form.

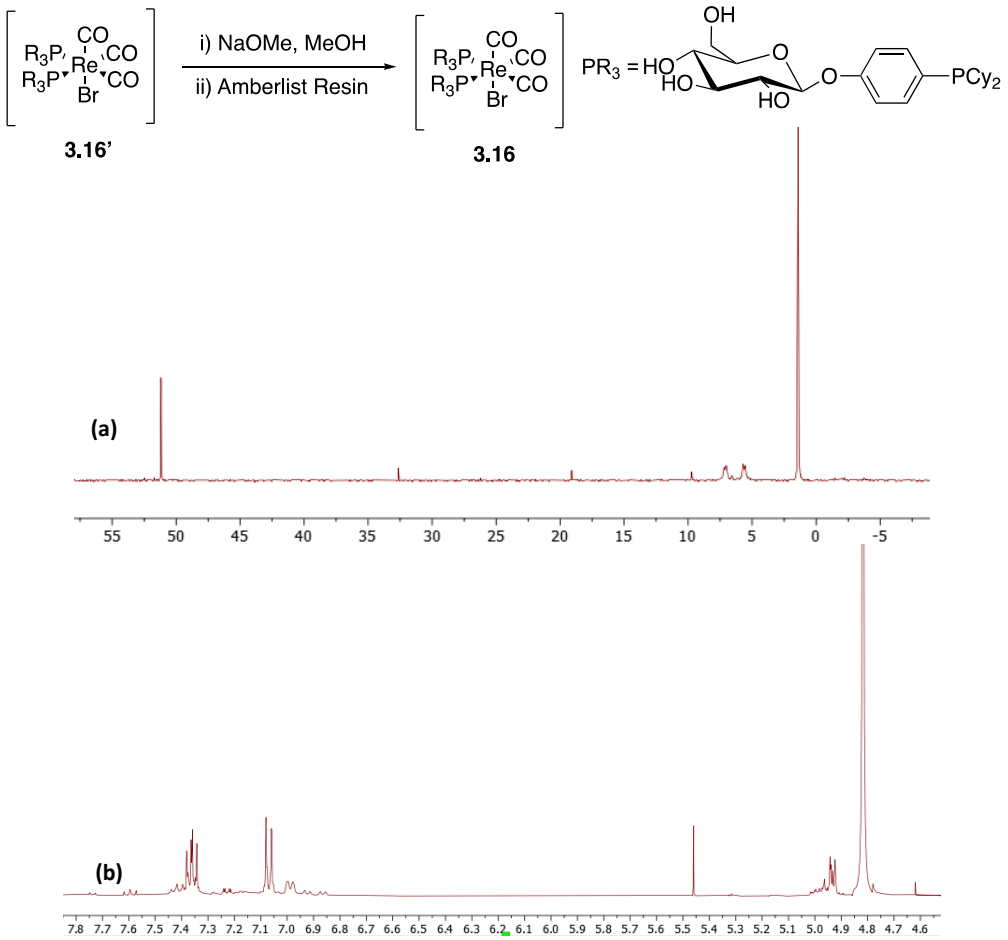

Figure 3.10 (a) The $^{31}P\{^{1}H\}$ NMR spectrum (CD_3OD, 162 MHz) and (b) partial ^{1}H NMR spectrum (CD_3OD, 400 MHz, 7.8-4.6 ppm) of the reaction shown schematically.

3.3.6. Coordination of diphenylphosphine-galactose conjugate 3.7

It was discovered that complex **3.17** could be formed directly from the deprotected ligand **3.7** (Figure 3.11) in 90% yield. This avoided the need to form a Re(I) complex with peracetylated **3.7′** and then deprotect the glycoconjugate ligand once coordinated to the Re(I) centre. An AB splitting pattern at -1.2 ppm (J_{PP} = 29.2 Hz) and -1.4 ppm (J_{PP} = 29.2 Hz, Figure 3.11) was observed by $^{31}P\{^{1}H\}$ NMR spectroscopy. The identity of the species was confirmed by HR-MS ($C_{51}H_{50}O_{15}P_2BrRe$ ([M+Na]+) = 1253.1249; obs. = 1253.1227) and ^{1}H NMR spectroscopy (see Chapter 6 for details). This result was unexpected as **3.17** is simply a stereoisomer of **3.11**.

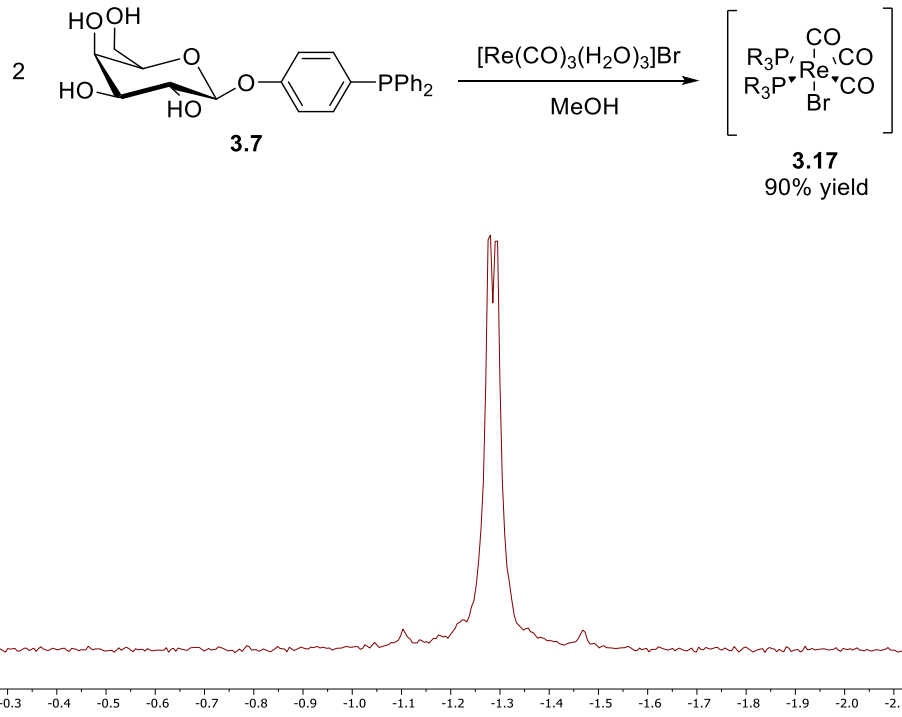

Figure 3.11 Synthesis of the Re(I) complex **3.17′**, and $^{31}P\{^{1}H\}$ NMR spectrum (CD_3OD, 162 MHz) between *ca*. 0 and -2 ppm. See Chapter 6 for full details.

3.3.7. Coordination of 3.10′

As discussed in Section 3.2.2.6, the synthesis of **3.10′** proved extremely challenging and **3.10′** was obtained in low yield (1% from D-lactose). Consequently, all purified material for **3.10′** was deprotected to give **3.10** (<10 mg) for radiolabelling (see Section 3.6). Crude material was therefore used to investigate whether complexation of **3.10′** to the $Re(CO)_3$ core was possible. The complexation was expected to proceed in a similar fashion to that of **3.1′** as the binding moiety does not differ for these two glycoconjugate ligands. Although crude **3.10′** contained multiple carbohydrate species, it only contained one phosphorus species (**3.10′**) and consequently, the reaction could be easily monitored by $^{31}P\{^{1}H\}$ NMR spectroscopy.

Addition of crude **3.10′** to $[Re(CO)_3(H_2O)_3Br]$ gave two new singlets in the $^{31}P\{^{1}H\}$ NMR spectrum at -0.8 ppm and +2.8 ppm. Based on similar chemical shifts being observed for related complexes, the broad signal at -0.8 ppm has been assumed to be the desired complex **3.18′** (Scheme 3.22). However, this signal should have resolved with an AB splitting pattern due to the C_1 symmetry within the complex. The formation of the expected species (**3.18′**) has been confirmed by HR-MS ($C_{91}H_{98}O_{39}P_2BrRe$ ([M+Na]+) = 2165.3799; obs. = 2165.3760). While this study confirms that the deprotected ligand, **3.10**, is likely to undergo radiolabelling with ^{99m}Tc, the quantities of **3.10′** have precluded further studies involving this ligand.

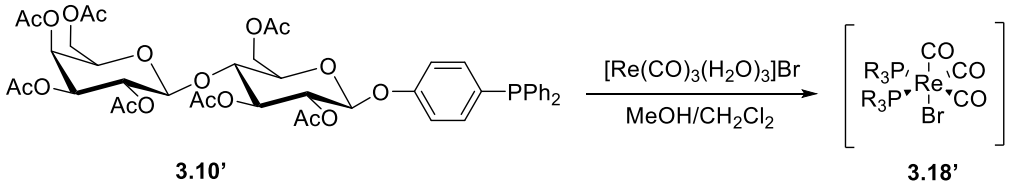

3.10' **3.18'**

Scheme 3.22 Synthesis of the Re(I) complex 3.18′.

3.3.8. Additional Re(I) Complexes, 3.19-3.21

Although crystallisation of the glycoconjugate complexes (Section 3.3.1-3.3.6) was unsuccessful, the expected geometry of these compounds has been established by growing crystals of the model complex $[Re(CO)_3(PPh_3)_2Br]$ (**3.19**) suitable for X-ray diffraction. Complex **3.19** was prepared in modest yield (34%) by addition of PPh_3 (2 eq.) to the Re(I) precursor (Scheme 3.23). The crystal structure confirms that two phosphorus ligands are bound in a *cis*-fashion, whilst the bromide ligand is *trans* to one of the three carbonyl ligands (

Figure **3.12**). Although **3.19** is known,[23] full characterisation has not previously been reported (see Chapter 6 for full details).

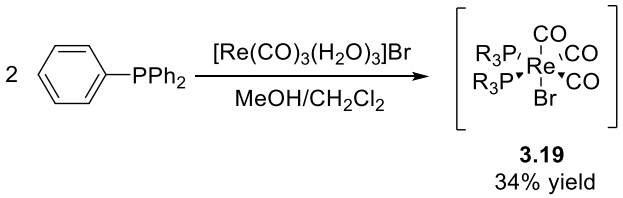

3.19
34% yield

Scheme 3.23 Synthesis of the Re(I) complex **3.19**

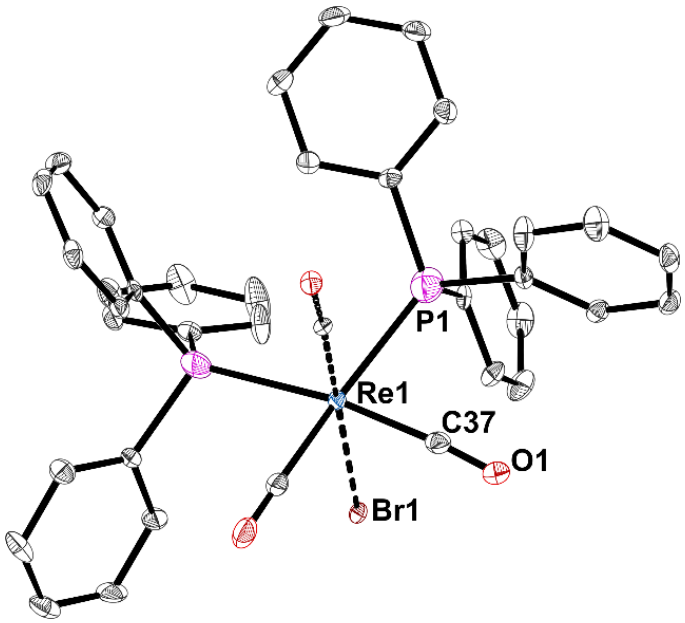

Figure 3.12 Crystal structure of **3.19**: Re-Br 2.570(4) Å, Re-P1 2.5323(8) Å, Re-P2 2.5279(7) Å, Re- C37 1.939(3), Re-C38 1.944(3), Re-C39A 1.945(9) Å, P1-Re-P2 102.43(2)º, C39A-Re-Br 172.6(7)º.

Cellular uptake studies were carried out using several Re(I) complexes to determine whether they could be transported into cells (Section 3.4). Synthesis of a Re(I) complex with a non-glycoconjugate phosphine ligand was required to determine whether uptake was a consequence of the carbohydrate moiety or simply the lipophilic nature of the phosphine moiety. The simplest analogue to prepare was **3.19**, but this proved to be insoluble in EtOH or water, making it unsuitable for cellular studies.

Consequently, tris(4-hydroxyphenyl)phosphine - prepared by deprotection of the phenol group of tris(4-methoxylphenyl)phosphine[24] - was added to $[Re(CO)_3(H_2O)_3]Br$. The $^{31}P\{^1H\}$ NMR spectrum revealed that two species were formed during this reaction. The major species (90% by $^{31}P\{^1H\}$ NMR spectroscopy) was a broad singlet at 3.8 ppm, whilst the minor species was a sharp singlet at -2.8 ppm (Figure 3.13). Previous complexation reactions, where $[Re(CO)_3(PR_3)_2]Br$ species are formed, exhibit resonances between *ca.* 0 and -3 ppm. Therefore, it is hypothesised that the species forming at -2.8 ppm is the expected complex **3.20**, with a coordination shift of $\Delta\delta$ = +7.2 ppm compared to the free ligand (δ_P = -10.0 ppm). The identity of the broad singlet at 3.8 ppm remains unknown, but is likely a second complex. As this mixture could not be separated by HPLC, this system was not deemed appropriate for cellular uptake studies.

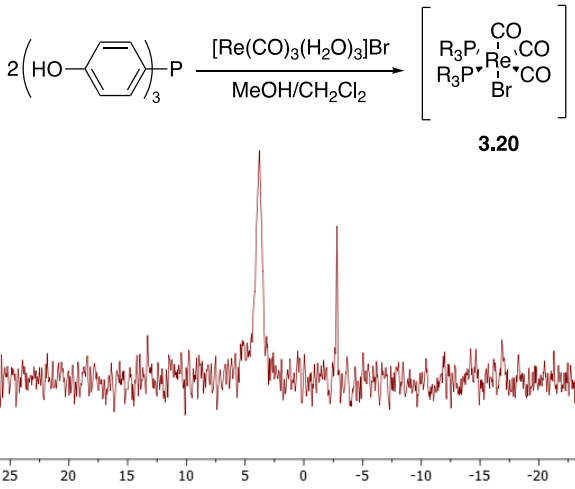

Figure 3.13 $^{31}P\{^{1}H\}$ NMR spectrum (CD_3OD, 121 MHz) produced from the above reaction involving tris(4-hydroxyphenyl)phosphine and $[Re(CO)_3(H_2O)_3]Br$.

Subsequently, (4-hydroxyphenyl)diphenylphosphine was acetylated with Ac_2O in pyridine to give (4-acetoxyphenyl)diphenylphosphine in good yield (77% yield) without the need for further purification (Scheme 3.24). Addition of two equivalents of the acetylated phosphine ligand to $[Re(CO)_3(H_2O)_3]Br$ in a mixture of CH_2Cl_2 and MeOH, gave **3.21** in 89% yield (Scheme 3.24). A singlet was present in the $^{31}P\{^{1}H\}$ NMR spectrum of **3.21** at -0.4 ppm and its identity was confirmed by HR-MS (*m/z* calcd. for $C_{43}H_{34}O_7P_2ReBrK$ ($[M+K]^+$) = 1029.0158; obs. = 1029.0132) and ^{1}H NMR spectroscopy (Chapter 6 for details). As **3.21** was soluble in EtOH, it was deemed a suitable candidate for cellular uptake studies.

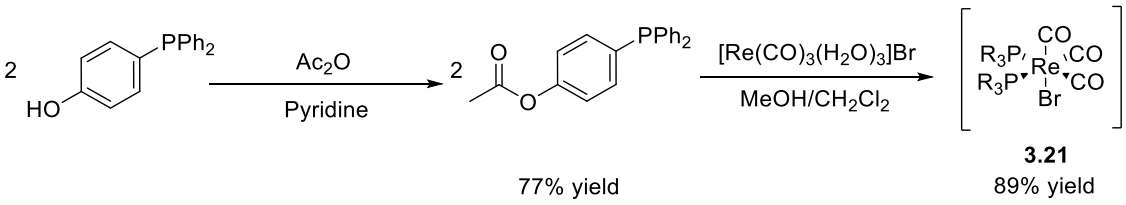

Scheme 3.24 Synthesis of (4-acetoxyphenyl)diphenylphosphine and its reaction with $[Re(CO)_3(H_2O)_3]Br$ to form the Re(I) complex **3.21.**

3.4. Cellular Studies

As discussed previously, 'cold' Re can be used as a non-radioactive analogue of ^{99m}Tc. This enables us to predict the behaviour of the radiolabelled analogues.[25] To quantify the cellular uptake of our compounds and determine whether the analogous ^{99m}Tc species will enter cells, it was necessary to perform uptake studies using the equivalent Re(I) complexes. These experimental results were analysed using ICP-MS (inductively coupled plasma mass spectrometry), a technique that can quantify the amount of a particular metal (*e.g.* Re) in cell extracts. Prior to performing uptake studies, it was necessary to determine whether the

complexes of interest were toxic towards the preferred cell lines, as uptake studies can only be performed on living cells.

All cellular studies discussed in this Section (toxicity testing and uptake studies) were carried out by Dr Radhe Shyam (Galan Group, University of Bristol). ICP-MS analysis was performed by researchers – Alexander Griffiths (KCL) and Maral Amrahli (KCL) - at the London Metallomics Factility (LMF), which is managed by Dr Theodora Stewart, at King's College London. The results of the ICP-MS work will be discussed in Section 3.4.2.

3.4.1. Alamar Blue Cell Viability Study

3.4.1.1. Background

The cytotoxicity of several Re(I) complexes and their precursor, $[Re(CO)_3(H_2O)_3]Br$, were tested on HeLa, HDF and EA.hy926 cell lines as model systems. These are cancerous, healthy and hybrid cells lines which consist of epithelial, fibroblast and endothelial cells, respectively. Complexes **3.11**, **3.15** and **3.17** (Figure 3.14) were chosen as they were stable to HPLC purification and could be isolated in >90% purity. The Re(I) complex **3.16**, containing the dicyclohexylphosphino-glucose conjugate, was not studied as it was not obtained in sufficient purity.

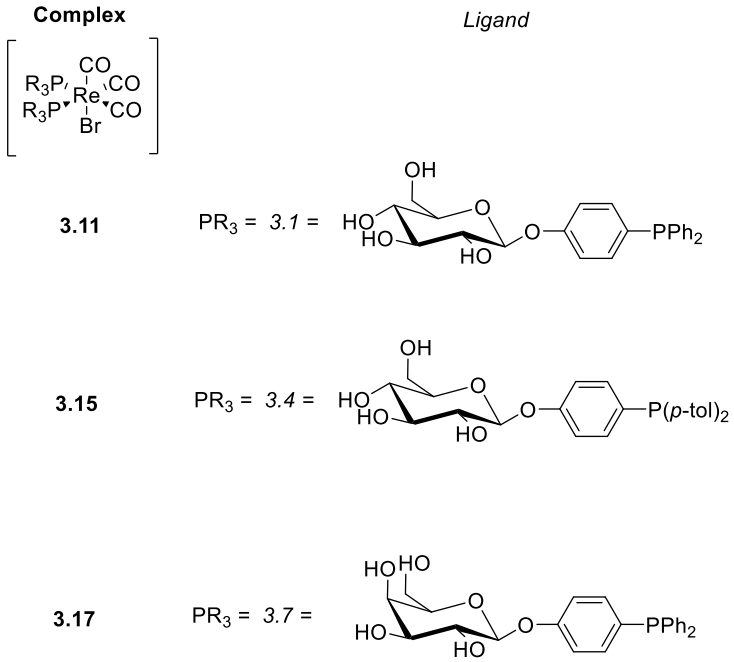

Figure 3.14 Structure of complexes **3.11**, **3.15** and **3.17**, which underwent toxicity testing on HeLa, HDF and EA.hy926 cells.

The viability of the HeLa, HFD and EA.hy926 cells after exposure to the complexes was assessed by Alamar Blue assay. This assay uses a dye (Alamar Blue) to quantify the metabolic activity within the cells so that the number of viable (live) cells can be determined. Alamar Blue is blue and non-fluorescent when oxidised, but pink and

fluorescent when reduced.[26] As the cells proliferate and grow, they reduce the Alamar Blue reagent so the dye turns from blue to pink. The extent by which this colour change happens is measured by UV absorbance or fluorescence and, by using calibration curve, the number of viable cells can be calculated.[26]

During our experiments, the viability of the cells was monitored after 2 h of exposure to the Re(I) complex, its associated ligand, or its ligand oxide at three different concentrations (25, 50 and 100 μM) in 96-well plates. This was necessary to determine which concentration would be optimal when performing the uptake studies since uptake studies can only be performed on live cells.

All ligand oxides were prepared by addition of iodine and then water to the peracetylated ligand before its subsequent deprotection (Scheme 3.25). For full details and characterisation data (^{1}H and ^{31}P{^{1}H} NMR, and HR-MS) see Chapter 6. The oxides were prepared because the Re(I) complexes (>90% purity) contained small amounts of the ligand oxide; it was important to ensure any toxicity that may be observed could be accounted for.

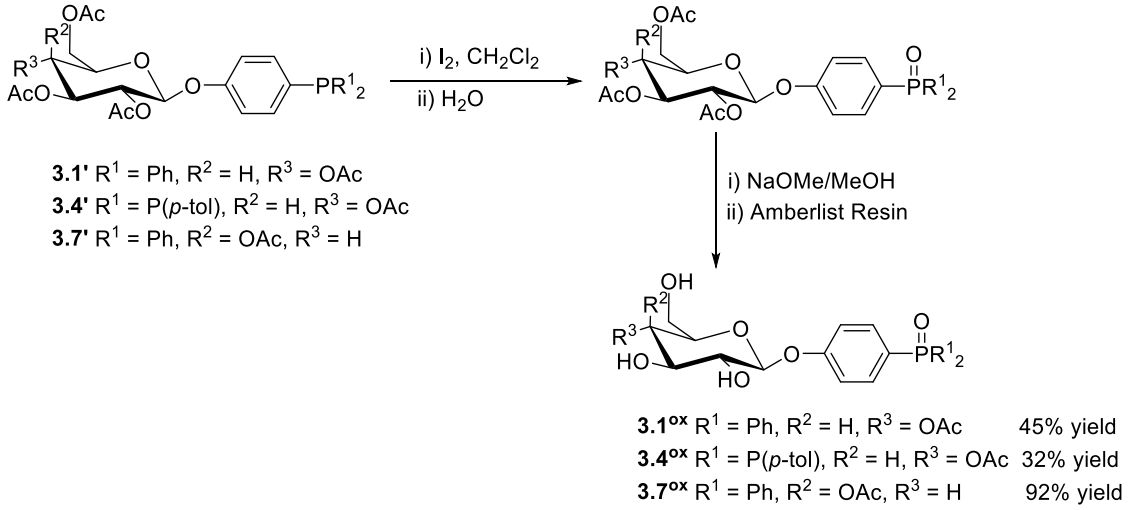

Scheme 3.25 Synthesis of phosphine oxide glycoconjugates 3.1^{ox}, 3.4^{ox} and 3.7^{ox}.

3.4.1.2. Results – Overall Summary

The number of viable cells increased over 2 h for all three cell lines. This effect was greatest in HDF (Figure 3.16, Section 3.4.1.4), then HeLa (Figure 3.15, Section 3.4.1.3), but minimal in EA.hy926 (Figure 3.17, Section 3.4.1.5). The change in cell viability appears negligible for cells that are treated with $[Re(CO)_3(H_2O)]Br$, and therefore increased metabolic activity can be attributed to treatment with the ligands and their Re complexes synthesised in this project.

Because a large increase in metabolic activity was observed when testing complexes **3.11**, **3.15** and **3.17** (and their ligands) on both HeLa and HDF cell lines, we reasoned that the molecules are somewhat cytotoxic, therefore putting the cells under increased stress and consequently, resulting in increased proliferation to ensure survival. This effect is referred to as hormesis and occurs when low levels of toxins stimulate repair mechanisms, thereby leading to increased viability.[27,28] As the concentration is further increased, a decrease in viability will eventually be overserved in line with higher levels of toxicity. In this study, although signs of toxicity are observed (*via* the hormetic effect), no significant cell death was detected and uptake studies could therefore be performed with these synthetic complexes (see Section 3.4.2).

3.4.1.3. Results - HeLa

Of the glycoconjugate samples tested on HeLa cells (Figure 3.15), the oxides were observed to have least impact, whilst the viability increased dramatically for cells treated with the ligands alone and, to a greater extent, the Re(I) complexes. The metabolic activity of the cells that were exposed to 100 µM of the Re(I) complexes was significantly increased to 153% (*para*-tolyl substituted complex **3.17**) and 164% (galactoside complex **3.15**). No statistically significant correlation between complex concentration (25, 50 and 100 µM) and cell viability was observed when the HeLa cells were incubated with the glucoside complexes, **3.11**, **3.15** and **3.17**. This result was unexpected as we had hoped to see a correlation between the sample concentration and the stress experienced by the cells.

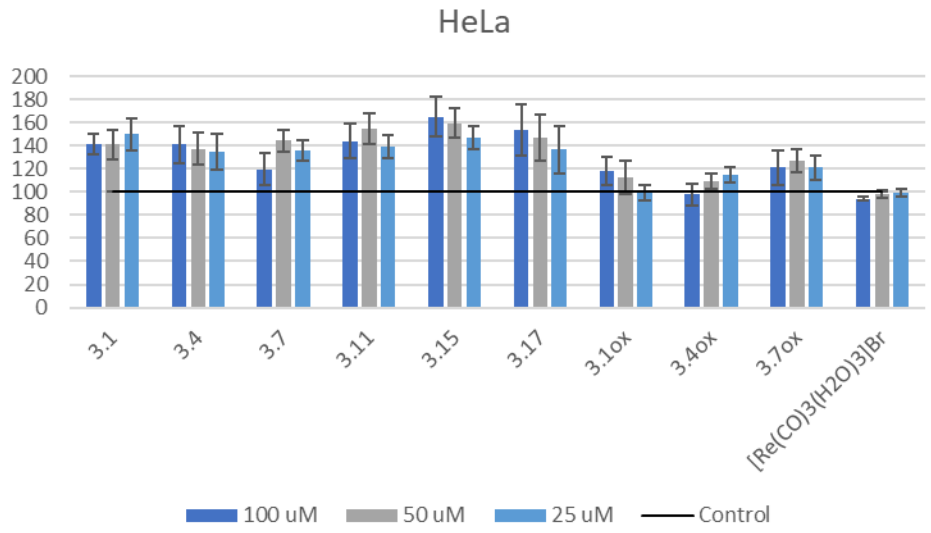

Figure 3.15 Cell viability data in HeLa cells. The error bars represent the calculated standard error of the mean (SEM) from three independent experiments, whilst the control line (in black) is set to 100% because this shows the number of cells after 2 h when left untreated.

3.4.1.4. Results - HDF

Similar effects to those seen in HeLa cells (Section 3.4.1.3) were observed for healthy HDF cells. Here, an increased viability was observed for the glycoconjugate ligands, oxides, and complexes (Figure 3.16). For the Re(I) complexes, the viability at 100 µM measured 133% (**3.17**), 180% (**3.11**) and 187% (**3.15**). Consequently, galactose-based **3.17** was found to affect the cellular metabolic activity ratios to a lesser extent compared to the two glucose containing complexes (**3.11** and **3.15**). When analysing the results of the assay with HeLa cells, no difference was noted between galactose and glucose containing complexes. Due to the standard errors between measurements, no overall trends could be discerned between concentration and viability.

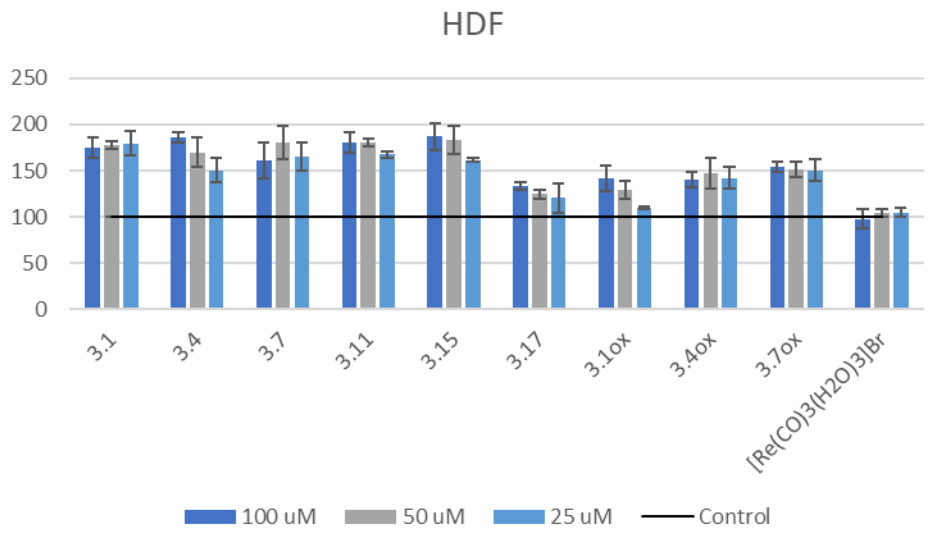

Figure 3.16 Cell viability data in HDF cells. The error bars represent the calculated standard error of the mean (SEM) from three independent experiments, whilst the control line (in black) is set to 100% because this shows the number of cells after 2 h when left untreated.

3.4.1.5. Results – EA.hy926

The Alamar Blue assay revealed that EA.hy926 - a hybrid cell line consisting of fused human umbilical cells and A594 lung carcinoma cells - showed the least response when these cells were incubated with our glycoconjugate-containing molecules (Figure 3.17). Nonetheless, increased viability (rather than cell death) was still observed. However, this was to a lesser extent than seen for the HeLa and HDF cells. The only sample which exhibited a notable increase in viability at all concentrations was the one with complex **3.17** (133% at 25 µM to 136% at 100 µM).

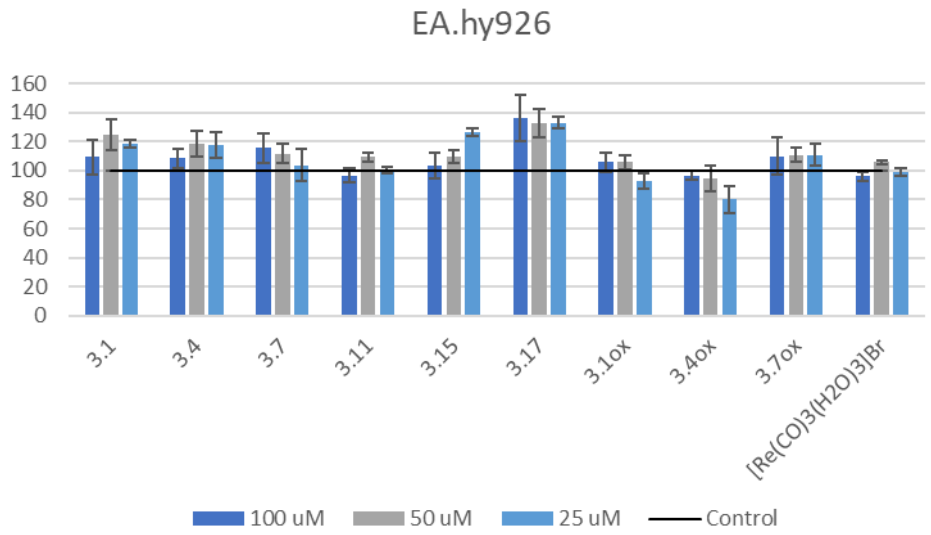

Figure 3.17 Cell viability data in EA.hy926 cells. The error bars represent the calculated standard error of the mean (SEM) from three independent experiments, whilst the control line (in black) is set to 100% because this shows the number of cells after 2 h when left untreated.

3.4.2. Uptake Studies

3.4.2.1. Pilot Study - Background

A pilot uptake study was initially performed to (i) ensure the method of sample preparation was compatible with ICP-MS analysis, and (ii) determine whether the Re content within the cells could be quantified. This was crucial as the London Metallomics Facility (LMF) had not previously analysed Re content. Based on the results in Section 3.4.1, the uptake study was performed at 50 µM concentration. This was because no cell death was observed after 2 h at this concentration, and uptake studies are generally performed at maximal concentrations. However, performing these studies at higher concentrations (100 µM) would be challenging due to the quantity of material that would be required *versus* the limited scale on which the complexes could be prepared.

In the pilot study, the uptake of the Re precursor, $[Re(CO)_3(H_2O)_3]Br$, and complex **3.11** were compared. The compounds were incubated with HeLa cells at 50 μM concentration for 2 h, before the cell lysis was performed using ultra-pure NaOH (99.99%) to ensure no Re contamination occurred. The ICP-MS results enabled us to calculate two different values: the accumulation ratio and the normalised Re uptake. The accumulation ratio reveals the amount of Re that was internalised as a percentage of the total amount of Re exposed to the cells, whilst the normalised uptake is expressed in terms of 'μg of Re per μg protein'. The quantity of protein in a sample is determined by performing a BCA assay. Quoting the normalised uptake in terms of 'μg Re/μg protein' means that the results were normalised for the number of cells within a sample. This is important because uptake increases with increasing cell count. However, it should be noted that this metric is more useful for making comparisons between different samples tested on a single cell line. This is because different cell lines grow at different rates, and contain different amounts of protein per cell, than others. Consequently, the accumulation ratio can be useful for making comparisons between different cell lines (such as HeLa *versus* HDF), as this shows efficiency of uptake.

3.4.2.2. Pilot Study - Results

As discussed in Section 3.4.1.2 the uptake of **3.11** and $[Re(CO)_3(H_2O)_3]Br$ was investigated in HeLa cells. Calculating the accumulation ratio as a percentage revealed that 19.6% of **3.11** was transported inside the HeLa cells after 2 h, compared with just 0.1% of $[Re(CO)_3(H_2O)_3]Br$. Because the quantity of cells in two samples is in agreement (see Table 3.2), the same trend is observed for the normalised uptake: 0.0547 μg Re/μg protein for complex **3.11**, and 0.0005 μg Re/μg protein for $[Re(CO)_3(H_2O)_3Br]$. It is therefore possible to confirm that complex **3.11** is transported inside the HeLa cells, and that ligand **3.1** has made this process 196-fold more efficient, compared with the aqua-ligated $[Re(CO)_3(H_2O)_3]Br$.

Table 3.2 Results of pilot Re uptake study in HeLa after 2 h incubation at 50 μM.

Sample	Cell Line	Accumulation Ratio (%)	Quantity of Re in cells (μg/mL)	Quantity of protein (μg/mL)	Normalised Re uptake (μg Re/μg protein)
$Re(CO)_3(H_2O)_3Br$	HeLa	0.10 ± 0.00%	0.034 ± 0.005	75.34 ± 0.74	0.0005 ± 0.0000
3.11	HeLa	19.65 ± 0.03%	4.301 ± 0.634	78.61 ± 2.88	0.0547 ± 0.0090

N.B. The experimental values for 'quantity of Re in cells' and 'quantity of protein' are quoted as means ± standard deviation for the experiment, which was performed in triplicate. The normalised uptake is calculated by dividing the 'quantity of Re in cells' by the 'quantity of protein'.

3.4.2.3. Full Uptake Study

As the pilot study indicated that we could measure differences in uptake between Re(I) samples, a larger study was designed to answer three specific questions about the uptake of our complexes: (i) is the cellular uptake a consequence of the carbohydrate moiety or the phosphine moiety; (ii) does the cellular uptake differ depend on the specific carbohydrate; (iii) are we able to distinguish between healthy and cancerous cell lines?

To answer the first of these questions, the uptake of complex **3.21** (Figure 3.18) was compared with that of complexes **3.11** and **3.17** (Figure 3.18). However, first the toxicity of **3.21** had to be assessed as uptake studies can only be performed on live cells.

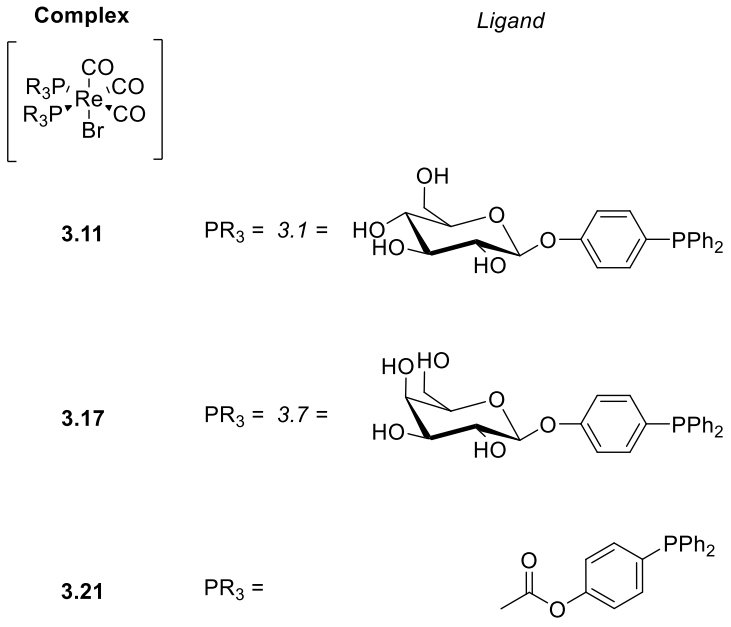

Figure 3.18 Structure of complexes tested in large scale Re uptake study.

Complex **3.21** was therefore incubated with HeLa, HDF and EA.hy926 cells at 25, 50 and 100 μM for 2 h. These results were performed in quintuplet, as opposed to triplicate, and the mean values plotted in the graphs below (see Figure 3.19). Depending on the concentration, a viability of *ca.* 101-110% was observed for HeLa (Figure 3.19(a)), a viability of *ca.* 92-97% for HDF (Figure 3.19(b)) and viability of *ca.* 96-103% for EA.hy926 (Figure 3.19(c)). Therefore, unlike the carbohydrate containing species, no significant increase in viability was observed for any cell line. Crucially, as no significant cell death was observed, uptake studies could be performed with complex **3.21**.

The second question was addressed by comparing the uptake of complex **3.11** (containing D-glucose) with complex **3.17** (the D-galactose analogue).

Lastly, the uptake of complex **3.11** was compared across all three cell lines – HeLa, HDF and EA.hy926 – in an attempt to answer our final question. If the uptake of **3.11** was greater in HeLa cells compared with HDF or EA.hy926 cells, then this would suggest we can differentiate between cell lines. As before, all results were recorded in triplicate and calculations were performed to convert the results into µg Re/µg protein. The results of this uptake study are shown in Table 3.3.

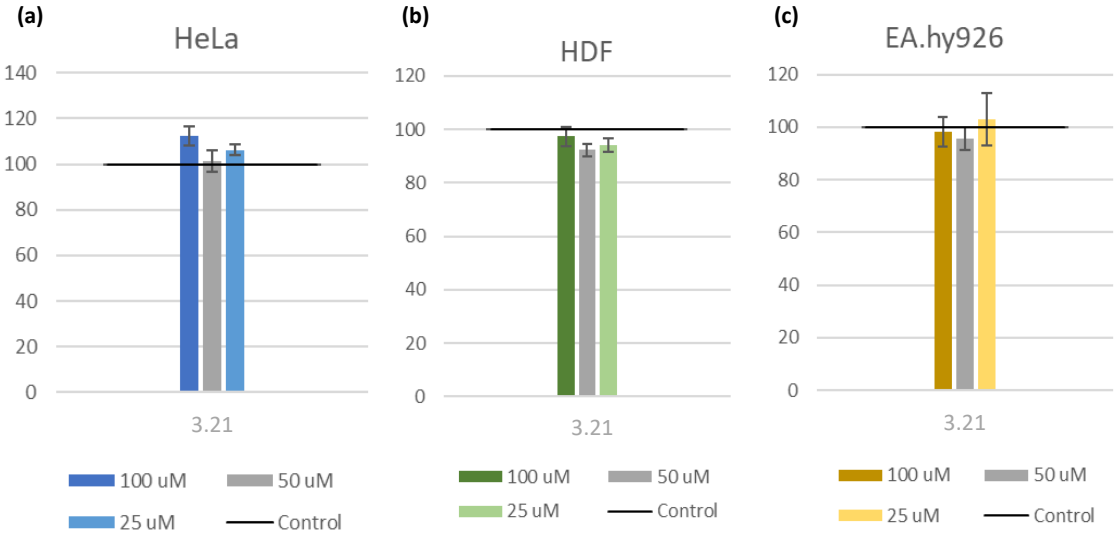

Figure 3.19 Cell viability data for **3.21** in (a) HeLa, (b) HDF and (c) EA.hy926 cells. The error bars represent the calculated standard error of the mean (SEM) from five different experiments, whilst the control line (in black) is set to 100% (untreated cells).

Table 3.3 Results of pilot Re uptake study in HeLa, HDF and EA.hy926 after 2 h incubation at 50 μM.

Sample	Cell Line	Accumulation Ratio (%)	Quantity of Re in cells (μg/mL)	Quantity of protein (μg/mL)	Normalised uptake (μg Re/μg protein)
3.11	HeLa	**8.18 ± 0.01%**	1.836 ± 0.147	72.37 ± 0.58	**0.0254 ± 0.0013**
3.17	HeLa	**8.85 ± 0.01%**	1.102 ± 0.097	90.95 ± 1.15	**0.0121 ± 0.0013**
3.21	HeLa	**3.25 ± 0.00%**	0.296 ± 0.019	53.45 ± 6.70	**0.0055 ± 0.0020**
$Re(CO)_3(H_2O)_3Br$	HeLa	**0.05 ± 0.00%**	0.026 ± 0.005	67.59 ± 4.43	**0.0004 ± 0.0000**
3.11	HDF	**5.40 ± 0.00%**	1.224 ± 0.087	50.89 ± 3.749	**0.0241 ± 0.0025**
3.17	HDF	**5.78 ± 0.01%**	0.682 ± 0.127	56.76 ± 1.301	**0.0120 ± 0.0041**
3.21	HDF	**4.47 ± 0.00%**	0.375 ± 0.036	51.20 ± 3.840	**0.0073 ± 0.0019**
$Re(CO)_3(H_2O)_3Br$	HDF	**0.05 ± 0.00%**	0.023 ± 0.002	61.13 ± 4.481	**0.0004 ± 0.0000**
3.11	EA.hy926	**3.86 ± 0.00%**	0.881 ± 0.087	52.37 ± 3.53	**0.0168 ± 0.0010**
3.17	EA.hy926	**3.34 ± 0.00%**	0.451 ± 0.030	49.72 ± 1.38	**0.0091 ± 0.0006**
3.21	EA.hy926	**1.45 ± 0.00%**	0.139 ± 0.020	46.15 ± 2.32	**0.0030 ± 0.0006**
$Re(CO)_3(H_2O)_3Br$	EA.hy926	**0.01 ± 0.00%**	0.007 ± 0.001	47.09 ± 2.78	**0.0001 ± 0.0000**

N.B. The experimental values for 'quantity of Re in cells' and 'quantity protein' are quoted as means ± standard deviation for an experiment performed in triplicate. The normalised uptake is calculated by dividing the 'quantity of Re in cells' by the 'quantity protein'.

As shown in Table 3.3, the uptake of glycoconjugate complexes **3.11** and **3.17** was significantly higher than that of **3.21** in all three cell lines. The normalised uptake of **3.11** was *ca.* 5-fold that of **3.21** in both HeLa (0.0254 *vs.* 0.0055 µg Re/µg protein) and EA.hy926 (0.0168 *vs.* 0.0030 µg Re/µg protein), and *ca.* 3-fold that of **3.21** in HDF (0.0241 *vs.* 0.0073 µg Re/µg protein). These results therefore confirm that the carbohydrate has a significant effect on uptake, independent of the lipophilic PR_3 moiety. However, as the uptake of **3.21** is between 14-fold (in HeLa) and 30-fold (in EA.hy926) that of $[Re(CO)_3(H_2O)_3Br]$, the phosphine does have some influence on uptake.

Furthermore, the choice in carbohydrate does affect cellular uptake; the quantity of the glucose-containing complex, **3.11**, is approximately twice that of the galactose-containing complex, **3.17**, for all three cell lines. Within HeLa cells, the normalised uptake of glucoside **3.11** is 0.0254 µg Re/µg protein, whilst the normalised uptake of galactoside **3.17** is 0.0121 µg Re/µg protein. This suggests that the Warburg Effect, is likely being exploited, as we see greater selectivity for the glucose containing complex than the galactose containing complex in the cancerous cell line.

When comparing the uptake of **3.11** across each of the three cell lines, the analysis is more complicated. We see essentially no difference in the normalised uptake when comparing HeLa (0.0254 µg Re/µg protein) and HDF (0.0241 µg Re/µg protein), but these values differ from that in EA.hy926 (0.0168 µg Re/µg protein). However, as discussed in Section 3.4.2.1, comparing normalised uptake between cell is not as good a measure as comparing the accumulation ratio for different cell lines and proliferation rates will be different. This is because cell lines grow at different rates[29], so although all studies began with the same number of cells, by the end of the 2 h experiment, the quantity of HeLa cells will exceed that of HDF, as cancerous cells grow more rapidly than healthy cells. Additionally, different cell types (*i.e.* epithelial cells in HeLa, fibroblast cells in HDF, endothelial in EA.hy926) will contain different amounts of protein. Therefore, to compare general uptake between different cell lines, it is more useful to look at accumulation ratios. When we compare the accumulation ratios of **3.11** in HeLa, HDF and EA.hy926 we see values of 8.18% ± 0.01%, 5.40% ± 0.00%, and 3.86% ± 0.00%. This therefore suggests that there are differential uptake rates for the complex, and this effect might be used to differentiate between cells lines in bioimaging applications. Additionally, it is important to note that HDF is not an exact model of a healthy cell line as it has been immortalised.

As a result of the uptake study, it is possible to determine that incorporation of a carbohydrate, such as glucose or galactose, has significantly improved the uptake of the Re(I) complex. Furthermore, the changes we have made to the carbohydrate (incorporation

of a phosphine ligand) have not prevented biorecognition as the cells appear to be able to distinguish between the glucose and galactose moieties, as exhibited by the different uptake of **3.11** *versus* **3.17** within each cell line. However, it is difficult to determine whether we can target cancerous cells in the presence of healthy cells based on the uptake of **3.11** in HeLa, HDF and EA.hy926. This should be further explored by performing *in vivo* tests with the ^{99m}Tc analogue of **3.11** (**3.22**, see Section 3.5.1).

Lastly, in order to put our results into context we have reviewed the literature for similar experiments. In 2014, ICP-MS was used to investigate uptake of a tricarbonyl-Re(I) complex with a selenium-based ligand (Figure 3.20) in HeLa. However, as all results were quoted in µM of Re per 1x10^6 cells, it is difficult to compare these literature uptake values with the ones we have generated in this project. As the dried weight of a HeLa cell is *ca.* 400 picograms, it can be inferred that there are approximately 2500 HeLa cells in 1 µg protein.[30] Therefore, the uptake of **3.11** in HeLa cells after 2 h is approximately 10 µg/1x10^6 cells, or 0.05 µM/1x10^6. This value is significantly lower than that reported for the diseleno-Re(I) complex (0.98 µM/1x10^6 cells), although the incubation time was significantly longer for the diseleno-Re(I) complex (48 h).[31]

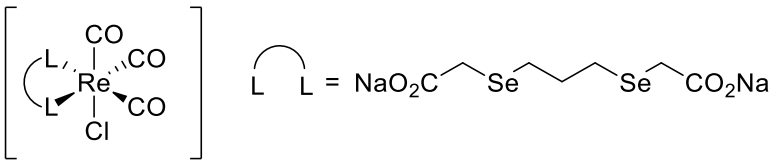

Figure 3.20 Structure of diseleno-Re(I) complex tested in uptake studies.[31]

In a further attempt to put our results into context, we have compared the uptake of our Re(I) complexes with FDA-approved Pt(II) anticancer drugs. Direct comparison again has difficulties because the Pt(II) study investigated the uptake in of these drugs in MCF-7, rather than HeLa, and involved a 24 h incubation of these complexes at 0.1 µM concentration, instead of 2 h incubation at 50 µM concentration. However, when comparing the accumulation ratio of **3.11** (8.18% or 0.082) with the Pt(II) complexes, this most closely resembles that of carboplatin, where the accumulation ration was *ca.* 50% greater (0.162 for carboplatin).[32] Whilst these results suggest that uptake of carboplatin is greater than **3.11**, this cannot be confirmed without testing both the Pt(II) and Re(I) complex in parallel experiments. Given the differences in experimental conditions and cell lines between the two studies, only accumulation ratios were considered.

3.5. Radiolabelling

As a result of the Re coordination studies performed in Section 3.3, radiolabelling of each of the deprotected ligands (**3.1**, **3.3**, **3.4**, **3.5** and **3.7**) was investigated with the $Tc(CO)_3$ core. Full experimental details of this work are reported in Chapter 6.

As discussed in Section 3.1.2, all radiolabelling with the Tc-tricarbonyl core involves a two-step process, as opposed to radiolabelling with the Tc-dioxo core (Chapter 2 & 4), where a single step is required. The tricarbonyl kit, $[^{99m}Tc(CO)_3(H_2O)_3]^+$, is prepared from $[TcO_4]^-$ according to a method outlined by P. Blower *et al.* that results in >90% yield by radio-TLC.[13] Once the ^{99m}Tc-tricarbonyl complex is formed, this can be added to the dissolved ligand. In this work, deprotected ligands were dissolved in a mixture of DMSO (HPLC grade) and MilliQ H_2O, to ensure a good level of solubility was achieved.

3.5.1. Radiolabelling Studies with 3.1

$[^{99m}Tc(CO)_3(H_2O)_3]^+$ was added to **3.1** in 10% DMSO:H_2O. After 30 min at room temperature the reaction mixture was directly injected into the HPLC. This is equipped with a gamma detector to enable the recording of radio-HPLC traces. As shown in the radio-chromatogram, many species were formed under these conditions (Figure 3.21). Note that the peaks at approximately 2.5 min and 3 min are unreacted $[TcO_4]^-$ and $[Tc(CO)_3(H_2O)_3]^+$, respectively.

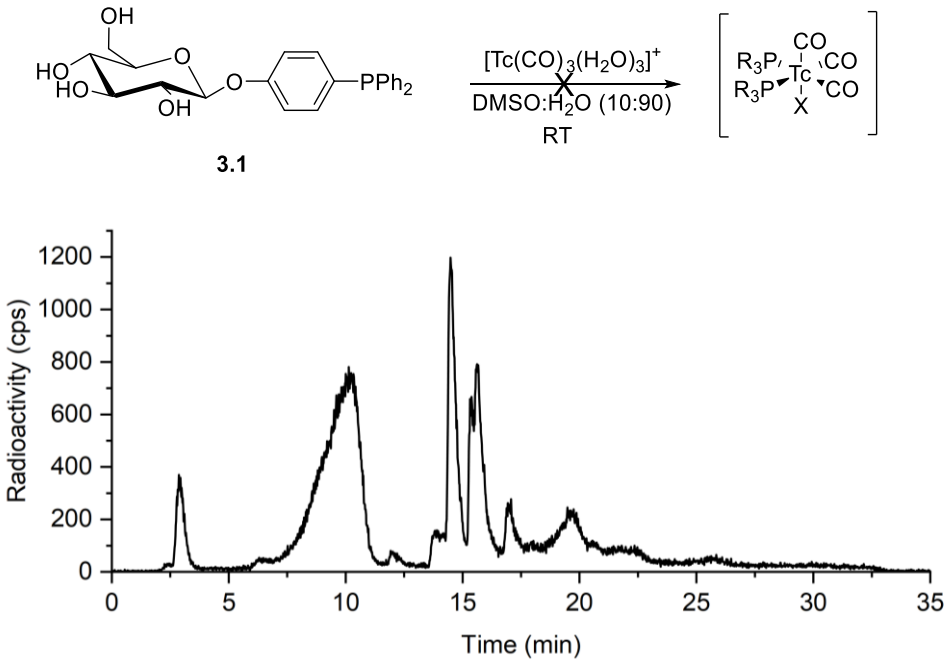

Figure 3.21 HPLC chromatogram for Tc(I) radiolabelling of **3.1** at room temperature, as shown schematically.

Modification of this method, by heating $[Tc(CO)_3(H_2O)_3]^+$ and ligand **3.1** (10% DMSO:H_2O) together at 50°C for 30 min, led to fewer species being formed as shown in the corresponding radio-HPLC chromatogram (Figure 3.22). The major species has a retention time of 13.9 min, when analysed using HPLC Method 1 (Chapter 6).

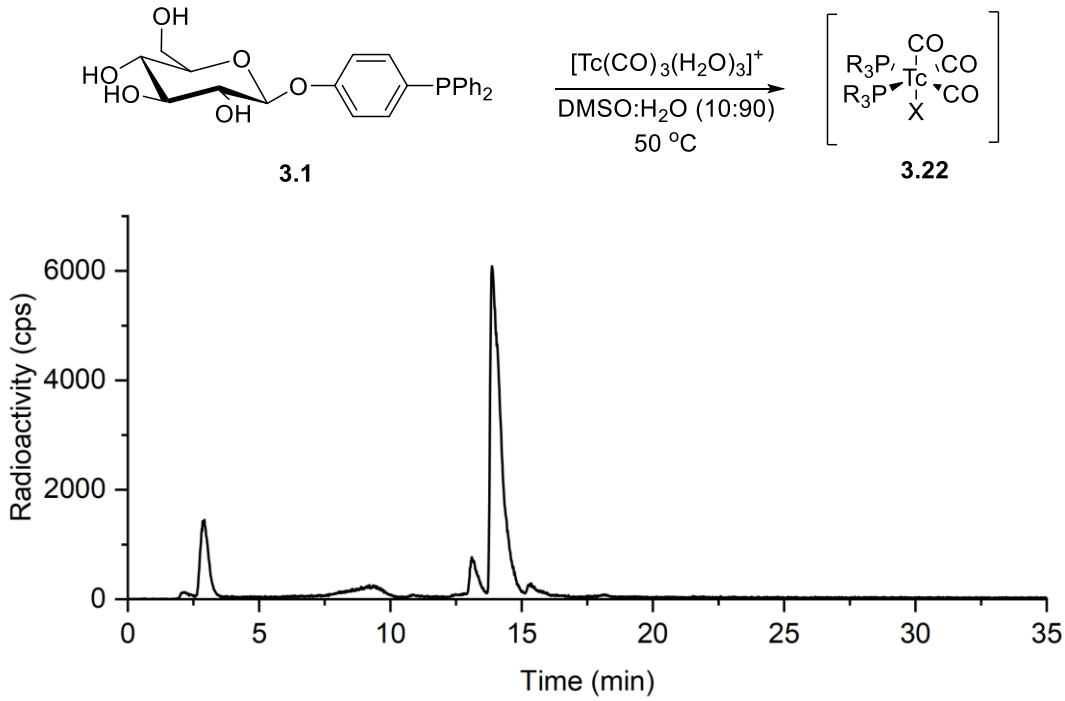

Figure 3.22 HPLC chromatogram for Tc(I) radiolabelling of **3.1** at 50 °C shown schematically.

Often Tc species are identified by co-elution of the non-radioactive analogous Re complex. Unfortunately, the analogous 'cold' Re complex (**3.11**) cannot be co-eluted as it is unstable in MeCN because this solvent displaces the phosphine ligands on the Re centre. Curiously, this effect was not observed for the ^{99m}Tc complex. To account for this, ^{99m}Tc ($t_{1/2}$ = 6h) radiolabelling has since been repeated, but the tricarbonyl kit has been spiked with ^{99}Tc ($t_{1/2}$ = $2x10^5$ years). This isotope of Tc, with a significantly longer half-life, has enabled the isolation of the compound with a 13.9 min retention time by semi-preparatory HPLC. MALDI HR-MS has established that this species is most likely complex **3.22** (*m/z* calcd. for $C_{51}H_{50}O_{15}P_2Cl^{99}Tc$ $[M\text{-}CO\text{-}Cl]^+$ = 1035.1733; obs. = 1035.1721), as the coordination of two ligands to ^{99}Tc can be observed.

The stability of complex **3.22** has been investigated in mouse serum at 37.5 °C, and after 2 h no significant changes were observed in the radio-HPLC trace. Full details of this stability study are given in Chapter 6. The outcome of this test is encouraging, given that this is a monophosphine glycoconjugate ligand. Note that the radio-HPLC chromatogram in Figure

3.23 is significantly noisier than Figure 3.22. This is due to loss in radioactivity over time because of the half-life of ^{99m}Tc ($t_{1/2}$ = 6 h).

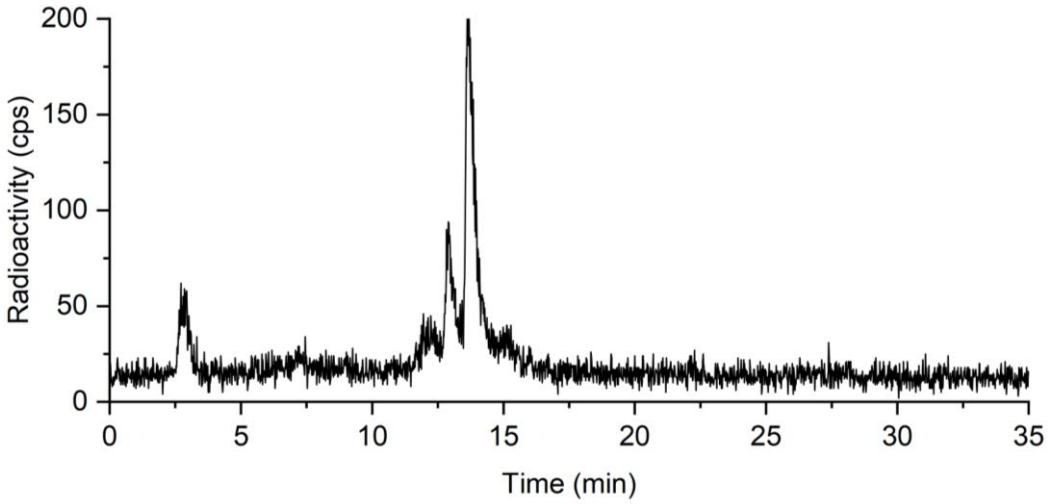

Figure 3.23 HPLC chromatogram from stability testing of complex **3.23** in mouse serum. Chromatogram shows result after 1 h due to decrease in cps over time.

All further radiolabelling work was carried out by Dr Michelle Ma (King's College London) due to the COVID-19 pandemic. This was a consequence of UK Government mandated travel restrictions within the UK (November 2020-March 2021), which was further compounded by the fact that all radiolaboratory facilities at King's College London are located within St Thomas's Hospital, London. The radiolabelling of **3.1** has been further improved by Ma. Increasing the quantity of DMSO from 10% to 37% when dissolving ligand **3.1** in MilliQ water (so DMSO accounts for 24% of the overall mixture once the $[Tc(CO)_3(H_2O)_3]^+$ has been added), has resulted in smaller quantities of unwanted species being formed. A shift in the retention time is observed, but this is a consequence of using a more rapid gradient during HPLC analysis (Method 2, see Chapter 6). Here, the HPLC method was modified so the concentration of solvent B increased from 5-95% over 20 mins (Method 2) as opposed to over 25 mins (Method 1). Therefore, a retention time of 9.3 min (Figure 3.24) is seen (instead of 13.9 min, Figure 3.22).

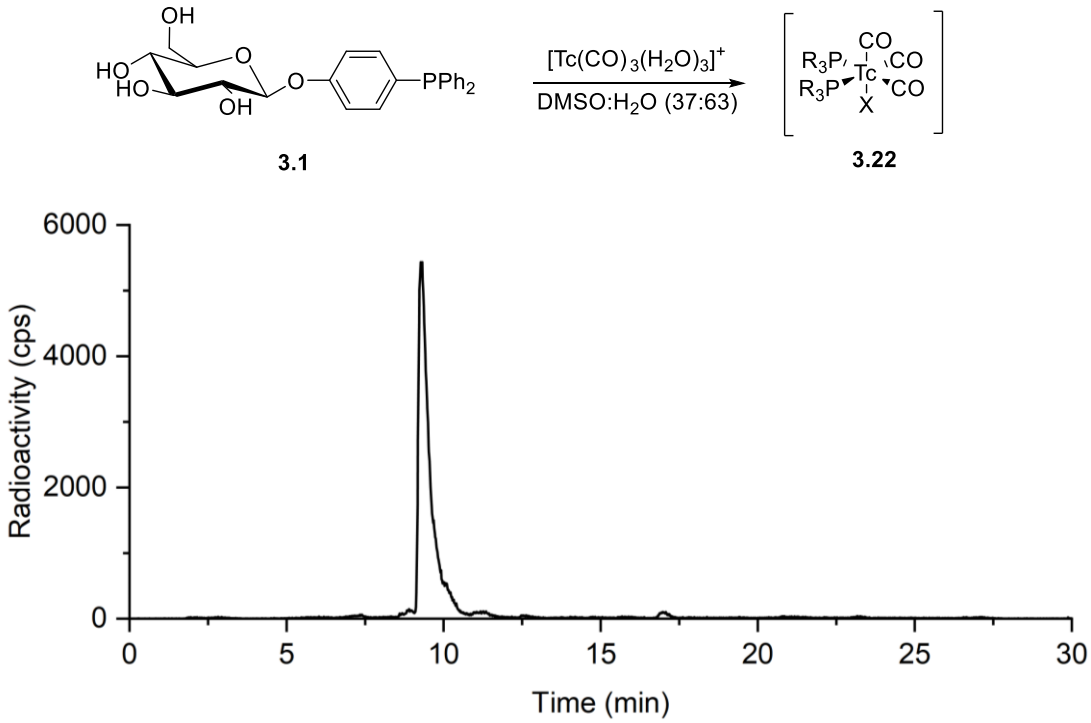

Figure 3.24 HPLC chromatogram for Tc(I) radiolabelling of **3.1** at 50 °C.

3.5.2. Radiolabelling of 3.3

Radiolabelling of **3.3**, where R = *o*-tolyl, was performed by Ma using the same method as before; $[Tc(CO)_3(H_2O)_3]$ (50 µL, 5 MBq) was added to **3.3** (100 DMSO µL in 270 µL H_2O) and the resulting mixture heated at 50°C for 30 min. Comparing the radio-chromatogram at the end of the experiment, with that of the starting material ($[Tc(CO)_3(H_2O)_3]^+$), has revealed that coordination did not occur and radiolabelling was unsuccessful (Figure 3.25). However, this result matches that expected based on the coordination chemistry of **3.3** and $[Re(CO)_3(H_2O)_3]Br$, and so, gives us confidence in our model system.

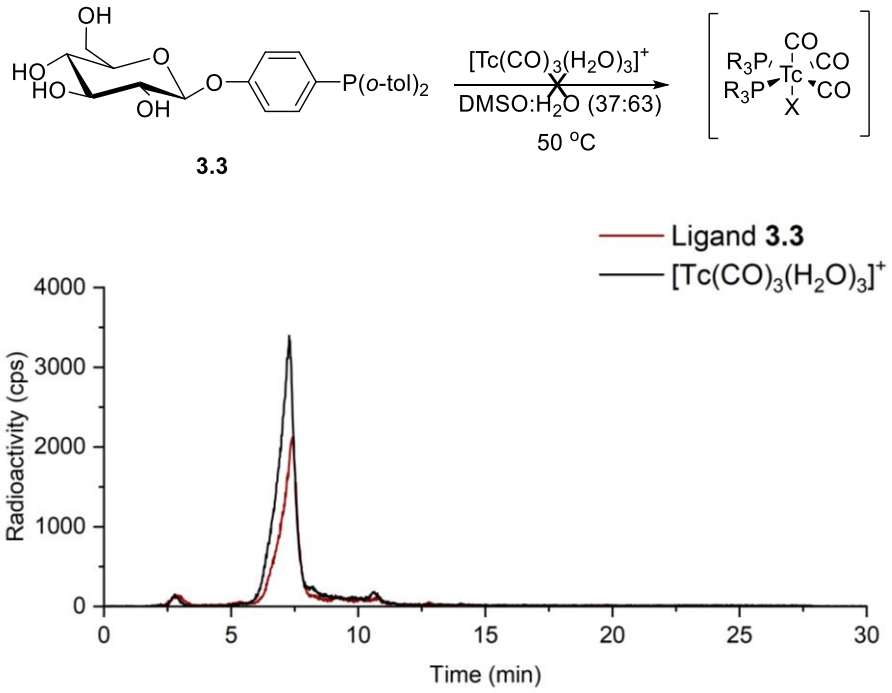

Figure 3.25 HPLC chromatograms of $[Tc(CO)_3(H_2O)]$ before (black trace) and after (red trace) being added to **3.3** at 50 °C.

3.5.3. Radiolabelling of 3.4

Using the same radiolabelling method, ligand **3.4**, where R = *p*-tolyl, was added to $[^{99m}Tc(CO)_3(H_2O)_3]^+$ and heated at 50 °C for 30 min to give the following radio-HPLC trace (Figure 3.26). A single major species was observed with a retention time of 11.4 min, and was assumed to be the expected complex, **3.23** ($[Tc(CO)_3(\mathbf{3.4})_2X]$); 'X' is likely to be a chloride ligand as the ^{99m}Tc tricarbonyl species is formed in saline. The radiolabelling of **3.4** does produce a greater number of unwanted species, compared with **3.1**, under the same conditions. A difference in retention time of +2.1 min is seen for **3.23** compared to **3.22** ($R\text{-}PPh_2$), which demonstrates the increased lipophilicity of **3.23** due to the incorporation of *p*-tolyl groups. As before, the analogous 'cold' Re complex, **3.17**, could not be co-eluted with the radiocomplex, as **3.17** is unstable in MeCN. Due to COVID-related constraints regarding access to facilities for users at KCL, no stability testing or ^{99}Tc labelling have been performed.

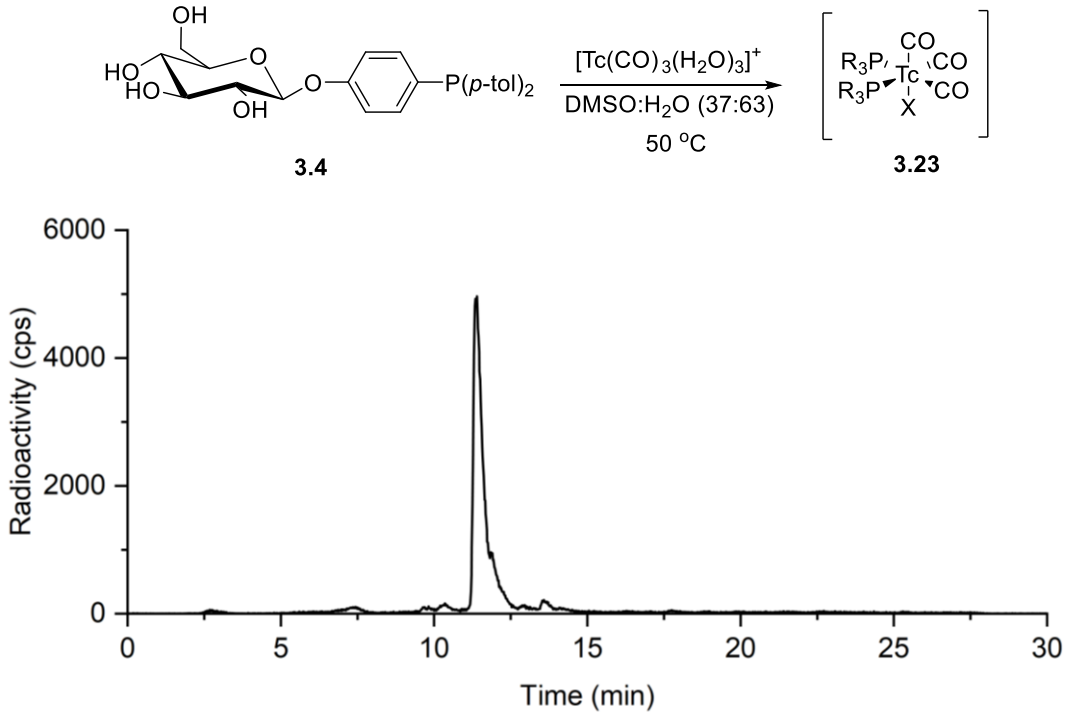

Figure 3.26 HPLC chromatogram for Tc(I) radiolabelling of **3.4** shown schematically.

3.5.4. Radiolabelling of 3.5

A number of species were formed when radiolabelling **3.5** with $[Tc(CO)_3(H_2O)_3]^+$ at 50 °C for 30 min. This was expected, based on the results of the Re coordination chemistry (Section 3.3.4), where complexation was less specific for this ligand compared with aryl R groups. The radio-chromatograph shows a major species at 13.3 min which is assumed to be $[Tc(CO)_3(\mathbf{3.5})_2X]$, where 'X' is likely to be a chloride ligand (Figure 3.27). The difference in retention time for the **3.24** ($PR_2 = PCy_2$) was +4.0 min compared with **3.22** ($PR_2 = PPh_2$). This result was expected, as Cy groups are significantly more lipophilic than Ph groups. As before, no further work has been performed on this complex due to COVID-related constraints regarding access to facilities for all users at KCL.

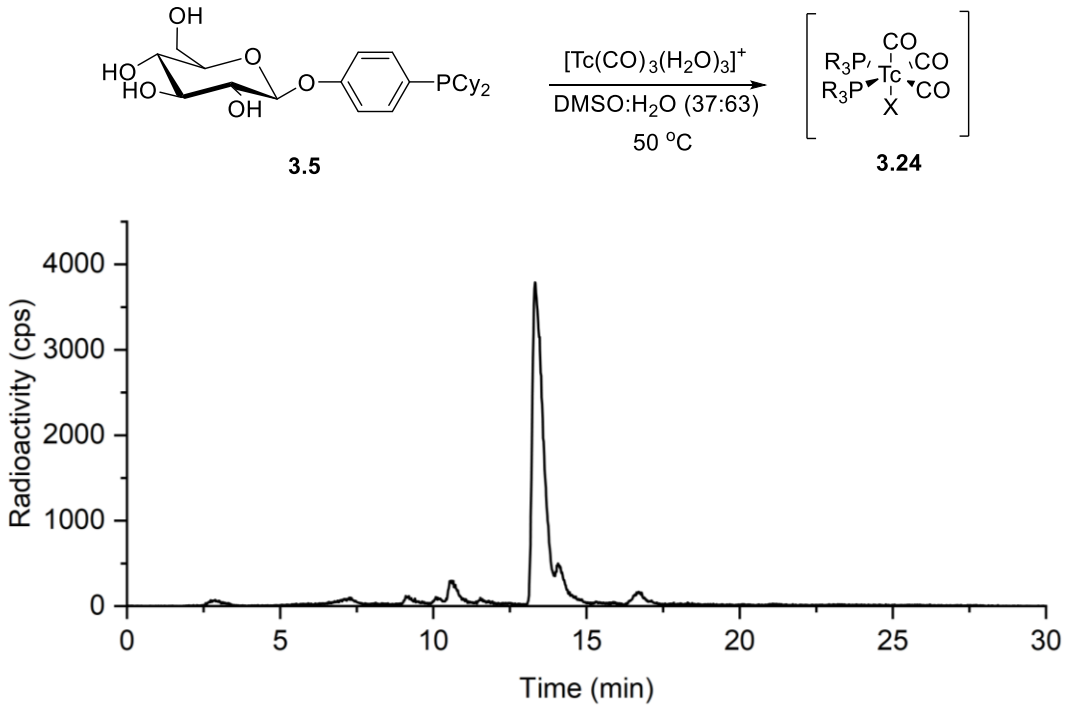

Figure 3.27 HPLC chromatogram for Tc(I) radiolabelling of **3.5** at 50 °C.

3.5.5. Radiolabelling of 3.7

Heating **3.7** (galactose-based glycoconjugate) with $[Tc(CO)_3(H_2O)_3]^+$ at 50 °C for 30 min resulted in the radio-HPLC chromatogram shown in Figure 3.28. A single major species with a retention time of 9.5 min can be seen in the trace which is assumed to be $[Tc(CO)_3$(**3.7**$)_2X]$ (**3.25**), where 'X' is likely a chloride ligand. Two other minor species can be seen at 9.2 and 11.4 min. The radiolabelling of **3.7** and **3.1** is therefore extremely similar, with almost identical retention times (9.5 min versus 9.3 min), and similar levels of product specificity. Based on the similarity of the HPLC chromatograms for **3.22** (Figure 3.24) and **3.25** (Figure 3.28), it is clear the carbohydrate has minimal influence on the radiolabelling. Again, no further work has been carried out on this system because of COVID-related constraints regarding access to facilities for all users at KCL.

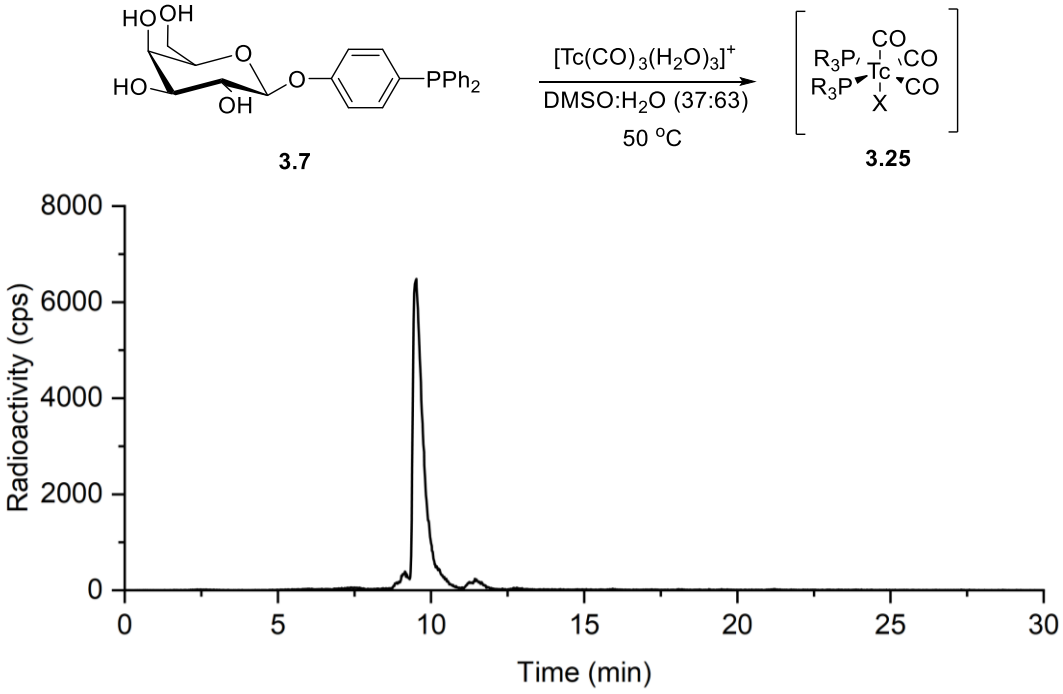

Figure 3.28 HPLC chromatogram for Tc(I) radiolabelling of **3.7** at 50 °C shown schematically.

It is clear from the radiolabelling studies that the Re(I) coordination chemistry of these ligands has provided an accurate model for predicting whether coordination of a ligand to the $^{99m}Tc(CO)_3$ core is possible. Furthermore, the specificity of the radiolabelling is affected by the identity of the R groups on the phosphine moiety, but not by the carbohydrate. Given these results, particularly for the radiolabelling of **3.1**, subsequent work should be directed at testing these ^{99m}Tc complexes *in vivo*. For this work to be done for ligands **3.4**, **3.5** and **3.7**, serum stability testing must first be carried out.

3.6. Conclusions and Future Work

Beller *et al.* have previously synthesised phosphine glycoconjugates **3.1** and **3.7** (Figure 3.29) for applications in biphasic catalysis. Our aim was to investigate the scope of these types of molecules for radio-imaging applications. The phosphine donor has been modified to give ligands where PR_2 = P(*o*-Tol)$_2$ (**3.3**), P(*p*-Tol)$_2$ (**3.4**) or PCy_2 (**3.5**). Furthermore, the carbohydrate moiety was also be modified and, through an alternative procedure for its synthesis, a lactose derivative (**3.10**) was prepared (see Section 3.2 and Figure 3.29). Unfortunately, because the synthesis of **3.10′** (the peracetylated analogue of **3.10**) was not achieved on a synthetically useful scale, the radiolabelling and cellular studies with **3.10** have not been investigated. Subsequent work should focus on improving the synthesis of this ligand to enable further studies, particularly given that this ligand should exhibit greater water solubility which is preferable when testing compounds *in vitro* or *in vivo*.

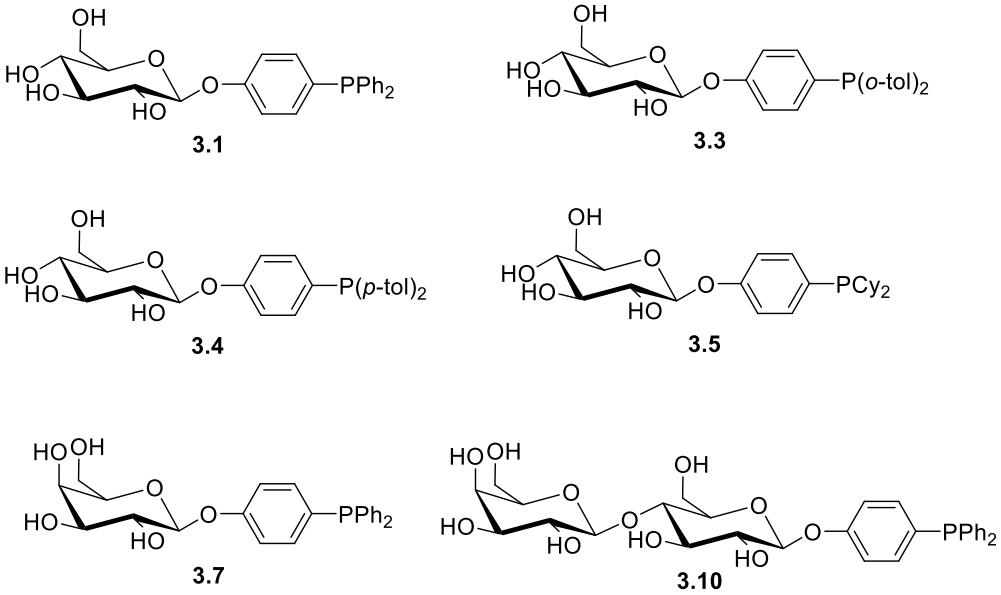

Figure 3.29 Structure of phosphine glycoconjugate ligands studied in this Chapter.

The Re(I) coordination chemistry has been explored for this series of ligands, and complexes with the $Re(CO)_3$ core have been readily synthesised for all the ligands apart from the sterically congested ligand **3.3′** (the peracetylated analogue of **3.3**). In most cases, only a singlet was observed when the rhenium complexes were analysed by $^{31}P\{^1H\}$ NMR spectroscopy. However, for all complexes containing phosphine glycoconjugate ligands an AB splitting pattern should be observed as the complexes exhibit C_1 symmetry, so the phosphine atoms are inequivalent.

The ^{99m}Tc radiolabelling of the glycoconjugate ligands has been investigated since the Re(I) coordination studies were encouraging. Ligands **3.1** and **3.7** gave the most promising ^{99m}Tc radiolabelling results, with high selectivity obtained. However, radiolabelling of **3.5** resulted

in the formation of a number of side products and no radiolabelling of **3.3** (where PR_2 = P(*o*-Tol)$_2$) was observed. The results obtained during the radiolabelling matched those seen in the Re(I) coordination study, and therefore give confidence in the reliability of using Re(I) as a model for ^{99m}Tc behaviour. The serum stability of complex **3.22** (the ^{99m}Tc(CO)$_3$ complex with ligand **3.1**) was investigated and **3.22** demonstrated good stability in mouse serum after 2 h. This is important for any future *in vivo* studies that may be performed.

To determine the effect of the carbohydrate moieties on cellular uptake, Re(I) uptake studies were performed in collaboration with the LMF. First, however, the toxicity of several complexes (**3.11**, **3.15**, **3.17**, **3.21** and [Re(CO)$_3$(H$_2$O)$_3$]Br) was investigated as uptake studies can only be performed on live cells. Although no significant cell death was noted after a 2 h incubation of these complexes with EA.hy926, an increase in metabolic activity was observed in both HeLa and HDF when the complex contained a carbohydrate (**3.11**, **3.15** and **3.17**). As no significant cell death was observed when testing all five complexes, uptake studies were performed. To date, the Re(I) uptake of **3.15** has not been studied but this should be studied in the future.

Re(I) uptake studies have shown that: (i) incorporation of a carbohydrate, such as glucose (**3.11**) or galactose (**3.17**), significantly improved the uptake of the Re(I) complex compared to the carbohydrate-free analogue, **3.21**; and (ii) chemical modifications to the carbohydrate, by incorporating a phosphine moiety, has not prevented biorecognition as each cell line displayed greater uptake for **3.11** *versus* **3.17**. This therefore confirms that receptor recognition is likely to be in effect. However, it has been difficult to determine whether we can target cancerous cells in the presence of healthy cells *in vivo* based on just the uptake data for **3.11** in HeLa, HDF and EA.hy926. This is because any differences in uptake between cell lines appears to depend on the metric chosen (accumulation ratio or normalised uptake). Because only a slight increase in uptake between target and non-target tissue is necessary to enable medical imaging (such as is exhibited by *Myoview*), our preliminary results are promising since small differences in accumulation ratio between different cell lines may be vital (8.18% for HeLa, 5.40% for HDF and 3.86% for EA.hy926 for **3.11**). To definitively answer this question, *in vivo* testing of **3.22** (the ^{99m}Tc analogue of **3.11)** is necessary and will be carried out in the future.

3.7. References

1 M. L. Bowen and C. Orvig, *Chem. Commun.*, 2008, 5077–5091.

2 M. Zhang, Z. Zhang, D. Blessington, H. Li, T. M. Busch, V. Madrak, J. Miles, B. Chance, J. D. Glickson and G. Zheng, *Bioconjug. Chem.*, 2003, **14**, 709–714.

3 B. Thomas, K. C. Yan, X. Le Hu, M. Donnier-Maréchal, G. R. Chen, X. P. He and S. Vidal, *Chem. Soc. Rev.*, 2020, **49**, 593–641.

4 M. Beller, J. G. E. Krauter and A. Zapf, *Angew. Chem. Int. Ed. Eng.*, 1997, **36**, 772–774.

5 K. Glegoła, E. Framery, C. Goux-Henry, K. Michał Pietrusiewicz and D. Sinou, *Tetrahedron*, 2007, **63**, 7133–7141.

6 M. Nishimura, M. Ueda and N. Miyaura, *Tetrahedron*, 2002, **58**, 5779–5787.

7 Y. Cheng, G. Shabir, X. Li, L. Fang, L. Xu, H. Zhang and E. Li, *Chem. Commun.*, 2020, **56**, 1070.

8 J. A. Jackson, I. N. Hungnes, M. T. Ma and C. Rivas, *Bioconjug. Chem.*, 2020, **31**, 483–491.

9 A. Boschi, L. Uccelli and P. Martini, *Appl. Sci.*, 2019, **9**, 1–16.

10 *Technetium-99m Radiopharmaceuticals: Manufacture of Kits*, International Atomic Energy Agency, Vienna, 2008.

11 R. Alberto, R. Schibli, A. Egli, A. P. Schubiger, U. Abram and T. A. Kaden, *J. Am. Chem. Soc.*, 1998, **120**, 7987–7988.

12 Ca Pat., WO 98/48848, 1998.

13 A. Badar, J. Williams, R. T. M. de Rosales, R. Tavaré, F. Kampmeier, P. J. Blower and G. E. D. Mullen, *EJNMMI Res.*, 2014, **4**, 1–8.

14 T. S. Pitchumony, B. Spingler, R. Motterlini and R. Alberto, *Chimia (Aarau).*, 2008, **62**, 277–279.

15 M. Beller, J. G. E. Krauter, A. Zapf and S. Bogdanovic, *Catal. Today*, 1999, **48**, 279–290.

16 Sigma Aldrich, https://www.sigmaaldrich.com/GB/en, (accessed 15 June 2021).

17 A. Chadwick, PhD Thesis, University of Bristol, 2019.

18 I. Hungnes, PhD Thesis, King's College London, 2021.

19 D. Benito-Alifonso, S. Tremel, B. Hou, H. Lockyear, J. Mantell, D. J. Fermin, P. Verkade, M. Berry and M. C. Galan, *Angew. Chem. Int. Ed.*, 2014, **53**, 810–814.

20 V. Carroll, D. W. Demoin, T. J. Hoffman and S. S. Jurisson, *Radiochim. Acta*, 2012, **100**, 653–667.

21 E. Deutsch, K. Libson, J. L. Vanderheyden, A. R. Ketring and H. R. Maxon, *Int. J. Radiat. Appl. Instrum.*, 1986, **13**, 465–477.

22 R. A. Baber, A. G. Orpen, P. G. Pringle, M. J. Wilkinson and R. L. Wingad, *Dalton*

Trans., 2005, **2**, 659–667.

23 G. Y. Kovalev and A. A. Johansson, *Bull. Acad. Sci. USSR Div. Chem. Sci.*, 1985, **34**, 2197–2200.

24 Jp, JP2015/858, 2015.

25 K. Libson, J. Vanderheyden, A. R. Ketring and H. R. Maxon, *Nucl. Med. Biol.*, 1986, **13**, 465–477.

26 S. N. Rampersad, *Sensors (Switzerland)*, 2012, **12**, 12347–12360.

27 E. Agathokleous and E. J. Calabrese, *Toxicology*, 2019, **145**, 152249.

28 C. Zhang, C. Li, S. Chen, Z. Li, L. Ma, X. Jia, K. Wang, J. Bao, Y. Liang, M. Chen, P. Li, H. Su, S. M. Y. Li, K. Liu, J. Wan and C. He, *Scientific Reports*, 2017, **7**, 41082.

29 A. L. Risinger, N. F. Dybdal-Hargreaves and S. L. Mooberry, *Anticancer Res.*, 2015, **35**, 5845–5850.

30 Thermofisher Scientific, https://www.thermofisher.com/uk/en/home/references/ambion-tech-support/rna-tools-and-calculators/macromolecular-components-of-e.html, (accessed 10 August 2021).

31 P. Collery, G. Bastian, F. Santoni, A. Mohsen, M. Wei, T. Collery, A. Tomas, D. Desmaele and J. D'Angelo, *Anticancer Res.*, 2014, **34**, 1679–1690.

32 A. R. Ghezzi, M. Aceto, C. Cassino, E. Gabano and D. Osella, *J. Inorg. Biochem.*, 2004, **98**, 73–78.

Chapter 4 : Towards Diphosphine Glycoconjugates

4.1. Introduction

The overall performance of a radiopharmaceutical is affected by several key components in its structure, and these include: the radiometal, the chelator, the targeting moiety and the linker (Figure 4.1). Each of these components affect the application, uptake, and stability of the radiopharmaceutical.

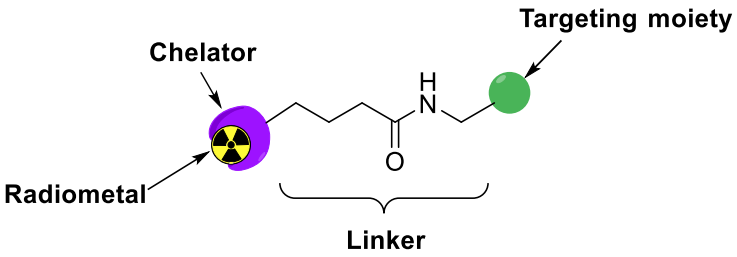

Figure 4.1 A general structure of a conjugated radiopharmaceutical.

The objective of this project is to develop imaging agents capable of detecting cancerous cells where the selected radiometal and targeting vector are ^{99m}Tc and a carbohydrate molecule, respectively. Because of the efficacy of *Myoview* (Figure 4.2), all binding moieties considered within this project have been phosphine-based, whilst the linker has been varied significantly to enable conjugation of the carbohydrate to the phosphine based binding moiety.[1]

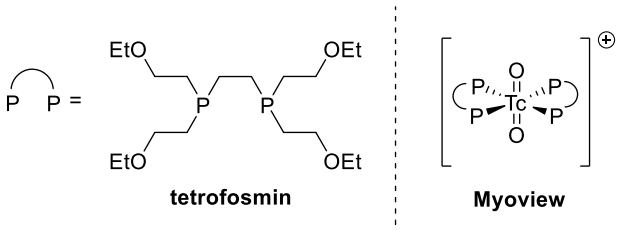

Figure 4.2 Structure of *Myoview*, and the diphosphine ligand that it utilises.

The ^{99m}Tc-glycoconjugates discussed previously (Chapters 2 and 3) have focused on mono-phosphine derivatives, and although the Tc-glycoconjugate containing ligand **3.1** (Chapter 3, Section 3.5.1) displayed good serum stability, ligand **2.21** (Chapter 2, Section 2.4) did not (Figure 4.3). Consequently, the aim of the work described in this Chapter was to improve on this.

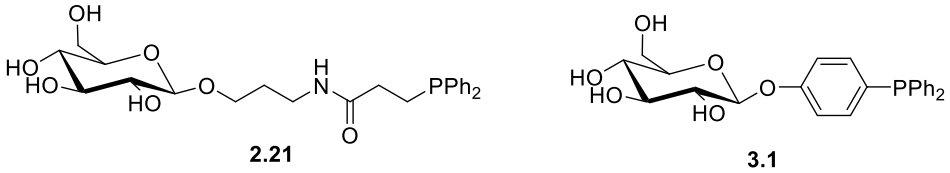

Figure 4.3 Structure of ligands **2.21** (Chapter 2) and **3.1** (Chapter 3) that were radiolabelled with ^{99m}Tc and underwent serum stability testing.

Whilst the choice of chelator is fairly simple for radio-metals that adopt just one oxidation state in an aqueous solution (*e.g.* Ga^{3+}), this choice becomes more complex for those which can adopt many (*e.g.* ^{99m}Tc/^{188}Re).[2,3] To generate an effective radiopharmaceutical the complexation kinetics, thermodynamic stability, kinetic inertness, and *in vivo* stability of the complex are vital. Each of these factors will be affected by the choice of chelator.

Fast complexation kinetics are important, especially for radio-metals with a short half-life, and consequently complexation within 15 min is preferred in the clinic. Additionally, complexation at lower temperatures (*e.g.* room temperature) is also beneficial, as many radiopharmaceuticals use biological targets, such as antibodies or peptides that are denatured at elevated temperatures.[4] In this respect, the choice of a carbohydrate as the targeting vector is advantageous as radiolabelling can be performed at higher temperatures (*e.g.* 80 °C) due to their thermal stability.[5,6] The thermodynamic stability of the complex also crucial when designing a radiopharmaceutical, and can be measured by the thermodynamic stability constant, as expressed in Equation 2. Whilst high values (K_{eq} > 1000) are favoured for radiometal-complexes, this becomes less important at high dilution (*i.e. in vivo*). At this point, the kinetic stability becomes increasingly important as dissociation of the ligand becomes significantly more likely (and $k_{dissociation}$ increases).[4] The kinetic stability dominated the *in vivo* stability. This is a critical factor in radiopharmaceutical performance because it is crucial that the ligand is not displaced from the radiometal by other molecules. If this occurs, it will disrupt the biodistribution and therefore the application of the radiopharmaceutical.[7]

$$M^{m+} + n\,L \rightleftharpoons ML_n^{m+} \qquad \text{Equation 1}$$

$$K_{ML} = \frac{[ML_n^{m+}]}{[M^{m+}][L]^n} = \frac{k_{complexation}}{k_{dissociation}} \qquad \text{Equation 2}$$

The chelate effect states that the coordination affinity of a ligand will increase with increasing denticity, compared with the monodentate counterpart.[8] This effect will have a positive impact on each of the factors highlighted above (*i.e.* rate of complexation, thermodynamics, kinetics and *in vivo* stability). Therefore, by synthesising bidentate

phosphine glycoconjugates, the stability and rate of coordination with ^{99m}Tc should increase, compared to monodentate phosphine glycoconjugates.

^{99m}Tc (and ^{188}Re) complexes in the +1 and +5 oxidation state are favoured for radiochemical applications, although these metals are capable of forming complexes with a wider range of oxidation states (-1 to +7).[9] When M = Tc/Re(I), the complexes contain the *fac*-$[M(CO)_3]^+$ moiety (Figure 4.4) and tridentate and bidentate ligands are favoured for stable radiopharmaceutical formation. Alternatively, $[M{=}O]^{3+}$, $[M{\equiv}N]^{2+}$ and $[MO_2]^+$ cores are the most favoured moieties for M = Tc/Re(V) complexes (Figure 4.4).[4] This project has focused on the $[MO_2]^+$ core when forming Tc/Re(V) complexes, which generally favours tetradentate and bidentate ligands.[4] The research described in this Chapter is focused on the synthesis of bidentate phosphine conjugates.

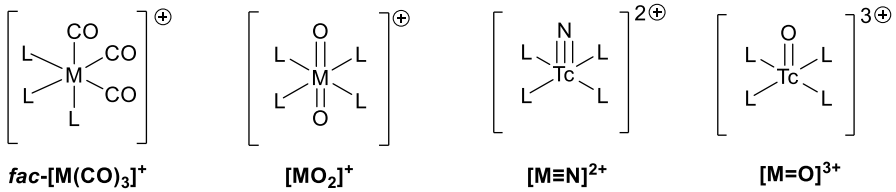

Figure 4.4 Commonly used cores in radiochemistry, where M = Tc/Re.

As discussed in Chapter 1, there are very few reported examples of phosphine glycoconjugate ligands, and even fewer that contain a bidentate phosphine. One such example is elpanphos-a'; this was reported by Ruffo *et al.* and has been formed *via* amide coupling (Figure 4.5).[10] This is beneficial because amide coupling is a more amenable method for the formation of a wide variety of structures compared with the sp^2-sp^2 Pd cross-coupling method used by Beller *et al.*[11] Elpanphos-a' is based on a ligand that was designed by Trost for asymmetric allylation catalysis.[12] However, the *trans*-cyclohexanediamine moiety of the Trost ligand was replaced by a glucodiamine group. Elpanphos-a' was tested as a ligand for the Pd catalysed desymmetrisation of meso-cyclopent-2-ene-1,4-diol, where an enantiomeric excess (ee) of 96%, and conversion of >99%, could be achieved after 5 min reacting in THF. Additionally, this Pd catalyst exhibited excellent enantioselectivity (90-94% ee) in ionic liquids, even after twice recycling the catalyst (79-77% ee).[10] Despite its reported ease of synthesis and desirable structural attributes, this particular glycoconjugate is unlikely to exhibit efficient GLUT-1 recognition due to its di-substituted glucosamine backbone (despite GLUT-1 possessing some affinity for D-glucosamine).[13] Nonetheless, it remains an interesting glycoconjugate within the context of this project.

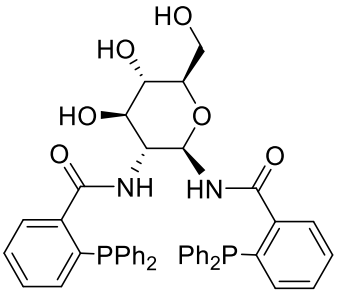

Figure 4.5 Structure of diphosphine glycoconjugate elpanphos-a', reported by Ruffo et al.[10]

4.2. Routes towards a 1,2-bis(diphenylphosphino)benzene-based glycoconjugate

Following the successful synthesis of a small library of monophosphine glycoconjugate ligands in Chapter 3, the next targets were bidentate phosphine glycoconjugates. The most obvious modification to ligand **3.1** (Chapter 3, Section 3.1), was to introduce a second PPh_2 moiety *ortho* with respect to the original PPh_2 group (Figure 4.6, **4.1**). As the binding moiety of **4.1** would mimic that of 1,2-bis(diphenylphosphino)benzene (dppbz), initial work was centred on the unexplored Re(I) and Re(V) coordination chemistry of dppbz.

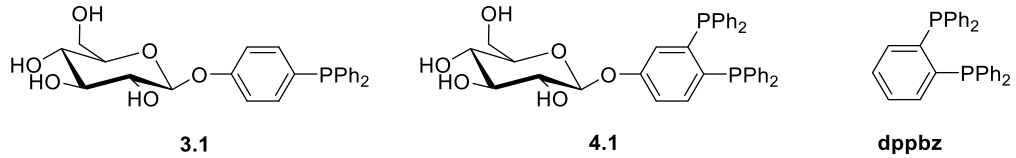

Figure 4.6 Structure of monophosphine glycoconjugate **3.1**, its bidentate analogue **4.1** and dppbz.

4.2.1. Coordination of dppbz to Re(I) and Re(V) cores

Complex **4.2** was formed overnight following addition of 1 eq. of dppbz to $[Re(CO)_3(H_2O)_3]Br$. As **4.2** precipitated from the reaction mixture, the product was isolated by filtration (Scheme 4.1). As expected, two water ligands were replaced by the phosphine ligand, whilst the third aqua group was replaced by the bromide counter-ion. This gave a neutral complex overall, as evidenced by a new a singlet at 30.4 ppm in the $^{31}P\{^{1}H\}$ NMR spectrum. The large coordination shift of $\Delta\delta$ = 44.4 ppm, contrasts with the coordination shifts for monophosphine ligands ($\Delta\delta$ = 5.3 ppm for the analogous complex with **3.1**). This difference is associated with the ring effect that is characteristic of 5-membered chelates such as those formed by dppbz. The identity of complex **4.2** has been confirmed by HR-MS (*m/z* calcd. for $C_{33}H_{24}O_3P_2Re$ ($[M\text{-}Br]^+$) = 717.0758; obs. = 717.0751), but unfortunately crystals suitable for X-ray diffraction have not been obtained.

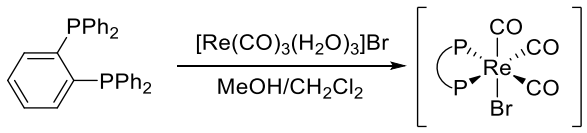

Scheme 4.1 Synthesis of the Re(I) complex **4.2**.

Two equivalents of dppbz were found to react rapidly with $[ReO_2I(PPh_3)_2]$ to give complex **4.3** (Scheme 4.2). Here, two dppbz ligands have coordinated to the Re(V)-dioxo core to give a positively charged complex, where the counter-ion is assumed to be an iodide. This species was precipitated from CH_2Cl_2 by addition of hexane to give **4.3**, which has a $^{31}P\{^1H\}$ NMR shift of 14.7 ppm and a coordination shift of $\Delta\delta$ = 28.7 ppm. The identity of **4.3** has also been confirmed by HR-MS ($C_{60}H_{48}O_2P_4Re$ ($[M]^+$) = 1111.2162; obs. = 1111.2150.). This contrasts with monodentate ligand **3.1,** that did not coordinate to the Re(V) core. This difference in reactivity has been attributed to the chelate effect, whereby dppbz readily displaces the PPh_3 ligands of the Re(V) precursor due to the chelate effect.

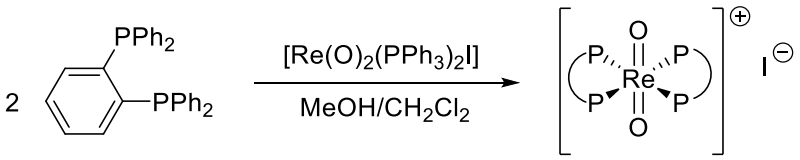

Scheme 4.2 Synthesis of the Re(I) complex **4.3**.

As Re coordination proceeded rapidly with dppbz, the synthesis of the glycoconjugate ligand **4.1** was attempted.

4.2.2. Routes towards 'dppbz'-based phosphine glycoconjugates

4.2.2.1. Modification of the phosphine moiety to prepare 'dppbz'-based diphosphine

Our aim was to synthesise **4.1** (Scheme 4.3(b)) using a similar method to the one outlined in Chapter 3 to give the lactosyl-based phosphine glycoconjugate **3.10** (Scheme 4.3(a)). When synthesising **3.10**, (4-hydroxyphenyl)diphenylphosphine was reacted with acetobromo-α-D-lactose. Crucially this phosphine can be synthesised from 4-bromophenol (Scheme 4.4(a)). To prepare **4.1** *via* a related route, acetobromo-α-D-glucose would be reacted with the novel 3,4-bis(diphenylphosphino)phenol (**4.4**). Unfortunately, only 3,4-dichlorophenol is commercially available, whilst the 3,4-dibromo- and 3,4-diiodophenol are not.

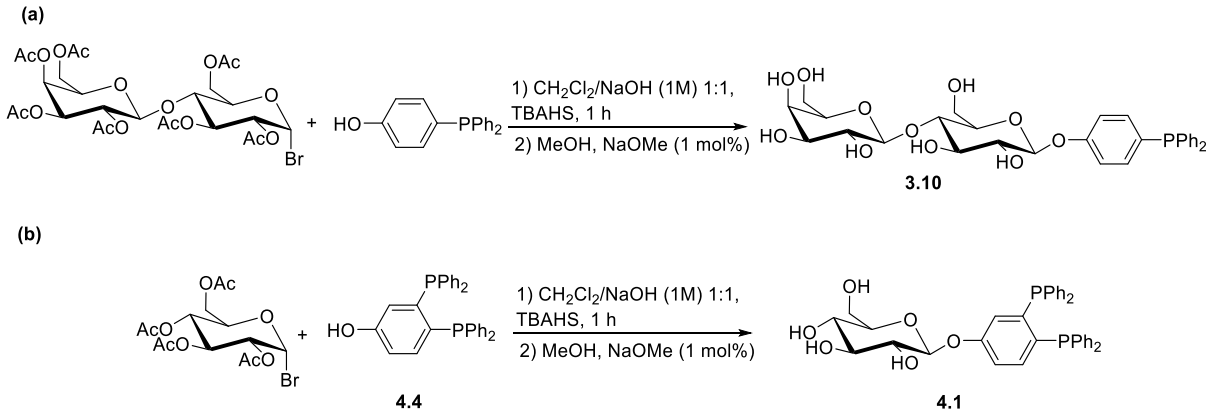

Scheme 4.3 (a) Synthesis of **3.10**, as reported in Chapter 3 and (b) a theoretical route for the synthesis of **4.1**. Both procedures are based on that by Beller *et al.* in 1997.[14]

Nonetheless, the synthesis of dppbz from 1,2-dichlorobenzene and $NaPPh_2$ has been reported in the literature (albeit with a yield of 10%), and therefore, this method was incorporated in *Step II* of our attempted synthesis of **4.4** (Scheme 4.4(b)).[15]

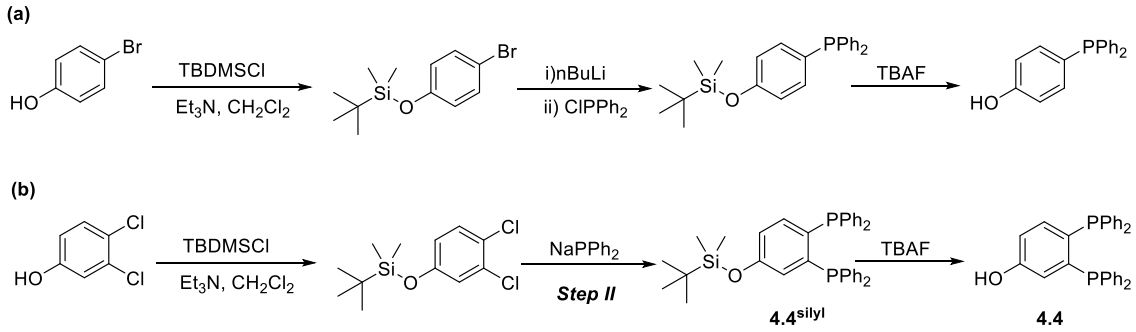

Scheme 4.4 (a) A literature route to (4-hydroxyphenyl)diphenylphosphine.[16] (b) A hypothetical route to **4.4** based on commercially available starting material, 3,4-dichlorophenol.

Prior to attempting the synthesis of **4.4**, initial work focused on reproducing the literature synthesis of dppbz from $NaPPh_2$ and 1,2-dichlorobenzene (Scheme 4.5) as this is analogous to our desired reaction between $NaPPh_2$ and *tert*-butyl(3,4-dichlorophenol)dimethyl silane (***Step II***, Scheme 4.4(b)).[15]

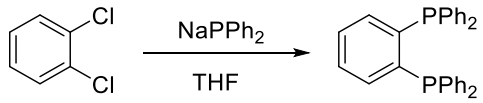

Scheme 4.5 Synthesis of dppbz from 1,2-dichlorophenol, as originally reported by Schmidbaur et al.[15]

Performing the reaction in THF gave rise to a number of signals in the $^{31}P\{^{1}H\}$ NMR spectrum of the crude product including: PPh_3 (-6.0 ppm, 45% *in situ* yield), 1-chloro-2-(diphenylphosphino)benzene (-11.5 ppm, 6.4% *in situ* yield), dppbz (-13.6 ppm, 4.5% *in situ* yield) and an unidentified species at -16.1 ppm (28% *in situ* yield) (Figure 4.7). Based on the chemical shift, it was postulated that this was either 4-diphenylphosphyl-butan-1-ol or Ph_2P-PPh_2. Because no rapid oxidation occurred when the product was exposed to air it seemed unlikely that this was Ph_2P-PPh_2. Therefore, the signal at -16.1 ppm was tentatively assigned to 4-diphenylphosphyl-butan-1-ol, as it can readily be formed by a ring-opening reaction between $NaPPh_2$ and the solvent, THF.[17]

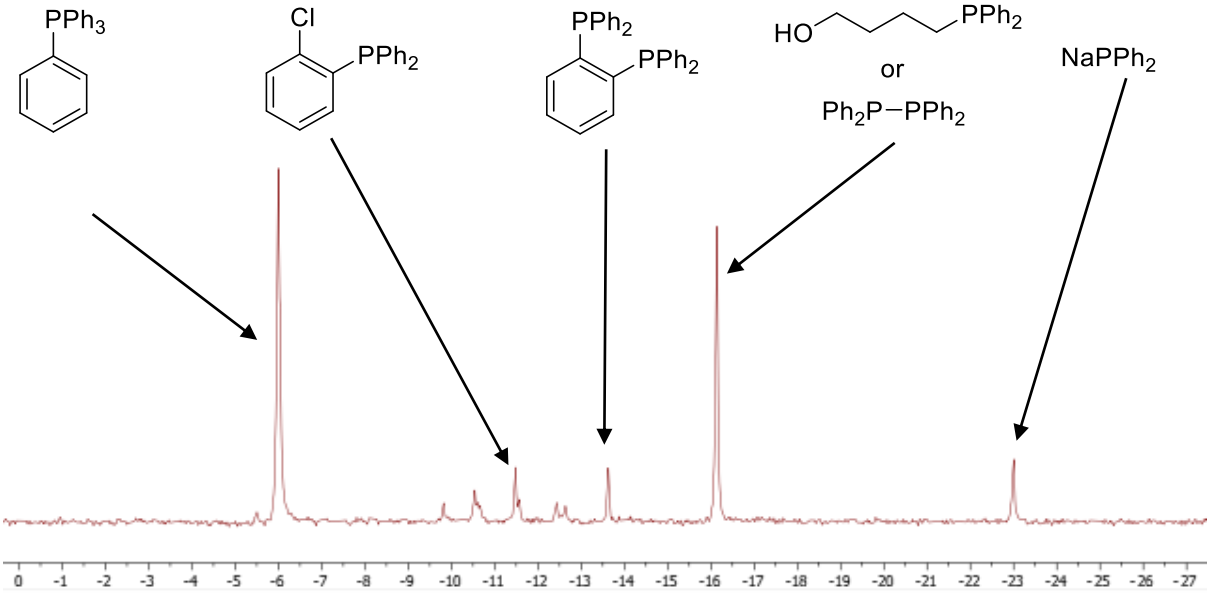

Figure 4.7 *In situ* $^{31}P\{^{1}H\}$ NMR spectrum showing the product mixture formed by reacting $NaPPh_2$ and 1,2-dichlorobenzene in THF for 16 h.

Repeating this reaction in 1,4-dioxane gave a similar product profile, although dppbz accounted for 6% of the $^{31}P\{^{1}H\}$ *in situ* mixture (Figure 4.8). This result therefore suggests that the species at -16.1 ppm, seen previously, may not be 4-diphenylphosphenyl-butan-1-ol, and instead may be $Ph_2P\text{-}PPh_2$. This was supported by aqueous work-up of the reaction in air, whereby oxidation of $Ph_2P\text{-}PPh_2$ was observed. Silica-plug purification after an aqueous work-up led to a final product mixture containing just PPh_3, 1-chloro-2-(diphenylphosphino)benzene and dppbz. No further purification steps were performed. We hypothesise that during the reaction, a chlorine is abstracted from 1,2-dichlorobenzene, thereby leading to the *in situ* formation of $ClPPh_2$ and 1-chlorobenzene. These intermediates can then react with $NaPPh_2$ to form $Ph_2P\text{-}PPh_2$ and PPh_3, respectively. This appears to be a major pathway during this reaction as these two species ($Ph_2P\text{-}PPh_2$ and PPh_3) account for 65-70% of the product mixture. Preventing these side-reactions from occurring would be essential to improving this reaction.

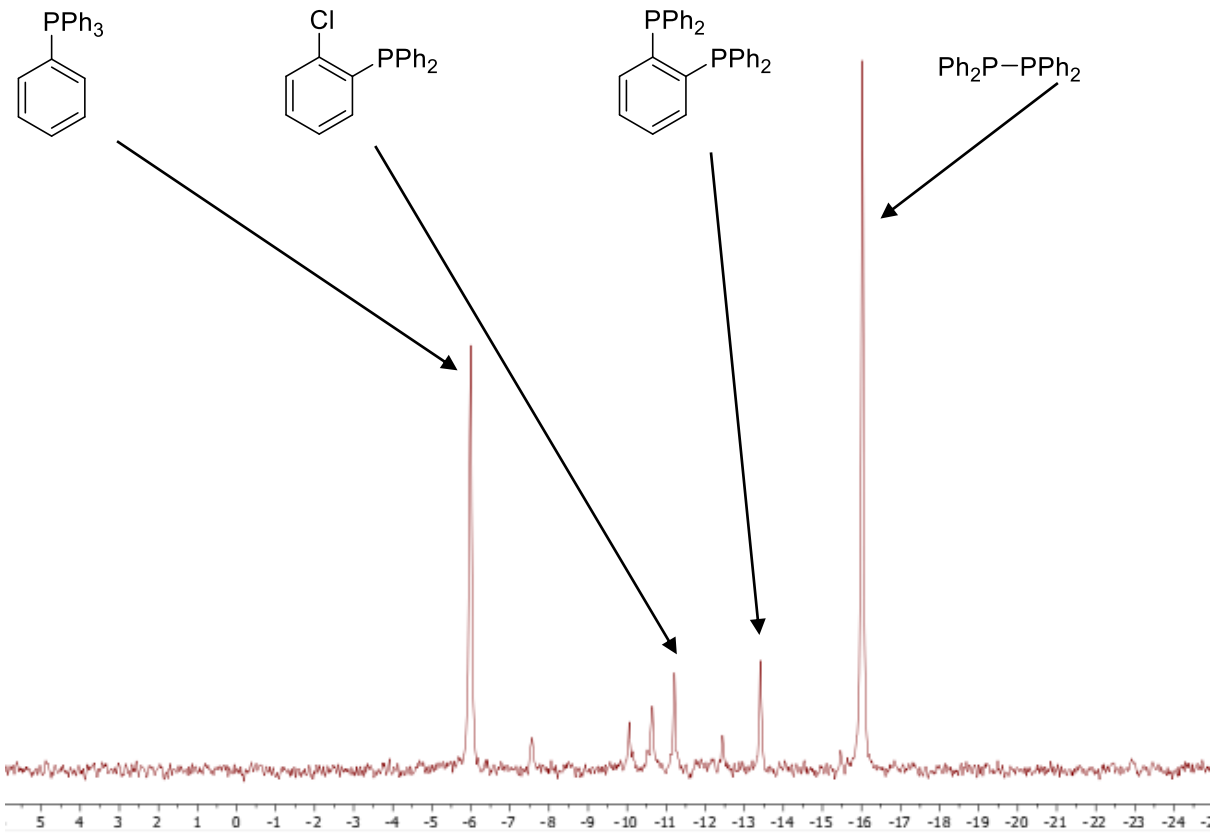

Figure 4.8 *In situ* $^{31}P\{^{1}H\}$ NMR spectrum showing the product mixture formed by reacting $NaPPh_2$ with 1,2-dichlorobenzene in dioxane for 16 h.

Due to time constraints on this project, the above reaction was applied to 3,4-dichlorophenol without any further optimisation, despite the issues described above when using 1,2-dichlorobenzene. The phenolic group was first protected by silylation as shown in Step 1 of Scheme 4.4(b). After work up, the silyl protected analogue was dried over P_2O_5 because 4 Å molecular sieves proved insufficient. Reacting **4.4**^{silyl} with $NaPPh_2$ in dioxane led to the formation of a complex mixture, as shown by $^{31}P\{^1H\}$ NMR spectroscopy (Figure 4.9). Aqueous work-up and silica plug purification led to the removal of the P^V by-products, and a majority of the Ph_2P-PPh_2 from the crude mixture. However, many species still remained and we hypothesise that these include: (3-hydroxphenyl)- and (4-hydroxyphenyl)diphenylphosphine (-6.1 and -7.2 ppm, 49% *in-situ* yield), 4-chloro-3- and 3-chloro-4-(diphenylphosphaneyl)phenol (-11.6 and -13.1 ppm or -13.1 and -14.4 ppm, 14-24% *in situ* yield), **4.4**^{silyl} (-15.4 ppm, 3% *in situ* yield) and Ph_2P-PPh_2 (-16.7 and ppm, 10% yield). Despite this, HR-MS has confirmed the presence of **4.4**^{silyl} in this mixture, and future work should investigate how to improve the synthesis of this molecule (Section 4.6).

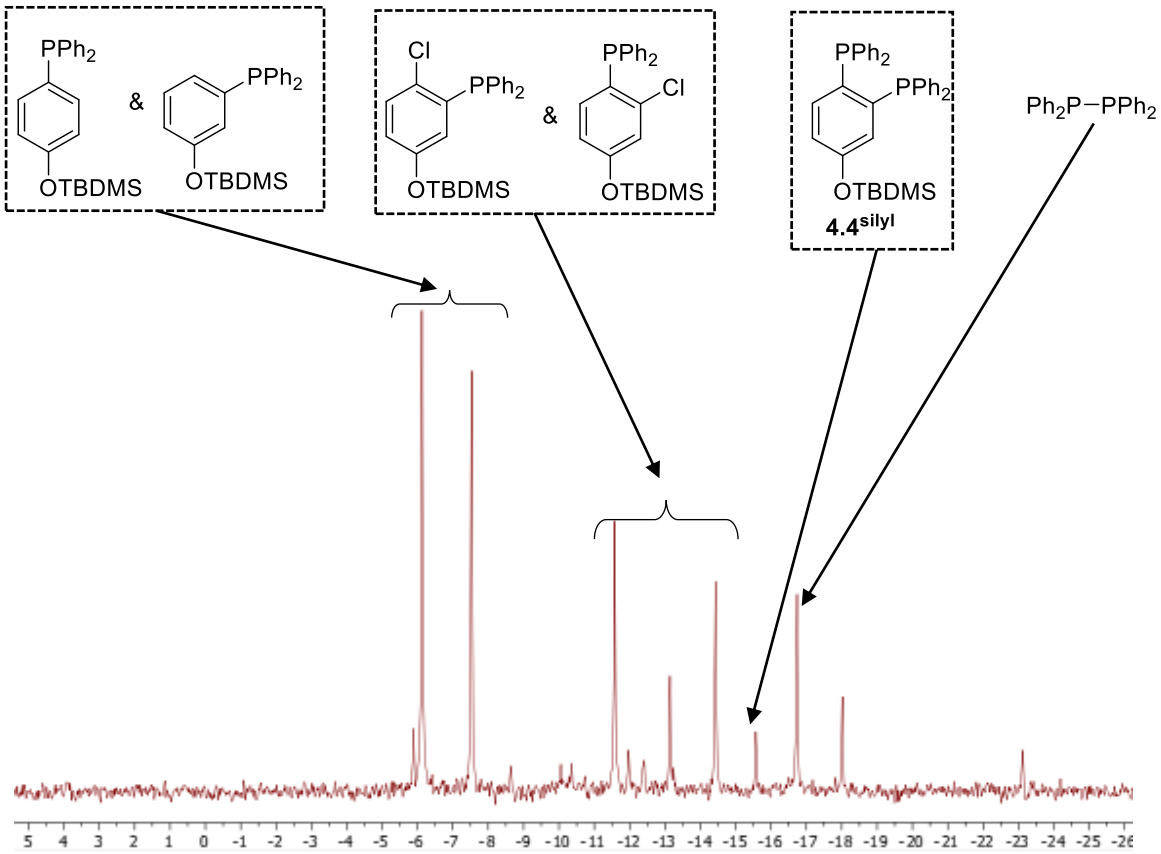

Figure 4.9 *In situ* $^{31}P\{^1H\}$ NMR spectrum showing the product mixture formed by reacting $NaPPh_2$ and **4.4**^{silyl} in dioxane for 16 h.

4.2.2.2. Modification of the carbohydrate moiety to prepare a 'dppbz'-based diphosphine

As pre-forming **4.4** proved unsuccessful, the palladium-catalysed route used to form **3.1** in Chapter 3 was re-investigated. Monophosphine **3.1** was prepared by reacting $HPPh_2$ with carbohydrate **3.2** (Figure 4.10(a)) in the presence of a palladacycle catalyst. Therefore, to prepare **4.1** *via* this method, we first needed to prepare carbohydrate **4.5** (Figure 4.10(b)).

Whilst carbohydrate **3.2** was prepared from acetobromo-α-D-glucose and 4-iodophenol, 3,4-diiodophenyl cannot be readily purchased or synthesised. As a result, **4.5** was deemed too challenging a target. There was however precedent in the literature for the synthesis of 1,2-diiodophenol (a structural isomer of 3,4-diiodophenol).[18] It was hoped that reacting acetobromo-α-D-glucose and 1,2-diiodophenol should give **4.6** (Figure 4.10(c)) and this could subsequently be reacted with $HPPh_2$ in the presence of a palladacycle catalyst to give **4.7** (a structural isomer of the original target, **4.1**, Scheme 4.6).

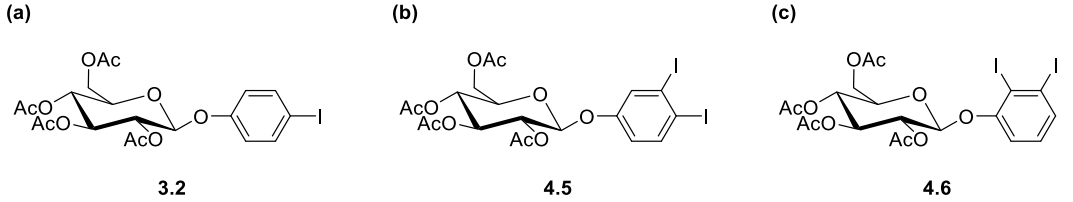

Figure 4.10 Structurally relevant mono- and diiodo-based glycoconjugates.

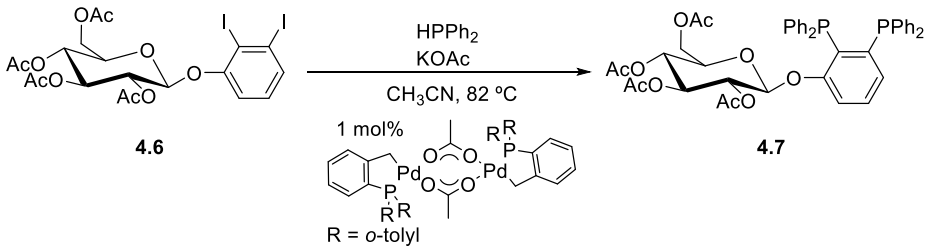

Scheme 4.6 Theoretical route to 4.7 from 4.6 and $HPPh_2$.

1,2-diiodophenol is prepared as described in the literature in three steps: (i) protection of the phenol group with a carbamate (ii) introduction of a second iodo-group and (iii) deprotection of the carbamate group (Scheme 4.7).[18] However, due to chemical supply issues, this literature procedure was modified and diisopropylcarbamoyl chloride was used instead of diethylcarbamoyl chloride. This small modification was expected to have a negligible impact on the outcome of the reaction. However, despite the first two steps proceeding in good yield (67% yield over two steps), the final deprotection step did not work. When using diethylcarbamoyl chloride we were able to access 1,2-diiodophenol (Scheme 4.7). The major flaw with this reaction is the scale that 1,2-diiodophenol can be synthesised on; only 90 mg of 1,2-diiodophenol could be isolated from 1 g of 3-iodophenol (10% yield for the deprotection step, and 4% yield overall), and consequently this significantly affected the

scale that subsequent reactions could be performed on. Nonetheless, routes to **4.6** were investigated.

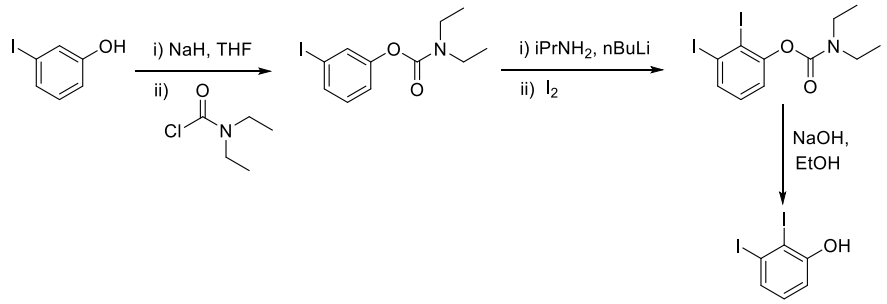

Scheme 4.7 Three-step literature route to 1,2-diiodophenol, by Byers *et al*.[18]

Because carbohydrate **4.8** has been previously reported,[19] this procedure was investigated for the synthesis of **4.6** (Scheme 4.8). Despite the similarity between **4.8** and the desired product **4.6**, no evidence of conjugation between acetobromo-α-D-glucose and 1,2-diiodophenol was observed when using the literature conditions. Instead, only 2,3,4,6-tetra-O-acetyl-β-D-glucose and starting materials were obtained.

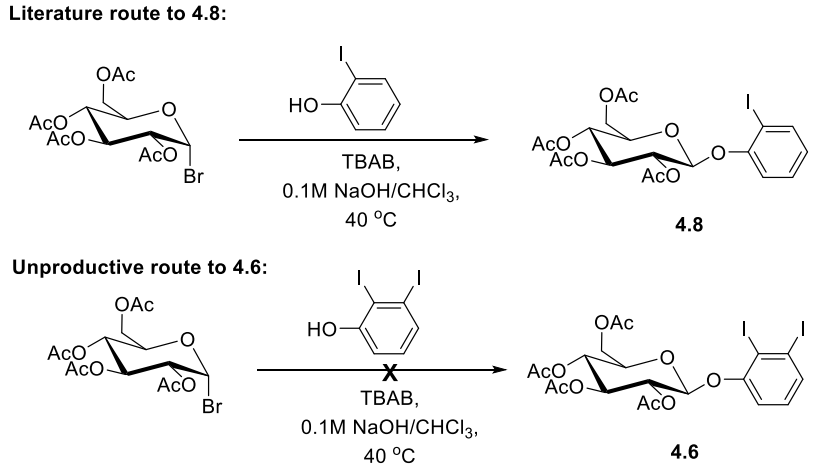

Scheme 4.8 Literature route to **4.8**, and equivalent unproductive route to **4.6**.

As trichloroacetimidate groups are more efficient glycosyl donors than bromides, this was next investigated for the synthesis of **4.6** (Scheme 4.9). Trichloroacetimidate donors require a Lewis acid for activation, and therefore TMSOTf (15 mol%) was added to the reaction mixture. As the carbohydrate starting material has an acetyl-group at the C-2 position, only the β-anomer was expected.[20] The crude reaction mixture contained several species and so a multi-step purification process was employed. To our surprise, crystallisation of the crude mixture from ice-cold EtOH gave us the α-anomer of **4.6**, whilst column chromatography gave us the expected product - the β-anomer of **4.6**. Despite chromatographic purification, the β-anomer required further recrystallisation from ice-cold EtOH.

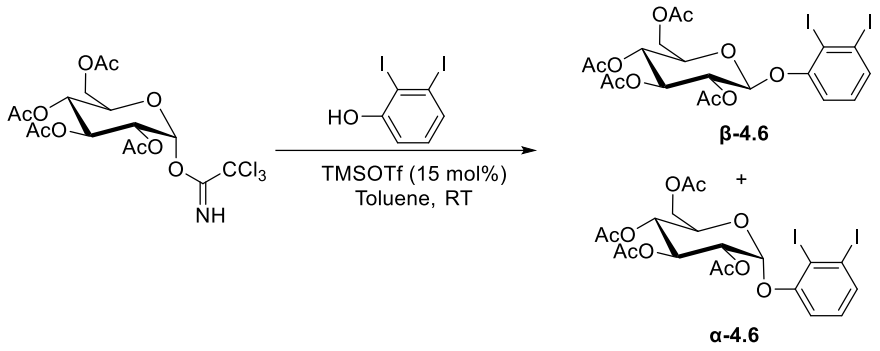

Scheme 4.9 Synthesis of **α-4.6** and **β-4.6**.

We postulate that a mixture of anomers was formed by the following mechanism (Figure 4.11), whereby the reaction of 1,2-diiodophenol occurred on a similar timescale to that of the triflate anion. This therefore led to inversion of the expected stereochemistry and enabled formation of the anomeric mixture. Just 3.2 mg of **α-4.6** and 2.5 mg of **β-4.6** were obtained, i.e. yields of 3% and 2%, respectively (see Chapter 6 for full characterisation). This result, compounded with the poor yield for 1,2-diiodophenol (4%), has meant no further work has been performed on this system. If the reaction to form **4.6** can be significantly improved, this could be a viable route to synthesising **4.7** (Scheme 4.6, pg. 10).

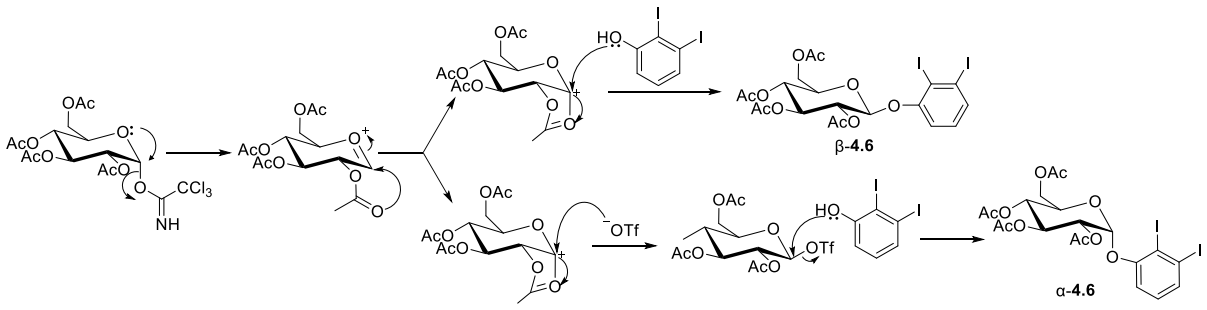

Figure 4.11 Tentative mechanism for the formation of an anomeric mixture during the reaction of 1,2-diiodophenol and imidate-based carbohydrate, despite acetyl protection at the C-2 position.

4.3. Routes toward unsymmetrical diphosphine glycoconjugates

Because of the issues with the synthesis of a dppbz-based phosphine glycoconjugate described above, subsequent steps looked to reduce the steric clash between the two phosphine moieties. One method by which this could be done was by synthesising an asymmetric 1,2-diphosphine glycoconjugate, as shown in Figure 4.12. Here, we investigated routes towards targets where R = Cy or Ph.

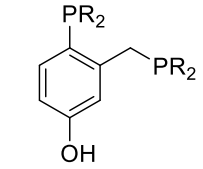

R = Cy or Ph

Figure 4.12 Structure of an unsymmetrical diphosphine, where R = Cy or Ph.

4.3.1. Attempted synthesis of a dicyclohexyl(2-dicyclohexylphosphaneyl)benzyl)phosphine-based glycoconjugate

Mecking *et al*. reported the synthesis of dicyclohexyl(2-dicyclohexylphosphino)benzyl)phosphine (**4.10**) from 2-bromobenzyl bromide, as shown in Scheme 4.10.[21]

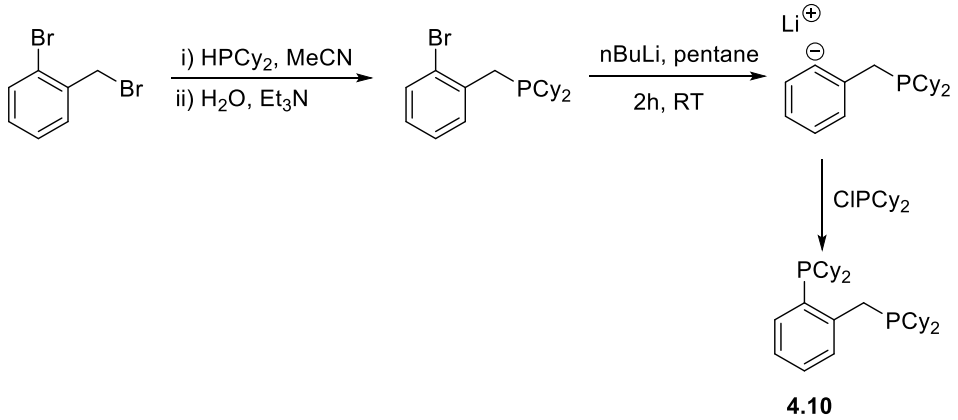

4.10

Scheme 4.10 Synthesis of **4.10**, as reported by Mecking *et al*.[21]

As we aim to introduce a carbohydrate moiety at a later stage of the synthesis, 2-bromo-5-methoxylbenzyl bromide was deemed to be an appropriate starting material. The aim was to use the same method reported by Mecking and co-workers to give the bidentate phosphine **4.12**, before cleaving the methyl ether to generate the phenolic product **4.13**. This should then react with acetobromo-α-D-glucose to give our desired final product, **4.14** (Scheme 4.11).

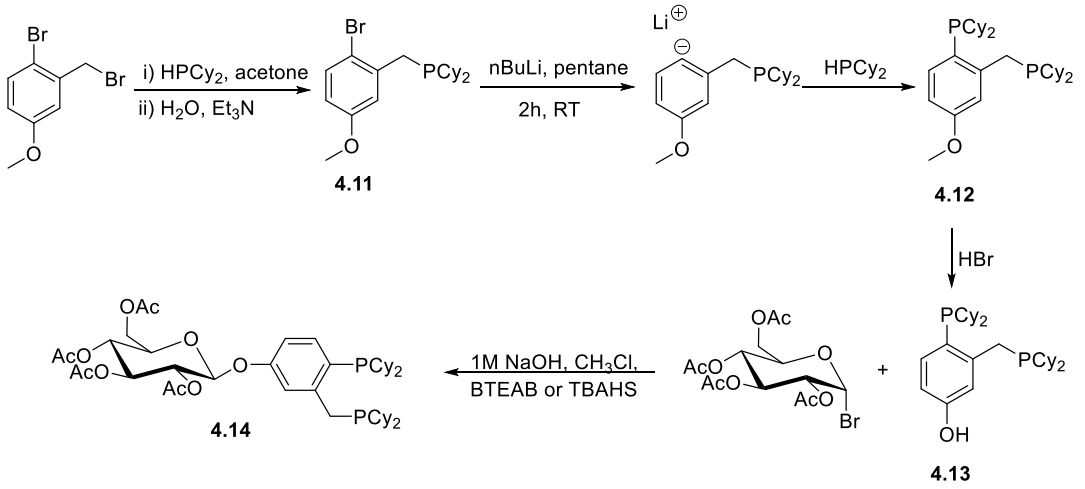

Scheme 4.11 Theoretical route to unsymmetrical diphosphine glycoconjugate **4.14**, from 2-bromo-5-methoxybenzyl bromide.

Monophosphine **4.11** was synthesised by heating $HPCy_2$ and 2-bromo-5-methoxylbenzyl bromide to reflux in acetone. After 18 h, no starting materials remained and only the phosphonium bromide (δ_P 21.5 ppm) was seen by $^{31}P\{^1H\}$ NMR spectroscopy. Following treatment of this species with Et_3N, the phosphonium salt was converted to **4.11**, which had a $^{31}P\{^1H\}$ NMR shift of 3.6 ppm (Scheme 4.12).

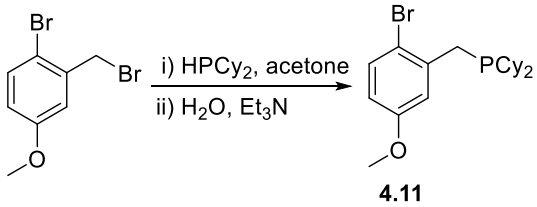

Scheme 4.12 Synthesis of **4.11** from 2-bromo-5-methoxylbenzyl bromide, *via* a phosphonium bromide intermediate.

Lithiation of **4.11** with *n*-butyllithium, and treatment with $ClPCy_2$, was expected to give **4.12**.[21] Performing this reaction under the same conditions reported by Mecking and co-workers gave a mixture of species by $^{31}P\{^1H\}$ NMR spectroscopy (Scheme 4.13). New signals in the $^{31}P\{^1H\}$ NMR spectrum at +7.0 ppm (doublet, J_{PP} = 8.9 Hz) and -18.1 ppm (broad singlet) accounted to 50% of the mixture, and were assigned as a single species. These chemical shifts are similar to those reported for **4.10** (δ_P +7.9 and -16.1 ppm) so suggested formation of **4.12**. Unfortunately, due to the methoxy group, recrystallisation of **4.12**, using the conditions for purification of **4.10**, was not possible. Repetition of this reaction and subsequent silica plug purification gave **4.12** as 74% of the mixture by $^{31}P\{^1H\}$ NMR spectroscopy. The $^{31}P\{^1H\}$ NMR spectrum contained two doublets at +6.6 (J_{PP} = 8.9 Hz) and -18.5 ppm (J_{PP} = 9.3 Hz) when recorded at 121 MHz rather than 162 MHz. The size of the ^4J coupling suggests that through-space coupling does not occur; this is consistent

with the molecule being arranged in solution as depicted in Scheme 4.13. The ^{1}H NMR spectrum showed several other impurities, and HR-MS was used to confirm that **4.12** had been formed (*m/z* calcd. for $C_{32}H_{53}P_2O$ ($[M+O]^+$) = 515.3563; obs. = 515.3572.). Attempts to improve the purity of **4.12** have been unsuccessful.

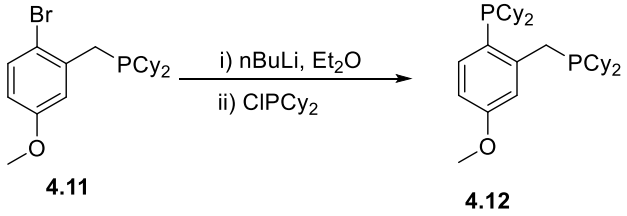

Scheme 4.13 Synthesis of diphosphine **4.12** from monophosphine **4.11**.

Consequently, cleavage of the methyl ester has been investigated as ester cleavage is critical to application of **4.12** as a relevant starting material. N_2-saturated aqueous HBr was added to **4.12**, and after heating the reaction mixture to 110 °C for 5 h, a new set of doublets at +53.2 (J_{PP} = 8.0 Hz) and -17.5 ppm (J_{PP} = 8.1 Hz) were seen in the ^{31}P{^{1}H} NMR spectrum alongside several other signals in the P(V) region. These chemical shifts suggested that oxidation of at least one of the PCy_2 groups had occurred to form **4.15**. These ether cleavage conditions have been successful for alternative targets[22] (Scheme 4.14(a)), and hence routes towards an alternative analogue, where R=Ph, were investigated. This is discussed in section 4.3.2.

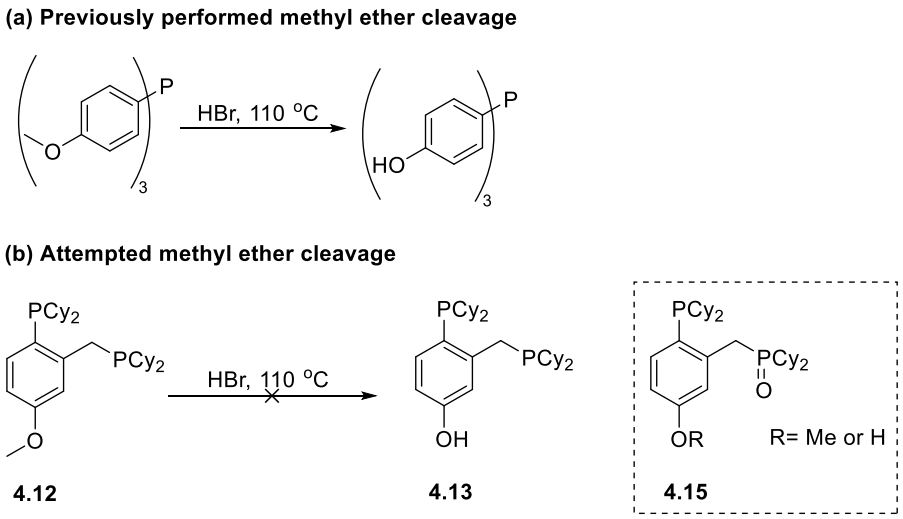

Scheme 4.14 Methyl ether cleavage of a phosphine containing molecule with HBr to (a) successfully form *tris*(4-hydroxylphenyl)phosphine or (b) unsuccessfully form **4.13**.

N.B. **4.15** is one of the of the potential products formed during the reaction with **4.12**.

Although ether cleavage proved unsuccessful, the Pt coordination chemistry of **4.12** was investigated. Complex **4.16** was formed by adding diphosphine **4.12** to [$PtCl_2$(COD)] (Figure 4.13). The formation of **4.16** produced doublets at 23.2 ppm (J_{PP} = 19.3 Hz) and 9.6 ppm (J_{PP} = 19.2 Hz) in the $^{31}P\{^{1}H\}$ NMR spectrum. The observed doublets have ^{195}Pt satellites that have *J* couplings of 3500 and 3512 Hz, respectively (Figure 4.13). The *J* values of the ^{195}Pt satellites are characteristic of a *cis*-PtP_2Cl_2 complex. Formation of **4.16** has also been confirmed by HR-MS (*m/z* calcd. for $C_{32}H_{52}P_2OClPt$ ($[M\text{-}Cl]^+$) = 744.2830; obs. = 744.2830).

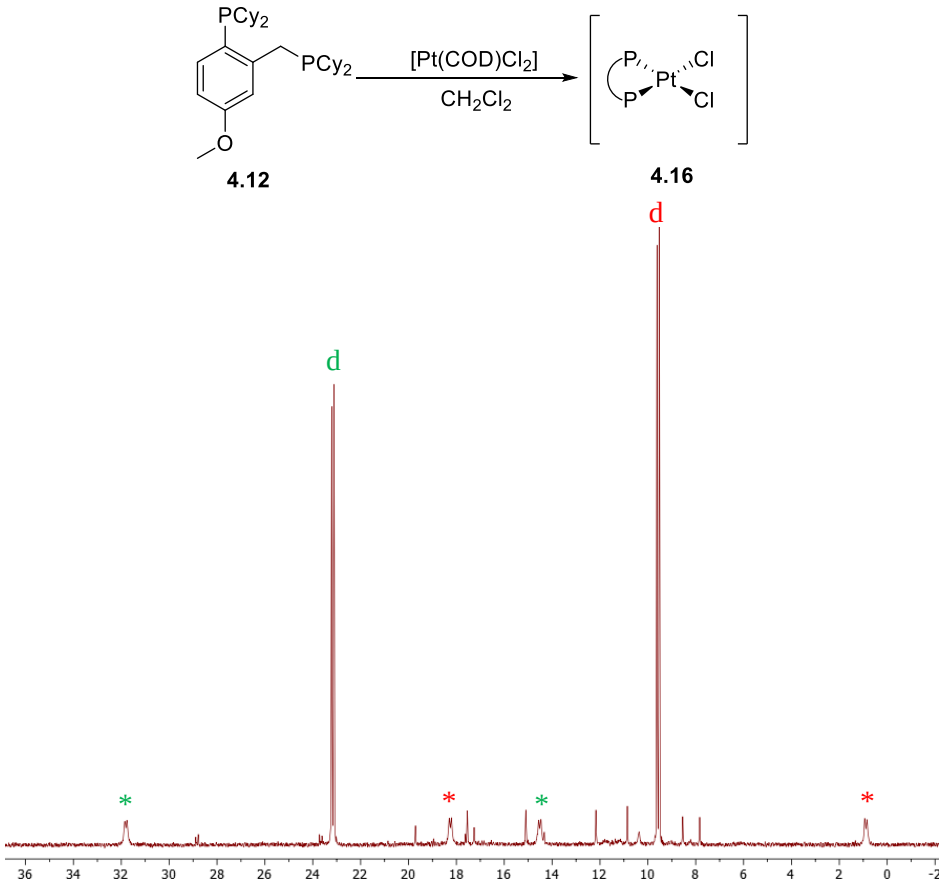

Figure 4.13 $^{31}P\{^{1}H\}$ NMR spectra (202 MHz, $CDCl_3$) of the product mixture after addition of [$PtCl_2$ (COD)] to **4.12** to give complex **4.16**. Asterix (*) mark the ^{195}Pt-^{31}P satellites, whilst the multiplicity of the signals is marked above those pertaining to the complex. The different colours (red and green) have been used to identify which ^{31}P signal relates to which set of ^{195}Pt satellites.

4.3.2. Attempted synthesis of a dicyclohexyl(2-dicyclohexylphosphaneyl)benzyl)phosphine-based glycoconjugate

As cleavage of the methyl ester was unsuccessful when the diphosphine contained PCy_2 groups (**4.12**), subsequently, the synthesis of a PPh_2 derivative was next investigated. Despite $HPCy_2$, 2-bromo-5-methoxybenzyl bromide and Et_3N reacting to give **4.11**, no evidence of the expected product **4.17** - or the intermediate phosphonium bromide - was observed when this method was investigated with $HPPh_2$ (Scheme 4.15).

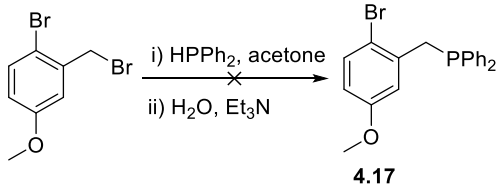

Scheme 4.15 Unproductive route to **4.17**, using $HPPh_2$ and 2-bromo-5-methoxybenzyl bromide.

The synthesis of compound **4.18** – which is structurally similar to **4.17** - has been previously reported by James,[23] who found **4.18 c**ould not be synthesised *via* Grignard routes (Scheme 4.16(a)). James also investigated a di-lithiation method which similarly proved unsuccessful for the formation of **4.18** (Scheme 4.16(b)), with large quantities of Ph_2P-PPh_2 formed. To successfully prepare **4.18**, a two-step lithiation procedure must be employed (Scheme 4.16(c)). James remarks that one caveat with this method is that ***Step II*** can, on occasion, produce a large number of side-products, and furthermore ***Step II*** appears to be highly sensitive regarding the purity of the monophosphine species. Consequently, this two-step lithiation method was investigated for the attempted synthesis of **4.17**.

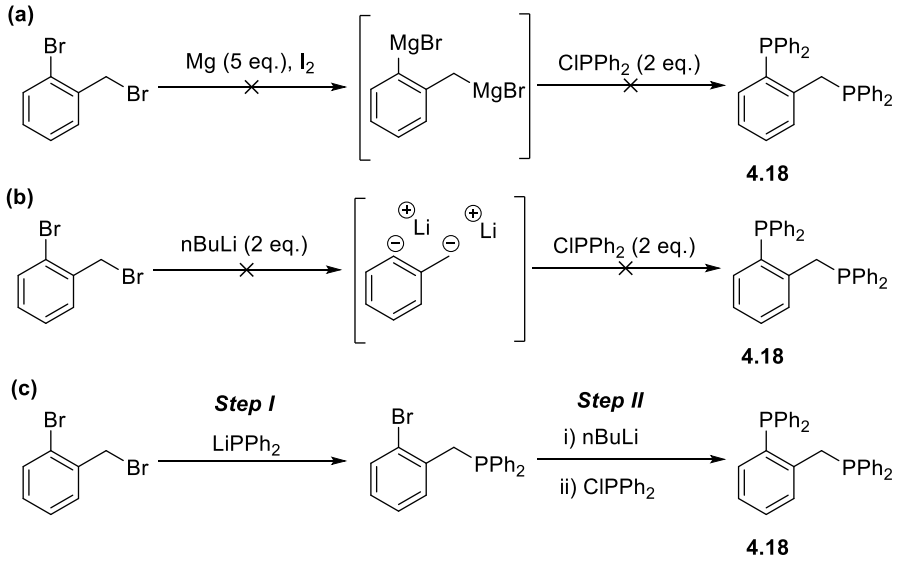

Scheme 4.16 A variety of routes to **4.18** as reported by S. James.[23] These include two unsuccessful routes: (a) a di-Gringard and (b) a dilithiation method, and (c) a successful two-step method to **4.18**.

When ***Step I*** was tested with 2-bromo-5-methoxybenzyl bromide several species were formed (Figure 4.14). These were identified by $^{31}P\{^{1}H\}$ NMR spectroscopy and included: **4.17** (35%), $Ph_2P\text{-}PPh_2$ (27%), **4.19** (11%) and several unidentified P(III) species (27%). The doublets at -8.6 ppm and -18.9 ppm ($J_{P\text{-}P}$ = 24 Hz) have been attributed to **4.19**. This is due to the similarity of these chemical shifts with those reported for **4.18** (-9.5 ppm and -17.2 ppm, J_{PP} = 24 Hz). Unfortunately, isolation of the desired product was unsuccessful, and so we attempted an alternative route from borane-protected lithium phosphide ($BH_3.LiPPh_2$).

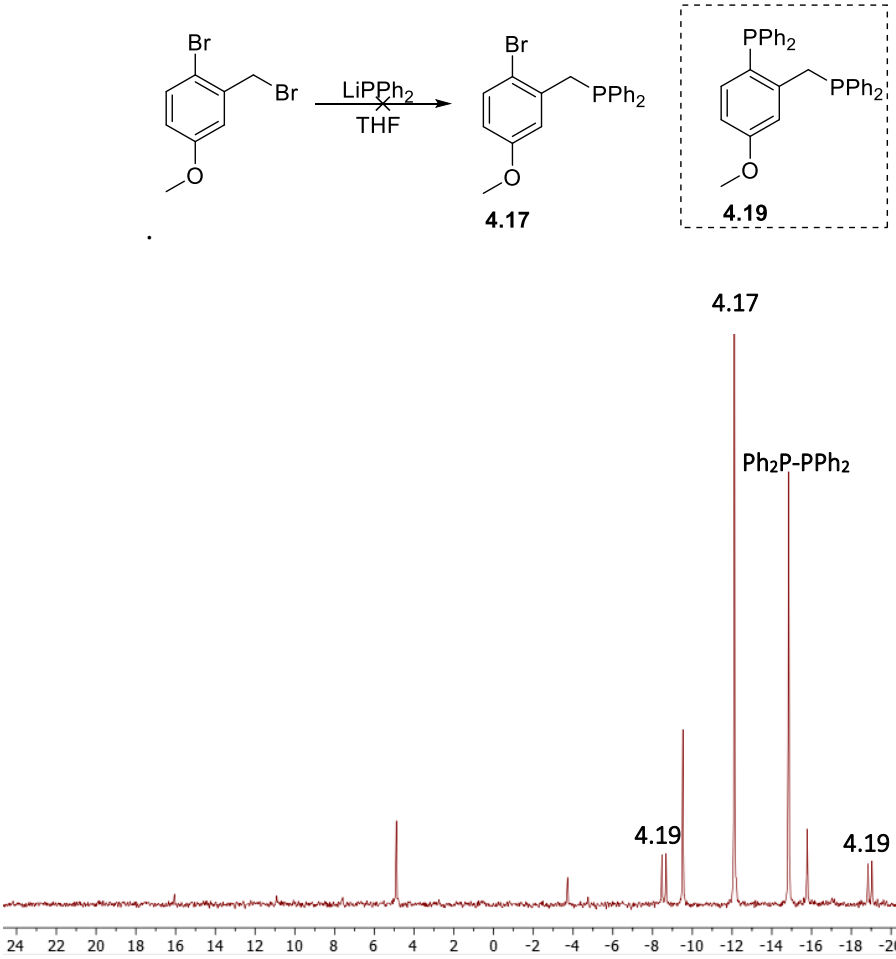

Figure 4.14 $^{31}P\{^{1}H\}$ NMR spectra (121 MHz, $CDCl_3$) of the product mixture formed from the reaction shown above. Signals referring to **4.17**, **4.19** and $Ph_2P\text{-}PPh_2$ have been labelled, whilst all other signals are assumed to correspond to unidentified P(III) species.

$BH_3.LiPPh_2$ was formed by addition $BH_3.SMe_2$ to $HPPh_2$, and its subsequent treatment with n-butyllithium[24]. Addition of $BH_3.LiPPh_2$ to 2-bromo-5-methoxybenzyl bromide gave a mixture of **4.20** (90% by $^{31}P\{^{1}H\}$ NMR spectroscopy) and $H(O{=})PPh_2$ (10%). This was easily purified by column chromatography (1:9, EtOAc:Hex) to give **4.20** in 65% yield (Scheme 4.17). This species displayed a broad multiplet at 19.2 ppm its $^{31}P\{^{1}H\}$ NMR spectrum.

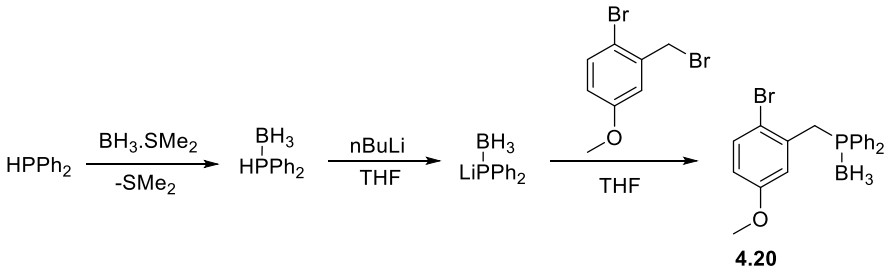

Scheme 4.17 Synthesis of **4.20**, a borane-protected monophosphine molecule.

Attempts to form diphosphine **4.21** by lithiation of **4.20** and subsequent addition of $ClPPh_2$ were unsuccessful (Scheme 4.18). After 2 h, *in situ* $^{31}P\{^1H\}$ NMR spectroscopy revealed that the main species in the reaction mixture were $ClPPh_2$ (83.0 ppm, 30%) and **4.20** (19.2 ppm, 62%). As a result of this lack of reactivity, borane deprotection was investigated.

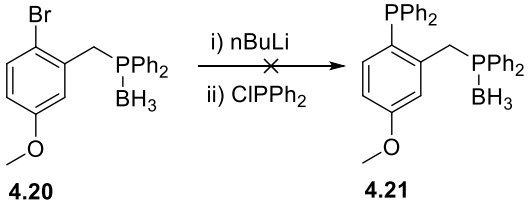

Scheme 4.18 Attempted synthesis of **4.21** using *n*BuLi and $ClPPh_2$.

The borane group was removed from **4.20** by addition of excess Et_2NH (Scheme 4.19, ***Step I***). Heating the reaction mixture to 50 °C for 16 h gave a mixture containing **4.17** and $Et_2NH.BH_3$. The amine-borane was simply removed by heating the viscous oil product mixture under vacuum at 80 °C for 1 h. This gave **4.17** in quantitative yield, with a chemical shift of δ_P -12.6 ppm.

Sequentially adding nBuLi and then $ClPPh_2$ to **4.17** gave a complex mixture by $^{31}P\{^1H\}$ NMR spectroscopy (Scheme 4.19, ***Step II***). As all signals in the $^{31}P\{^1H\}$ NMR spectrum were singlets, there was no evidence of formation of **4.18**.

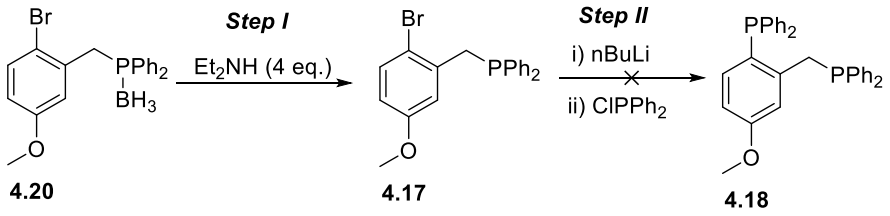

Scheme 4.19 Successful borane deprotection of **4.20** to give **4.17**, and the attempted synthesis of **4.18**.

The work described in Sections 4.2 and 4.3 shows that we have experienced no success in forming aryl diphos ligands suitable for conjugation by routes which require formation of Ar-P bonds. As a result, we turned our attention to forming aliphatic diphos ligands that would be amenable to bioconjugation (Sections 4.4 and 4.5 below).

4.4. Attempts to prepare a glycoconjugate of a derivative of bis(diphenylphosphinomethyl)aniline

Given the difficulties associated with the synthesis of phenolic diphosphines with Ar-P bonds (Sections 4.2 and 4.3), the synthesis of the 4-aminophenol ligand (**4.23**) was explored (Figure 4.15). Compound **4.23** has been reported previously, and can be prepared by several routes, two of which will briefly be discussed here.

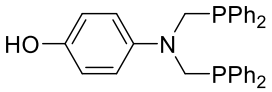

4.23

Figure 4.15 Structure of **4.23**, previously reported in literature by de Jesús et al.[25]

De Jesús *et al.* reported the synthesis of **4.23** from $HPPh_2$, formaldehyde and 4-aminophenol (**Scheme 4.20**(a)).[25] It could also be prepared by pre-forming the phosphonium salt (bis(hydroxymethyl)diphenylphosphonium chloride, **4.22**) and adding this to 4-aminophenol in the presence of Et_3N (**Scheme 4.20**(b)). As accurate stoichiometry during these reactions is important to prevent formation of a complex mixture, the second route was favoured as **4.22** is a bench-stable solid. Therefore, it is easier to handle and measure out accurately (compared with $HPPh_2$) when performing reactions on a small scale (<100 mg). This is particularly relevant when considering the small scale on which multi-step carbohydrates are often prepared. Consequently, **4.23** was prepared in moderate yield (49%) using the route shown in Scheme 4.20(b).

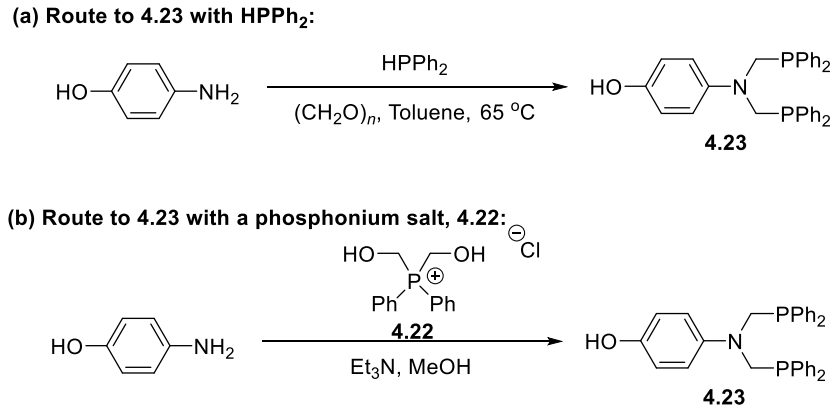

Scheme 4.20 Two alternative routes to **4.23** that involve either (a) $HPPh_2$ (reported by de Jesús *et al.*)[25] or (b) bis(hydroxymethyl)diphenylphosphonium chloride (**4.22**).

Method (b) in Scheme 4.20 was used to prepare **4.23** in 49% yield. The aim was then to use **4.23** as the precursor to the phosphine glycoconjugate **4.24** (Figure 4.16). However, before the bioconjugation, it was important to investigate the coordination chemistry of **4.23**, to establish that a glycoconjugate with this binding motif would be capable of forming complexes suitable for radio-imaging.

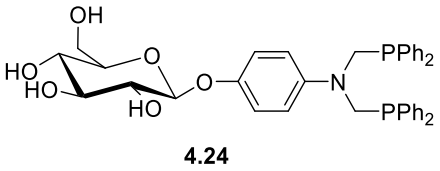

Figure 4.16 Structure of a bidentate N-phosphano glycoconjugate, **4.24**.

4.4.1. Rhenium coordination chemistry of 4.23

The coordination chemistry of **4.23** was initially investigated with respect to the $[Re(CO)_3]^+$ core by adding 1 eq. of **4.23** to the Re(I) precursor $[Re(CO)_3(H_2O)_3]Br$ (Scheme 4.21). Three new phosphorus-containing species were formed during the reaction, according to $^{31}P\{^1H\}$ NMR spectroscopy. The major species had a δ_P of -19.8 ppm and accounted for 84% of the mixture. This species has tentatively been assigned as complex **4.25**, based on the reported chemical shift (δ_P -19.6 ppm) for a structurally similar complex, **4.26** (Figure 4.17).[26] Two unidentified minor species at δ_P +4.6 ppm and -15.2 ppm accounted for 9% and 7% of the mixture, respectively. Evidence of both the expected complex (**4.25**) and the other unidentified species could be observed in the ^1H NMR spectrum. However, HR-MS did not confirm the identity of complex **4.25** and instead, only the molecular weight of the protonated ligand was observed, with other ion fragments unable to be assigned.

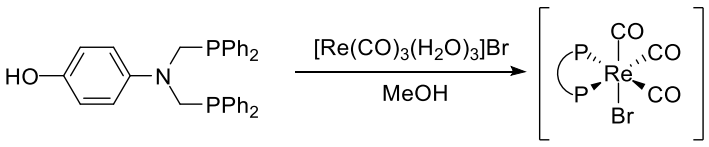

4.23 **4.25**

Scheme 4.21 Reaction of **4.23** and Re(I) precursor, to give complex **4.25**.

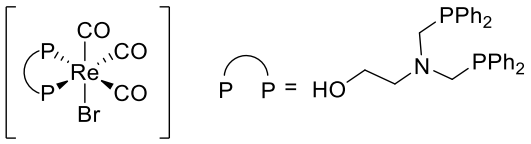

4.26

Figure 4.17 Structure of reported Re(I) complex **4.26** by Yan et al.[26]

Addition of 2 eq. of diphos ligand **4.23** to the Re(V) precursor, $[ReO_2I(PPh_3)_2]$, resulted in formation of a new species (**4.27**) with a δ_P of -34.0 ppm (Scheme 4.22). This shift is upfield of the free ligand, which has a δ_P of -26.8 ppm. The identity of complex **4.27** has been confirmed by HR-MS (*m/z* calcd. for $C_{64}H_{58}O_4N_2P_4Re$ ($[M]^+$) = 1229.2905; obs. = 1229.2930). As only a single species was formed when reacting **4.23** with $[ReO_2I(PPh_3)_2]$, all subsequent Re coordination studies therefore focused on the Re(V)-dioxo core.

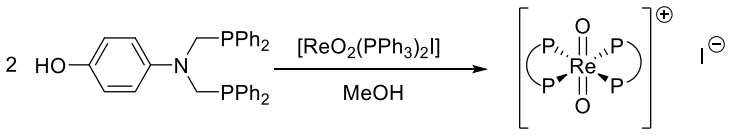

4.23 **4.27**

Scheme 4.22 Synthesis of Re(V) complex **4.27**, from **4.23**.

4.4.2. Towards glycoconjugates derived from a phenolic diphosphine

To prepare phosphine glycoconjugate **4.24**, the synthesis of the carbohydrate precursor **4.28** was first attempted (Scheme 4.23).

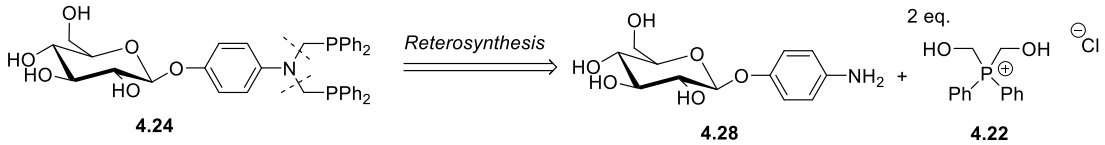

4.24 **4.28** **4.22**

Scheme 4.23 Structure of carbohydrate **4.28**, which is necessary for the formation of **4.24**, as shown retrosynthetically.

The most obvious route to **4.28**, would be to react 4-aminophenol with acetobromo-α-D-glucose. However, this is precluded by the greater nucleophilicity of the aniline-NH_2 group, compared with the phenolic-OH group. Consequently, **4.28** was instead prepared following literature procedures from the Cyrański and Boratynski groups.[27,28] First, 4-nitrophenol was

reacted with acetobromo-α-D-glucose in the presence of Ag_2CO_3 as reported by Cyrański *et al*.[27] This was followed by removal of the acetyl protecting groups using NaOMe in MeOH, and reduction of the -NO_2 group using Pd/C and $NH_4.HCO_3$ in MeOH, as reported by Boratynski *et al*. (Scheme 4.24)[28]. Carbohydrate **4.28** was therefore synthesised in 37% yield overall, in three steps from acetobromo-α-D-glucose, compared with a hypothetical overall yield of 30%, based off the combined literature methods.[29] Full characterisation was not reported by Cyrański or Borantynski, but the data recorded for **4.28** (^{1}H NMR, ^{13}C NMR and HR-MS) was consistent with that reported by Y. Zhao *et al.*[30]

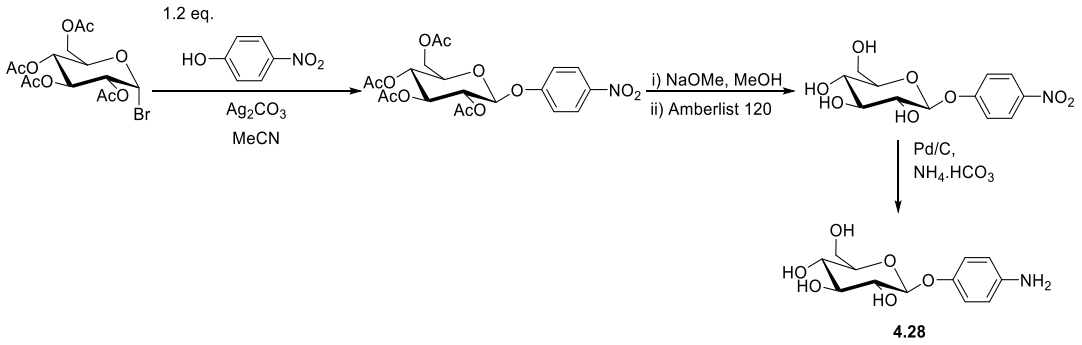

Scheme 4.24 Three step route to **4.28** from aceto-bromo-α-D-glucose, previously reported by Cyrański *et al*. (Step 1)[27] and Boratynski *et al.* (Steps 2 and 3)[28].

In an attempt to synthesise **4.24**, carbohydrate **4.28** was added to the phosphonium salt, **4.22**, which was dissolved in a mixture of Et_3N, MeOH and H_2O (Scheme 4.25). After heating this mixture to 70 °C overnight, no starting material was present according to TLC, and a new species was formed as confirmed by *in situ* $^{31}P\{^1H\}$ NMR spectroscopy (δ_P = -28.2 ppm). The new product was isolated after aqueous work up. However, analysis by ^{1}H NMR spectroscopy revealed an absence of signals relating to a carbohydrate molecule. Additionally, HR-MS did not support the formation of **4.24**. We suggest that the loss of the carbohydrate moiety is due to the $Et_3N.HCl$ by-product being a weak acid and catalysing the hydrolysis of the glycosidic bond between the D-glucose and 4-aminophenoxy group. Any D-glucose formed by hydrolysis will be simply removed during the aqueous work-up, and this would therefore account for the lack of carbohydrate signals in the ^{1}H NMR spectrum of the product. Subsequent work has therefore turned to the conjugation of **4.23** and acetobromo-α-D-glucose.

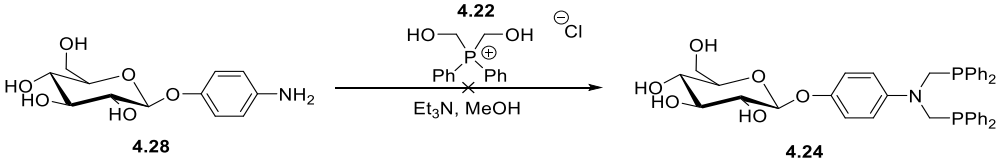

Scheme 4.25 Unsuccessful route to **4.24**, from carbohydrate **4.28** and phosphonium salt **4.22**.

As phenols can undergo direct conjugation with acetobromo-α-D-glucose, this method was next explored for the formation of peracetylated **4.24**, i.e. **4.29**. This reaction was attempted using three different conjugation conditions, as listed in Table 4.1.

Table 4.1 Reaction conditions tested for the formation of **4.29**.

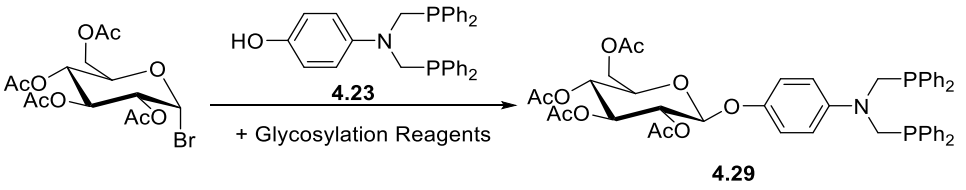

Entry	Reagents	4.23 (eq.)	Carbohydrate (eq.)	Temp/°C	Time/hr	4.29 (*in situ* $^{31}P\{^{1}H\}$ NMR)
1	Ag_2CO_3, DIEA	1.2	1.0	21	48	No
2	NaOH, TBAHS	1.0	5.0	21	24	Yes
3	NaOH, BTEAB	2.0	1.0	60	4	Yes

Exclusive formation of **4.29** did not occur using any of the above conditions. However, Entry 3 appeared to be the most promising. Here, addition of **4.23** (2 eq.) to acetobromo-α-D-glucose in the presence of NaOH and benzyltriethylammonium bromide (BTEAB) led to **4.29** accounting for 36% of the crude mixture, according to $^{31}P\{^{1}H\}$ NMR spectroscopy with a chemical shift at -27.2 ppm. An unidentified species at -27.1 ppm (18%) and the excess of **4.23** at -26.8 ppm (45%) were also observed in the $^{31}P\{^{1}H\}$ NMR spectrum. Purification of **4.29** using column chromatography was attempted, but **4.29** was only isolated with a purity of 66% according to $^{31}P\{^{1}H\}$ NMR spectroscopy (Figure 4.18). Additionally, ^{1}H NMR spectroscopy has confirmed that the impurities are not carbohydrates. This therefore suggests that the by-products, which account for 34% of the mixture by $^{31}P\{^{1}H\}$ NMR spectroscopy, are not carbohydrate-based by-products, but instead are unidentified aromatic tertiary phosphines. The formation of **4.29** was confirmed by HR-MS (*m/z* calcd. for $C_{46}H_{48}O_{10}NP_2$ ($[M+H]^+$) = 836.2753; obs. = 836.2744), but subsequent attempts to improve the efficacy of this reaction were unsuccessful.

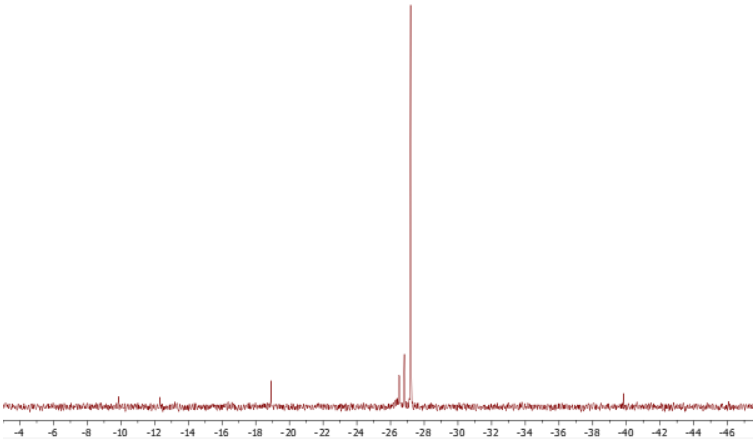

Figure 4.18 $^{31}P\{^{1}H\}$ ($CDCl_3$, 121 Hz) spectrum of **4.29** (66% purity) after column chromatography.

Despite this, the coordination chemistry of **4.29** has been investigated by adding 2 eq. to $[ReO_2I(PPh_3)_2]$. The major product of this reaction was the expected complex **4.30**, which is evidenced by a singlet at -33.0 ppm in the $^{31}P\{^{1}H\}$ NMR spectrum (Figure 4.19(b)), and by HR-MS analysis (*m/z* calcd. for $C_{92}H_{94}O_{22}N_2P_4Re$ ($[M]^+$) = 1889.4806; obs. = 1889.4757).

However, not surprisingly in view of the low purity of **4.29**, several other species were also formed upon addition of the Re(V) precursor (Figure 4.19(b)). Future research should be carried out to improve the synthesis of **4.29**, and its deprotected analogue **4.24**, as our preliminary results indicate that the ^{99m}Tc analogue of **4.30** would be a promising target for radiolabelling studies.

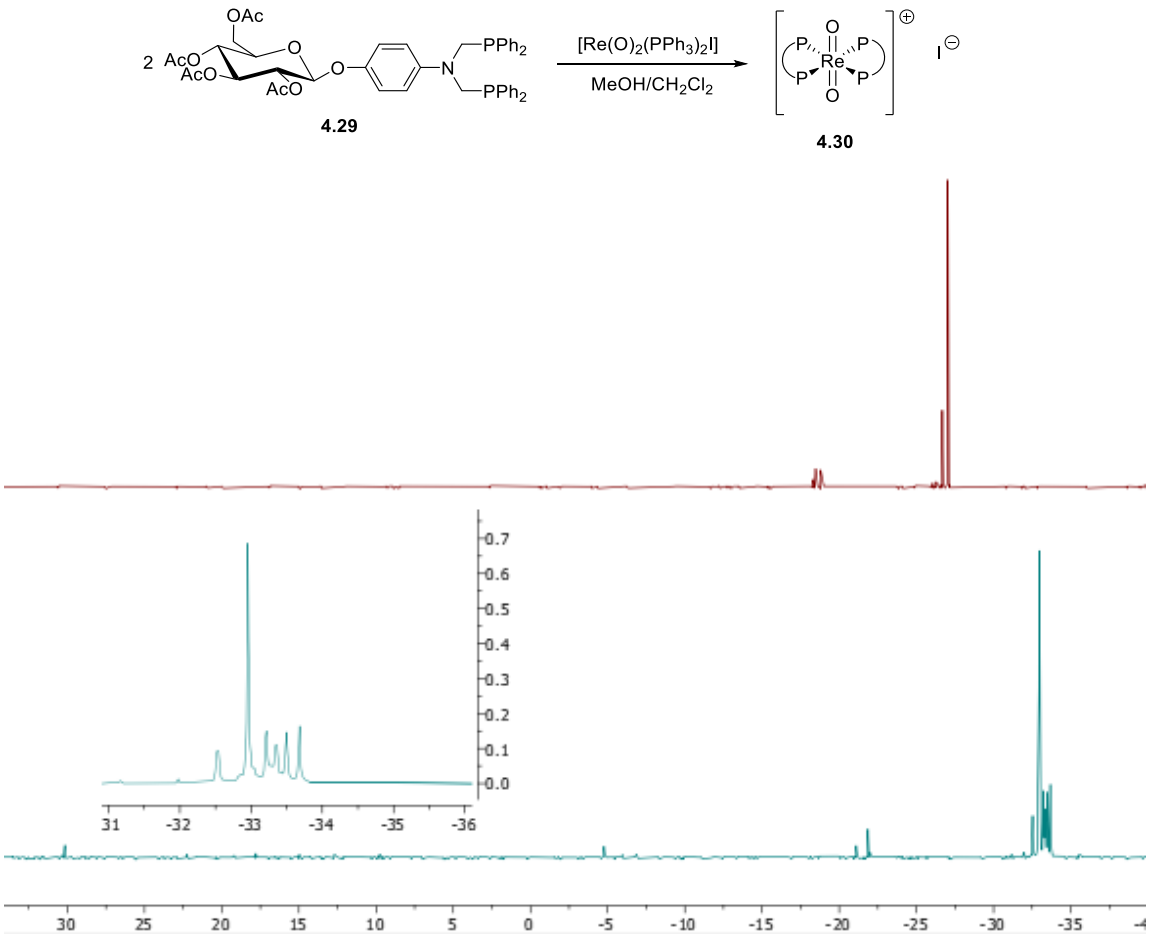

Figure 4.19 $^{31}P\{^{1}H\}$ NMR spectra (121 MHz, $CDCl_3$) of (a) the batch of ligand (**4.29**) before complexation with $[ReO_2I(PPh_3)_2]$ and (b) after complexation to give **4.30** (major species).

4.5. Towards glycoconjugates derived from an amide-linked diphosphine

As outlined in Chapter 2, amide coupling chemistry provided the most successful route to an alkyl linked monophosphine glyconconjugate (**2.21**, Figure 4.20(a)). Whilst **2.21** radiolabelled efficiently when reacted with pertechnetate ($[^{99m}TcO_4]$) to give a single species, the resulting complex, **2.25**, did not exhibit good serum stability (Figure 4.20(b)). Consequently, further work was not performed on this system.

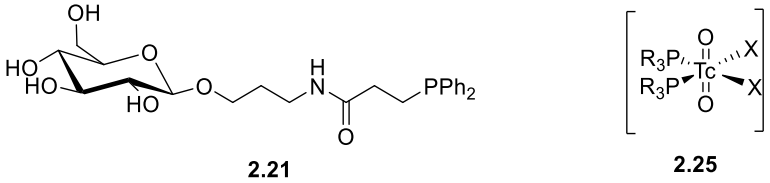

Figure 4.20 Structure of **2.21**, and its ^{99m}Tc complex (**2.25**), as reported in Chapter 2.

This route to glycoconjugate formation has been redirected to the formation of a diphosphine glycoconjugate; the chelate complexes should demonstrate greater serum stability when coordinated to ^{99m}Tc. To synthesise such a ligand the carbohydrate moiety remains

unchanged, and so will be referred to as **2.18** (**Figure 4.21**). However, novel diphosphine carboxylic acids are required for the coupling and these will be discussed below in Section 4.5.1.

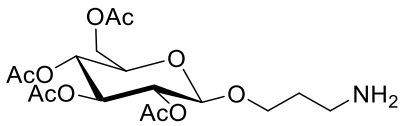

2.18

Figure 4.21 Structure of carbohydrate **2.18**, previously reported in Chapter 2.

4.5.1. Attempted synthesis of a diphosphine carboxylic acid (3-carbon backbone)

Synthesis of a diphosphine carboxylic acid with a 3-carbon backbone (**4.33**) was initially investigated (Scheme 4.26) for conjugation with carbohydrate **2.18**. This should give access to a Re(V) (or ^{99m}Tc(V)) complex with a 6-membered chelate, using a binding motif that would be analogous to that of 1,3-bis(diphenylphosphine)propane (dppp). As the dppp-coordinated Re(V)-dioxo complex has previously been reported (Figure 4.22), this gave us confidence in our ligand design.[31]

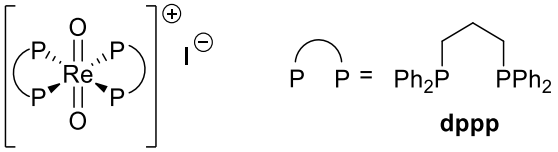

Figure 4.22 Re(V)-dioxo complex, with two dppp ligands, published by Castiniras *et al.*.[31]

A plausible route to **4.33** starts from commercially available 3-bromo-2-(bromomethyl)propionic acid. ***Step I*** involved the ester protection of the carboxylic acid, which was carried out under acidic conditions with isopropanol. This reaction proceeded to give the novel ester, isopropyl 3-bromo-2-(bromomethyl)propionate, in high yield (89%), following a simple aqueous work up.

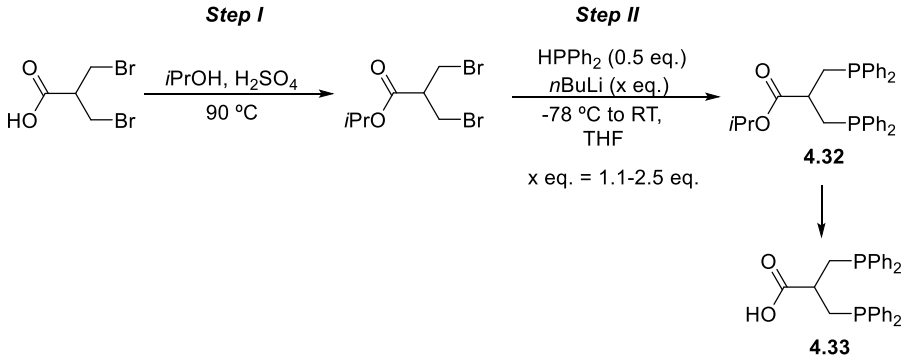

Scheme 4.26 Proposed route to **4.33**, in three steps from 3-bromo-2-(bromomethyl)propionic acid.

Step II (to give **4.32**) involved addition of $LiPPh_2$ (*n*BuLi + $HPPh_2$) to isopropyl 3-bromo-2-(bromomethyl)propionate to install the two diphenylphosphine moieties. This reaction gave a number of tertiary phosphine products, but no evidence of the desired product, **4.32**, was observed by ^{1}H, ^{13}C or HR-MS. Despite varying the reaction conditions (the order of addition, the rate of addition, the reactant concentrations), this result could not be improved and instead, subsequent work focused on formation of an alternative diphosphine carboxylic acid with a 1-carbon backbone, using chemistry originally developed in the Webster group.[32]

4.5.2. Synthesis of a diphosphine carboxylic acid (1-carbon backbone)

The Webster Group has shown that a variety of 1,1-diphosphines, often containing an ester 'R' group, can be synthesised *via* hydrophosphination by $HPPh_2$ (or H_2PPh) of the terminal alkyne (Scheme 4.27).[32] Using hydrophosphination chemistry to install both 'PPh_2' groups means there is a 1-carbon backbone, and so these molecules are derivatives of 1,1-bis(diphenylphosphine)methane (dppm).

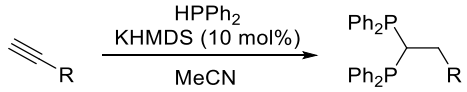

Scheme 4.27 General route to 1,1-diphosphines from $HPPh_2$.[32]

Although not investigated by Webster and co-workers, hydrolysis of the ester should give the corresponding carboxylic acid. Base catalysed hydrolysis of the methyl ester did not occur at ambient or elevated temperatures (Scheme 4.28(a)). However, hydrolysis of the ethyl ester was found to proceed at room temperature, over a period of 5 d, to give the novel phosphine carboxylic acid **4.34** with a $^{31}P\{^{1}H\}$ NMR shift of -7.4 ppm in an 87% yield for this step (Scheme 4.28(b)). For full characterisation see Chapter 6. Next, the conjugation of **4.34** and carbohydrate **2.18** was investigated.

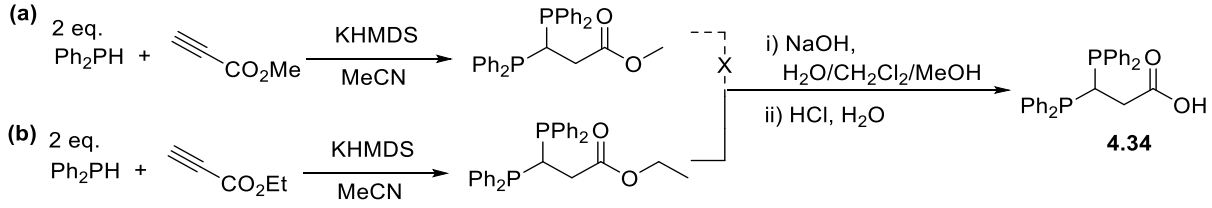

Scheme 4.28 Productive and unproductive routes to **4.34** from esterified 1,1-diphosphines.

4.5.3. Synthesis of bidentate phosphine glycoconjugates with a 1-carbon backbone

Using the amide-coupling conditions optimised in Chapter 2, **4.34** was conjugated to the amine-functionalised carbohydrate, **2.18**, to give **4.35**. This gave a singlet at 7.1 ppm in its $^{31}P\{^{1}H\}$ NMR spectrum (Scheme 4.29). Several other products were formed during this reaction, and purification by inert-atmosphere column chromatography was necessary to purify **4.35** due to its air-sensitivity. A low yield (24%) was obtained for the amide coupling step, but the material was pure and the deprotection of the acetyl groups was next investigated. **4.35** has been fully characterised by ^{31}P, ^{1}H and ^{13}C NMR spectroscopy and HR-MS (see Chapter 6 for details).

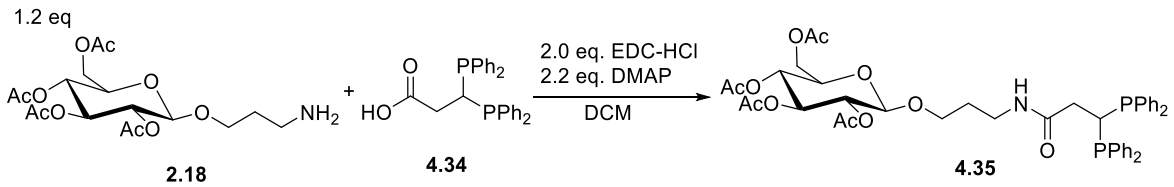

Scheme 4.29 Synthesis of **2.20** and **4.35** *via* amide coupling chemistry.

The deprotection of **4.35** proceeded to give the novel glycoconjugate **4.36** in 54% yield, with a $^{31}P\{^{1}H\}$ NMR chemical shift of -6.4 ppm (Scheme 4.30). Pleasingly, no hydrolysis of the amide bond was observed, and the identity of this species was confirmed by HR-MS (m/z

calcd. $C_{36}H_{31}NO_7P_2Na$ ($[M+Na]^+$) = 684.2256; obs. = 684.2255). Production of significant quantities of **4.36** has proved difficult, with an overall yield of 0.5% from 10 steps, and total of just 7 mg isolated (*versus* 1.5% yield and 50 mg isolated for monophos analogue **2.21**).

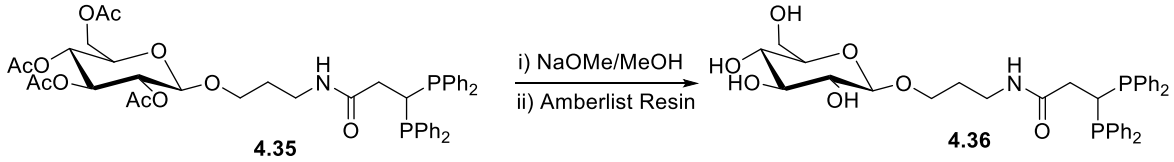

Scheme 4.30 Deprotection of ligand **4.35**, to give **4.36**.

The lowest yielding steps in the synthesis of **4.36** were (i) the reduction of the $-N_3$ group (to an $-NH_2$ group) in the synthesis of carbohydrate **2.18** and (ii) the amide coupling reaction between **2.18** and **4.34** (Scheme 4.29). As a result, changes were made in both of these steps in an attempt to improve the overall yield. By deprotecting the carbohydrate prior to reduction of the $-N_3$ group, the yield for this transformation was increased from 48% to 90% to give carbohydrate **4.37** (Scheme 4.31); see Experimental Chapter for details. A possible explanation for this significant yield increase is that an acetyl migration, likely from the C-2 position, to the $-NH_2$ group, is inhibiting formation of the desired carbohydrate when reducing the $-N_3$ group of the peracetylated carbohydrate.

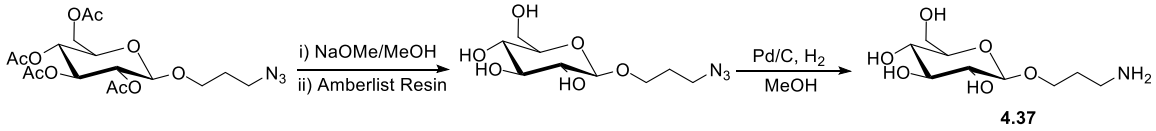

Scheme 4.31 Synthesis of carbohydrate **4.37**.

The amide coupling reaction was therefore repeated with **4.34** and carbohydrate **4.37** (rather that its peracetylated analogue, **2.18**). The amide coupling reaction gave a mixture of two products according to the $^{31}P\{^1H\}$ NMR spectrum of the product (Figure 4.23). Furthermore, two anomeric proton signals at 4.16 ppm (**4.36**) and 4.33 ppm (**4.38**) are evident in the ^1H NMR spectrum; the ratio of these anomeric protons is reflected in the $^{31}P\{^1H\}$ NMR spectrum with singlets seen at -6.2 ppm (**4.36**, 33%) and -6.4 ppm (**4.38**, 67%) (Figure 4.23). It should be noted that DMAP was not added during this reaction, as the presence of a base promotes ester formation to give **4.38** instead of amide formation to give **4.36**. Hence, this route to **4.36** was discontinued and subsequent work on the Re(V) coordination chemistry and radiolabelling of **4.36** proceeded with the ligand made *via* the original route, *via* **4.35**.

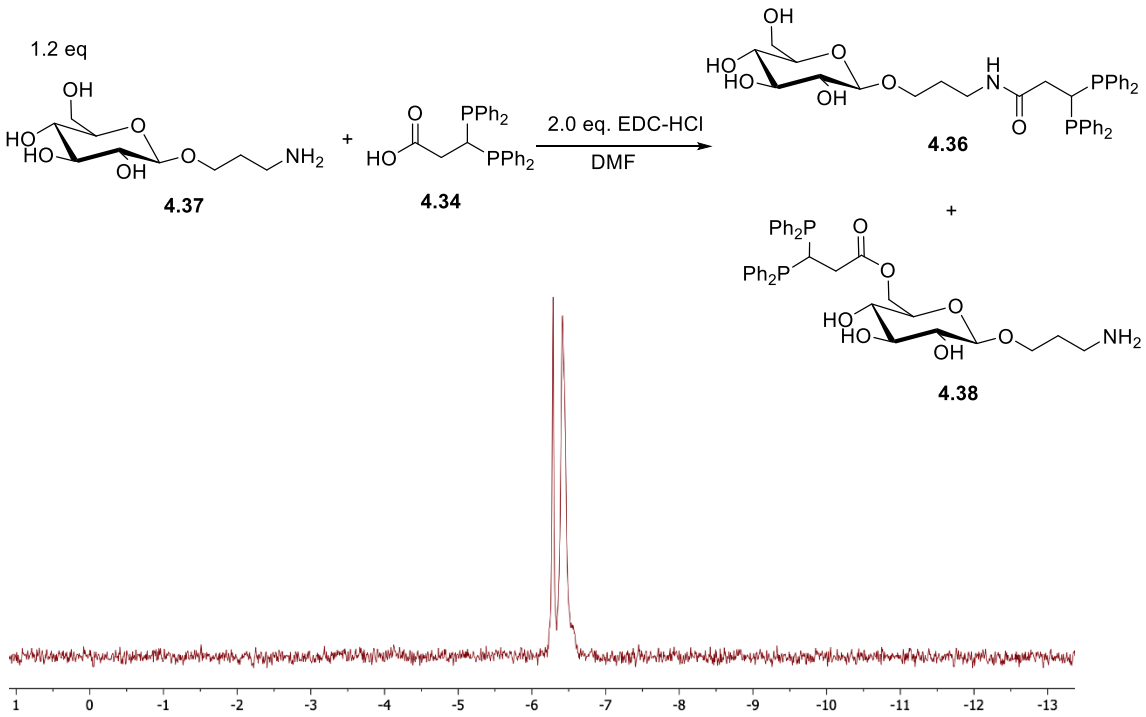

Figure 4.23 Reaction between **4.34** and **4.37**. A mixture of products was formed, as shown by the $^{31}P\{^{1}H\}$ NMR (202 MHz, CD_3OD) spectrum where the broad signal corresponds to **4.38**, and the sharper signal to **4.36**.

4.5.4. Rhenium coordination chemistry of bidentate phosphine glycoconjugates with a 1-carbon backbone

The synthesis of Re(I) complexes with ligands **4.35/4.36** was not investigated because of the observed hydrolytic instability of the amide bond when reacting the monophosphine analogue (**2.20**) with $[Re(CO)_3(H_2O)_3]Br$ (Chapter 2, Section 2.3.1). Coordination studies therefore focused on reacting the bidentate phosphine glycoconjugate with $[ReO_2I(PPh_3)_2]$. In the literature, the bis(dppm) Re(V)-dioxo complex has been reported by Midollini *et al.*, which suggested that the dppm derivates **4.35**/**4.36** should be capable of coordinating to the Re-dioxo (and ^{99m}Tc-dioxo) core (Figure 4.24).[33]

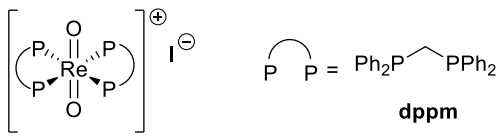

Figure 4.24 Re(V)-dioxo complex, with two dppm ligands, published by Midollini *et al.*.[33]

Addition of 2 eq. of **4.35** to the Re(V) precursor, $[ReO_2I(PPh_3)_2]$ led to multiple signals in the ^{31}P NMR spectrum of the product (**Figure 4.25**). The minor resonances around -35.0 ppm, with an upfield coordination shift of $\Delta\delta$ 28.3 ppm and an AB splitting pattern, have tentatively been assigned as the hoped-for bis(chelate) complex, **4.39**. A mixture of diastereoisomers of **4.39** would be anticipated due to the *cis* and *trans* relationship of the R

groups on the backbone C atoms. The upfield phosphorus chemical shift is characteristic of the formation of a four-membered chelate at a metal centre. However, the main product has signals at 38.2 (d), -14.3 (m) and -34.8 (br s) ppm which have tentatively been assigned as the environments labelled 'A', 'B' and 'C' in complex **4.40**, where an O atom of a Re=O group has inserted between the Re-P bond (**Figure 4.25**); there would be several diastereoisomers of this compound too.

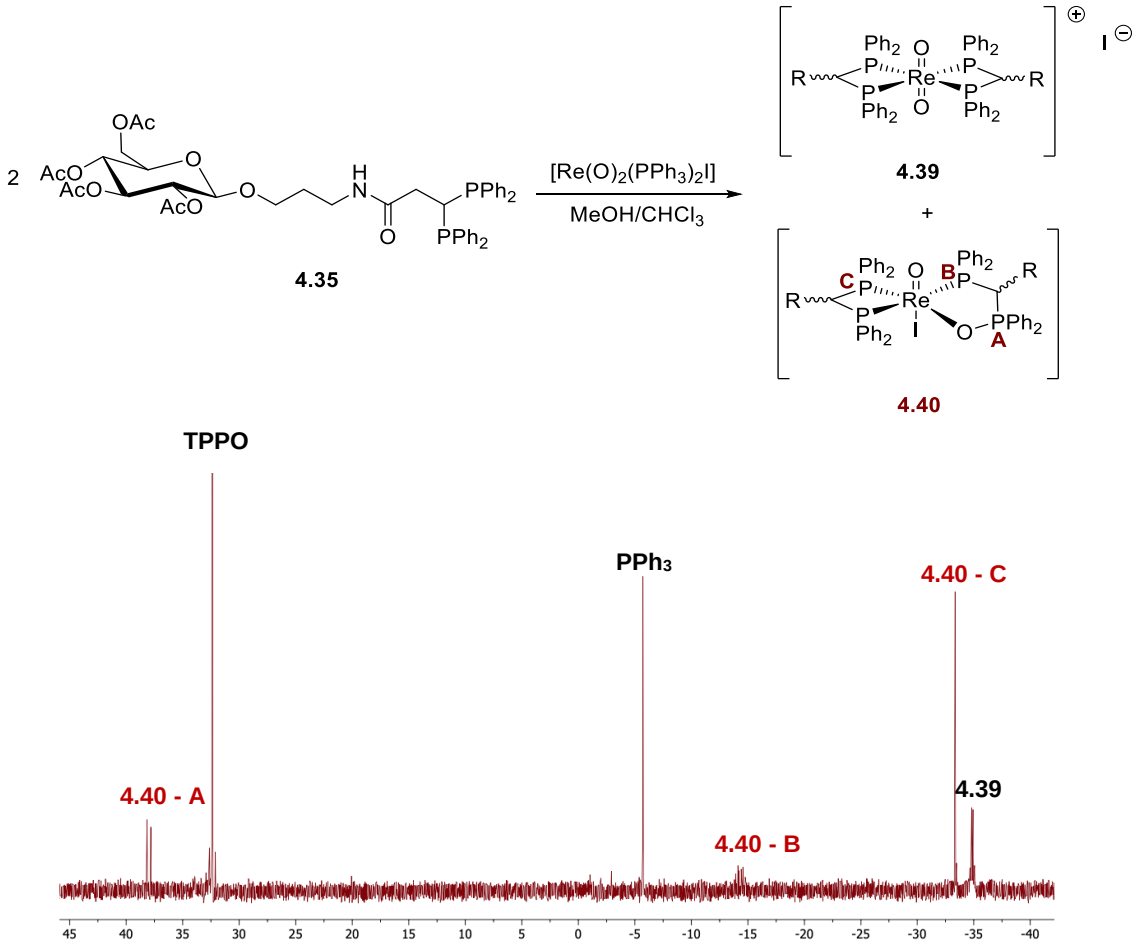

Figure 4.25 The reaction scheme and the $^{31}P\{^{1}H\}$ NMR spectrum (202 MHz, ^{d4}MeOD) of the proposed species (**4.39** and **4.40**) formed by addition of **4.35** to $[ReO_2I(PPh_3)_2]$.

N.B. Additional TPPO was added to confirm the identity of this species in the mixture.

The assignments of **4.40** are based on reports for the binding of dppm to $[ReOCl_3(PPh_3)_2]$ - an alternative Re(V) core. In 1993, Graziani and co-workers found that rather than forming the expected $[ReOCl(dppm)_2]$ structure, they isolated the $[ReCl_3(dppm\text{-}P,P)(dppom\text{-}P)]$ species (Figure 4.26). This structural rearrangement is likely favoured by the release of ring strain in the 4-membered chelates. Graziani reported that refluxing this species in toluene, gave rise to a mixture of two new products - $[ReOCl_3(dppm\text{-}P,P')]$ and $[ReCl_4(dppom\text{-}P,O)]$, the second of which was characterised by X-ray diffraction (Figure 4.26).[34]

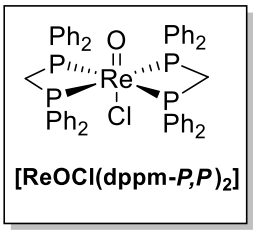

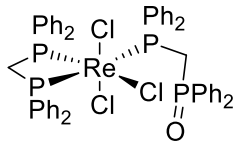

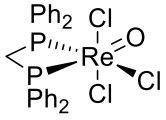

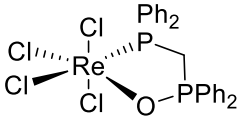

Figure 4.26 Complexes synthesised by Grazini *et al.* when investigating Re(V) coordination of dppm, and the expected complex [ReOCl(dppm)$_2$].[34]

As shown in Figure 4.24, Midollini *et al.* reported the first $Re^{V}(dppm)_2$ complex, $[ReO_2(dppm)_2]I$, in 2000.[33] However, Midollini and co-workers only achieved exclusive formation of the expected bis(chelate) complex by using a high ligand to Re ratio (10:1, ligand:rhenium). Due to the limited scale of synthesis for **4.35** (Section 4.5.2), this was not attempted here.

Attempts to prepare a Re(V) complex of **4.36** (deprotected **4.35**) from $[ReO_2I(PPh_3)_2]$ were inconclusive, with signals observed only for PPh_3 and TPPO by ^{31}P NMR spectroscopy. This is akin to the difficulties that arose when reacting **2.21** with $[ReO_2I(PPh_3)]$ described in Chapter 2 (Section 2.3.2).

4.5.5. ^{99m}Tc Radiolabelling of a bidentate phosphine glycoconjugate with a 1-carbon backbone

^{99m}Tc radiolabelling studies are typically performed in a mixture of saline and milliQ water, although co-solvents such as EtOH or DMSO can be added to improve ligand solubility. Consequently, these studies are preferentially performed on molecules with high water solubility. As diphosphine glycoconjugate **4.35** is insoluble in water, whilst **4.36** exhibits reasonable water solubility, all ^{99m}Tc radiolabelling was performed on ligand **4.36**. Full details of this work are given in Chapter 6.

Tc(V)-dioxo radiopharmaceuticals are typically prepared by adding $[^{99m}TcO_4]^-$ to a lyophilised kit that contains the ligand (in this case **4.36**), a reducing agent (stannous chloride), a buffer (sodium hydrogen carbonate) and a weak chelator for stabilisation of intermediates (sodium tartrate). In this project, the Tc(V) kits have been based on those used for *Myoview*, but the diphosphine ligand (tetrofosmin) has been replaced with a diphosphine glycoconjugate ligand. The following kits were prepared with ligand **4.36** (Table 4.2):

Table 4.2 Kit preparation for diphosphine ligand **4.36**

Kit	Ligand (μmol)	$SnCl_2.2H_2O$ (μmol)	Sodium tartrate dihydrate (μmol)	$NaHCO_3$ (μmol)
1	0.76	0.38	0.38	0.30
2	0.76	0.38	0.19	0.30
3	1.06	0.53	0	0

It was hoped only the bis(chelate)-Tc(V) complex would form when radiolabelling **4.36** with $[^{99m}TcO_4]^-$ because in the radiochemical synthesis a large excess of ligand with respect to Tc is present. As stated above, Midollini *et al.* showed that the bis(chelate)-Re(V) complex was exclusively formed when a large excess of dppm was added to $[ReO_2I(PPh_3)_2]$ at 30 °C.[33]

The ^{99m}Tc radiolabelling of **4.36** was first explored with Kit 1 (Table 4.2). This kit is comprised of the same ratio of reagents as that which gave the best results when radiolabelling **2.21** (Kit 2, Table 2.4 in Chapter 2). Heating Kit 1 with $[TcO_4]^-$ for 30 min at 30 °C gave a disappointing radio-HPLC trace; the chromatogram (Figure 4.27) shows an intense peak at 2.5 min indicating unreacted $[TcO_4]^-$, and weak, broad peaks with a retention time of 10-13 min signalling formation of several unidentified species.

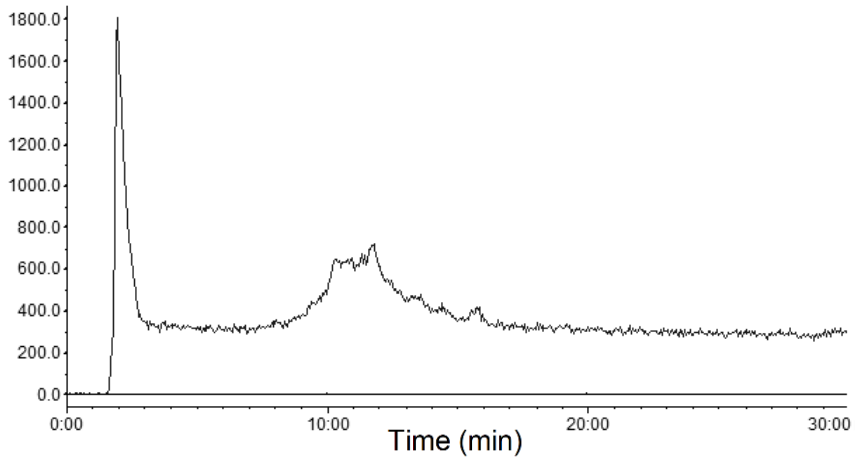

Figure 4.27 HPLC chromatogram for the radiolabelling of Kit 1 with $[^{99m}TcO_4]^-$.

If radiolabelling of **4.36** had proceeded efficiently, the HPLC chromatogram would have shown a minor peak for free $[TcO_4]^-$, and a shaper, more significant peak for the ^{99m}Tc complex with **4.36**. The absence of any sharp peaks in the chromatogram, when using Kit 1, has led us to hypothesise that the sodium tartrate (added for intermediate stabilisation) is competing with **4.36** for coordination to $^{99m}Tc^V$.

Accordingly, radiolabelling with Kit 2 was investigated as this kit contained less of the tartrate weak chelator. However, despite testing Kit 2 at both 30 and 60 °C, no notable improvement was observed.

Subsequently, Kit 3 was prepared. This kit was simplified as much as possible; it contained no sodium tartrate or sodium hydrogen carbonate. The stannous chloride was not removed from the kit as it is necessary for the reduction of pertechnetate, $[TcO_4]^-$, from oxidation state +7 to +5. By removing any species that may interfere with the coordination of **4.36**, it was hoped radiolabelling may occur. Kit 3 was heated with $[TcO_4]^-$ for 30 min at 30 °C and pertechnetate (at 2 min) and a single broad but more intense peak at 12 min were seen in the radio-HPLC trace (Figure 4.28). Although this result is more promising than those seen for Kits 1 & 2, LC-MS analysis did not detect any molecular weights that corresponded to chemically sensible reaction products.

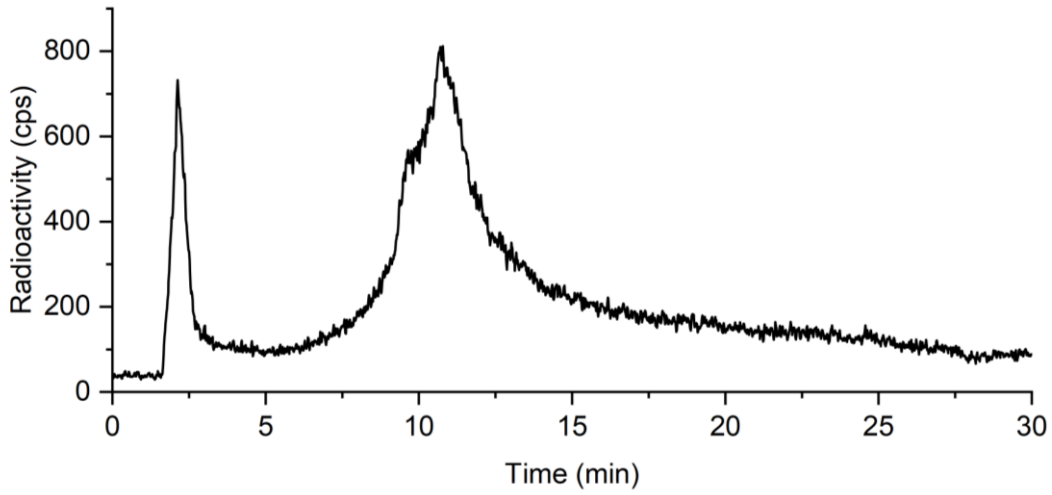

Figure 4.28 HPLC chromatogram of radiolabelling of Kit 3 with $[^{99m}TcO_4]^-$ (30 min, 30 °C).

The radiolabelling of Kit 3 was repeated at 60°C for 30 mins and gave radio-HPLC trace shown in Figure 4.29. Again, the well-defined peak with a retention time of approximately 2 mins corresponds to a large quantity of unreacted $[TcO_4]^-$. A series of broad and overlapping peaks of low intensity are present between 10-14 mins, but there is no evidence of a single species being formed in good yield. Heating this kit for a longer period (60 min) resulted in no improvement to the chromatogram. Consequently, despite testing a number of kits and conditions, clean and efficient radiolabelling of **4.36** was not achieved. Poor radiolabelling of **4.36** has precluded further testing of this compound, and these results suggest that the 4-membered chelate may be too strained for efficient ^{99m}Tc radiolabelling. Larger chelates should therefore be investigated in the future (Section 4.6).

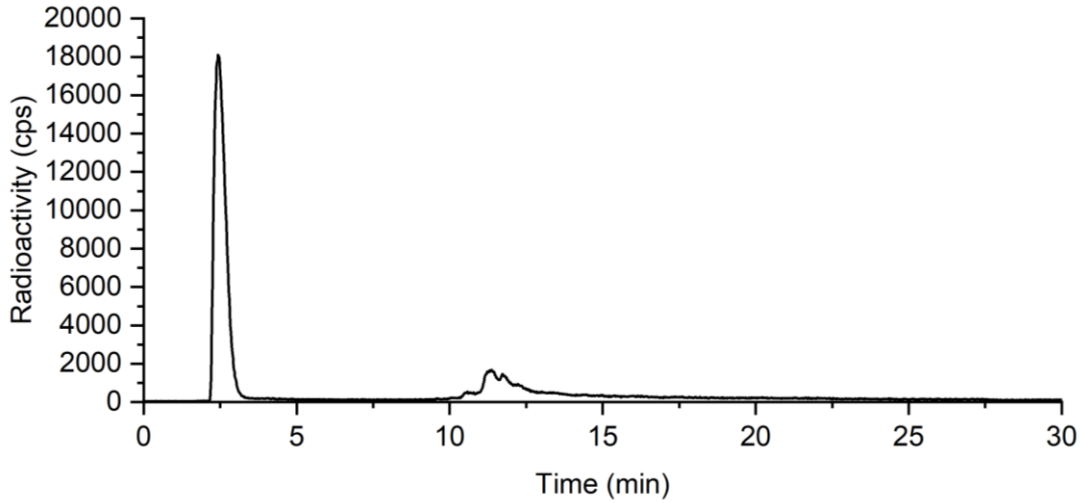

Figure 4.29 HPLC chromatogram of the radiolabelling of kit RD3.3 with $[^{99m}TcO_4]^-$ (30 min, 60 °C).

4.6. Conclusions & Future Work

Several methods have been investigated for the synthesis of bidentate phosphine glycoconjugates. Routes involving the synthesis of phenolic diphosphines from haloarenes were found to be unproductive (Section 4.2 and 4.3). Consequently, the methods investigated in Sections 4.4 and 4.5 avoided the direct synthesis of Ar-P bonds from Ar-X species (where X=Cl, Br, I). Instead, diphosphines containing phenolic or carboxylic acid functions were prepared and investigated for bioconjugation. The two novel bidentate phosphine glycoconjugates, **4.29** and **4.36** have been obtained (Figure 4.30).

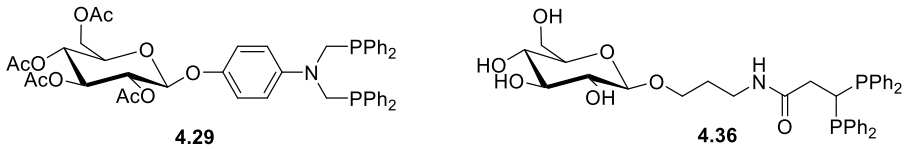

Figure 4.30 Structure of bidentate phosphine glycoconjugates, **4.29** and **4.36**.

Unfortunately, both **4.29** and **4.36** had features (see discussion below) that prevented their successful incorporation into ^{99m}Tc radio-complexes. However, synthesis of these ligands has increased the number of examples of bidentate phosphine glycoconjugates as, to the best of our knowledge, there has only been one previously reported example of a fully-deprotected bidentate phosphine glycoconjugate (Figure 4.31).

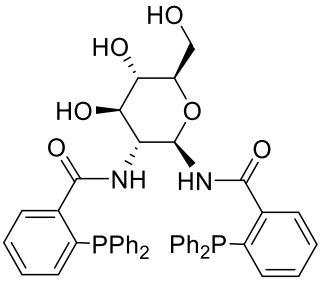

Figure 4.31 Bidentate phosphine glycoconjugate, reported by Ruffo *et al*.,[8] where the native carbohydrate is intact and fully deprotected.

Compound **4.24** (deprotected **4.29**) could not be formed when the diphenylphosphonium salt (**4.22**) and carbohydrate **4.28** were reacted together using the conditions outlined in Scheme 4.25. However, **4.29** was prepared when **4.23** was reacted with acetobromo-α-D-glucose in the presence of NaOH and BTEAB (Table 4.1). Unfortunately, **4.29** was not formed exclusively, and we were unable to purify it sufficiently for it to be investigated for radiolabelling with ^{99m}Tc. As **4.29** exhibits promise when reacting with a Re(V)-dioxo core, to give **4.30**, future work should focus on the improving the synthesis of **4.29**/**4.24**. Alternative routes for glycolysis, should therefore be investigated.

Compound **4.36** was formed using amide coupling chemistry, and column chromatography gave this product, although in poor yield (0.5% yield over 10 steps) as a single product. However, reacting **4.35** (the peracetylated analogue of **4.36**) with $[ReO_2I(PPh_3)_3]$ did not give exclusive formation of the bis(chelate) complex, **4.39**. Unexpectedly, a second complex, **4.40**, was also formed. Here, the Re(V) centre has been reduced to Re(III), and the bidentate P(III)/P(III)-diphosphine ligand is partially oxidised to give a bidentate P(III)/P(V) species. Despite these disappointing results, the ^{99m}Tc coordination chemistry of **4.36** was investigated, but conditions for the successful radiolabelling of **4.36** with ^{99m}Tc(V) were not identified. It is postulated that the ^{99m}Tc complex formed by **4.36** may be destabilised by the 4-membered ring strain.

Future research should look to combine the successful Re(V) coordination chemistry of **4.29**, and more reproducible amide coupling chemistry of **4.36**. Hence compound **4.41** (Scheme 4.32) combines both of these aspects, making it a promising target for the future.

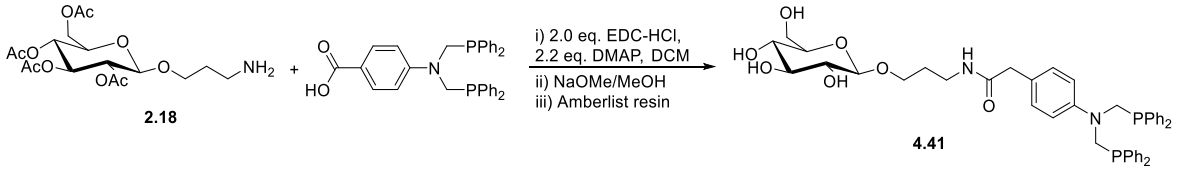

Scheme 4.32 Proposed route to target **4.41**, which should overcome the associated issues with **4.29** and **4.36**.

Lastly, the synthesis of **4.4** (3,4-bis(diphenylphosphino)phenol), or its glycoconjugate analogue **4.1**, proved to be especially challenging. However, we now propose an alternative route to **4.1** that uses commercially available 3,4-difluorophenol as the starting material (Scheme 4.33(b)). ***Step II*** of this proposed method is based on a procedure for the synthesis of dppbz from 1,2-difluorobenzene, which was published by Lipshutz *et al.* (Scheme 4.33(a)).[35] The reported yield for this reaction was 75%, which is a considerable improvement on that reported by Schmidbaur *et al.* when starting from 1,2-dichlorobenzene (10% yield).[15] This suggests that the reaction with difluroroarene is significantly cleaner, and therefore should be investigated in the future.

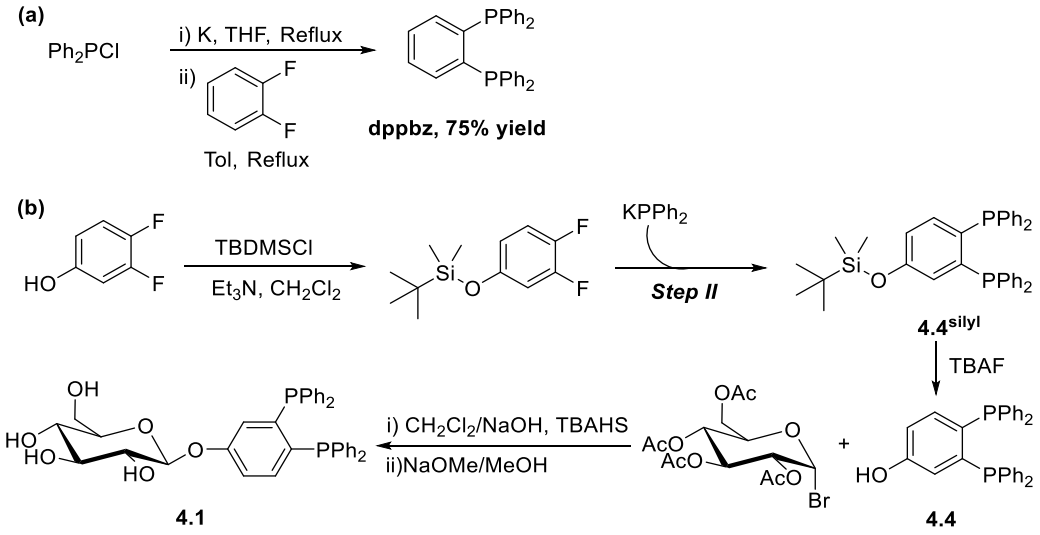

Scheme 4.33 (a) The synthesis of dppbz, published by Lipshutz *et al.*, and (b) the proposed route to **4.1** incorporating method (a) in Step *II*.

4.7. References

1 S. Jones and R. C. Hendel, *J Nucl Med*, 1993, **21**, 191–195.

2 WO, 2015, WO2015129926.

3 E. Deutsch, K. Libson, J. L. Vanderheyden, A. R. Ketring and H. R. Maxon, *Int. J. Radiat. Appl. Instrum.*, 1986, **13**, 465–477.

4 N. C. Okoye, J. E. Baumeister, F. N. Khosroshahi, H. M. Hennkens and S. S. Jurisson, *Radiochim. Acta*, 2019, **107**, 1087–1120.

5 I. S. Fagerson, *J. Agric. Food Chem.*, 1969, **17**, 747–750.

6 P. Tomasik, M. Palasinski and S. Wiejak, *Adv. Carbohydr. Chem. Biochem.*, 1989, **47**, 203–278.

7 M. L. Bowen and C. Orvig, *Chem. Commun.*, 2008, 5077–91.

8 R. Breslow, *Recl. des Trav. Chim. des Pays-Bas*, 1994, **113**, 493–498.

9 A. Boschi, L. Uccelli and P. Martini, *Appl. Sci.*, 2019, **9**, 1–16.

10 V. Benessere, A. De Roma, R. Del Litto, M. Lega and F. Ruffo, *Eur. J. Org. Chem.*, 2011, 5779–5782.

11 M. Beller, J. G. E. Krauter, A. Zapf and S. Bogdanovic, *Catal. Today*, 1999, **48**, 279–290.

12 B. M. Trost and C. Marschner, *Bull Soc Chim Fr*, 1997, **134**, 263–274.

13 M. Mueckler and B. Thorens, *Mol. Aspects Med.*, 2013, 34, 121–138.

14 M. Beller, J. G. E. Krauter and A. Zapf, *Angew. Chem. Int. Ed. Eng.*, 1997, **36**, 772–774.

15 G. A. Bowmaker, R. Herr and H. Schmidbaur, *Chem. Ber.*, 1983, **116**, 3567–3579.

16 F. Sieber, P. Wentworth, J. D. Toker, A. D. Wentworth, W. A. Metz, N. N. Reed and K. D. Janda, *J. Org. Chem.*, 1999, **64**, 5188–5192.

17 N. A. Bondarenko, E. I. Matrosov, E. N. Tsvetkov and M. I. Kabachnik, *Bull. Acad. Sci. USSR*, 1980, **29**, 92–98.

18 P. M. Byers and I. V. Alabugin, *J. Am. Chem. Soc.*, 2012, **134**, 9609–9614.

19 Y. Hu, K. Yu, L.-L. Shi, L. Liu, J.-J. Sui, D.-Y. Liu, B. Xiong and J.-S. Sun, *J. Am. Chem. Soc.*, 2017, **139**, 12736–12744.

20 J. Guo and X.-S. Ye, *Molecules*, 2010, **15**, 7235–7265.

21 J. T. Christl, P. Roesle, F. Stempfle, P. Wucher, I. Göttker-Schnetmann, G. Müller and S. Mecking, *Chem. Eur. J.*, 2013, **19**, 17131–17140.

22 Jp, JP2015/858, 2015.

23 S. L. James, PhD Thesis, University of Bristol, 1992.

24 G. Barozzino Consiglio, P. Queval, A. Harrison-Marchand, A. Mordini, J.-F. Lohier, O. Delacroix, A.-C. Gaumont, H. Gérard, J. Maddaluno and H. Oulyadi, *J. Am. Chem. Soc.*, 2011, **133**, 6472–6480.

25 S. Vigo, R. Andrés, P. Gómez-Sal, J. De La Mata and E. De Jesús, *J. Organomet. Chem.*, 2012, **717**, 88–98.

26 J. Zhang, J. J. Vittal, W. Henderson, J. R. Wheaton, I. H. Hall, T. S. A. Hor and Y. K. Yan, *J. Organomet. Chem.*, 2002, **650**, 123–132.

27 A. Temeriusz, T. Gubica, P. Rogowska, K. Paradowska and M. K. Cyrański, *Carbohydr. Res.*, 2005, **340**, 1175–1184.

28 R. Roy, F. D. Tropper, T. Morrison and J. Boratynski, *J. Chem. Soc. Chem. Commun.*, 1991, 536–538.

29 R. Roy, F. D. Tropper, T. Morrison and J. Boratynski, *J. Chem. Soc. Chem. Commun.*, 1991, 536–538.

30 X. Li, M. Zangiabadi and Y. Zhao, *J. Am. Chem. Soc.*, 2021, **143**, 5172–5181.

31 C. Kremer, M. Rivero, E. Kremer, L. Suescun, A. W. Mombrú, R. Mariezcurrena, S. Domínguez, A. Mederos, S. Midollini and A. Castiñeiras, *Inorganica Chim. Acta*, 1999, **294**, 47–55.

32 N. T. Coles, M. F. Mahon and R. L. Webster, *Chem. Commun.*, 2018, **54**, 10443–10446.

33 M. Rivero, C. Kremer, J. Gancheff, E. Kremer, L. Suescun, A. Mombrú, R. Mariezcurrena, S. Domínguez, A. Mederos and S. Midollini, *Polyhedron*, 2000, **19**, 2249–2254.

34 R. Rossi, A. Marchi, L. Marvelli, L. Magon, M. Peruzzini, U. Casellato and R. Graziani, *Inorganica Chim. Acta*, 1993, **204**, 63–71.

35 B. A. Baker, Ž. V. Bošković and B. H. Lipshutz, *Org. Lett.*, 2008, **10**, 289–292.

Chapter 5 :Summary

5.1. Overall summary and conclusions of Chapters 2-4

In this project, a variety of different routes towards phosphine glycoconjugates have been explored. Whilst many of these routes proved challenging several new examples were prepared, which primarily exploited palladium cross coupling or amide coupling methodology. This work is of note as previously few examples of fully deprotected phosphine glycoconjugates ligands have been reported in the literature.[1-3]

Chapter 2 focused on the preparation of monophosphine glycoconjugates that incorporated an alkyl linker into their structure. This was based on previous reports by Schibli and Orvig *et al.*, whereby poor transport of ^{99m}Tc amino glycoconjugate complexes into cells were attributed to either too short or too inflexible a linker being incorporated into their structures.[4] Traditional methods towards the synthesis of glycoconjugates (Lewis acid mediated glycolysis chemistry) or tertiary phosphines (lithiation, hydrophosphination or quaternisation chemistry) proved unsuccessful. This has been attributed to incompatibilities between the starting materials and reagents necessary to promote these coupling reactions. Therefore, amine coupling was probed and led to the synthesis of **2.21** (Figure 5.1). A kit was prepared with **2.21** and successful radiolabelling was achieved with the Tc(V)-dioxo core. Unfortunately, stability testing in mouse serum was poor. This has been attributed to displacement of the phosphine ligand by cysteine on the Tc(V)-dioxo core. Whilst poor stability has precluded further testing of the ^{99m}Tc complex (**2.25**) this is, to the best of our knowledge, the first example of a phosphine glycoconjugate that has been radiolabelled with ^{99m}Tc. This is therefore an interesting example within the field of radiochemistry.

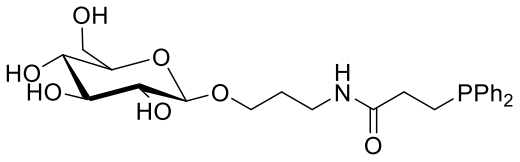

2.21

Figure 5.1 Monophosphine glycoconjugate **2.21**, prepared *via* amide coupling chemistry.

Chapter 3 built on the examples of phosphine glycoconjugates published by Beller in 1997 and led to the generation of a small library of such ligands.[1] The rhenium coordination chemistry of these ligands (Figure 5.2) was investigated before they were radiolabelled with ^{99m}Tc. The tricarbonyl core was used this time, and consequently a two-kit process was necessary. Radiolabelling was successful for ligands **3.1**, **3.4**, **3.5** and **3.7**, and the stability of the ^{99m}Tc complex formed with ligand **3.1** (**3.11**) proved favourable. Further studies have therefore looked at the cellular uptake of some of the Rhenium complexes, with ICP-MS

revealing that these complexes could be transported into the cells. The uptake appears to be dependant on the carbohydrate moiety, as opposed to the phosphine moiety, and the cells can distinguish between the carbohydrate (Glucose *versus* Galactose). These results have demonstrated that a shorter linker between the phosphine and carbohydrate moieties can be suitable, and this does not preclude the uptake of these complexes, despite previous results by Schibli and Orvig *et al*.[4] These results corroborate those seen by Li *et al.* and has led to a consensus within the Pringle and Galan groups that incorporation of synthetically challenging longer linkers may not be necessary.[5] This is therefore of importance for all future studies.

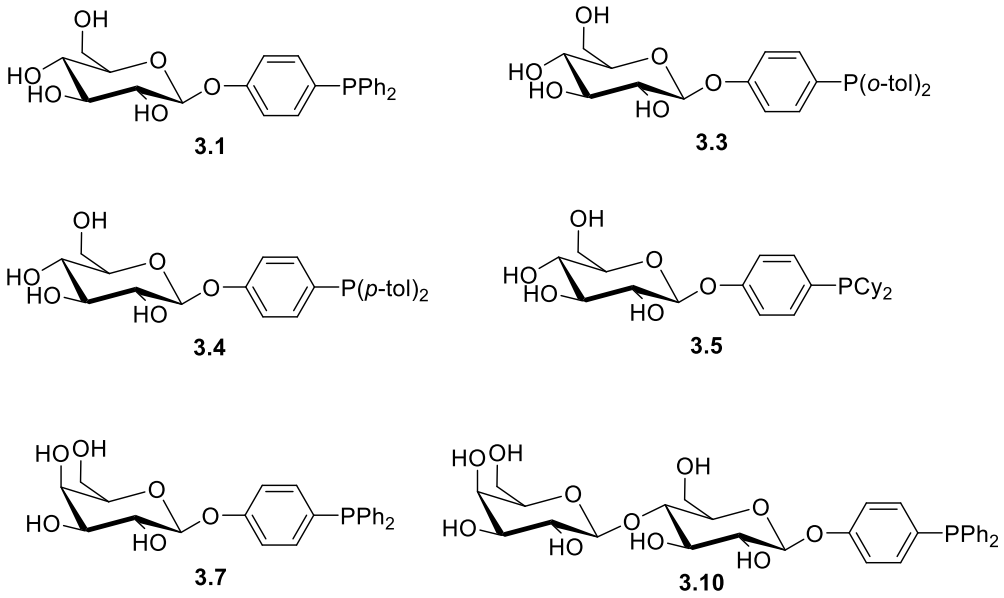

Figure 5.2 Structure of molecules synthesised in Chapter 3.

Chapter 4 investigated routes towards bidentate phosphine glycoconjugates. Several were investigated, but routes involving the synthesis of phenolic diphosphines from haloarenes were generally unproductive (Section 4.2-4.3). Instead, amide coupling proved to be more reliable and led to the synthesis of **4.36** (Figure 5.3). Unfortunately, rhenium coordination chemistry did not proceed as expected and suitable conditions for radiolabelling of **4.36** with ^{99m}Tc were not found. Whilst the radiochemical result was disappointing, the synthesis of **4.36** and **4.29** (see Chapter 4, Figure 5.3) has increased the number of reported examples of bidentate phosphine glycoconjugates as, to the best of our knowledge, there has only been one previously reported example of a fully-deprotected bidentate phosphine glycoconjugate by Ruffo *et al.*[3]

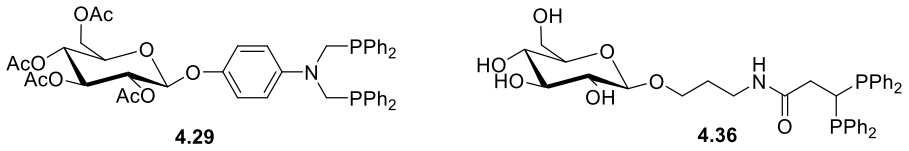

Figure 5.3 Structure of bidentate glycoconjugates synthesised in Chapter 4.

Chapter 4 has demonstrated that there is a significant increase in complexity when forming bidentate analogues, which has primarily stemmed from the difficultly in preparing the phosphine moiety. Additionally, it can be observed throughout the thesis that conjugation of phenolic moieties is not particularly reliable. Amide coupling has proved to be a much more reliable method and should be exploited more in when preparing future phosphine glycoconjugate molecules.

Beyond synthesising a variety of interesting molecules, a number of other important discoveries have been made from a productivity perspective. We have discovered useful conditions for the HPLC purification of Re(I) complexes, for which there is little precedent for in the literature. Additionally, this was the first time the London Metallomics Facility have investigated the uptake of rhenium in cells. We now have a protocol in place, both for performing these cellular uptake tests and for analysing the uptake in cells, which will be of significant use for subsequent group members researching in this area, and for students at KCL (where the LMF are based) who want to look at quantification of rhenium content in cells.

5.2. References

1 M. Beller, J. G. E. Krauter and A. Zapf, *Angew. Chem. Int. Ed. Eng.*, 1997, **36**, 772–774.

2 T. N. Mitchell and K. Heesche-Wagner, *J. Organomet. Chem.*, 1992, **436**, 43–53.

3 V. Benessere, A. De Roma, R. Del Litto, M. Lega and F. Ruffo, *Eur. J. Org. Chem.*, 2011, **29**, 5779–5782.

4 M. L. Bowen and C. Orvig, *Chem. Commun.*, 2008, **41**, 5077–5091.

5 Y. Cheng, G. Shabir, X. Li, L. Fang, L. Xu, H. Zhang and E. Li, *Chem. Commun.*, 2020, **56**, 1070.

Chapter 6 : Experimental

6.1. General Considerations

6.1.1. Reagents and Experimental Conditions

All reactions were performed under a nitrogen atmosphere using standard Schlenk techniques and oven dried glassware, unless otherwise stated. Oxygen and/or moisture sensitive compounds were manipulated and stored in an MBraun glove box with an argon atmosphere. CH_2Cl_2, MeCN, THF, Et_2O and hexane were collected from the University of Bristol Grubbs-type solvent system and stored over 4 Å molecular sieves. MeOH and EtOH were purchased as anhydrous solvents from Sigma Aldrich and stored over 3 Å molecular sieves. Non-deuterated solvents were deoxygenated by sparging with N_2 for 30-60 min. $CDCl_3$ and ^{d6}DMSO were dried over activated 4 Å molecular sieves and deoxygenated by three successive freeze-pump-thaw cycles, whilst CD_3OD was dried over activated 3 Å molecular sieves and deoxygenated by sparging with N_2 for 30 min. Wet solvents were provided by Fisher or Merck and used without further purification. HPLC grade MeCN, MeOH, DMSO and H_2O were used for all HPLC analysis and preparation of such samples. Technetium-99m was provided as pertechnetate ($[TcO_4]^-$) in saline by the radio pharmacy department Guy's Hospital and normal mouse serum was purchased form Sigma Aldrich (M5905-5ML) and stored at -20 °C. Tc tricarbonyl CRS kits were purchased from the Centre for Radiopharmaceutical Science at the Paul Scherrer Institute and stored at 4 °C.

The following molecules were prepared as reported in the literature and the spectroscopic data matches that previously reported: Glucose pentaacetate[1], acetobromo-α-D-glucose[1], (diphenylphosphino)ethan-1-ol (**2.3**)[2], O-(2,3,4,6-tetra-O-acetyl-α-D-glucopyranosyl)trichloroacetimidate (**2.4**)[1], O-(2,3,4,6-tetra-O-benzyl-α,β-D-glucopyranosyl) trichloroacetimidate **2.12**[3], (3-azido-propyl)-(tetra-O-acetyl-β-D-glucopyranoside)[1], (3-amino-propyl)-(tetra-O-acetyl-β-D-glucopyranoside) (**2.18**)[1], $[Re(CO)_3(H_2O)_3]Br$[4], acetobromo-α-D-galactose[5], lactose-octaacetate[6], acetobromo-α-D-lactose (**3.8**)[5], 1-(4-iodophenol)-tetra-acetyl-glucopyranose (**3.2**)[7], 1-(4-iodophenol)-tetra-acetylgalactopyranose (**3.6**)[8], $[Pd_2(P(o\text{-tol})_3)_2(OAc)_2]$[9], $HP(p\text{-Tol})_2$[10], 4-aminophenol-β-D-glucopyranoside (**4.28**)[11], 1,2-diiodophenol[12], ethyl 3,3-bis(diphenylphosphaneyl)propanoate[13] and 3-azidopropyl β-D-glucopyranoside[14].

Other commercial reagents and chemicals were used without further purification unless stated otherwise.

6.1.2. Characterisation

^{1}H, ^{13}C and ^{31}P and NMR spectra were recorded on Bruker cryo500, Varian 500-MR, Jeol ECZ 400, Jeol ECS 400, or Jeol ECS 300 spectrometers at room temperature, unless otherwise stated. The spectra were processed using MestReNova software with chemical shifts (δ) reported in parts per million (ppm) and coupling constants (*J*) measured in Hertz (Hz). Residual solvent peak signals were used for the calibration of ^{1}H and ^{13}C NMR spectra ($CDCl_3$ δ_H 7.26, δ_C 77.2 ppm, CD_3OD δ_H 7.26, δ_C 77.2 ppm, ^{d6}DMSO δ_H 7.26, δ_C 77.2 ppm). ^{31}P chemical shifts are reported with reference to an external standard (85% H_3PO_4). Infrared data was collected using a Perkin-Elmer Spectrum One FTIR machine with a scanning range of 4000-400 cm^{-1}. Mass spectrometry data (ESI+) obtained at the University of Bristol Mass Spectrometry Service was recorded on a Bruker Daltonics micrOTOF II instrument, whilst mass spectra data recorded at King's College London was collected by an Advion Expression Compact Mass spectrometer equipped with an ESI probe. X-ray crystallographic data was obtained using a Bruker Kappa Apex II diffractometer, and all structures were processed using Olex2 software (see Chapter 6, Section 6.1 for details).

The carbohydrate numbering system follows nomenclature for pyranoside species and is shown below in Figure 6.1. This will be referred to for NMR assignments of pyranose-containing species. Where a mixture of anomers occur, partial integrals will be given.

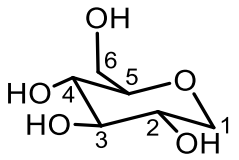

Figure 6.1 Numbering system for pyranose-type carbohydrates.

6.1.3. HPLC Methods

Purification of radioactive samples was performed as follows: Semi-preparative and analytical HPLC purification were both performed on an Agilent 1200 series HPLC system. The HPLC system, operated using Laura software, was equipped with a Rheodyne 200 µL sample loop and Eclipse XBD-C18 column (4.6 x 150 mm, 5 µm) to perform reverse-phase HPLC with a flow rate of 1 mL min^{-1}. Mobile phase A was water with 0.1% TFA and mobile phase B was acetonitrile with 0.1% TFA. For Method 1 (35 mins) UV detection was set to 220 nm, and the concentration of B was increased from 5% to 100% over 25 min. The concentration of B was maintained at 100% for 5 min, before the gradient decreased back to 5% of B over the last 5 min. For Method 2 (30 min) UV detection was set to 220 nm, and the concentration of B was increased from 5% to 100% over 20 min. The concentration of B

was maintained at 100% for 5 min, before the gradient decreased back to 5% of B over the last 5 min.

Purification of non-radioactive rhenium samples were performed as follows: Preparative HPLC purification was performed on a Grace Discovery Series Reveleris Prep system. The HPLC system, operated using BUCHI software, was equipped with a 5 mL sample loop and Phenomenex Luna 5 µm C18(2) AXIA packed column (250 x 21.2 mm, 100 Å) to perform reverse phase HPLC with a flow rate of 14 mL min^{-1}. Mobile phases A and B were water and MeOH, respectively. For this method (Method 3, 55 mins) the instrument was set to monitor the ELSD signal as well as performing 220, 265 and 254 nm UV detection. The concentration of B was held at 5% for 5 mins, then increased from 5% to 95% over 30 mins. Next, the concentration of B was maintained at 95% for 10 mins, before the gradient was decreased to 5% of B over 5 mins, and 5% of B was maintained for a further 5 mins to re-equilibrate the column prior to the next run. The fractions were combined and concentrated as would be for flash column chromatography.

6.2. Experimental Procedures and Characterisation Data - Chapter 2

6.2.1. Synthesis of 3-(diphenylphosphino)propan-1-ol, 2.5[15]

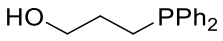

AIBN (23.0 mg, 10 mol%) and $HPPh_2$ (0.250 mL, 1.43 mmol) were stirred for 10 mins, then allyl alcohol (0.100 mL, 1.43 mmol) was added and the resulting solution was heated to 70 ºC for 48 h. All volatiles were removed *in vacuo* and the product, 3-(diphenylphosphino)propan-1-ol (**2.5**), was isolated as a colourless oil without need for further purification (290 mg, 1.19 mmol, 83% yield). **$^{31}P\{^{1}H\}$ NMR** δ_P (121 MHz, $CDCl_3$) (δ, ppm): -15.6 (s). **^{1}H NMR** (300 MHz, $CDCl_3$) (δ, ppm): 7.69-7.19 (m, 10H, Ar*H*), 3.64 (m, 2H, CH_2OH), 2.09-2.02 (m, 2H, PCH_2), 1.08 (br s, 1H, O*H*), 1.68-1.58 (m, 2H, PCH_2CH_2). $^{31}P\{^{1}H\}$ and ^{1}H NMR data match that previously reported in literature.[15]

6.2.2. Synthesis of 3-(boraneyldiphenylphosphino)propan-1-ol, 2.6

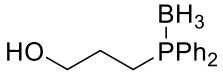

3-(diphenylphosphino)propan-1-ol (290 mg, 1.19 mmol) in CH_2Cl_2 (5 mL) was cooled to 0 ºC and $BH_3.SMe_2$ (0.340 mL, 3.73 mmol) was added dropwise. The reaction was left to warm-up to ambient temperature and after 48 h all volatiles were removed *in vacuo*. The residue was partitioned between CH_2Cl_2 (5 mL) and brine (10 mL), and the aqueous phase was extracted into CH_2Cl_2 (2 x 5 mL). The organic phases were combined, dried over anhydrous $MgSO_4$, filtered and the solvent was removed *in vacuo* to give a clear oil as the final product (180 mg, 0.700 mmol, 59% yield). **$^{31}P\{^{1}H\}$ NMR** δ_P (121 MHz, $CDCl_3$) (δ,

ppm): 16.4-14.9 (br m, Ph_2P-BH_3). **$^{11}B\{^1H\}$ NMR** δ_B (96 MHz, $CDCl_3$) (δ, ppm) -41.8 (d, $^1J_{B\text{-}P}$ = 57.9 Hz, Ph_2P-BH_3). **^1H NMR** δ_H (300 MHz, $CDCl_3$) (δ, ppm): 7.71-7.66 (m, 4H, Ar*H*), 7.53-7.42 (m, 6H, Ar*H*), 3.70-3.63 (m, 2H, CH_2OH), 2.36-2.30 (m, 2H, PC$H_2$$CH_2$), 1.80-1.73 (m, 2H, PCH_2CH_2), 1.60-0.60 (m, 3H, BH_3). $^{31}P\{^1H\}$, $^{11}B\{^1H\}$ and ^1H NMR data matches that previously reported in literature.[16]

6.2.3. Synthesis of 3-(boraneyldiphenylphosphino)propan-1-ol tethered glycoconjugate, 2.10

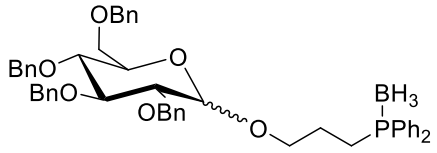

O-(2,3,4,6-tetra-O-benzyl-α-D-glucopyranosyl) trichloroacetimidate, **2.8**, (68.0 mg, 0.100 mmol) was dried under vacuum for 30 min then dissolved in CH_2Cl_2 (2 mL). To this, a solution of **2.6** (24.0 mg, 0.080 mmol) in CH_2Cl_2 (0.5 mL) was added and the resulting mixture cooled to 0 °C. After stirring at 0 °C for 10 min, TMSOTf in CH_2Cl_2 (50 µL, 0.2 M, 0.010 mmol) was added to the reaction and the temperature maintained at 0 °C for 1 h. The resulting mixture was left to warm to room temperature and after stirring for 40 h, the reaction was quenched by addition of saturated NH_4Cl (1 mL). The reaction was diluted with EtOAc (5 mL) and the organics were washed with brine (2 x 5 mL), dried over $MgSO_4$, filtered and all solvent removed *in vacuo* to give a residue (71.0 mg). This was purified by column chromatography (EtOAc:Hex gradient from 10:90 to 100:0, R_f = 0.40) and **2.10** (4.50 mg, 5.76 µmol, 6% yield) was isolated as a 1.8:1 α:β mixture. **$^{31}P\{^1H\}$ NMR** (121 MHz, $CDCl_3$) (δ, ppm): 15.9 (br s, Ph_2P-BH_3). **$^{11}B\{^1H\}$ NMR** δ_B (96 MHz, $CDCl_3$) (δ, ppm) -40.7 (d, $^1J_{B\text{-}P}$ = 57.2 Hz, Ph_2P-BH_3). **MS (ESI+)**: *m/z* calcd. for $C_{49}H_{58}NBO_6P$ ($[M+NH_4]^+$) =798.8; obs. = 798.6; *m/z* calcd. for $C_{49}H_{54}BO_6PNa$ ($[M+Na]^+$) =803.7; obs. = 803.5.

6.2.4. Synthesis of 1-(3-bromopropoxy)-2,3,4,6-tetra-O-benzyl-D-glucopyranose, 2.14

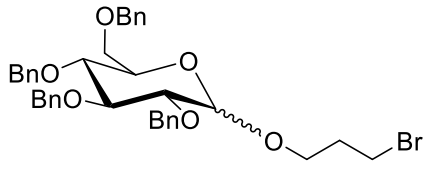

O-(2,3,4,6-tetra-O-benzyl-α,β-D-glucopyranosyl) trichloroacetimidate, **2.12**, (1.14 g, 1.46 mmol) was dried under vacuum for 1.5 h then dissolved in anhydrous CH_2Cl_2 (10 mL). To this, 3-bromopropan-1-ol (0.265 mL, 2.92 mmol) was added and the reaction stirred at room temperature for 1 h. $BF_3.OEt_2$ (0.900 mL, 7.30 mmol) was added dropwise to the reaction at -40 °C and the reaction was maintained at -40 °C for 2 h. The reaction was left to warm to room temperature and stirred overnight before being quenched with saturated $NaHCO_3$ (15

mL). The organics were extracted into CH_2Cl_2 (3 x 20 mL), washed with brine (30 mL), dried over $MgSO_4$, filtered and all volatiles removed *in vacuo* to give the crude product. The product was recrystallised from a mixture of CH_2Cl_2 and pentane at -20 °C to give **2.14** (880 mg, 1.33 mmol, 91% yield). **^{1}H NMR** (500 MHz, $CDCl_3$) (δ, ppm): 7.38-7.28 (m, 20H, Ar*H*), 5.02-4.88 (m, 8H, 4 x OC*H*$_2$Ph), 4.80 (d, 0.55H, *J* = 2.3 Hz, H-1α), 4.43 (d, 0.45H, *J* = 7.8 Hz, H-1β), 4.07 (app. dt, 0.45H, *J* = 10.0, 5.6 Hz, H-3β), 3.98 (d, 0.55H, *J* = 9.2 Hz, H-3α), 3.87-3.45 (m, 9H, H-2, H-4, H-5, H-6a, H-6b, 2 x C*H*$_2$), 2.35-1.99 (m, 2H, C*H*$_2$). Partial integrals are quoted for ^{1}H signals that correspond to the H-1α/β and H-3α/β signals, with all other signals overlapping significantly. **HR-MS (ESI+)**: *m/z* calcd. for $C_{37}H_{41}BrO_6Na$ ($[M+Na]^+$) =683.1984; obs = 683.1996. The characteristic bromide isotope pattern can be observed in the HR-MS.

6.2.5. Synthesis of 3-bromopropyl 2,3,4,6-tetra-O-acetyl-β-D-glucopyranoside, 2.16[17]

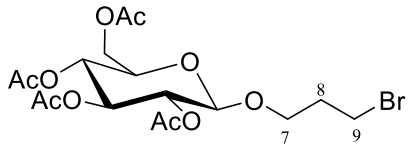

O-(2,3,4,6-tetra-O-acetyl-α-D-glucopyranosyl)trichloroacetimidate, **2.4**, (4.60 g, 9.34 mmol) was dried under vacuum for 1 h then dissolved in anhydrous CH_2Cl_2 (30 mL). To this, 3-bromopropan-1-ol (1.70 mL, 18.80 mmol) was added and the reaction stirred at room temperature for 1 h. $BF_3.OEt_2$ (5.70 mL, 46.18 mmol) was added dropwise to the reaction at -40 °C and the reaction was maintained at this temperature for 2 h. The reaction was left to warm up to room temperature and was stirred overnight before being quenched with saturated $NaHCO_3$ (40 mL). The organics were extracted into CH_2Cl_2 (3 x 100 mL), washed with brine (150 mL), dried over $MgSO_4$, filtered and all volatiles removed *in vacuo* to give the crude product (5.27 g). The crude product was purified by column chromatography (EtOAc:Hex, 1:1, which gave **2.16** (2.81 g, 5.99 mmol, 64% yield). **^{1}H NMR** (400 MHz, $CDCl_3$) (δ, ppm): 5.22 (app. t, 1H, *J* = 9.5 Hz, H-3), 5.08 (app. t, 1H, *J* = 9.7 Hz, H-4), 4.99 (dd, 1H, *J* = 9.6, 7.9 Hz, H-2), 4.51 (d, 1H, *J* = 7.9 Hz, H-1), 4.27 (dd, 1H, *J* = 12.3, 4.8 Hz, H-6a), 4.14 (dd, 1H, *J* = 12.2, 2.4 Hz, H-6b), 3.99 (dt, *J* = 9.9, 5.1 Hz, 1H, H-5), 3.76-3.73 (m, 2H, H-7a & H-7b), 3.16 (br. d, 2H, H-9a & H-9b), 2.12 (s, 3H, OAc), 2.20-2.11 (m, 2H, H-8a & H-8b), 2.11 (s, 3H, OAc), 2.03 (s, 3H, OAc), 2.01 (s, 3H, OAc). The ^{1}H NMR data matches that previously reported in the literature.[17]

6.2.6. Synthesis of 1-(3-aminopropoxy)-2,3,4,6-tetra-acetyl-glucopyranose, 2.18

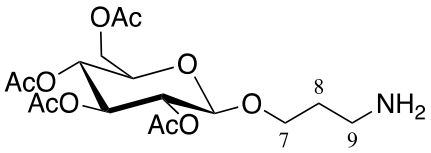

The following procedure was modified from literature.[1] To a solution of 3-azidopropyl-2,3,4,6-tetra-O-acetyl-β-D-glucopyranoside (1.10 g, 2.55 mmol) in MeOH (35 mL) was added Pd catalyst (10% Pd-C, 110 mg). The reaction was stirred under a hydrogen atmosphere (1 atm) for 4 h. The reaction mixture was filtered through a Celite bed, washed with MeOH (15 mL) and the filtrate concentrated *in vacuo*. This residue was dissolved in CH_2Cl_2 (20 mL), washed with brine (20 mL) and the organic layer then dried over anhydrous $MgSO_4$. Filtration and solvent removal *in vacuo* gave **2.18** as a colourless residue (0.461 g, 1.13 mmol, 44% yield). **^{1}H NMR** δ_H (400 MHz, $CDCl_3$) (δ, ppm): 5.22 (app. t, 1H, *J* = 9.7 Hz, H-3), 5.08 (app. t, 1H, *J* = 9.7 Hz, H-4), 4.96 (dd, 1H, *J* = 9.7, 8.0 Hz, H-2), 4.54 (d, 1H, *J* = 8.0 Hz, H-1), 4.29-4.19 (m, 2H, H-6a & H-6b), 4.05-3.98 (m, 1H, H-5), 3.76-3.73 (m, 2H, H-7a & H-7b), 3.16 (br. d, 2H, H-9a & H-9b), 2.12 (s, 3H, OAc), 2.11 (s, 3H, OAc), 2.03 (s, 3H, OAc), 2.01 (s, 3H, OAc). HSQC analysis has shown that signals for H-8a and H-8b are buried under OAc signals in the ^{1}H NMR spectrum.**HR-MS** (ESI+): m/z calcd. for $C_{17}H_{27}NO_{10}$ ($[M+H]^+$) = 406.1708; obs. = 406.1710.

6.2.7. Synthesis of 3-(diphenylphosphine)propanoic acid, 2.19[19]

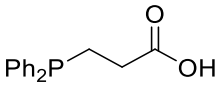

The following procedure was modified from literature methods.[18,19] $HPPh_2$ (0.280 mL, 1.61 mmol) was added to $Pt(nbe)_3$ (1.90 mg, 2.50 mol%) in DCM (8 mL), and the resulting orange solution was stirred for 10 min. *t*BuOH (3.00 mL, 31.4 mmol) was added to the orange reaction mixture, followed by slow dropwise addition of methyl acrylate (0.150 mL, 1.67 mmol). The reaction was stirred at room temperature for 6 h before this mixture was filtered through a silica plug and all volatiles removed *in vacuo*. The yellow solid was re-dissolved in de-oxygenated MeOH (3 mL) and 10 M NaOH (1.5 mL) was added. This mixture was stirred for 2 h before 2M HCl was added to adjust the pH to *ca.* pH 2. The product was extracted into CH_2Cl_2 (3 x 10 mL) and isolated by removal of the solvent *in vacuo* to give **2.19** as a white solid (0.310 g, 1.20 mmol, 75% yield). **^{31}P{^{1}H} NMR** δ_P (121 MHz, $CDCl_3$) (δ, ppm) -16.6 (s). **^{1}H NMR** δ_H (300 MHz, $CDCl_3$) (δ, ppm): 7.46-7.27 (m, 10H, Ar*H*), 2.48-2.40 (m, 2H, CH_2), 2.38-2.32 (m, 2H, CH_2).^{31}P and ^{1}H NMR data matches that previously reported in the literature.[19]

6.2.8. Synthesis of ^{OAc}Glc-O-$(CH_2)_3$NHC(O)$(CH_2)_2PPh_2$, 2.20

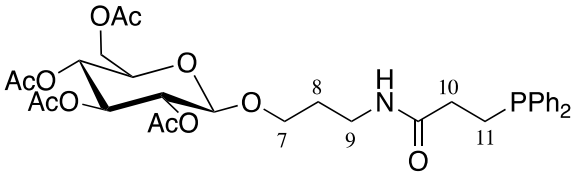

DMAP (100 mg, 0.819 mmol) and EDC-HCl (140 mg, 0.730 mmol) were added to 3-(diphenylphosphino)propanoic acid (90.0 mg, 0.348 mmol) in CH_2Cl_2 (7 mL). This mixture was stirred for 30 min at room temperature and **2.18** (141 mg, 0.348 mmol) in CH_2Cl_2 (3 mL) was added. After stirring at room temperature for 16 h, the reaction was diluted with CH_2Cl_2 (15 mL) and washed with HCl (1 M, 15 mL), saturated $NaHCO_3$ (15 mL) and brine (15 mL). The organics were dried over anhydrous $MgSO_4$, filtered and the solvent removed *in vacuo* to give the crude product as an oil. This was purified by flash chromatography (EtOAc:Hex, 2:1, R_f = 0.16) and **2.20** (94.0 mg, 0.146 mmol, 42% yield) was isolated as a colourless oil. **^{31}P{^{1}H} NMR** (121 MHz, $CDCl_3$) (δ, ppm): -14.9 (s). **^{1}H NMR** (400 MHz, $CDCl_3$) (δ, ppm): 7.46-7.41 (m, 4H, ArH), 7.35-7.31 (m, 6H, ArH), 5.89 (br t, 1H, $^1J_{NH}$ = 5.5 Hz, C(O)N*H*), 5.20 (app. t, 1H, *J* = 9.5 Hz, H-3), 5.06 (app. t, 1H, $^3J_{HH}$ = 9.7 Hz, H-4), 4.94 (dd, 1H, *J* = 9.7, 8.0 Hz, H-2), 4.46 (d, 1H, *J* = 8.0 Hz, H-1), 4.24-4.12 (m, 2H, H-6a & H-6b), 3.89 (ddd, 1H, *J* = 9.6, 7.1, 4.7 Hz, H-7a), 3.65 (ddd, 1H, *J* = 10.0, 4.6, 2.4 Hz, H-5), 3.54 (ddd, 1H, *J* = 9.7, 6.7, 4.8 Hz, H-7b), 3.40-3.16 (m, 2H, H-9a & H-9b), 2.39-2.33 (m, 2H, H-11a & H-11b), 2.31-2.23 (m, 2H, H-10a & H-10b), 2.05 (s, 3H, OAc), 2.02 (s, 3H, OAc), 2.01 (s, 6H, OAc), 1.81-1.66 (m, 2H, H-8a & H-8b). **^{13}C NMR** δ_C (100 MHz, $CDCl_3$) (δ, ppm): 172.5 (br. s, 1C, *C*(O)NH), 172.4 (s, 1C, CH_3*C*OO), 172.3 (s, 1C, CH_3*C*OO), 169.6 (s, 1C, CH_3*C*OO), 169.5 (s, 1C, CH_3*C*OO), 133.0 (d, 2C, $^3J_{PC}$ = 5.3 Hz, Ar*C*), 132.8 (d, 2C, $^3J_{PC}$ = 5.2 Hz, Ar*C*), 129.1 (s, 1C, Ar*C*), 129.0 (s, 1C, Ar*C*), 128.9 (s, 2C, Ar*C*), 128.6 (s, 2C, Ar*C*), 101.0 (s, 1C, C-1), 72.7 (s, 1C, C-3), 72.1 (s, 1C, C-2), 71.4 (s, 1C, C-4), 68.6 (s, 1C, C-7), 68.5 (s, 1C, C-5), 61.9 (s, 1C, C-6), 37.3 (s, 1C, C-9), 32.9 (d, 1C, $^1J_{PC}$ = 18.5 Hz, C-11), 29.9 (s, 1C, C-8), 29.4 (d, 1C, $^2J_{PC}$ = 11.6Hz, C-10), 20.93 (s, 1C, *C*H_3COO), 20.86 (s, 1C, *C*H_3COO), 20.79 (s, 1C, *C*H_3COO), 20.77 (s, 1C, *C*H_3COO). The quaternary ArC atom could not be observed in the ^{13}C NMR spectrum. **HR-MS (ESI+)**: *m/z* calcd. for $C_{32}H_{41}NO_{11}P$ ($[M+H]^+$) = 646.2412; obs. = 646.2404. **IR**: 2930 (br, N-H stretch), 1746 (s, R_2C(=O) stretch), 1659 (m, NHC(=O) stretch).

6.2.9. Synthesis of ^{OH}Glc-O-$(CH_2)_3$NHC(O)$(CH_2)_2PPh_2$, 2.21

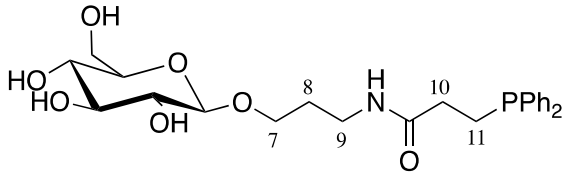

1M sodium methanolate (0.200 mL, 0.200 mmol) was added to **2.20** (87.0 mg, 0.135 mmol) dissolved in EtOAc (5 mL) and MeOH (5 mL). After stirring at room temperature for 24 h, Amberlyst 120 resin was added to reduce the pH to 7. The Amberlyst 120 resin was prepared by washing with MeOH then drying the resin in air. The reaction was filtered and concentrated *in vacuo* to give **2.21** as white solid (50 mg, 0.105 mmol, 78% yield). **$^{31}P\{^1H\}$ NMR** (121 MHz, D_2O) (δ, ppm): -14.8 (s). **^{1}H NMR** (500 MHz, D_2O) (δ, ppm): 7.55-7.50 (m, 4H, ArH), 7.46-4.45 (m, 6H, ArH), 4.42 (d, 1H, *J* = 8.0 Hz, H-1), 3.99-3.86 (m, 2H, H-6a & H-7a), 3.70-3.62 (m, 3H, H-6b & H-7b), 3.47 (app. t, 1H, *J* = 9.0 Hz, H-3), 3.44-3.40 (m, 1H, H-5), 3.36 (dd, 1H, *J* = 9.9, 8.9 Hz, H-4), 3.25 (dd, 1H, *J* = 9.4, 8.0 Hz, H-2), 3.20-3.11 (m, 2H, H-9a & H-9b), 2.47-2.36 (m, 4H, H-10a, H-10b, H-11a & H-11b), 1.80-1.70 (m, 2H, H-8a & H-8b). Amide and alcohol protons cannot be observed in D_2O, trace impurities are observed. **^{13}C NMR** (126 MHz, D_2O) (δ, ppm): 173.7 (d, 1C, $^3J_{PC}$ = 8.7 Hz, *C*(O)NH), 131.1 (d, 2C, $^3J_{PC}$ = 5.9 Hz, *o*-Ar*C*), 131.0 (d, 2C, $^3J_{PC}$ = 5.8 Hz, *o*-Ar*C*), 127.9 (s, 1C, *p*-Ar*C*), 127.8 (s, 1C, p-Ar*C*), 127.30 (d, 2C, $^3J_{PC}$ = 7.0 Hz, *m*-Ar*C*), 127.29 (d, 2C, $^3J_{PC}$ = 7.1 Hz, *m*-Ar*C*), 102.2 (1C, s, C-1), 75.9 (s, 1C, C-5), 75.7 (s, 1C, C-3), 73.1 (s, 1C, C-2), 69.7 (s, 1C, C-4), 67.8 (s, 1C, C-7), 60.7 (s, 1C, C-6), 36.3 (s, 1C, C-9), 32.1 (d, 1C, $^1J_{PC}$ = 16.6 Hz, C-11), 28.3 (s, 1C, C-8), 22.4 (d, 1C, $^2J_{PC}$ = 8.3 Hz, C-10). **HR-MS (ESI+)**: *m/z* calcd. for $C_{24}H_{32}NO_7PNa$ ($[M+Na]^+$) = 500.1814; obs. = 500.1825. Impurity signals observed at 3.63 and 1.63 ppm in the ^{1}H NMR, correlate to signals at 59.1 ppm and 31.4 ppm in the ^{13}C NMR. Additionally, the quaternary Ar*C* signal cannot be observed in ^{13}C NMR spectrum.

6.2.10. General Procedure for Re(I) Complexes with Phosphine Ligands

Phosphine ligand (2 eq.) in CH_2Cl_2 (0.5 mL) or MeOH (0.5 mL) was added to $[Re(CO)_3(H_2O)_3]Br$ (1 eq.) in MeOH (0.3 mL) at room temperature. Once the reaction reached completion, as determined by ^{31}P NMR spectroscopy, all volatiles were removed *in vacuo* to isolate the $[Re(CO)_3(PR_3)_2Br]$ complex.

6.2.11. Synthesis of [Re(CO)$_3$(2.20)$_2$Br], 2.22

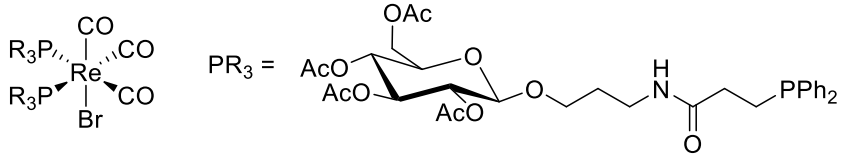

2.22 was synthesised according to the general procedure outlined in Section 5.2.10. Further data could not be recorded due to the instability of this compound in solution (see Chapter 2, Section 2.3.1, where it hydrolyses to give **2.23**). **^{31}P{^{1}H} NMR** (121 MHz, $CDCl_3$) (δ, ppm) 7.1 (s, 2P). **MS (ESI+)**: *m/z* calcd. for $C_{67}H_{82}BrN_2O_{25}P_2Re$ ($[M+2H]^+$) = 1643.3; obs. = 1643.3. The characteristic bromide isotope pattern can be observed in the MS.

6.2.12. Synthesis of [Re(CO)$_3$(2.19)$_2$Br], 2.23

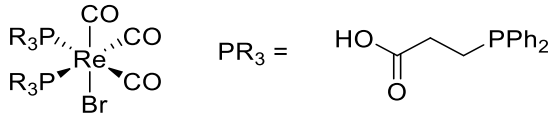

2.23 was synthesised according to the general procedure outlined in Section 5.2.10. Crystals of the methyl ester product suitable for X-ray diffraction we obtained upon leaving the reaction to stand. **^{31}P{^{1}H} NMR** (121 MHz, CD_3OD) (δ, ppm) -10.4 (s, 2P).

6.2.13. Synthesis of [ReO$_2$I(2.20)$_2$], 2.24

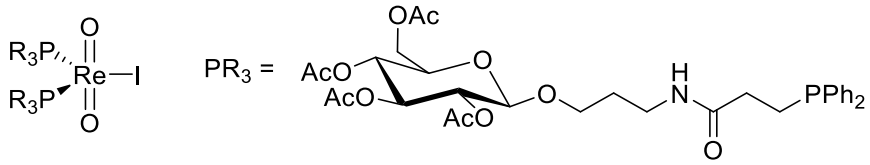

2.20 (21.0 mg, 32.50 μmol) in MeOH (0.5 mL) was added to $[Re(O)_2(PPh_3)_2I]$ (14.0 mg, 16.10 μmol) in CH_2Cl_2 (0.3 mL) and the reaction was stirred at room temperature. Once the reaction had reached completion, as determined by ^{31}P NMR spectroscopy, all volatiles were removed *in vacuo* to isolate the Re(V) complex, **2.24**. Removal of PPh_3 (from the Re(V) precursor) was performed by repeated washing of the solid with ice-cold Et_2O (4 x 5 mL) to give **2.24** (10.0 mg, 6.15 μmol, 38% yield). Further purification by washing with portions of hot hexane was attempted, however this proved unsuccessful. **^{31}P{^{1}H} NMR** (121 MHz, $CDCl_3$) (δ, ppm) -0.3 (s, 2P). **^{1}H NMR** (400 MHz, $CDCl_3$) (δ, ppm): 8.34 (br s, C(O)N*H*), 7.36-7.28 (m, 12H, ArH), 7.19-7.13 (m, 8H, ArH), 5.24 (app. t, 2H, *J* = 9 Hz, H-3), 5.05 (app. t, 2H, *J* = 10 Hz, H-2), 4.93 (app. t, 2H, *J* = 9 Hz, H-4), 4.63 (d, 2H, *J* = 8 Hz, H-1), 4.30-4.14 (m, 4H, H-6a & H-6b), 4.05-3.99 (m, 2H, H-7a), 3.83-3.74 (m, 4H, H-5 & H-7b), 3.68-3.59 (m, 4H, H-9a & H-9b), 3.12-2.86 (m, 8H, H-10a, H-10b, H-11a & H-11b), 2.08 (s, 6H, OAc), 2.06 (s, 6H, OAc), 2.02 (s, 6H, OAc), 2.00 (br s, 4H, H-8a & H-8b) 1.98 (s, 6H, OAc). **MS (ESI+)**: *m/z* calcd. for $C_{64}H_{80}N_2O_{24}P_2Re$ ($[M-I]^+$) = 1509.4; obs. = 1509.4; *m/z* calcd. for $C_{64}H_{82}IN_2O_{25}P_2Re$ ($[M+H_2O]^+$) = 1654.3; obs. = 1654.3.

6.2.14. Synthesis of ^{99m}Tc(V) complexes with 2.21

Kits for radiolabelling **2.21** are listed in Chapter 2, Section 2.4, Table 2.4. Standard solutions of the reagents that were added to the kit (ligand, stannous chloride, sodium tartrate and sodium hydrogen carbonate) were prepared in purified water or ethanol. The kits were freeze-dried in Eppendorf tubes immediately after preparation then stored under a nitrogen or argon atmosphere at -20 ºC in a freezer.

Synthesis of the ^{99m}Tc(V) complexes was performed by addition of the $[^{99m}TcO_4]^-$ saline solution (5-10 µL, 10-20 MBq) and saline (500 µL) to a thawed kit. The solubilised kit was incubated at room temperature or 50 ºC for 30 min. Aliquots of these samples were analysed by analytical HPLC (Method 2, 100-150 µL).

6.2.15. Serum stability testing of ^{99m}Tc complexes

Mouse serum (850 µL) was added to a 150 µL aliquot of the Tc complex and this mixture heated at 37.5 ºC. After incubation for 1 and 2 h, a 150 µL aliquot was removed and shaken vigorously with MeCN to precipitate the proteins in the serum. This mixture was centrifuged (130,000 rpm, 2 mins) and the supernatant removed without disturbing the pellet. The supernatant was centrifuged (130,000 rpm, 2 mins) for a second time and then placed in a clean Eppendorf tube to remove any remaining traces of protein. The MeCN was evaporated under a flow of N_2, and the contents of the Eppendorf tube re-dissolved in saline (150 µL) then analysed by analytical HPLC (Method 2, 150 µL).

6.3. Experimental Procedures and Characterisation Data - Chapter 3

6.3.1. General Procedure for the Synthesis of 3.1′, 3.3′, 3.4′, 3.5′ & 3.7′

This general procedure was adapted from a literature procedure.[20] Carbohydrate **3.2** or **3.6** (1 eq.), KOAc (1.2 eq.) and $[Pd_2(P(o\text{-tol})_3)_2(OAc)_2]$ (1 mol%) were dissolved in MeCN (5 mL per 0.2 mmol of carbohydrate). After 10 min, the secondary phosphine was added to this mixture and heated to reflux for 16 hrs if $HPPh_2$ (1 eq.), $HP(o\text{-Tol})_2$ (1 eq.), $HP(p\text{-Tol})_2$ (1 eq.) or 5 d if $HPCy_2$ (2 eq.). Upon cooling, the mixture was concentrated *in vacuo* and the residue dissolved in CH_2Cl_2 and washed with deionised water (2 x 5mL) and brine (5 mL). The organics were dried over anhydrous $MgSO_4$, and filtration then evaporation under a reduced pressure gave the crude product. Removal of excess of secondary phosphine was performed by dissolving the crude product in MeCN and washing with hexane. Oxide impurities were removed by silica plug purification (EtOAc:Hex 50:50), to give the desired final product.

6.3.2. Synthesis of ^{OAc}Glc-O-Ph-PPh$_2$, 3.1′

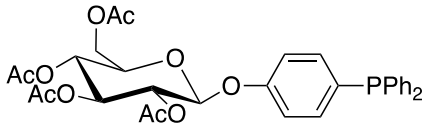

3.1′ (122 mg, 0.278 mmol, 77% yield) was prepared according to the general procedure outlined in Section 5.3.1. **^{31}P{^{1}H} NMR** (162 MHz, $CDCl_3$) (δ, ppm): -6.3 (s). **^{1}H NMR** (400 MHz, $CDCl_3$) (δ, ppm): 7.33-7.23 (m, 12H, Ar-H), 6.95 (dd, 2H, *J* = 8.8, 1.0 Hz, Ar-H), 5.29-5.25 (m, 2H, H-3 & H-2), 5.17-5.13 (m, 1H, H-4), 5.09 (d, 1H, *J* = 8.0 Hz, H-1), 4.27 (dd, 1H, *J* = 12.3, 5.4 Hz, H-6a), 4.13 (dd, 12.3, 2.4 Hz, H-6b), 3.84 (ddd, 1H, *J* = 10.0, 5.4, 2.4 Hz, H-5), 2.04 (s, 3H, OAc), 2.03 (s, 3H, OAc), 2.02 (s, 6H, OAc). **^{13}C NMR** (121 MHz, $CDCl_3$) (δ, ppm): 170.7, 170.4, 169.5, 169.4 (s, 4C, 4 x CH_3*C*OO), 157.5 (s, 1C, quart. Ar*C*), 135.6 (d, 4C, J_{PC} = 20.9 Hz, Ar*C*), 133.7 (d, 4C, J_{PC} = 19.5 Hz, Ar*C*), 130.2-128.0 (m, 4C, Ar*C*), 117.0 (d, 2C, J_{PC} = 7.6 Hz, Ar*C*), 98.8 (s, 1C, C-1), 72.9 (s, 1C, C-2/3), 72.2 (s, 1C, C-2/3), 71.3 (s, 1C, C-5), 68.4 (s, 1C, C-4), 62.1 (s, 1C, C-6), 20.80, 20.77. 20.75, 20.72 (s, 4C, 4 x *C*H_3COO).**HR-MS** (ESI+): m/z calcd. for $C_{32}H_{33}O_{10}PNa$ ([M+Na]$^+$) = 631.1709; obs. = 631.1723. Quaternary Ar*C* atoms (that were directly bound to phosphorus) could not be observed in the ^{13}C spectrum.

6.3.3. Synthesis of ^{OAc}Glc-O-Ph(*o*-Tol), 3.3′

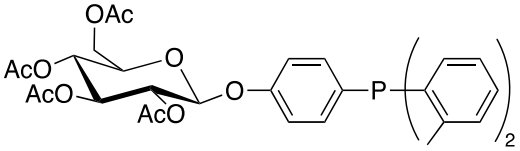

3.3′ (77.9 mg, 0.122 mmol, 67% yield) was prepared according to the general procedure outlined in Section 5.3.1. **^{31}P{^{1}H} NMR** (162 MHz, $CDCl_3$) (δ, ppm): -21.9 (s). **^{1}H NMR** (400 MHz, $CDCl_3$) (δ, ppm): 6.62-6.50 (m, 6H, Ar*H*), 6.43 (app. t, 2H, *J* = 7.2 Hz, Ar*H*), 6.31 (dd, 2H, *J* = 8.8, 1.0 Hz, Ar*H*) 6.03 (dd, 2H, *J* = 7.6, 4.6 Hz, Ar*H*), 4.67-4.60 (m, 2H, H-3 & H-2), 4.53-4.44 (m, 2H, *J* = 8.0 Hz, H-4 & H-1), 3.64 (dd, 1H, *J* = 12.3, 5.4 Hz, H-6a), 3.50 (dd, 12.3, 2.4 Hz, H-6b), 3.20 (ddd, 1H, *J* = 10.0, 5.4, 2.4 Hz, H-5), 1.71 (br s, 6H, *o*-Tol), 1.40 (s, 3H, OAc), 1.39 (s, 3H, OAc), 1.380 (s, 3H, OAc), 1.375 (s, 3H, OAc). **^{13}C NMR** (121 MHz, $CDCl_3$) (δ, ppm): 170.9, 170.6, 169.8, 169.7 (s, 4C, 4 x CH_3*C*OO), 157.7 (s, 1C, quart. Ar*C*), 142.6 (d, 2C, J_{PC} = 22.6 Hz, quart. Ar*C*), 136.4 (d, 2C, J_{PC} = 21.4 Hz, Ar*C*), 135.4-135.2 (m, 1C, quart. Ar*C*), 133.6 (s, 2C, Ar*C*), 130.5 (d, 2C, J_{PC} = 5.0 Hz, Ar*C*), 129.5 (d, 2C, J_{PC} = 10.1 Hz quart. Ar*C*-CH_3), 128.7 (s, 2C, ArC), 117.4 (d, 2C, J_{PC} = 7.6 Hz, Ar*C*), 99.0 (s, 1C, C-1), 73.1 (s, 1C, C-2/3), 72.5 (s, 1C, C-2/3), 71.5 (s, 1C, C-5), 68.7 (s, 1C, C-4), 62.3 (s, 1C, C-6), 21.6 (s, 1C, *o*-CH_3), 21.5 (s, 1C, *o*-CH_3), 21.1, 21.1, 21.0, 21.0 (s, 4C, 4 x *C*H_3COO). **HR-MS** (Nanospray+): m/z calcd. for $C_{34}H_{38}O_{10}P$ ([M+H]$^+$) = 637.2203; obs. = 637.2184.

6.3.4. Synthesis of ^{OAc}Glc-O-Ph-P(*p*-Tol)$_2$, 3.4′

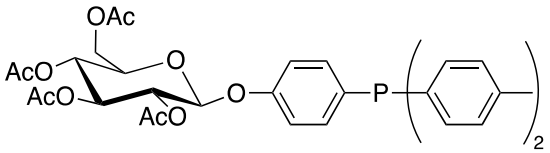

3.4′ (125 mg, 0.196 mmol, 73% yield) was prepared according to the general procedure outlined in Section 5.3.1. **^{31}P{^{1}H} NMR** (162 MHz, $CDCl_3$) (δ, ppm): -7.9 (s). **^{1}H NMR** (400 MHz, $CDCl_3$) (δ, ppm): 7.23 (dd, 2H, *J* = 8.7, 7.0 Hz, Ar*H*), 7.21-7.09 (m, 10H, Ar*H*), 6.93 (dd, 2H, *J* = 8.7, 1.0 Hz, Ar*H*), 5.33-5.21 (m, 2H, H-3 & H-2), 5.18-5.13 (m, 1H, H-4), 5.09 (m, 1H, H-1), 4.27 (dd, 1H, *J* = 12.3, 5.4 Hz, H-6a), 4.13 (dd, 12.3, 2.5 Hz, H-6b), 3.86 (ddd, 1H, *J* = 10.0, 5.3, 2.5 Hz, H-5), 2.33 (s, 6H, *p*-C*H*$_3$), 2.03 (s, 3H, OAc), 2.03 (s, 3H, OAc), 2.02 (s, 3H, OAc), 2.02 (s, 6H, OAc). **^{13}C NMR** (121 MHz, $CDCl_3$) (δ, ppm): 170.7, 170.4, 169.5, 169.4 (s, 4C, 4 x CH_3*C*OO), 157.3 (s, 1C, quart. Ar*C*), 138.7 (s, 2C, quart. Ar*C*-CH_3), 135.3 (d, 2C, J_{PC} = 20.7 Hz, Ar*C*), 133.7 (d, 4C, J_{PC} = 19.7 Hz, Ar*C*), 129.5 (d, 4C, J_{PC} = 7 Hz, Ar*C*), 117.0 (d, 2C, J_{PC} = 7.3 Hz, Ar*C*), 98.8 (s, 1C, C-1), 72.9 (s, 1C, C-2/3), 72.2 (s, 1C, C-5), 71.3 (s, 1C, C-2/3), 68.4 (s, 1C, C-4), 62.1 (s, 1C, C-6), 21.4 (s, 2C, *p*-*C*H_3) 20.79, 20.76, 20.74, 20.71 (s, 4C, 4 x *C*H_3COO). **HR-MS** (Nanospray+): m/z calcd. for $C_{34}H_{38}O_{10}P$ ([M+H]$^+$) = 637.2203; obs. = 637.2219. Quaternary Ar*C* atoms (that were directly bound to phosphorus) could not be observed in the ^{13}C spectrum.

6.3.5. Synthesis of ^{OAc}Glc-O-Ph-PCy$_2$, 3.5′

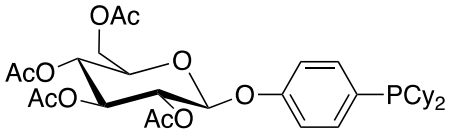

3.6′ (122 mg, 0.196 mmol, 55% yield) was prepared according to the general procedure outlined in Section 5.3.1 **^{31}P{^{1}H} NMR** (162 MHz, $CDCl_3$) (δ, ppm): -2.2 (s). **^{1}H NMR** (400 MHz, $CDCl_3$) (δ, ppm): 7.39 (app. t, 2H, *J* = 7.3 Hz, Ar*H*), 6.95 (d, 2H, *J* = 8.5 Hz, Ar*H*), 5.33-5.24 (m, 2H, H-3 & H-2), 5.20-5.12 (m, 2H, H-4 & H-1), 4.30 (dd, 1H, *J* = 12.3, 5.4 Hz, H-6a), 4.18 (dd, 12.3, 2.5 Hz, H-6b), 3.88 (ddd, 1H, *J* = 10.0, 5.4, 2.5 Hz, H-5), 2.07 (s, 3H, OAc), 2.06 (s, 3H, OAc), 2.05 (s, 3H, OAc), 2.04 (s, 3H, OAc), 1.88-1.53 (m, 12H, CH_2) 1.35-1.04 (m, 12H, CH_2). **^{13}C NMR** (121 MHz, $CDCl_3$) (δ, ppm): 170.4, 170.1, 169.2, 169.2 (s, 4C, 4 x CH_3*C*OO), 136.0 (d, 2C, J_{PC} = 19.9 Hz, Ar*C*), 116.0 (d, 2C, J_{PC} = 10.0 Hz, Ar*C*), 98.5 (s, 1C, C-1), 72.6 (s, 1C, C-2/3), 71.9 (s, 1C, C-4), 71.0 (s, 1C, C-2/3), 68.2 (s, 1C, C-5), 61.8 (s, 1C, C-5), 32.5 (d, 2C, J_{PC} = 10.0 Hz, P-*Cy*), 29.8 (d, C, J_{PC} = 21.0 Hz, *Cy*), 27.3-27.0 (m, 4C, *Cy*), 29.8 (d, 2C, J_{PC} = 7.0 Hz, *Cy*), 26.2 (s, 4C, *Cy*), 20.5, 20.5, 20.4, 20.4 (s, 4C, 4 x *C*H_3COO). **HR-MS** (Nanospray+): m/z calcd. for $C_{32}H_{46}O_{10}P$ ([M+H]$^+$) = 621.2829; obs. = 621.2836.

6.3.6. Synthesis of ^{OAc}Gal-O-Ph-PPh$_2$, 3.7′

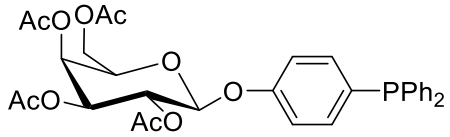

3.7′ (120 mg, 0.197 mmol, 69% yield) was prepared according to the general procedure outlined in Section 5.3.1 **^{31}P{^{1}H} NMR** (162 MHz, $CDCl_3$) (δ, ppm): -6.4 (s). **^{1}H NMR** (400 MHz, $CDCl_3$) (δ, ppm): 7.36-7.15 (m, 12H, Ar-H), 6.96 (dd, 2H, *J* = 8.8, 1.0 Hz, Ar-H), 5.50-5.43 (m, 2H, H-3 & H-2), 5.09 (dd, 1H, *J* = 10.5, 3.5 Hz, H-4) , 5.05 (d, 1H, *J* = 8.0 Hz, H-1), 4.25-4.08 (m, 2H, H-6a & H-6b), 4.03 (ddd, 1H, *J* = 7.2, 6.2, 1.2 Hz, H-5), 2.16 (s, 3H, OAc), 2.04 (s, 3H, OAc), 2.00 (s, 3H, OAc), 2.00 (s, 3H, OAc).

6.3.7. Synthesis of ^{OAc}Lac-O-Ph-I, 3.9

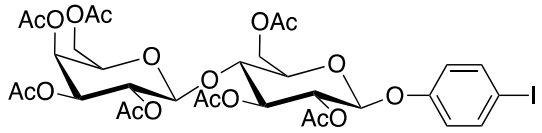

α-D-Lactosyl bromide heptaacetate (**3.8**) (2.50 g, 3.57 mmol), benzyltriethylammonium bromide (0.82 g, 3.01 mmol), 4-iodophenol (1.56 g, 7.09 mmol) and 1.25 M NaOH (11.5 mL) were dissolved in CH_3Cl (20 mL). This reaction mixture was heated to 60 °C for 4 h and upon cooling, diluted with deionised water (10 mL). The organics were separated, washed with 1.25 M NaOH (2 x 10 mL), dried over anhydrous $MgSO_4$, and filtered before the volatiles removed *in vacuo*. The crude product was purified by column chromatography (1:1 EtOAc:Hex, R_f = 0.24) to give **3.9** as a white powder (340 mg, 0.406 mmol, 11% yield). **^{1}H NMR** (500 MHz, $CDCl_3$) (δ, ppm): 7.57 (d, 2H, *J* = 8.7 Hz, Ar-H), 6.75 (d, 2H, *J* = 8.8 Hz, Ar-H), 5.35 (dd, 1H, *J* = 3.5, 1.2 Hz, Gal-H-4), 5.27 (t, 1H, *J* = 9.0 Hz, Glu-H-3), 5.15 (t, 1H, J = 9.2 Hz, Glu-H-2), 5.14-5.09 (m, 1H, Gal-H-2), 5.00 (d, 1H, J = 7.7 Hz, Glu-H-1), 4.96 (dd, 1H, J = 10.4, 3.4, Gal-H-3), 4.50 (d, 1H, J = 7.8 Hz, Gal-H-1), 4.48 (dd, 1H, J = 11.9, 2.2 Hz, Glu-H-6a), 4.18-4.04 (m, 3H, Glu-H-6b, Gal-H-6a & Gal-H-6b), 3.94-3.83 (m, 2H, Glu-H-5 & Glu-H-4), 3.76 (ddd, 1H, J = 9.9, 5.8, 2.2 Hz, Gal-H-5), 2.15 (s, 3H, OAc), 2.07 (s, 3H, OAc), 2.07 (s, 3H, OAc), 2.06 (s, 3H, OAc), 2.05 (s, 6H, 2 x OAc), 1.96 (s, 3H, OAc). **^{13}C NMR** (121 MHz, $CDCl_3$) (δ, ppm): 170.3, 170.2, 170.1, 170.0, 169.7, 169.5, 169.1, 156.6 (s, 7C, 7 x CH_3*C*OO), 138.44 (s, 2C, Ar*C*), 119.2 (s, 2C, Ar*C*), 101.1 (s, 1C, Gal-C-1), 98.6 (s, 1C, Glu-C-1), 86.1 (s, 1C, Ar*C*-I), 76.1 (s, 1C, Glu-C-4/C-5), 72.9 (s, 1C, Gal-C-5), 72.7 (s, 1C, Glu-C-3), 71.4 (s, 1C, Glu-C-2), 70.9 (s, 1C, Gal-C-3), 70.7 (s, 1C, Glu-C-4/5), 69.1 (s, 1C, Gal-C-2), 66.6 (s, 1C, Gal-C-4), 61.9 (s, 1C, Glu-C-6b), 60.8 (s, 3C, Gal-C-6a, Gal-C-6b& Glu-C-6), 20.76, 20.73, 20.64 20.62, 20.62, 20.60, 20.5 (s, 7C, 7 x *C*H_3COO). **HR-MS** (ESI+): m/z calcd. for $C_{32}H_{39}O_{18}INa$ ($[M+Na]^+$) = 861.1073; obs. =

861.1037. The quaternary Ar*C* atom directly bonded to iodine was not observed by ^{13}C NMR spectroscopy.

6.3.8. Synthesis of ^{OAc}Lac-O-Ph-PPh$_2$, 3.10′

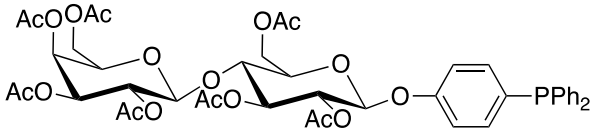

This procedure was modified from the literature.[21] 1M NaOH solution (2.00 mL, 2.00 mmol) was added to 4-hydroxydiphenylphosphine (50.0 mg, 0.18 mmol) and TBAHS (30.0 mg, 0.09 mmol) in CH_2Cl_2 (3.6 mL). After 15 min stirring at room temperature, α-D-lactosyl bromide heptaacetate (**3.8**) (380 mg, 0.54 mmol) was added. The reaction was vigorously stirred at room temperature for 16 h. The reaction was diluted with EtOAc (10 mL) and the organics were separated, washed with 1.25 M NaOH (2 x 4 mL) and brine (4 mL), dried (anhydrous $MgSO_4$) and filtered before the volatiles removed *in vacuo*. The crude product was purified by column chromatography (1:1 EtOAc:Hex, Rf = 0.28) to give the desired final product (15 mg, 16.7 μmol, 9% yield). **^{31}P NMR** (162 MHz, $CDCl_3$) (δ, ppm): -6.3 ppm. **^{1}H NMR** (400 MHz, $CDCl_3$) (δ, ppm): 7.48-7.20 (m, 12H, Ar-H), 7.00-6.93 (m, 2H, Ar-H), 5.38 (dd, 1H, *J* = 3.5, 1.2 Hz, Gal-H-4), 5.30 (t, 1H, *J* = 9.0 Hz, Glu-H-3), 5.24-5.12 (m, 2H, Glu-H-2 & Gal-H-2), 5.10 (d, 1H, J = 7.7 Hz, Glu-H-1), 4.99 (dd, 1H, J = 10.4, 3.4, Gal-H-3), 4.52 (d, 1H, J = 7.9 Hz, Gal-H-1), 4.49 (dd, 1H, J = 11.9, 2.2 Hz, Glu-H-6a), 4.18-4.09 (m, 3H, Glu-H-6b, Gal-H-6a & Gal-H-6b), 3.95-3.87 (m, 2H, Glu-H-5 & Glu-H-4), 3.79 (ddd, 1H, J = 9.9, 5.8, 2.2 Hz, Gal-H-5), 2.18 (s, 3H, OAc), 2.09 (s, 3H, OAc), 2.08 (s, 3H, OAc), 2.07 (s, 3H, OAc), 2.07 (s, 3H, OAc), 2.05 (s, 3H, OAc), 1.99 (s, 3H, OAc). **^{13}C NMR** (121 MHz, $CDCl_3$) (δ, ppm): 170.5, 170.4, 170.3, 170.2, 169.8, 169.7, 169.2 (s, 7C, 7 x CH_3COO), 157.5 (s, 1C, quart. Ar*C*), 137.5 (dd, 2C, J_{PC} = 10.6, 7.3 Hz, quart. Ar*C*), 135.6 (d, 2C, J_{PC} = 21.0 Hz, Ar*C*), 133.6 (d, 4C, J_{PC} = 19.3 Hz, Ar*C*), 131.3 (d, 1C, J_{PC} = 10.0 Hz, quart. Ar*C*), 128.8 (s, 2C, Ar*C*), 128.6 (d, 4C, J_{PC} = 6.8 Hz, Ar*C*), 117.0 (d, 2C, J_{PC} = 7.8 Hz, Ar*C*), 101.3 (s, 1C, Gal-C-1), 98.4 (s, 1C, Glu-C-1), 76.4 (s, 1C, Glu-C-4/C-5), 72.9 (s, 1C, Gal-C-5), 71.6 (s, 1C, Glu-C-3), 71.1 (s, 1C, Glu-C-2), 70.9 (s, 1C, Gal-C-3), 69.2 (s, 1C, Glu-C-4/5), 66.3 (s, 1C, Gal-C-2), 65.0 (s, 1C, Gal-C-4), 62.2 (s, 1C, Glu-C-6b), 61.0 (s, 3C, Gal-C-6a, Gal-C-6b & Glu-C-6a), 20.9, 20.86, 20.80, 20.77, 20.77, 20.75, 20.6 (s, 7C, 7 x CH_3COO). **HR-MS** (ESI+): m/z calcd. for $C_{44}H_{49}O_{18}P$ ($[M+H]^+$) = 897.2735; obs. = 897.2718.

6.3.9. General procedure for the synthesis of 3.1, 3.3, 3.4, 3.5, 3.7 and 3.10

1M sodium methanolate solution (0.66 eq) was added to the peracetylated glycoconjugate (1 eq.) in EtOAc:MeOH (1:1, 1 ml per 10 μmol of carbohydrate). After stirring at room temperature for 30-60 min, pre-prepared Amberlyst 120 resin was added to reduce the pH to

7. The reaction was filtered and concentrated *in vacuo* to give the deprotected glycoconjugate as the product. The Amberlyst 120 resin was prepared by washing with MeOH, then filtering and drying the resin in air.

6.3.10. Synthesis of ^{OH}Glc-O-Ph-PPh$_2$, 3.1

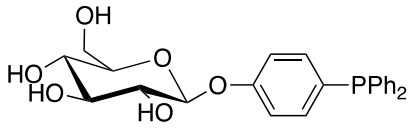

3.1 (17.7 mg, 40.2 µmol, 98% yield) was prepared according to the general procedure outlined in Section 5.3.9. **^{31}P{^{1}H} NMR** (162 MHz, CD_3OD) (δ, ppm): -6.6 (s). **^{1}H NMR** (400 MHz, CD_3OD) (δ, ppm): 7.36-7.24 (m, 12H, Ar*H*), 7.12 (d, 2H, *J* = 8.9 Hz, Ar*H*), 4.96 (d, 1H, *J* = 8.1 Hz, H-1), 3.90 (dd, 1H, *J* = 12.1, 2.1 Hz, H-6a), 3.70 (dd, 1H, *J* = 12.1, 5.5 Hz, H-6b), 3.51-3.37 (m, 3H, H-2,-3,-4,-5).**^{13}C NMR** (121 MHz, CD_3OD) (δ, ppm): 158.6 (s, 1C, quart. Ar*C*), 135.1 (d, 2C, J_{PC} = 21.4 Hz, Ar*C*), 133.2 (d, 4C, J_{PC} = 19.3 Hz, Ar*C*), 128.7-128.1 (m, 6C, Ar*C*), 116.5 (d, 2C, J_{PC} = 7.8 Hz, Ar*C*), 100.6 (s, 1C, C-1), 76.9 (s, 1C, C-2/3), 76.6 (s, 1C, C-2/3), 73.6 (s, 1C, C-5), 70.0 (s, 1C, C-4), 61.1 (s, 1C, C-6). **HR-MS** (ESI+): m/z calcd. for $C_{24}H_{25}O_6PNa$ ($[M+Na]^+$) = 463.1286; obs. = 463.1272. Quaternary Ar*C* atoms (that were directly bound to phosphorus) could not be observed in the ^{13}C spectrum.

6.3.11. Synthesis of ^{OH}Glc-O-Ph-P(*o*-Tol)$_2$, 3.3

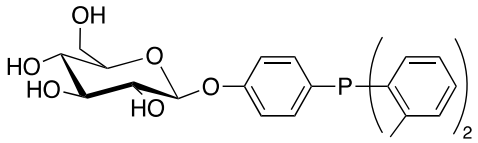

3.3 (11.5 mg, 24.5 µmol, 78% yield) was prepared according to the general procedure outlined in Section 5.3.9. **^{31}P{^{1}H} NMR** (162 MHz, CD_3OD) (δ, ppm): -22.9 (s). **^{1}H NMR** (400 MHz, CD_3OD) (δ, ppm): 7.26-6.98 (m, 10H, Ar*H*), 6.65 (dd, 2H, *J* = 7.5, 4.6 Hz, Ar*H*), 4.93 (dd, 1H, *J* = 5.4, 2.2 Hz, H-1), 3.86 (dd, 1H, *J* = 12.1, 2.2 Hz, H-6a), 3.66 (dd, 1H, *J* = 12.1, 5.4 Hz, H-6b), 3.49-3.32 (m, 4H, H-2,-3,-4,-5), 2.30 (s, 6H, *o*-CH_3). **^{13}C NMR** (126 MHz, CD_3OD) (δ, ppm): 159.9 (s, 1C, quart. Ar*C*), 143.1 (d, 2C, J_{PC} = 24.9 Hz, quart. Ar*C*), 136.9 (d, 2C, J_{PC} = 21.9 Hz, Ar*C*), 136.7 (d, 2C, J_{PC} = 10.9 Hz, quart. Ar*C*), 133.4 (d, 2C, J_{PC} = 2.6 Hz, Ar*C*), 131.0 (d, 2C, J_{PC} = 4.7 Hz, Ar*C*), 129.6 (s, 2C, Ar*C*), 128.9 (d, 1C, J_{PC} = 7.6 Hz, quart. Ar*C*), 126.9 (s, 2C, Ar*C*), 117.80 (d, 2C, J_{PC} = 7.8 Hz, Ar*C*), 101.7 (s, 1C, C-1), 78.0 (s, 1C, C-2/3), 77.8 (s, 1C, C-2/3), 74.7 (s, 1C, C-5), 71.2 (s, 1C, C-4), 62.3 (s, 1C, C-6), 22.8 (d, 2C, J_{PC} = 21.4 Hz, 2 x *o*-*C*H_3). **HR-MS** (Nanospray+): m/z calcd. for $C_{26}H_{29}O_6PNa$ ($[M+Na]^+$) = 491.1599; obs. = 491.1587.

6.3.12. Synthesis of ^{OH}Glc-O-Ph-P(*p*-Tol)$_2$, 3.4

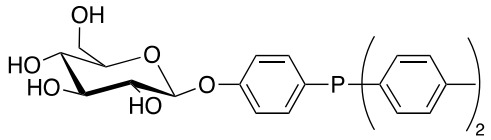

3.4 (46.7 mg, 99.7 µmol, 84% yield) was prepared according to the general procedure outlined in section 5.3.9. **^{31}P{^{1}H} NMR** (162 MHz, CD_3OD) (δ, ppm): -8.3 (s). **^{1}H NMR** (400 MHz, CD_3OD) (δ, ppm): 7.23-7.06 (m, 12H, Ar*H*), 4.93 (m, 1H, H-1), 3.89 (dd, 1H, *J* = 12.1, 2.1 Hz, H-6a), 3.69 (dd, 1H, *J* = 12.1, 5.4 Hz, H-6b), 3.50-3.36 (m, 4H, H-2,-3,-4,-5), 2.30 (s, 6H, 2 x *p*-CH_3). **^{13}C NMR** (121 MHz, CD_3OD) (δ, ppm): 139.9 (s, 2C, quart. Ar*C*), 136.2 (d, 4C, J_{PC} = 21.0 Hz, Ar*C*), 134.5 (d, 2C, J_{PC} = 20.0 Hz, Ar*C*), 130.2 (d, 4C, J_{PC} = 7.0 Hz Ar*C*), 116.5 (d, 2C, J_{PC} = 7.7 Hz, Ar*C*), 101.9 (s, 1C, C-1), 78.2 (s, 1C, C-2/3), 78.0 (s, 1C, C-2/3), 74.9 (s, 1C, C-5), 71.4 (s, 1C, C-4), 62.5 (s, 1C, C-6), 22.8 (s, 2C, *p*-CH_3). **HR-MS** (Nanospray+): m/z calcd. for $C_{26}H_{29}O_6PNa$ ($[M+Na]^+$) = 491.1599; obs. = 491.1592. The quaternary Ar*C* atoms bound directly to the phosphorus and oxygen atoms could not be observed in the ^{13}C spectrum.

6.3.13. Synthesis of ^{OH}Glc-O-Ph-PCy$_2$, 3.5

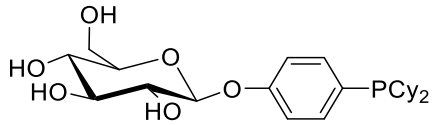

3.5 (19.7 mg, 43.5 µmol, 90% yield) was prepared according to the general procedure outlined in Section 5.3.9. **^{31}P{^{1}H} NMR** (162 MHz, CD_3OD) (δ, ppm): 1.9 (s). **^{1}H NMR** (400 MHz, CD_3OD) (δ, ppm): 7.37 (d, 2H, *J* = 8.5, 6.7 Hz, Ar*H*), 7.07 (d, 2H, *J* = 8.6 Hz, Ar*H*), 4.94-4.91 (m, 1H, H-1), 3.88 (dd, 1H, *J* = 12.0, 2.2 Hz, H-6a), 3.68 (dd, 1H, *J* = 12.1, 5.6 Hz, H-6b), 3.47-3.41 (m, 4H, H-2,-3,-4,-5), 1.95-1.50 (m, 11H, Cy), 1.41-0.87 (m, 11H, Cy). **HR-MS** (Nanospray+): m/z calcd. for $C_{24}H_{38}O_6P$ ($[M+H]^+$) = 453.2404; obs. = 453.2406.

6.3.14. Synthesis of ^{OH}Gal-O-Ph-PPh$_2$, 3.7

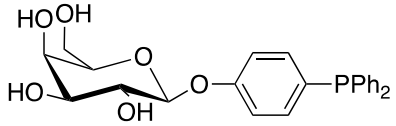

3.7 (69.5 mg, 0.16 mmol, 96% yield) was prepared according to the general procedure outlined in Section 5.3.9. **^{31}P{^{1}H} NMR** (162 MHz, ^{d6}DMSO) (δ, ppm): -7.9 (s). **^{1}H NMR** (400 MHz, ^{d6}DMSO) (δ, ppm): 7.39-7.38 (m, 6H, ArH), 7.19-7.13 (m, 6H, ArH), 7.02 (dd, 2H, *J* = 8.7, 0.8 Hz, ArH), 5.17 (d, 1H, *J* = 5.0 Hz, O*H*), 4.85 (d, 1H, *J* = 7.7 Hz, H-1), 4.62 (t, 1H, *J* = 5.0 Hz, O*H*), 4.50 (d, 1H, *J* = 4.5 Hz, O*H*), 3.70 (t, 1H, *J* = 3.6 Hz, H-5), 3.60-3.39 (m, 5H, H-2, H-3, H-4, H-6a & H-6b), 3.17 (d, 1H, *J* = 4.9 Hz, O*H)*. One OH group is

not observed in the 1H NMR spectrum. **^{13}C NMR** (100 MHz, ^{d6}DMSO) (δ, ppm): 158.4 (s, 1C, quart. Ar*C*), 137.3 (app. dd, 2C, J_{PC} = 11.3, 2.2 Hz, quart. Ar*C*), 135.0 (d, 2C, J_{PC} = 21.3 Hz, Ar*C*), 133.0 (d, 4C, J_{PC} = 19.1 Hz, Ar*C*), 128.8 (s, 2C, Ar*C*) 128.7 (d, 4C, J_{PC} = 21.3 Hz, Ar*C*), 128.2 (d, 1C, J_{PC} = 6.6 Hz, quart. Ar*C*), 116.6 (d, 2C, J_{PC} = 9.1 Hz, ArC), 100.7 (s, C-1), 75.6 (s, C-2), 73.3 (s, C-3), 70.2 (s, C-4), 68.2 (s, C-5), 60.4 (s, C-6). **HR-MS (ESI+)**: *m/z* calcd. for $C_{24}H_{25}O_6PNa$ ([M+Na]$^+$) = 463.1281; obs. = 463.1261. **[α]$^{23}_D$ =** 155.0 (*c* 0.43, MeOH).

6.3.15. Synthesis of ^{OH}Lac-O-Ph-PPh$_2$, 3.10

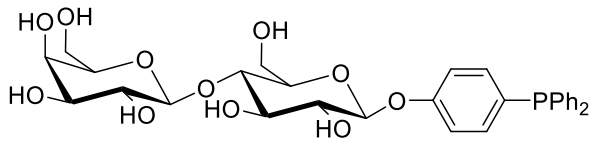

3.10 (10.9 mg, 0.02 mmol, 64% yield) was prepared according to the general procedure outlined in Section 5.3.9. **^{31}P{^{1}H} NMR** (162 MHz, CD_3OD) (δ, ppm): -6.6 (s). **^{1}H NMR** (500 MHz, CD_3OD) (δ, ppm): 7.40-7.30 (m, 6H, ArH), 7.29-7.18 (m, 6H, ArH), 7.10 (d, 2H, *J* = 8.2 Hz, ArH), 5.00 (dd, 1H, J = 7.8, 1.7 Hz, Glu-H-1), 4.40 (dd, 1H, J = 7.7, 1.7 Hz, Gal-H-1), 3.97-3.77 (m, 4 H), 3.77-3.48 (m, 8H). Only anomeric signals can be distinguished due overlapping multiplicities for all other ^{1}H NMR shifts. **^{13}C NMR** (126 MHz, CD_3OD) (δ, ppm): 158.4 (s, 1C, quart. Ar*C*), 137.7 (dd, 2C, J_{PC} = 10.7, Ar*C*), 135.1 (d, 2C, J_{PC} = 21.3 Hz, Ar*C*), 133.1 (app. dd, 4C, J_{PC} = 19.5, 1.1 Hz, Ar*C*), 130.0-129.3 (m, 1C, quart. Ar*C*), 128.3 (s, 2C, Ar*C*), 128.2 (d, 4C, J_{PC} = 6.8 Hz, Ar*C*), 117.5 (d, 2C, J_{PC} = 7.9 Hz, Ar*C*), 103.7 (s, 1C, Gal-C-1), 100.2 (s, 1C, Glu-C-1), 78.7 (s, 1C, C*H*), 75.7 (s, 1C, C*H*), 75.3 (s, 1C, C*H*), 74.9 (s, 1C, C*H*),73.4 (s, 1C, C*H*), 73.1 (s, 1C, C*H*), 71.2 (s, 1C, C*H*), 68.9 (s, 1C, C*H*), 61.2 (s, 3C, Glu/Gal-C-6a/b), 60.2 (s, 1C, Glu/Gal-C-6a/b). Only C1 and C6 atoms can be defined in ^{13}C NMR. **HR-MS (Nanospray+)**: *m/z* calcd. for $C_{30}H_{35}O_{11}PNa$ ([M+Na]$^+$) = 625.1815; obs. = 625.1807.

6.3.16. General Procedure for the Synthesis of 3.11′, 3.15′, 3.16′ and 3.18′

Peracetylated phosphine glycoconjugate (2 eq.) in CH_2Cl_2 (0.5 mL) was added to $[Re(CO)_3(H_2O)_3]Br$ in MeOH (0.3 mL) at room temperature. Once the reaction had reached completion (typically 1-2 hr) as determined by ^{31}P NMR spectroscopy, all volatiles were removed *in vacuo* to isolate the Re(I) complex.

6.3.17. Synthesis of [Re(CO)$_3$(^{OAc}Glc-Ph-O-PPh$_2$)$_2$Br], 3.11′

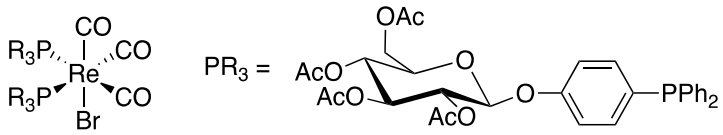

3.11′ (45.5 mg, 29.03 μmol, 88% yield) was synthesised according to the general procedure outlined in Section 5.3.16. **^{31}P{^{1}H} NMR** (202 MHz, CD_3OD) (δ, ppm): -1.9 (app. s, 2P). **HR-MS** (Nanospray): *m/z* calcd. for $C_{24}H_{25}O_6PNa$ ([M+Na]$^+$) = 1589.2109; obs. = 1589.2076. The characteristic bromide isotope pattern can be observed in the HR-MS.

6.3.18. Synthesis of [Re(CO)$_3$(^{OAc}Glc-Ph-O-P(*p*-Tol)$_2$)$_2$Br], 3.15′

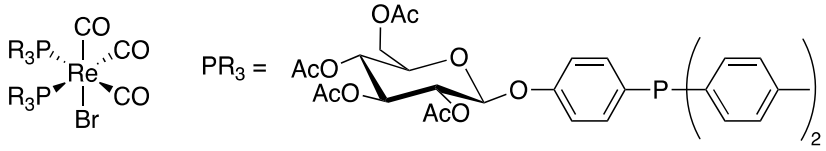

3.15′ (28 mg, 17.55 μmol, 88% yield) was synthesised according to the general procedure outlined in Section 5.3.16. **^{31}P{^{1}H} NMR** (202 MHz, CD_3OD) (δ, ppm): -1.9 (app. s, 2P). **HR-MS** (Nanospray+): *m/z* calcd. for $C_{71}H_{74}O_{23}P_2BrReNa$ ([M+Na]$^+$) = 1645.2735; obs. = 1645.2715. The characteristic bromide isotope pattern can be observed in the HR-MS.

6.3.19. Synthesis of [Re(CO)$_3$(^{OAc}Glc-Ph-O-PCy$_2$)$_2$Br, 3.16′

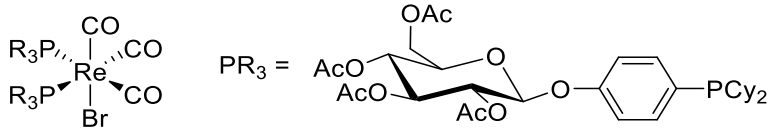

3.16′ (28 mg, 17.6 μmol, 88% yield) was synthesised according to the general procedure outlined in Section 5.3.16. **^{31}P{^{1}H} NMR** (162 MHz, CD_3OD) (δ, ppm): -2.7 (d, J_{PP} = 24.2 Hz, s, *P*Cy$_2$), -5.3 (br s, *P*Cy$_2$). **HR-MS** (Nanospray+): *m/z* calcd. for $C_{67}H_{90}O_{23}P_2BrReNa$ ([M+Na]$^+$) = 1613.3956; obs. = 1613.3987. The characteristic bromide isotope pattern can be observed in the HR-MS.

6.3.20. Synthesis of [Re(CO)$_3$(^{OAc}Lac-Ph-O-PPh$_2$)$_2$Br], 3.17′

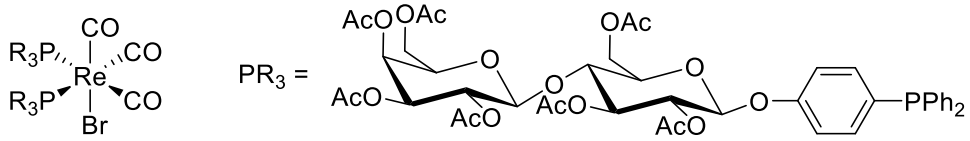

3.17′ was synthesised according to the general procedure outlined in Section 5.3.16, however no yield is quoted as this compound is impure and was produced using crude ligand material (Chapter 3, Section 3.3.6). **^{31}P{^{1}H} NMR** (121 MHz, CD_3OD) (δ, ppm): -0.8 (br. s, 2P). **HR-MS** (Nanospray+): *m/z* calcd. $C_{91}H_{98}O_{39}P_2BrRe$ ([M+Na]+) = 2165.3799; obs. = 2165.3760. The characteristic bromide isotope pattern can be observed in the HR-MS.

6.3.21. General Procedure for the synthesis of 3.11, 3.15 and 3.16

1M sodium methanolate solution (1 eq.) was added to the peracetylated Re(I) complex (1 eq.) dissolved in MeOH:EtOAc (1:1, 2 mL per 20 mg of starting material). After stirring at room temperature for 1 h, pre-prepared Amberlyst 120 resin was added to reduce the pH to 7. The reaction was filtered and concentrated *in vacuo* to isolate the deprotected Re(I) complex. The Amberlyst 120 resin was prepared by washing with MeOH then filtering and drying the resin in air.

6.3.22. Synthesis of [Re(CO)$_3$(^{OH}Glc-Ph-O-PPh$_2$)$_2$Br], 3.11

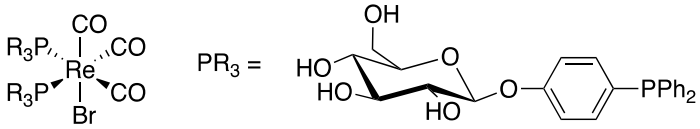

3.11 (14 mg, 11.4 μmol, 93% yield) was synthesised according to the general procedure outlined in Section 5.3.21. The product was further purified by reverse phase HPLC (Method 3) to give **3.11** with 96% purity for toxicity testing. **^{31}P{^{1}H} NMR** (162 MHz, CD_3OD) (δ, ppm): -1.1 (d, J_{PP} = 29.2 Hz), -1.3 (d, J_{PP} = 29.2 Hz). **^{1}H NMR** (400 MHz, CD3OD) (δ, ppm): 7.45-7.14 (m, 24H, Ar*H*), 6.93-6.90 (d, 4H, Ar*H*), 4.94-4.88 (m, 2H, H-1), 3.90-3.81 (m, 2H, H-6a), 3.71-3.61 (m, 2H, H-6b), 3.45-3.33 (m, 8H, H-2,-3,-4,-5). **HR-MS** (ESI+): *m/z* calcd. for $C_{51}H_{50}O_{15}P_2BrReNa$ ($[M+Na]^+$) = 1253.1264; obs. = 1253.1240. The characteristic bromide isotope pattern can be observed in the HR-MS.

6.3.23. Synthesis of [Re(CO)$_3$(^{OH}Glc-O-Ph-P(*p*-Tol)$_2$)Br], 3.15

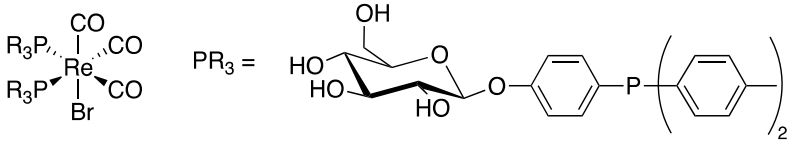

3.15 (18 mg, 14.2 μmol, 83% yield) was synthesised according to the general procedure outlined in Section 5.3.21. The product was further purified by reverse phase HPLC (Method 3) to give **3.15** with 94% purity for toxicity testing. **^{31}P{^{1}H} NMR** (202 MHz, CD_3OD) (δ, ppm): -3.0 (d, J_{PP} = 28.3 Hz), -3.2 (d, J_{PP} = 28.3 Hz). **^{1}H NMR** (500 MHz, CD_3OD) (δ, ppm): 7.07-7.00 (m, 20H, Ar*H*), 6.94-6.90 (m, 4H, Ar*H*), 4.93-4.89 (m, 2H, H-1), 3.89 (dd, 2H, *J* = 11.9, 2.2 Hz, H-6a), 3.67 (dd, 2H, *J* = 12.1, 5.5 Hz, H-6b), 3.49-3.33 (m, 8H, H-2,-3,-4,-5), 2.33 (s, 12H, *p*-C*H*$_3$). **HR-MS** (Nanospray+): *m/z* calcd. for $C_{55}H_{58}O_{15}P_2BrReNa$ ($[M+Na]^+$) = 1309.1890; obs. = 1309.1879. The characteristic bromide isotope pattern can be observed in the HR-MS.

6.3.24. Synthesis of [Re(CO)$_3$(^{OH}Glc-Ph-O-PCy$_2$)$_2$Br], 3.16

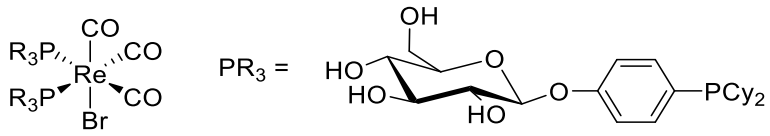

3.16 (25.2 mg, 20.1 μmol) was synthesised with *ca.* 55% purity according to the general procedure outlined in Section 5.3.21. **^{31}P{^{1}H} NMR** (202 MHz, CD_3OD) (δ, ppm): 1.4 (app. s, 2P). **^{1}H NMR** (500 MHz, CD_3OD) (δ, ppm): 7.36 (dd, 4H , *J* = 8.7, 6.7 Hz, Ar*H*), 7.07 (d, 4H, *J* = 8.5 Hz, Ar*H*), 4.94-4.92 (m, 2H, H-1), 3.88 (ddd, *J* = 12.1, 2.1 Hz, 2H, H-6a), 3.69 (dd, 2H, *J* = 12.1, 5.6 Hz, H-6b), 3.54 – 3.34 (m, 8H, H-2,-3,-4,-5), 1.91-1.51 (m, 22H, Cy), 1.38-1.01 (m, 22H, Cy). Additional unidentified impurities were also observed in the ^{1}H NMR spectrum.

6.3.25. Synthesis of [Re(CO)$_3$(^{OH}Gal-Ph-O-PPh$_2$)$_2$Br], 3.17

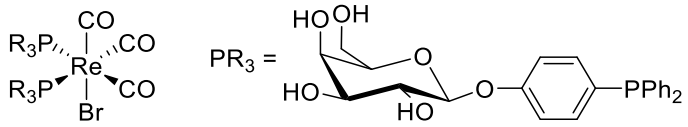

3.7 (30.0 mg, 68.11 μmol) in MeOH (1 mL) was added to [Re(CO)$_3$(H$_2$O)$_3$]Br (15.0 mg, 37.11 μmol) in MeOH (0.5 mL) at room temperature. Once the reaction had reached completion, as determined by ^{31}P NMR spectroscopy, all volatiles were removed *in vacuo* to isolate **3.17** (37.6 mg, 30.54 μmol, 90% yield). The product was further purified by reverse phase HPLC (Method 3) to give **3.17** with *ca.* 95% purity for toxicity testing. **^{31}P{^{1}H} NMR** (162 MHz, CD_3OD) (δ, ppm): -1.2 (d, J_{PP} = 29.2 Hz), -1.4 ppm (d, J_{PP} = 29.2 Hz). **^{1}H NMR** (400 MHz, CD_3OD) (δ, ppm): 7.50-7.19 (m, 24H, Ar*H*), 6.98-6.90 (m, 4H, Ar*H*), 4.87 (dd, 2H, *J* = 7.8, 1.4 Hz, H-1), 3.88 (app. d, 2H, *J* = 3.5 Hz, H-2/3), 3.82-3.65 (m, 8H, H-2/-3 and H-4,-5,-6a), 3.58 (d, 2H, *J* = 9.7, 3.4 Hz Hz, H-6b). **MS** (ESI+): *m/z* calcd. for $C_{51}H_{50}BrO_{15}P_2ReNa$ ($[M+Na]^+$) = 1254.0; obs. = 1254.0. **IR**: 3360 (br s, O-H stretch), 2927 (w, ArC-H stretch), 2029 (s, CO stretch), 1954 (s, CO stretch), 1914 (s, CO stretch). The characteristic bromide isotope pattern can be observed in the HR-MS.

6.3.26. Synthesis of [AuCl(^{OAc}Glc-O-Ph-P(*o*-Tol)$_2$)], 3.13′

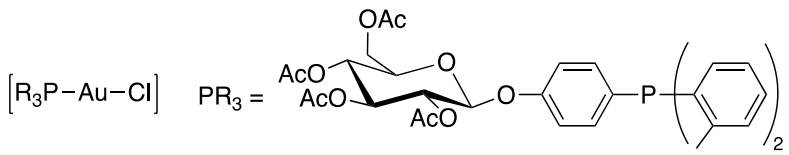

3.3′ (16.0 mg, 25.1 μmol) in CH_2Cl_2 (0.5 mL) was added to [Au(SMe$_2$)Cl] (7.5 mg, 25.5 μmol) in CH_2Cl_2 (0.5 mL). The reaction reached completion after 1.5 h and the solvent was removed *in vacuo* to give a sticky residue, that when washed with hexane gave **3.13′** (15.9 mg, 18.3 μmol, 73% yield) as a free-flowing white powder. **^{31}P{^{1}H} NMR** (121 MHz,

CD_3OD) (δ, ppm): 14.6 (s). **^{1}H NMR** (300 MHz, CD_3OD) (δ, ppm): 7.55-7.38 (m, 4H, Ar*H*), 7.32 (app. t, 2H, *J* = 6.4 Hz, Ar*H*), 7.21-7.16 (m, 2H, Ar*H*), 7.06 (dd, 2H, *J* = 8.9, 1.8 Hz, 2H, Ar*H*), 6.88-6.73 (m, 2H, Ar*H*), 5.37-5.11 (m, 4H, H-1,-2,-3,-4), 4.30 (dd, 1H, *J* = 12.4, 5.3 Hz, H-6a), 4.14 (dd, 1H, *J* = 12.3, 2.4 Hz, H-6b), 3.89 (ddd, 1H, J = 9.8, 5.3, 2.4 Hz, H-5), 2.64 (s, 6H, *p*-C*H*$_3$), 2.06 (s, 3H, OAc), 2.04 (s, 3H, OAc), 2.03 (s, 6H, 2 x OAc). **HR-MS** (Nanospray+): *m/z* calcd. for $C_{34}H_{37}O_{10}PClAuNa$ ([M+Na]$^+$) = 891.1376; obs. = 891.1365. The characteristic chloride isotope pattern can also be observed in the HR-MS.

6.3.27. Synthesis of *trans*-[PtCl$_2$(^{OAc}Glc-O-Ph-P(*o*-Tol)$_2$)], 3.14′

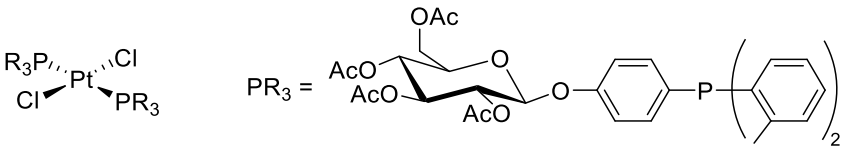

3.3′ (20.0 mg, 31.4 μmol) in CH_2Cl_2 (1 mL) was added dropwise to [$PtCl_2(NC^tBu)_2$] (6.40 mg, 14.8 μmol) in CH_2Cl_2 (1 mL) and the resulting solution stirred for 3 h. All volatiles were removed *in vacuo* and the complex was re-dissolved in $CHCl_3$ (0.5 mL) then precipitated in air by addition of hexane (*ca.* 15 mL). This mixture was left to settle over several h and the supernatant removed by pipette before any residual solvent removed *in vacuo* to give **3.14′** (11.2 mg, 10.1 μmol, 67% yield). **^{31}P{^{1}H} NMR** (202 MHz, $CDCl_3$) (δ, ppm): 15.0 (s, $^1J_{PPt}$ = 2583 Hz, 2P).

6.3.28. Synthesis of [Re(CO)$_3$(PPh$_3$)$_2$Br], 3.19

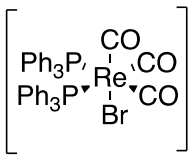

PPh_3 (50.0 mg, 0.191 mmol) in CH_2Cl_2 (1 mL) was added to [$Re(CO)_3(H_2O)_3$]Br (36.7 mg, 90.8 μmol) in MeOH (0.5 mL) and the product precipitated from solution after 40 min. The solid was isolated by filtration (27.0 mg, 31.0 μmol, 34% yield). Re-dissolving the product in CH_2Cl (0.5 mL) and layering this with MeOH in a sealed NMR tube gave crystals of **3.19**, that were suitable for X-ray diffraction, after several days. **^{31}P{^{1}H} NMR** (121 MHz, $CDCl_3$) (δ, ppm) -0.3 (s, 2P). **^{1}H NMR** (400 MHz, $CDCl_3$) (δ, ppm): 7.37-7.32 (m, 18H, ArH), 7.24-7.19 (m, 12H, ArH). **^{13}C NMR** δ_C (100 MHz, $CDCl_3$) (δ, ppm) 134.5 (t, 12C, J_{PC} = 5.3 Hz, *m*-Ar*C*), 133.0 (t, 6C, J_{PC} = 21.1 Hz, quart. *i*-Ar*C*), 130.4 (s, 6C, *p*-Ar*C*), 128.3 (t, 12C, J_{PC} = 4.8 Hz, *o*-Ar*C*). **HR-MS (ESI+)**: *m/z* calcd. for $C_{39}H_{30}O_3P_2Re$ ([M-Br]$^+$) = 793.1200; obs. = 723.1201. **IR**: 3060 (w, ArC-H stretch), 2025 (s, CO stretch), 1946 (s, CO stretch), 1888 (s, CO stretch).

6.3.29. Synthesis of (4-acetoxyphenyl)diphenylphosphine

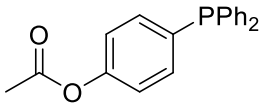

(4-hydroxyphenyl)diphenylphosphine (250 mg, 0.898 mmol) was dissolved in pyridine (1 mL) and to this, acetic anhydride (0.11 mL, 1.17 mmol) was added at 0 °C. After stirring for 5 min at 0 °C, the reaction was left to warm to room temperature and stirred for 80 min. The reaction was diluted by addition of EtOAc (10 mL) and washed with H_2O (10 mL), HCl (1M, 10 mL) and brine (10 mL), then the organics dried over anhydrous $MgSO_4$, filtered and all volatiles removed *in vacuo* to give (4-acetoxyphenyl)diphenylphosphine (0.220 g, 0.687 mmol, 76% yield) as a white solid. No further purification was required. **$^{31}P\{^1H\}$ NMR** (162 MHz, $CDCl_3$) (δ, ppm): -5.5 (s). **^{1}H NMR** (400 MHz, $CDCl_3$) (δ, ppm): 7.43-7.25 (m, 12H, Ar*H*), 7.06 (d, 2H, *J* = 8.1 Hz, Ar*H*), 2.28 (s, 3H, OAc). **^{13}C NMR** (121 MHz, $CDCl_3$) (δ, ppm): 169.3 (s, 1C, CH_3*C*OO), 151.3 (s, 1C, quart. Ar*C*), 137.1 (d, 1C, J_{PC} = 10.6 Hz, quart. Ar*C*), 135.0 (d, 2C, J_{PC} = 20.5 Hz, Ar*C*), 134.7 (d, 2C, J_{PC} = 11.7 Hz, quart. Ar*C*), 133.8 (d, 4C, J_{PC} = 19.6 Hz, Ar*C*), 128.9 (s, 2C, Ar*C*), 128.7 (d, 4C, J_{PC} = 7.1 Hz, Ar*C*), 121.8 (d, 2C, J_{PC} = 7.4 Hz, Ar*C*), 21.3 (s, 1C, *C*H_3COO). **HR-MS** (Nanospray+): *m/z* calcd. for $C_{20}H_{18}O_2PRe$ ($[M+H]^+$) = 321.1044; obs. = 321.1050.

6.3.30. Synthesis of $[Re(CO)_3(^{OAc}PhPPh_2)_2Br]$, 3.21

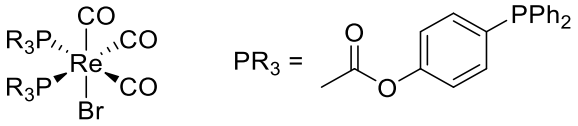

(4-acetoxyphenyl)diphenylphosphine (29.0 mg, 90.6 µmol) in CH_2Cl_2 (1 mL) was added to $[Re(CO)_3(H_2O)_3]Br$ (20.2 mg, 50.0 µmol) in MeOH (1 mL) and the reaction stirred at room temperature for 3 h. All volatiles were removed *in vacuo* to isolate **3.21** (41.5 mg, 47.1 µmol, 89% yield) with *ca*. 93% purity. No further purification was necessary. **$^{31}P\{^1H\}$ NMR** (121 MHz, CD_3OD) (δ, ppm) -0.4 (s, 2P). **^{1}H NMR** (400 MHz, $CDCl_3$) (δ, ppm): 7.36-7.20 (m, 24H, ArH), 6.99-6.93 (m, 4H, ArH), 2.28 (s, 6H, OAc). **HR-MS (Nanospray+)**: *m/z* calcd. for $C_{43}H_{34}O_7P_2ReK$ ($[M+K]^+$) = 1029.0158; obs. = 1029.0132. The characteristic bromide isotope pattern can be observed in the HR-MS.

6.3.31. General Procedure for the Synthesis of Deprotected Oxidised Phosphine Glycoconjugates

This general procedure was modified from the literature.[22] I_2 (2 eq.) in CH_2Cl_2 (1 mL) was added to the peracetylated phosphine glycoconjugate ligand (10 mg) in CH_2Cl_2 (1 mL) and this mixture then stirred at ambient temperature for 2 h. Deionised H_2O (2 mL) was added and the product extracted into CH_2Cl_2 (5 mL), washed with saturated $Na_2S_2O_3$ solution (2 mL), and the organics dried over anhydrous $MgSO_4$. The mixture was filtered and the

solvent was removed *in vacuo* to give the oxidised peracetylated product. To this, 1M sodium methanolate solution (20 μL, 20 μmol) in MeOH:EtOAc (1:1, 2 mL) was added. After stirring at ambient temperature for 1 h, Amberlyst 120 resin was added to reduce the pH of the mixture to 7, and this was then filtered and concentrated *in vacuo* to give the desired final product. The Amberlyst 120 resin was prepared by washing with MeOH, then filtering and drying the resin in air.

6.3.32. Synthesis of ^{OH}Glc-O-Ph-P(O)Ph$_2$

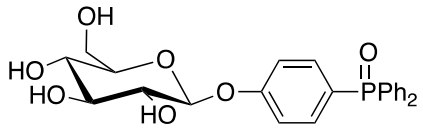

3.1^{ox} (3.3 mg, 7.23 μmol, 45% yield) was prepared according to the general procedure outlined in Section 5.3.31. **^{31}P{^{1}H} NMR** (202 MHz, CD_3OD) (δ, ppm): 32.3 (s). **^{1}H NMR** (500 MHz, CD_3OD) (δ, ppm): 7.71-7.56 (m, 12H, Ar*H*), 7.27 (dd, 2H, *J* = 8.9, 2.2 Hz Ar*H*), 5.07-5.03 (m, 1H, H-1), 3.90 (dd, 1H, *J* = 12.1, 2.2 Hz, H-6a), 3.70 (dd, 1H, *J* = 12.1, 5.7 Hz, H-6b), 3.55-3.46 (m, 3H, H-2,-3,-4), 3.44-3.39 (m, 1H, H-5). **HR-MS** (Nanospray+): *m/z* calcd. for $C_{24}H_{25}O_7PNa$ ([M+Na]$^+$) = 479.1236; obs. = 479.1246.

6.3.33. Synthesis of ^{OH}Glc-O-Ph-P(*p*-Tol)$_2$

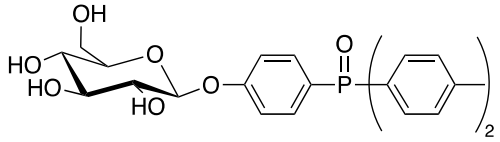

3.4^{ox} (2.4 mg, 4.95 μmol, 32% yield) was prepared according to the general procedure outlined in Section 5.3.31. **^{31}P{^{1}H} NMR** (202 MHz, CD_3OD) (δ, ppm): 32.9 (s). **^{1}H NMR** (500 MHz, CD_3OD) (δ, ppm): 7.48-7.43 (m, 6H, Ar*H*), 7.35-7.31 (m, 4H, Ar*H*), 7.16-7.13 (m, 2H, Ar*H*), 4.94 (br d, 1H, *J* = 7.5 Hz, H-1), 3.65 (dd, 1H, *J* = 11.9, 2.0 Hz, H-6a), 3.28-3.21 (m, 3H, H-2/-3/-4 and H-5),1.62 (s, 6H, *p*-CH_3). The ^{1}H NMR signals for H-6b and either H-2, H-3 or H-4 is obscured by the CD_3OD signal at 3.31 ppm. **HR-MS** (Nanospray+): *m/z* calcd. for $C_{26}H_{29}O_7PNa$ ([M+Na]$^+$) = 507.1549; obs. = 507.1564.

6.3.34. Synthesis of ^{OH}Gal-O-Ph-P(O)Ph$_2$

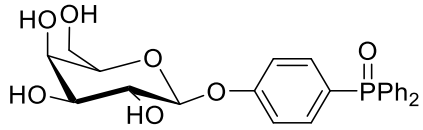

3.7^{ox} (6.9 mg, 15.1 μmol, 92% yield) was prepared according to the general procedure outlined in Section 5.3.31. **^{31}P{^{1}H} NMR** (161 MHz, CD_3OD) (δ, ppm): 33.1 (s). **^{1}H NMR** (400 MHz, CD_3OD) (δ, ppm): 7.64-7.49 (m, 12H, Ar*H*), 7.23 (dd, 2H, *J* = 8.9, 2.3 Hz, Ar*H*), 4.96 (d, 1H, *J* = 7.7 Hz, H-1), 3.88 (dd, 1H, *J* = 3.3, 1.0 Hz, H-2/3), 3.84 – 3.64 (m, 4H, H-

2/3,-4,-5,-6a), 3.57 (dd, 1H, *J* = 9.7, 3.4 Hz, H-6b). **HR-MS** (Nanospray+): *m/z* calcd. for $C_{24}H_{25}O_7PNa$ ($[M+Na]^+$) = 479.1236; obs. = 479.1221.

6.3.35. Synthesis of $[Tc(CO)_3(H_2O)_3]^+$

$[^{99m}TcO_4]^-$ saline solution (200 µL, 200-250 MBq) and saline (800 µL) were added to a commercially available CRS Isolink® tricarbonyl kit, which are manufactured and supplied by the Centre for Radiopharmaceutical Science, Paul Scherrer Institute, Villigen, Switzerland. The resulting solution was heated at 100 ºC for 30 min in a heating block before being left to cool to room temperature. Once cooled, 1 M HCl was added to kit to reduce the pH to 7.5-6.5. The formation of **$[Tc(CO)_3(H_2O)_3]^+$** was confirmed by TLC (1% HCl:MeOH) using glass backed silica plates, which were visualised using a CycloPlus Phorphor Imager (Perkin Elmer).

6.3.36. Synthesis of ^{99m}Tc(I) complexes

$[Tc(CO)_3(H_2O)_3]^+$ (50 µL, 5 MBq) was added to **3.1**, **3.3-3.5** or **3.7** (0.5 mg) in a mixture of DMSO (100 µL) and milliQ water (270 µL) then incubated at 50 ºC for 30 min. Aliquots of these samples were analysed by direct addition to an analytical HPLC (Method 1 or 2 for radiolabelling of **3.1**, and Method 2 for radiolabelling of **3.3-3.5** & **3.7**).

6.4. Experimental Procedures and Characterisation Data - Chapter 4

6.4.1. Synthesis of $[Re(dppbz)(CO)_3Br]$, 4.2

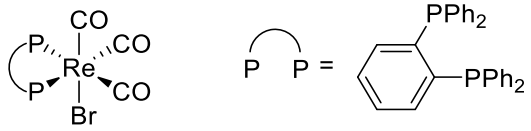

To a stirred solution of $[Re(CO)_3(H_2O)_2Br]$ (18.0 mg, 44.5 µmol) in MeOH (0.5 mL), dppbz (20.0 mg, 44.8 µmol) in CH_2Cl_2 (1 mL) was added dropwise. The reaction was stirred at ambient temperature for 16 h and the product precipitated from the solution overnight. Filtration gave the product, $[Re(dppbz)(CO)_3Br]$ (**4.2**), as a white solid (32.4 mg, 40.2 µmol, 91%). **$^{31}P\{^1H\}$ NMR** (162 MHz, $CDCl_3$) (δ, ppm): 30.4 (s, 2P). **^1H NMR** (400 MHz, $CDCl_3$) (δ, ppm): 7.84 (ddd, 4H, *J* = 11.0, 8.0, 1.7 Hz, Ar*H*), 7.57 (m, 4H, Ar*H*), 7.42 (m, 6H, Ar*H*), 7.22 (m, 6H, Ar*H*), 7.09 (m, 4H, Ar*H*). (Nanospray+): *m/z* calcd. for $C_{33}H_{24}O_3P_2Re$ ($[M-Br]^+$) = 717.0758; obs. = 717.0751.

6.4.2. Synthesis of $[Re(dppbz)_2O_2]I$, 4.3

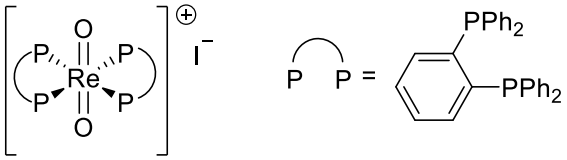

To a stirred solution of $[Re(O)_2(PPh_3)_2I]$ (19.5 mg, 22.4 µmol) in CH_2Cl_2 (1 mL), dppbz (20.0 mg, 44.8 µmol) in CH_2Cl_2 (1 mL) was added dropwise. The reaction was stirred at ambient temperature for 16 h. The solvent was removed *in vacuo*, the product re-dissolved in CH_2Cl_2 (0.5 mL) and then precipitated by addition of hexane (5 mL). The solid was washed with additional hexane (2 x 5 mL) and dried to give $[Re(dppbz)_2O_2]I$ (**4.3**) as the final product (16.6 mg, 13.4 µmol, 60% yield). **$^{31}P\{^1H\}$ NMR** (162 MHz, $CDCl_3$) (δ, ppm): 14.7 (s, 4P). **^{1}H NMR** (400 MHz, $CDCl_3$) (δ, ppm): 7.60 (m, 8H, Ar*H*), 7.38 (m, 8H, Ar*H*), 7.12 (m, 16H, Ar*H*), 6.95 (m, 16H, Ar*H*). **HR-MS** (Nanospray+): *m/z* calcd. for $C_{60}H_{48}O_2P_4Re$ ($[M-I]^+$) = 1111.2162; obs. = 1111.2150.

6.4.3. Synthesis of *tert*-butyl(3,4-dichlorophenol)dimethyl silane

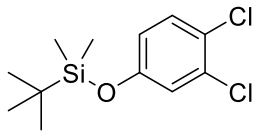

Et_3N (2.30 mL, 16.5 mmol) was added in portions (0.5 mL per min) to 3,4-dichlorophenol (2.50 g, 15.3 mmol) in CH_2Cl_2 (20 mL). To this mixture, TBDMSCl (2.87 g, 19.0 mmol) was added in portions (0.5 g per min), and the reaction flask covered with foil to prevent exposure to light whilst the mixture was stirred for 1.5 h. The reaction was washed with deionised water (50 mL) and the organic solvent removed *in vacuo*. The residue was re-dissolved in hexane (20 mL), washed with deionised water (2 x 50 mL), the organics dried over anhydrous $MgSO_4$ and the reaction filtered before the solvent was removed *in vacuo* to give *tert*-butyl(3,4-dichlorophenol)dimethyl silane as an oil (3.05 g, 11.0 mmol, 72% yield). The sample was placed inside a vial without a cap, and then stored in a Schlenk flask containing P_2O_5 for 96 h to achieve an anhydrous final product. **^{1}H NMR** (400 MHz, $CDCl_3$) (δ, ppm): 7.27 (d, 1H, J_{HH} = 8.7 Hz, Ar*H*), 6.94 (d, 1H, J_{HH} = 2.8 Hz, Ar*H*), 6.68 (dd, 1H, J_{HH} = 8.7, 2.8 Hz, Ar*H*), 0.97 (s, 9H, tBu), 0.20 (s, 6H, 2 x Me). **^{13}C NMR** (100 MHz, $CDCl_3$) (δ, ppm): 155.0 (s, 1C, quart. Ar*C*), 132.7 (s, 1C, quart. Ar*C*), 130.7 (s, 1C, Ar*C*), 124.8 (s, 1C, quart. Ar*C*), 122.3 (s, 1C, Ar*C*), 119.9 (s, 1C, Ar*C*), 25.7 (s, 3C, tBu), 18.3 (s, 1C, quart. tBu), -4.4 (s, 2C, 2 x Me). **HR-MS** (EI+): *m/z* calcd. for $C_{12}H_{18}OSiCl_2$ ($[M]^+$) = 276.0497; obs. = 276.0498. The EI mass spectrum exhibited the expected dichloride isotope pattern.

6.4.4. Synthesis of 2,3-diiodophenyl glucose, α-4.6 and β-4.6

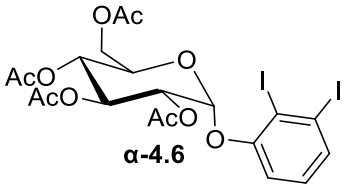

α-4.6

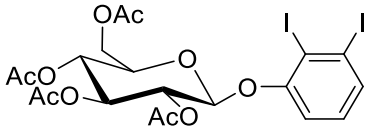

β-4.6

To a solution of 2,3-diiodophenol (60.0 mg, 0.173 mmol) and 2,3,4,6-tetra-O-acetoxy-α-D-glucopyranolsyl trichloroacetimidate (85.0 mg, 0.173 mmol) in toluene (2.5 mL), freshly distilled TMSOTf (5.00 µL, 27.7 µmol) was added. The reaction mixture which was stirred at room temperature for 4 h before dilution with EtOAc (5 mL). The reaction was quenched with saturated sodium bicarbonate (10 mL) and the organics were extracted into EtOAc (2 x 10 mL). The combined organic layers were dried over anhydrous $MgSO_4$, filtered and all volatiles removed *in vacuo* to isolate the crude product. The alpha anomer (**α-4.6**) was crystalised from EtOH in the freezer (3.2 mg, 4.73 µmol, 3% yield), whilst the beta anomer (**β-4.6**) was isolated by column chromatography (EtOAc:Hex, 1:1) and subsequent recrystallisation from EtOH in the freezer (2.5 mg, 3.7 µmol, 2% yield). **Data for α-4.6: ^{1}H NMR** (500 MHz, $CDCl_3$) (δ, ppm): 7.62 (dd, 1H, J_{HH} = 5.8, 3.3 Hz, Ar*H*), 6.94 (m, 2H, Ar*H*), 5.83 (dd, 1H, J_{HH} = 9.7 Hz, H-3), 5.80 (d, 1H, J_{HH} = 3.7z Hz, H-1), 5.18 (t, 1H, J_{HH} = 9.7 Hz, H-4), 4.99 (dd, 1H, J_{HH} = 10.2, 3.6 Hz, H-2), 4.25 (dd, 1H, J_{HH} = 12.1, 4.2 Hz, H-6a), 4.12-4.05 (m, 2H, H-5 & H-6b), 2.09 (s, 3H, OAc), 2.06 (s, 3H, OAc), 2.05 (s, 6H, 2 x OAc). **^{13}C NMR** (126 MHz, $CDCl_3$) (δ, ppm): 170.6, 170.5, 170.1, 169.9 (s, 4C, 4 x CH_3*C*OO), 156.3 (s, 1C, quart. Ar*C*), 134.0 (s, 1C, Ar*C*), 130.8 (s, 1C, Ar*C*), 113.2 (s, 1C, Ar*C*), 110.0 (s, 1C, quart. Ar*C*), 101.7 (s, 1C, quart. Ar*C*), 95.6 (s, 1C, C-1), 70.6 (s, 1C, C-2), 70.2 (s, 1C, C-3), 68.9 (s, 1C, C-5), 68.2 (s, 1C, C-4), 61.6 (s, 1C, C-6), 21.0, 20.9, 20.82, 20.77 (s, 4C, 4 x *C*H_3COO). **HR-MS** (ESI+): *m/z* calcd. for $C_{20}H_{22}O_{10}NaI_2$ ($[M+Na]^+$) = 698.9200; obs. = 698.9216. **Data for β-4.6: ^{1}H NMR** (500 MHz, $CDCl_3$) (δ, ppm): 7.64 (dd, 1H, J_{H-H} = 7.8, 1.4 Hz, Ar*H*), 7.05 (app. t, 1H, J_{HH} = 8.0 Hz, Ar*H*), 6.98 (dd, 1H, J_{HH} = 8.2, 1.4 Hz, Ar*H*), 5.40 (dd, 1H, J_{HH} = 9.4, 7.8 Hz, H-2), 5.29 (t, 1H, J_{HH} = 9.4 Hz, H-3), 5.19 (t, 1H, J_{HH} = 9.6 Hz, H-4), 5.05 (d, 1H, J_{HH} = 7.8, Hz, H-1), 4.28 (dd, 1H, J_{HH} = 12.3, 5.3 Hz, H-6a), 4.20 (dd, 1H, J_{HH} = 12.3, 2.5 Hz, H-6b), 3.87 (m, 1H, H-5), 2.10 (s, 3H, OAc), 2.08 (s, 3H, OAc), 2.05 (s, 3H, OAc), 2.04 (s, 3H, OAc). **^{13}C NMR** (126 MHz, $CDCl_3$) (δ, ppm): 170.6, 170.4, 169.5, 169.3 (s, 4C, 4 x CH_3*C*OO), 157.2 (s, 1C, quart. Ar*C*), 134.4 (s, 1C, Ar*C*), 130.7 (s, 1C, Ar*C*), 114.5 (s, 1C, Ar*C*), 110.1 (s, 1C, quart. Ar*C*), 101.9 (s, 1C, quart. Ar*C*), 100.0 (s, 1C, C-1), 72.8 (s, 1C, C-3), 72.4 (s, 1C, C-5), 70.8 (s, 1C, C-2), 68.3 (s, 1C, C-4), 62.0 (s, 1C, C-6), 21.3, 20.83, 20.78, 20.7 (s, 1C, *C*H_3COO). **HR-MS** (ESI+): *m/z* calcd. for $C_{20}H_{22}O_{10}NaI_2$ ($[M+Na]^+$) = 698.9194; obs. = 698.9172.

6.4.5. Synthesis of (2-bromo-5-methoxybenzyl)dicyclohexylphosphine, 4.11

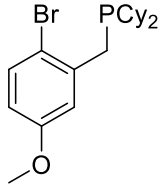

The following procedure was based on that reported by Clark *et al.*[23] $HPCy_2$ (0.36 mL, 1.78 mmol) was added to 2-bromo-5-methoxylbenzyl bromide (0.50 g, 1.79 mmol) in deoxygenated acetone (2.40 mL) and the resulting solution was heated to reflux (65 °C) for 16 h. The mixture was then cooled to room temperature and concentrated *in vacuo* to give a foam-like solid that was washed with ice-cold Et_2O (10 mL). The solid was dried under reduced pressure, re-dissolved in CH_2Cl_2 (10 mL) and Et_3N (2 mL) was then added. This solution was stirred at room temperature for 2 h before removal of the volatiles *in vacuo*. The crude residue was re-dissolved in toluene (5 mL) and the insoluble salts removed by filter cannula. These insoluble salts were washed with a two portions of toluene (2 x 5 mL) and all organics were then concentrated to give (2-bromo-5-methoxybenzyl)dicyclohexylphosphine (**4.11**) as a pale yellow, partially crystalline solid (0.420 g, 1.06 mmol, 59% yield) with *ca.* purity of 94%. **$^{31}P\{^1H\}$ NMR** (162 MHz, $CDCl_3$) (δ, ppm): 3.85 (s). **^{1}H NMR** (400 MHz, $CDCl_3$) (δ, ppm): 7.37 (d, 1H, *J* = 8.8 Hz, Ar*H*), 6.95 (app. t, 1H, *J* = 3 Hz, Ar*H*), 7.64 (dd, 1H, *J* = 8.8, 3 Hz, Ar*H*), 3.76 (s, 3H, OCH_3), 2.91 (d, 2H, *J* = 2.5 Hz, CH_2PCy_2), 2.21-1.67 (m, 11H, Cy), 1.33-1.08 (m, 11H, Cy). **^{13}C NMR** (121 MHz, $CDCl_3$) (δ, ppm): 158.8 (s, 1C, quart. Ar*C*-OCH_3), 141.04 (d, 1C, *J* = 8.8 Hz, quart. Ar*C*-CH_2PCy_2), 133.4 (s, 1C, Ar*C*), 116.7 (d, 1C, *J* = 11.1 Hz, Ar*C*), 115.5 (d,1C, *J* = 3.9 Hz, quart. Ar*C*-Br), 113.5 (s, 1C, Ar*C*), 55.5 (s, 1C, OCH_3), 33.7 (d, 2C, *J* = 15.1 Hz, Cy), 29.83 (dd, 4C, *J* = 11.1, 5.4 Hz, Cy), 29.5 (d, 2C, *J* = 20.6 Hz, CH_2PCy_2), 27.5 (dd, 4C, *J* = 9.3, 3.0 Hz, Cy), 26.6 (s, 2C, Cy). **HR-MS** (ESI+): *m/z* calcd. for $C_{20}H_{31}BrPO$ ($[M+H]^+$) = 397.129041; obs. = 397.129042. The characteristic bromide isotope pattern can be observed in the HR-MS.

6.4.6. Synthesis of (2-dicyclohexylphosphino-5-methoxybenzyl)dicyclohexylphosphine, 4.12

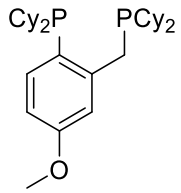

nBuLi (1.6 M in Hexanes, 0.2 mL, 0.32 mmol) was added dropwise over 10 min to (2-bromo-5-methoxybenzyl)dicyclohexylphosphine (108 mg, 0.272 mmol) in THF (4 mL) at -78 °C. The reaction was stirred at -78 °C for 15 min, then left to warm to room temperature

over 15 min. $ClPPh_2$ (60 µL, 0.272 mmol) in THF (0.54 mL) was added to the lithiated mixture at -78 °C and the resulting solution stirred for 15 min at this temperature. The reaction was left to warm up to room temperature and stirred for 1 h. All volatiles were removed *in vacuo* and the residue was re-dissolved in Et_2O (10 mL), washed with water (10 mL), dried over anhydrous $MgSO_4$, filtered and the solvent removed under reduced pressure. The crude residue was passed through a silica plug (EtOAc:Hex, 50:50) to give **4.12** with *ca.* 66% purity by $^{31}P\{^1H\}$ NMR. **$^{31}P\{^1H\}$ NMR** (122 MHz, $CDCl_3$) (δ, ppm): 6.6 (d,$^4J_{PP}$ = 8.9 Hz, $ArCH_2PCy_2$), -18.5 (d,$^4J_{PP}$ = 9.3 Hz, $ArPCy_2$). **HR-MS** (ESI+): *m/z* calcd. for $C_{32}H_{53}P_2O$ ($[M+O]^+$) = 515.3563; obs. = 515.3572.

6.4.7. Synthesis of [Pt(4.12)$_2$Cl$_2$], 4.16

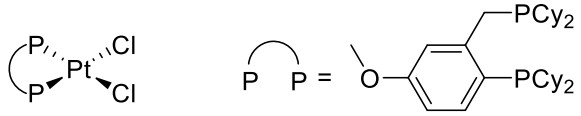

(2-dicyclohexylphophino-5-methoxybenzyl)dicyclohexylphosphine (27.0 mg, 52.4 µmol, *ca.* 70% purity) in CH_2Cl_2 (1 mL) was added dropwise to [$PtCl_2$(COD)] (17.0 mg, 45.4 µmol) in CH_2Cl_2 (2 mL) and stirred at room temperature for 1.5 h. All volatiles were removed *in vacuo* and the residue was redissolved in $CHCl_3$ (0.5 mL). In air, the product was precipitated by addition of hexane (15 mL) and left to stand so that the supernatant could be removed by pipette. Residual solvent was removed *in vacuo* and **4.16** was isolated as a white solid (28.8 mg, 36.9 mmol, 81% yield). **$^{31}P\{^1H\}$ NMR** (122 MHz, $CDCl_3$) (δ, ppm): 23.8 (d,$^4J_{PP}$ = 19.4 Hz, $^1J_{PPt}$ = 3499 Hz, $ArCH_2PCy_2$), 10.2 (d,$^4J_{PP}$ = 19.2 Hz, $^1J_{PPt}$ = 3519 Hz, $ArPCy_2$). **HR-MS** (Nanospray+): *m/z* calcd. for $C_{32}H_{52}P_2OClPt$ ($[M-Cl]^+$) = 744.2830; obs. = 744.2830.

6.4.8. Synthesis of 4.20

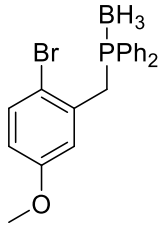

$BH_3.SMe_2$ (0.15 mL, 1.64 mmol) was added to $HPPh_2$ (0.28 mL, 1.61 mmol) in THF (3 mL) at 0 °C, and the resulting mixture was stirred for 10 min then left to warm to room temperature and stirred for a further 3 h. nBuLi (1.6 M in Hexanes, 1.1 mL, 1.76 mmol) was added dropwise to BH_3-protected phosphine at -78 °C and the resulting mixture was stirred at this temperature for 15 min, then left to warm to room temperature and stirred for 20 min. Next, the lithiated solution was added dropwise to (2-bromo-5-methoxybenzyl)bromide (442 mg, 1.58 mmol) in THF (10 mL) at -78 °C over a period of 20 min and this mixture was left

to warm to room temperature and stirred for 1 h. All volatiles were removed *in vacuo* and the residue was partitioned between CH_2Cl_2 (10 mL) and H_2O (10 mL), then extracted into CH_2Cl_2 (2 x 20 mL). The organics were combined, dried over anhydrous $MgSO_4$, filtered and the solvent removed *in vacuo*. The crude product was purified by column chromatography (EtOAc:Hex, 1:9, Rf = 0.17) which gave the desired final product, **4.20** (410 mg, 1.02 mmol, 65% yield). **^{31}P{^{1}H} NMR** (162 MHz, $CDCl_3$) (δ, ppm): 19.8 (m). **^{11}B{^{1}H} NMR** (128 MHz, $CDCl_3$) (δ, ppm): -39.4 (d, $^{1}J_{BP}$ = 56 Hz). **^{1}H NMR** (400 MHz, $CDCl_3$) (δ, ppm): 7.65-7.60 (m, 4H, Ar*H*), 7.52-7.37 (m, 6H, Ar*H*), 7.26 (dd, 1H, *J* = 9.1, 2.6 Hz, Ar*H*), 6.84-6.81 (m, 1H, Ar*H*), 6.64-6.59 (m, 1H, Ar*H*), 3.81 (dd, 2H, *J* = 11.9, 2.8 Hz, C*H*$_2$), 3.65 (s, 3H, OC*H*$_3$), 1.56-0.53 (m, 3H, B*H*$_3$). **^{13}C NMR** (121 MHz, $CDCl_3$) (δ, ppm): 158.5 (d, 1C, J_{PC} = 2.6 Hz, Ar*C*-OCH$_3$), 133.3 (d, 1C, J_{PC} = 9.1 Hz, Ar*C*), 133.0 (d, 4C, J_{PC} = 9.1 Hz, Ar*C*), 131.5 (d, 2C, J_{PC} = 2.5 Hz, Ar*C*), 128.8 (d, 4C, J_{PC} = 9.9 Hz, Ar*C*),128.5 (s, 1C, quart. Ar*C*), 128.0 (s, 1C, quart. Ar*C*), 116.2 (d, 1C, J_{PC} = 9.3, 3.4 Hz, Ar*C*), 116.0 (d, 1C, J_{PC} = 9.3, 3.4 Hz, Ar*C*), 55.48 (s, 1C, OC*H*$_3$), 33.69 (d, 1C, $^{1}J_{PC}$ = 31.9 Hz, C*H*$_2$PPh$_2$). Quaternary Ar*C* atoms (that were directly bound to phosphorus) could not be observed in the ^{13}C spectrum. **HR-MS** (ESI+): *m/z* calcd. for $C_{20}H_{31}BrPO$ ($[M+H]^+$) = 397.129041; obs. = 397.129042. The ESI mass spectrum exhibits the expected bromide isotope pattern.

6.4.9. Synthesis of 4.17

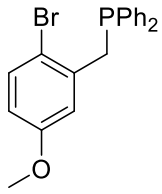

Compound **4.20** (150 mg, 0.376 mmol) in Et_2NH (0.5 mL, 4.84 mmol) was heated to 50 °C for 20 h. All volatiles were removed *in vacuo* and the residue heated under vacuum at 80 °C to ensure complete removal of $Et_2NH.BH_3$. This gave **4.17** as a colourless solid without any further purification (141 mg, 0.366 mmol, 97% yield). **^{31}P{^{1}H} NMR** (162 MHz, $CDCl_3$) (δ, ppm): -12.3 (s). **^{1}H NMR** (400 MHz, $CDCl_3$) (δ, ppm): 7.42-7.39 (m, 5H, Ar*H*), 7.36-7.29 (m, 6H, Ar*H*), 6.57 (ddd, 1H, *J* = 8.8, 3.1, 1.5 Hz, Ar*H*), 6.24 (dd, 1H, *J* = 3.1, 2.1 Hz, Ar*H*), 3.51 (br s, 2H, C*H*$_2$), 3.49 (s, 3H, OC*H*$_3$). **HR-MS** (APCI+): *m/z* calcd. for $C_{20}H_{19}BrPO_2$ ($[M+O+H]^+$) = 401.0301; obs. = 401.0301 and $C_{20}H_{19}BrPO$ ($[M+H]^+$) = 385.0351; obs. = 385.0356. The APCI mass spectrum exhibits the expected bromide isotope pattern.

6.4.10. Synthesis of bis(hydroxymethyl)diphenylphosphonium chloride, 4.22[25]

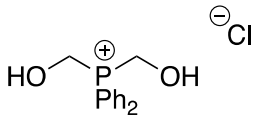

The following procedure was modified from the literature.[24] HCl (37% w/w, 0.5 mL) was added to a stirred solution of formaldehyde solution (37% w/w, 1 mL) and $HPPh_2$ (0.903 mL, 5.20 mmol). The self-heating mixture was stirred for 0.33 h. Upon cooling, all volatiles were removed *in vacuo* and the crude product was isolated as a white solid. Recrystallisation of this solid from boiling MeOH (4 mL) gave bis(hydromethyl)diphenylphosphonium chloride as a crystalline, white solid (1.15 g, 4.08 mmol, 78% yield). **^{31}P NMR** (162 MHz, $CDCl_3$) (δ, ppm): -17.0 (s). **^{1}H NMR** (400 MHz, $CDCl_3$) (δ, ppm): 7.97-7.91 (m, 4H, Ar*H*), 7.89 (td, 2H, *J* = 7.5, 1.7 Hz, Ar*H*), 7.75 (td, 4H, *J* = 7.7, 3.3 Hz, Ar*H*), 5.16 (d, 4H, *J* = 1.6 Hz, 2 x CH_2). Spectroscopic data matches that previously reported.[25]

6.4.11. Synthesis of 4-bis((diphenylphosphino)methyl)aminophenol, 4.23

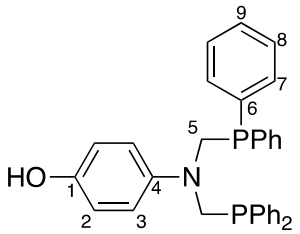

Et_3N (0.3 mL, 2.15 mmol) was added to solution of **4.22** (0.550 g, 1.95 mmol) in deionised H_2O (10 mL) and MeOH (5 mL). To this, 4-aminophenol (106 mg, 0.971 mmol) was added and the resulting mixture heated 70 °C for 1.5 h. Upon cooling, the reaction mixture was diluted by addition of CH_2Cl_2 (50 mL) and deionised H_2O (25 mL). The product was extracted into CH_2Cl_2 (2 x 25 mL) and the organic fractions combined, dried over anhydrous $MgSO_4$ and filtered before all volatiles were removed *in vacuo* to give the crude product as a sticky, clear solid. Purification by column chromatography (50:50 EtOAc:Hex, Rf = 0.70) gave **4.23** (240 mg, 0.475 mmol, 49% yield). **^{31}P NMR** (162 MHz, $CDCl_3$) (δ, ppm): -26.7 (s, 2P). **^{1}H NMR** (400 MHz, $CDCl_3$) (δ, ppm): 7.33-7.27 (m, 20H, PPh_2), 6.75 (d, 2H, *J* = 8.9 Hz, Ar*H*), 6.66 (d, 2H, *J* = 8.8 Hz, Ar*H*), 3.99 (d, 4H, *J* = 4.0 Hz, 2 x CH_2). **^{13}C NMR** (121 MHz, $CDCl_3$) (δ, ppm): 149.0 (s, 1C, C-1), 143.5 (s, 1C, C-4), 137.7 (d, 4C, J = 14.4 Hz, C-6), 133.3 (d, 8C, J = 19.3 Hz, C-7), 128.7 (s, 4C, C-9), 128.6-128.3 (m, 8C, C-8), 119.1 (s, 2C, C-2), 115.9 (s, 2C, C-3), 56.1 (s, 4C, C-5). **HR-MS** (ESI+): m/z calcd. for $C_{32}H_{30}NOP_2$ ([M+H]+) = 506.1797; obs. = 506.1811.

6.4.12. Synthesis of [Re(4.23)(CO)$_3$Br], 4.25

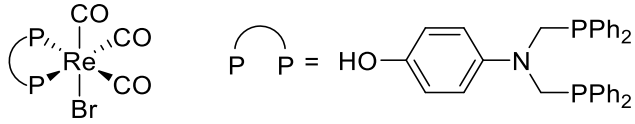

To a stirred solution of [Re(CO)$_3$(H$_2$O)$_2$Br] (16.0 mg, 39.5 µmol) in MeOH (0.5 mL), **4.23** (20.0 mg, 39.5 µmol) in CH_2Cl_2 (1 mL) was added dropwise. The reaction was stirred at ambient temperature for 16 h and the solvent removed *in vacuo* to give the expected final product, **4.25** (32.4 mg, 37.9 µmol, 96% yield), with *ca.* 84% purity by $^{31}P\{^1H\}$ NMR spectroscopy. **^{31}P{^{1}H} NMR** (162 MHz, $CDCl_3$) (δ, ppm): -19.8 (s, 2P). **^{1}H NMR** (400 MHz, $CDCl_3$: CD_3OD, 1:1) (δ, ppm): 7.50-7.31 (m, 20H, Ar*H*), 6.56 (d, 2H, *J* = 8.7 Hz, Ar*H*), 6.19 (d, 2H, *J* = 8.8 Hz, Ar*H*), 3.36 (br s, 4H, 2 x CH_2).

6.4.13. Synthesis of [Re(4.23)$_2$O$_2$]I, 4.27

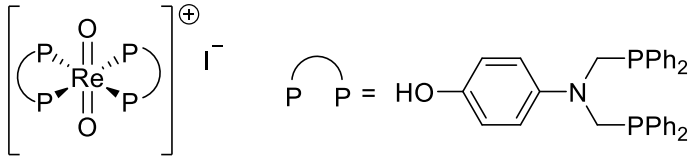

To a stirred solution of [Re(O)$_2$(PPh$_3$)$_2$I] (16.4 mg, 18.9 µmol) in CH_2Cl_2 (1 mL), **4.23** (20.0 mg, 39.5 µmol) in CH_2Cl_2 (2 mL) was added dropwise. The reaction was stirred at ambient temperature for 16 h. The solvent was removed *in vacuo*, the product re-dissolved in CH_2Cl_2 (0.25 mL) and MeOH (0.25 mL) then the product precipitated by addition of hexane (5 mL). The solid was washed with additional hexane (5 mL) and dried to give **4.27** as the final product (16.6 mg, 12.2µmol, 62% yield). **^{31}P{^{1}H} NMR** (162 MHz, $CDCl_3$: CD_3OD, 1:1) (δ, ppm): -34.1 (s, 4P). **^{1}H NMR** (400 MHz, $CDCl_3$: CD_3OD, 1:1) (δ, ppm): 7.44-7.26 (m, 14H, Ar*H*), 7.14 (app. t, 10H, *J* = 7.6 Hz, Ar*H*), 6.53 (d, 2H, *J* = 8.8 Hz, Ar*H*), 6.33 (d, 2H, *J* = 8.9 Hz, Ar*H*), 4.28 (br s, 4H, 2 x CH_2). **HR-MS** (Nanospray+): *m/z* calcd. for $C_{64}H_{58}O_4N_2P_4Re$ ($[M-I]^+$) = 1229.2905; obs. = 1229.2930.

6.4.14. Synthesis of 4.29

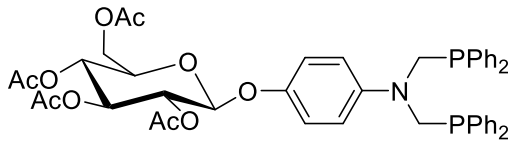

Acetobromo-α-D-glucose (165 mg, 0.401 mmol), BTEAB (326 mg, 1.20 mmol) and **4.23** (304 mg, 0.602 mmol) were dissolved in a mixture of CH_3Cl (15 mL) and 1.25 M NaOH (1.5 mL). The resulting biphasic mixture was stirred rapidly and heated to 60 °C for 4 h before the reaction was cooled to room temperature and diluted with $CHCl_3$ (20 mL). The organic layer was washed with deionised water (15 mL) and 1M NaOH (2 x 20 mL), then dried over $MgSO_4$, filtered and all volatiles removed *in vacuo* to give the crude product. The

crude product was purified by column chromatography (1:1 EtOAc:Hex, Rf = 0.44) to give **4.29** (34.0 mg, 0.0407 mmol, 10% yield) with *ca.* 63% purity, as measured by $^{31}P\{^{1}H\}$ NMR spectroscopy. **$^{31}P\{^{1}H\}$ NMR** (162 MHz, $CDCl_3$) (δ, ppm): -27.2 (s, 2P). **^{1}H NMR** (400 MHz, $CDCl_3$) (δ, ppm): 7.36-7.23 (m, 20H, 4 x Ph), 6.84 (d, 2H, J_{HH} = 9.2 Hz, Ar*H*), 6.73 (d, 2H, J_{HH} = 9.3 Hz, Ar*H*), 5.28-5.22 (m, 2H, H-2 and H-3), 5.17 (t, 1H, J_{HH} = 9.6 Hz, H-4), 4.94 (d, 1H, J_{HH} = 7.5 Hz, H-1), 4.31 (dd, 1H, J_{HH} = 12.2, 5.2 Hz, H-6a), 4.17 (dd, 1H, J_{HH} = 12.2, 2.5 Hz, H-6b), 3.94 (d, 4H, J_{HH} = 4.3 Hz, 2 x C*H*$_2$PPh$_2$), 3.79 (ddd, 1H, J_{HH} = 9.6, 5.2, 2.3 Hz, H-5), 2.09 (s, 3H, OAc), 2.08 (s, 3H, OAc), 2.05 (s, 3H, OAc), 2.04 (s, 3H, OAc). **^{13}C NMR** (126 MHz, $CDCl_3$) (δ, ppm): 170.8, 170.4, 169.5, 169.4 (s, 4C, 4 x CH_3*C*OO), 149.7 (s, 1C, quart. Ar*C*), 145.0 (s, 1C, quart. Ar*C*), 137.5 (d, 4C, J_{PC} = 14.4 Hz, quart. Ph), 133.3 (d, 8C, J_{PC} = 19.7 Hz, Ph), 130.7-127.7 (m, 8C, Ph), 128.9 (s, 4C, Ph), 118.5 (s, 2C, Ar*C*), 116.7 (s, 2C, Ar*C*), 100.5 (s, 1C, C-1), 73.0 (s, 1C, C-2/3), 72.0 (s, 1C, C-5), 71.4 (s, 1C, C-2/3), 68.5 (s, 1C, C-4), 62.1 (s, 1C, C-6), 55.4 (s, 4C, C*H*$_2$PPh$_2$), 20.9, 20.8, 20.72, 20.68 (s, 4C, 4 x *C*H_3COO). **HR-MS** (Nanospray+): *m/z* calcd. for $C_{46}H_{48}O_{10}NP_2$ ($[M+H]^+$) = 836.2753; obs. = 836.2744.

6.4.15. Synthesis of [Re(4.29)$_2$O$_2$]I, 4.30

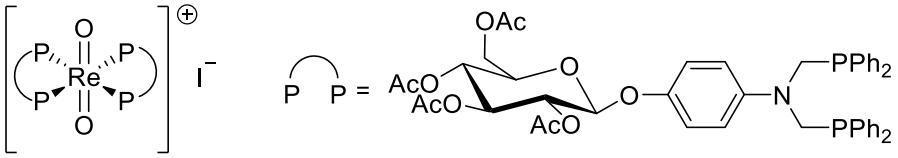

A solution of **4.29** (18.8 mg, 22.5 μmol, *ca.* 63% pure) in MeOH (1 mL) and CH_2Cl_2 (1 mL) was added dropwise to $[ReO_2I(PPh_3)_2]$ (9.8 mg, 11.3 μmol) in CH_2Cl_2 (1 mL). The resulting mixture was stirred at room temperature for 3 h and all volatiles were removed *in vacuo*. The residue was redissolved in $CHCl_3$ (0.5 mL) and the product was precipitated by addition of hexane (5 mL) and left to stand so that the supernatant could be removed by pipette. The solid was washed with further portions of hexane (2 x 5 mL) and the solid dried *in vacuo* to give **4.30** (13.3 mg) with *ca*. 40% purity by $^{31}P\{^{1}H\}$ NMR; complexes **4.27**, **4.31** and other unidentifiable ^{31}P-containing species were present (Chapter 4, Section 4.4.2). Data for **4.30**: **$^{31}P\{^{1}H\}$ NMR** (162 MHz, $CDCl_3$) (δ, ppm): -33.0 (s, 4P). **HR-MS** (Nanospray+): *m/z* calcd. for $C_{92}H_{94}O_{22}NP_4Re$ ($[M-I]^+$) = 1889.4806; obs. = 1889.4757. Data for **4.27**: **HR-MS** (Nanospray+): *m/z* calcd. for $C_{64}H_{58}O_4N_2P_4Re$ ($[M-I]^+$) = 1229.2800; obs. = 1229.4720. Data for **4.31**: **HR-MS** (Nanospray+): *m/z* calcd. for $C_{78}H_{76}O_{13}N_2P_4Re$ ($[M-I]^+$) = 1559.5690; obs. = 1559.5552.

6.4.16. Synthesis of isopropyl 3-bromo-2-(bromomethyl)propionate

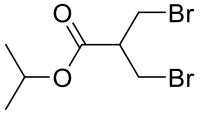

3-Bromo-2-(bromomethyl)propionic acid (200 mg, 0.813 mmol) was dissolved in isopropyl alcohol (10 mL) before conc. H_2SO_4 (0.220 mL) was added, and the resulting solution was heated to reflux for 24 h. Upon cooling to room temperature, the reaction was concentrated *in vacuo* and the residue re-dissolved in EtOAc (10 mL) before being neutralised with sat. $NaHCO_3$ and further diluted in a mixture of CH_2Cl_2:EtOAc (1:1, 30 mL). The organic phase was separated and washed with brine (15 mL), dried over anhydrous $MgSO_4$, filtered and the crude product was purified by column chromatography (EtOAc:Hex: 1:1: R_f = 0.50) to give isopropyl 3-bromo-2-(bromomethyl)propionate (131 mg, 0.455 mmol, 56% yield) as a clear, off-white oil. **^{1}H NMR** (400 MHz, $CDCl_3$) (δ, ppm): 5.09 (p, 1H, $^3J_{HH}$ = 6.3 Hz, iPr-C*H*), 3.76 (dd, 2H, $^3J_{HH}$ = 10.4, 5.1 Hz, C*H*$_2$Br), 3.70 (dd, 2H, $^3J_{HH}$ = 10.4, 6.5 Hz, C*H*$_2$Br), 3.12 (tt, 1H, $^3J_{HH}$ = 6.5, 5.0 Hz, C*H*($CH_2Br)_2$), 1.27 (s, 3H, CH_3), 1.26 (s, 3H, CH_3).) **^{13}C NMR** (126 MHz, CD_3OD) (δ, ppm): 169.5 (s, 1C, *C*=O), 70.0 (s, 1C, *C*H($CH_3)_2$), 49.2 (s, 1C, *C*H($CH_2Br)_2$), 31.3 (s, 2C, 2 x *C*H_2Br), 22.1 (s, 2C, 2 x *C*H_3).

6.4.17. Synthesis of HO(O)CCH$_2$CH(PPh$_2$)$_2$, 4.34

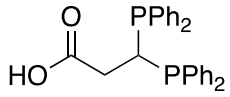

NaOH (0.770 g, 19.3 mmol) and ethyl 3,3-bis(diphenylphosphaneyl)propanoate (0.600 g, 1.28 mmol) were dissolved in a mixture of MeOH (18 mL), CH_2Cl_2 (10 mL) and deoxygenated H_2O (3 mL). After 5 days stirring at room temperature, the reaction was neutralised by addition of 2M HCl and extracted into CH_2Cl_2 (3 x 15 mL) and EtOAc (2 x 10 mL). The combined organics were dried over anhydrous $MgSO_4$, filtered and all volatiles removed *in vacuo* to give **4.34** as a white solid (0.490 g, 1.11 mmol, 87% yield). **^{31}P{^{1}H} NMR** (121 MHz, CD_3OD) (δ, ppm): -7.4 (s, 2P). **^{1}H NMR** (500 MHz, CD_3OD) (δ, ppm): 7.87-7.11 (m, 20H, ArH), 3.84 (t, 1H, $^3J_{HH}$ = 6.0 Hz, C*H*($PPh_2)_2$), 2.47 (td, 2H, *J* = 9.2, 6.0 Hz, C*H*$_2$CH($PPh_2)_2$). **^{13}C NMR** (126 MHz, CD_3OD) (δ, ppm): 175.4 (s, 1C, *C*OOH), 134.5 (app. t, 4C, $^3J_{PC}$ = 11.1 Hz, *o*-Ar*C*), 133.3 (t, 4C, $^3J_{PC}$ = 10.4 Hz, *o*-Ar*C*), 131.1 (s, 2C, *i*-Ar*C*), 131.0 (s, 2C, *i*-Ar*C*), 129.2 (s, 2C, *p*-Ar*C*), 128.8 (s, 2C, *p*-Ar*C*), 127.30 (m, 8C, *m*-Ar*C*), 32.1 (t, 1C, $^1J_{PC}$ = 9.4 Hz, CH$_2$*C*H), 27.7 (t, 1C, $^2J_{PC}$ = 25.3 Hz, *C*H$_2$CH). **HR-MS (ESI-)**: *m/z* calcd. for $C_{27}H_{23}O_2P$ ([M-H]$^-$) = 441.1173; obs. = 441.1179. *Ethyl 3,3-bis(diphenylphosphaneyl)propanoate was prepared as reported by Webster et al.*[13]

6.4.18. Synthesis of ^{OAc}Glc-O-$(CH_2)_3$NHC(O)CH_2CH$(PPh_2)_2$, 4.35

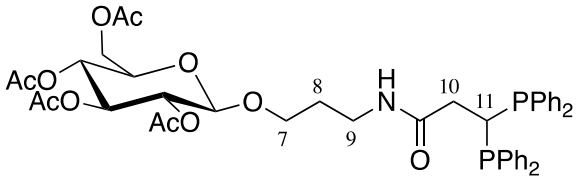

DMAP (108 mg, 0.884 mmol) and EDC-HCl (153 mg, 0.798 mmol) were added to carboxylic acid **4.34** (180 mg, 0.407 mmol) in CH_2Cl_2 (12 mL) and stirred for 30 min at room temperature. Carbohydrate **2.18** (205 mg, 0.506 mmol) in CH_2Cl_2 (3 mL) was added and the resulting solution stirred at room temperature for 24 h. All volatiles were removed *in vacuo* and the residue was re-dissolved in CH_2Cl_2 (20 mL). The organics were washed with HCl (2 M, 10 mL), saturated $NaHCO_3$ (20 mL) and brine (20 mL), then dried over anhydrous $MgSO_4$ and product (150 mg, 0.181 mmol) was purified by flash chromatography (EtOAc:Hex:Et_3N, 2:1:0.01, R_f = 0.41) and **4.35** (40.0 mg, 0.0483 mmol, 24% yield) was isolated as a colourless oil. *N.B* The yield is 24% as only 50% of the crude material underwent purification. **^{31}P{^{1}H} NMR** (121 MHz, $CDCl_3$) (δ, ppm): -7.1 (s, 2P). **^{1}H NMR** (500 MHz, $CDCl_3$) (δ, ppm): 7.60-7.56 (m, 4H, ArH), 7.50-7.45 (m, 4H, ArH), 7.29-7.22 (m, 12H, ArH), 5.18 (app. t, 1H, *J* = 9.5 Hz, H-3), 5.06 (app. t, 1H, *J* = 9.7 Hz, H-4), 4.91 (dd, 1H, *J* = 9.7, 8.0 Hz, H-2), 4.87 (br. t, 1H, $^1J_{NH}$ = 7.5 Hz, C(O)N*H*), 4.38 (d, 1H, *J* = 8.0 Hz, H-1), 4.14-4.09 (m, 2H, H-6a and H-6b), 4.08-4.05 (m, 1H, H-11a), 3.69-3.62 (m, 2H, H-7a & H-5), 3.36-3.31 (m, 2H, H-7b), 2.77 (m, 2H, H-9a & H-9b), 2.25 (td, 2H, *J* = 9.6, 5.7 Hz, H-10a & H-10b), 2.04 (s, 3H, OAc), 2.03 (s, 3H, OAc), 2.02 (s, 3H, OAc), 1.98 (s, 3H, OAc), 1.43 (tt, 2H, *J* = 13.7, 7.4 Hz, H-8a & H-8b). **^{13}C NMR** (126 MHz, $CDCl_3$) (δ, ppm): 171.2 (t, $^3J_{PC}$ = 3.5 Hz 1C, *C*(O)NH), 170.7 (s, 1C, CH_3*C*OO), 170.3 (s, 1C, CH_3*C*OO), 169.5 (s, 1C, CH_3*C*OO), 169.4 (s, 1C, CH_3*C*OO), 136.5 (m, 2C, *i*-Ar*C*), 136.3 (d, 2C, *i*-Ar*C*), 134.8 (m, 4C, *o*-Ar*C*), 133.8 (m, 4C, *o*-Ar*C*), 128.8 (s, 2C, *p*-Ar*C*), 128.7 (s, 2C, *p*-Ar*C*), 128.4 (m, 4C, *m*-Ar*C*), 128.2 (m, 4C, *m*-Ar*C*), 100.3 (s, 1C, C-1), 72.7 (s, 1C, C-3), 72.0 (s, 1C, C-5), 71.3 (s, 1C, C-2), 68.5 (s, 1C, C-4), 68.1 (s, 1C, C-7), 61.9 (s, 1C, C-6), 37.2 (s, 1C, C-9),36.3 (t, 1C, $^2J_{PC}$ = 9.2 Hz, C-10), 28.9 (s, 1C, C-8), 28.9 (t, 1C, $^1J_{PC}$ = 22.9 Hz, C-11), 20.9 (s, 1C, *C*H_3COO), 20.77 (s, 1C, *C*H_3COO), 20.75 (s, 1C, *C*H_3COO), 20.72 (s, 1C, *C*H_3COO). **HR-MS (ESI+)**: *m/z* calcd. for $C_{44}H_{50}NO_{11}P$ ($[M+H]^+$) = 830.2859; obs. = 830.2871.

6.4.19. Synthesis of ^{OH}Glc-O-$(CH_2)_3$NHC(O)$CH_2CH(PPh_2)_2$, 4.36

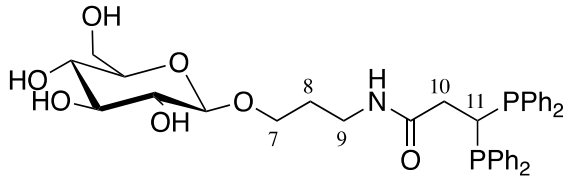

1M sodium methanolate (0.20 mL, 0.200 mmol) was added to **4.35** (7.00 mg, 8.44 µmol) in methanol (2 mL). After stirring at room temperature for 18 h the reaction was diluted with MeOH (4 mL). Amberlyst 120 resin was added to reduce the pH to 7 and the reaction was filtered and concentrated *in vacuo* to give **4.36** as white foam (3.00 mg, 4.54 µmol, 54% yield). The Amberlyst 120 resin was prepared by washing with MeOH then drying the resin in air. **$^{31}P\{^1H\}$ NMR** (121 MHz, MeOH) (δ, ppm): -6.7 (s, 2P). **HR-MS (ESI+)**: *m/z* calcd. for $C_{36}H_{41}NO_7P_2Na$ ($[M+Na]^+$) = 684.2256; obs. = 684.2255.

6.4.20. Synthesis of 3'-aminopropyl-β-D-glycopyranoside, 4.37

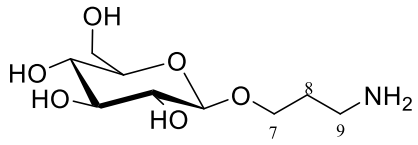

3-azidopropyl β-D-glucopyranoside (330 mg, 1.25 mmol) was dissolved in MeOH (10 mL) and Pd/C (36.0 mg) was added to the solution under a flow of N_2. The reaction was sparged with 1 balloon of H_2 before a second balloon was added to the sealed system to maintain a H_2 atmosphere throughout the reaction. After leaving the mixture to stir at room temperature for 3 h, the mixture was filtered through MeOH-wet Celite and all volatiles were removed *in vacuo* to give **4.37** (280 mg, 1.18 mmol, 94% yield). **^{1}H NMR** (400 MHz, CD_3OD) (δ, ppm): 4.27 (d, 1H, *J* = 7.8 Hz, H-1), 4.05-3.94 (m, 1H, H-7a), 3.88 (dd, 1H, *J* = 11.9, 1.6 Hz, H-6a), 3.73-3.61 (m, 2H, H-7b and H-6b), 3.31-3.25 (m, 2H, H-3/-4 or -5), 3.17 (dd, 1H, *J* = 9.1, 7.8 Hz, H-2), 2.80 (td, 2H, *J* = 6.7, 2.0 Hz, H-9a and H-9b), 1.84-1.74 (m 2H, H-8a and H-8b). The ^{1}H NMR signal for H-3/-4 or -5 is obscured by the CD_3OD signal at 3.31 ppm.**^{13}C NMR** (126 MHz, $CDCl_3$) (δ, ppm): 104.5 (s, 1C, C-1), 78.1 (s, 1C), 77.8 (s, 1C) 75.1 (s, 1C), 71.7 (s, 1C), 68.8 (s, 1C), 62.8 (s, 1C), 39.7 (s, 1C, C-9), 33.2 (s, 1C, C-8).

6.4.21. Synthesis of ^{99m}Tc(V) complexes with 4.36

Kits for radiolabelling **4.36** are listed in Chapter 4, Section 4.5.5, Table 4.2. Standard solutions of the reagents added to the kit (ligand, stannous chloride, sodium tartrate and sodium hydrogen carbonate) were prepared in purified water or ethanol. The kits were freeze-dried in Eppendorf tubes immediately after preparation and stored under nitrogen or argon gas at -20 ºC in a freezer.

Synthesis of the ^{99m}Tc(V) complexes was performed by addition of the [^{99m}TcO$_4$]$^-$ saline solution (5-10 µL, 10-20 MBq) and saline (500 µL) to a thawed kit. The solubilised kit was incubated at room temperature or 50 ºC for 30 min. Aliquots of these samples were analysed by analytical HPLC (Method 2, 100-150 µL).

6.5. References

1 J. Ma, X. Yang, W. Hao, Z. Huang, X. Wang and P. G. Wang, *Eur. J. Med. Chem.*, 2017, **128**, 45–55.

2 J. Ipaktschi and W. Sulzbach, *J. Organomet. Chem.*, 1992, **434**, 287–302.

3 I. Damager, C. Erik Olsen, B. Lindberg Møller and M. Saddik Motawia, *Carbohydr. Res.*, 1999, **320**, 19–30.

4 N. Lazarova, S. James, J. Babich and J. Zubieta, *Inorg. Chem. Commun.*, 2004, **7**, 1023–1026.

5 G. Zhao, W. Yao, J. N. Mauro and M. Y. Ngai, *J. Am. Chem. Soc.*, 2021, **143**, 1728–1734.

6 S. De Munari, S. Sandoval, E. Pach, B. Ballesteros, G. Tobias, D. C. Anthony and B. G. Davis, *Inorganica Chim. Acta*, 2019, **495**, 118933.

7 D. A. Learmonth, *Synth. Commun.*, 2004, **34**, 1565–1575.

8 H. P. Kleine, D. V. Weinberg, R. J. Kaufman and R. S. Sidhu, *Carbohydr. Res.*, 1985, **142**, 333–337.

9 W. A. Hermann, C. Brossmer, K. Ofele, C.-P. Reisinger, T. Priermeier, M. Beller and H. Fischer, *Angew. Chem. Int. Ed. Engl.*, 1995, **5**, 1844–1847.

10 M. K. Rong, K. Van Duin, T. Van Dijk, J. J. M. De Pater, B. J. Deelman, M. Nieger, A. W. Ehlers, J. C. Slootweg and K. Lammertsma, *Organometallics*, 2017, **36**, 1079–1090.

11 R. Roy, F. D. Tropper, T. Morrison and J. Boratynski, *J. Chem. Soc. Chem. Commun.*, 1991, 536–538.

12 P. M. Byers and I. V. Alabugin, *J. Am. Chem. Soc.*, 2012, **134**, 9609–9614.

13 N. T. Coles, M. F. Mahon and R. L. Webster, *Chem. Commun.*, 2018, **54**, 10443–10446.

14 A. K. Yadav, D. L. Shen, X. Shan, X. He, A. R. Kermode and D. J. Vocadlo, *J. Am. Chem. Soc.*, 2015, **137**, 1181–1189.

15 V. Fehring, R. Kadyrov, M. Ludwig, J. Holz, K. Haage and R. Selke, *J. Organomet. Chem.*, 2001, **621**, 120–129.

16 C. Clarke, D. J. Fox, S. Pedersen and S. Warren, *Org. Biomol. Chem.*, 2009, 1329–

1336.

17 A. Shavnya, K. D. Hesp and A. S. Tsai, *Adv. Synth. Catal.*, 2018, **360**, 1768–1774.

18 A. Chadwick, PhD Thesis, University of Bristol, 2019.

19 E. L. Myers and R. T. Raines, *Angew. Chem. Int. Ed.*, 2009, **48**, 2359–2363.

20 M. Beller, J. G. E. Krauter, A. Zapf and S. Bogdanovic, *Catal. Today*, 1999, **48**, 279–290.

21 M. Beller, J. G. E. Krauter and A. Zapf, *Angew. Chem. Int. Ed. Eng.*, 1997, **36**, 772–774.

22 S. Sasaki, *Phosphorus, Sulfur Silicon Relat. Elem.*, 2016, **191**, 1513–1514.

23 S. E. Wright, S. Richardson-Solorzano, T. N. Stewart, C. D. Miller, K. C. Morris, C. J. A. Daley and T. B. Clark, *Angew. Chem. Int. Ed.*, 2019, **58**, 2834–2838.

24 J. Fawcett, P. A. T. Hoye, R. D. Kemmitt, D. J. Law and D. R. Russell, *J. Am. Chem. Soc., Dalton Trans.*, 1993, 2563–2568.

25 M. Siebert, M. Seibicke, A. F. Siegle, S. Kräh and O. Trapp, *J. Am. Chem. Soc.*, 2019, **141**, 334–341.

Chapter 7 : Appendix

7.1. X-ray Crystallography

X-ray crystallographic data was recorded by Dr Hazel Sparkes and Dr Natalie Pridmore on a Bruker Kappa Apex II diffractometer at 100 K, using Mo-Kα radiation (λ = 0.71073 Å). Intensities were integrated in SAINT[1] and absorption corrections, based on equivalent reflections, were applied with SADABS[2]. Crystal structures were solved with ShelXT[3], and each structure was refined against F^2 using ShelXL[4] in Olex2[5]. The crystal structure and refinement data for **2.23** and **3.19** are given in Table **7.1**.

Table 7.1 Crystal data and structure refinement for complexes **2.23** and **3.19**.

Identification code	Complex 2.23	Complex 3.19
Empirical formula	$C_{35}H_{34}BrO_7P_2Re$	$C_{39}H_{30}BrO_3P_2Re$
Formula weight	894.67	874.68
Temperature/K	100(2)	100(2)
Crystal system	triclinic	monoclinic
Space group	P-1	$P2_1/c$
a/Å	10.6414(5)	9.39030(10)
b/Å	11.4634(6)	37.9563(5)
c/Å	16.1289(8)	9.83770(10)
α/°	79.727(3)	90
β/°	75.741(3)	108.2890(10)
γ/°	63.261(2)	90
Volume/$Å^3$	1697.79(15)	3329.24(7)
Z	2	4
$\rho_{calc}g/cm^3$	1.750	1.745
μ/mm^{-1}	4.897	4.984
F(000)	880.0	1712.0
Crystal size/mm^3	0.358 × 0.21 × 0.119	0.352 × 0.318 × 0.224
Radiation	MoKα (λ = 0.71073)	MoKα (λ = 0.71073)
2Θ range for data collection/°	3.99 to 56.038	4.292 to 55.918
Index ranges	$-11 \le h \le 14$, $-15 \le k \le 15$, $-21 \le l \le 21$	$-12 \le h \le 12$, $-49 \le k \le 50$, $-11 \le l \le 12$
Reflections collected	31701	30381
Independent reflections	8192 [R_{int} = 0.0347, R_{sigma} = 0.0320]	7994 [R_{int} = 0.0360, R_{sigma} = 0.0350]
Data/restraints/parameters	8192/0/417	7994/41/443
Goodness-of-fit on F^2	1.024	1.055
Final R indexes [I>=2σ (I)]	R_1 = 0.0220, wR_2 = 0.0484	R_1 = 0.0266, wR_2 = 0.0484
Final R indexes [all data]	R_1 = 0.0254, wR_2 = 0.0497	R_1 = 0.0326, wR_2 = 0.0499
Largest diff. peak/hole / e $Å^{-3}$	1.01/-1.17	0.63/-0.85

7.2. Inductively Coupled Plasma Mass Spectrometry (ICP-MS)

7.2.1. Sample Preparation for ICP-MS analysis

Aliquots of samples (0.3 mL) were digested in concentrated Optima Grade HNO_3 (0.1 mL, 68% w/w; Fisher Scientific trace metal grade acid) at 60 °C for *ca.* 12 h. After digestion, samples were diluted with purified water (resistivity ≥18.2 MΩ cm from a Milli-Q system by Merck Millipore) to give a total sample volume of 3 mL. Calibration standards were prepared volumetrically using a High Purity Standard (HPS) ICP-MS multi-element standard solution (HPS multi-element standard solution D) that contained 10 mg/L of Re. Calibration solutions (0.1 to 1000 µg/L) were doped with a Leehman Labs 100 ppm Tb standard (Teledyne) so each solution had a standard concentration of Tb (50 µg Tb/L).

7.2.2. ICP-MS Measurements

All ICP-MS measurements were performed at the London Metallomics Facility (LMF) at King's College London with a Perkin Elmer NexION 350D Inductively Coupled Plasma Quadrupole Mass Spectrometer (ICP-QMS) that was operated in standard mode. The ICP-QMS was equipped with a Cetac ASX-100 autosampler that was coupled to a SeaSpray glass nebulizer and quart cyclonic spray chamber. Further details are given in Table 7.2 and Table 7.3.

ICP-QMS results were verified though the repeated checking of blanks, calibrants and a certified reference material (CRM); trace metal drinking water (CRM-TMDW-100) from High Purity Standards. As it was not possible to obtain a CRM for Re, Mo was used as a proxy to assess the system bias in ICP-QMS calibration, and Ga was used as an internal standard for Mo measurements.

To account for instrument drift and matrix effects, all results were normalised relative to the internal Tb standard. Intensities of samples and standards were blank corrected by subtracting the average isotopic intensity (counts per second, cps) of repeat blank measurements. Corrected isotopic intensity values were converted from counts per second (cps) to concentration (µg/L) by interpolation of neighbouring calibrants. The quality of the interpolation was assessed by measuring the linearity of the calibration curve.

Table 7.2 Settings for ICP-QMS (PerkinElmer NexION 350D).

PerkinElmer NexION 350D ICP Mass Spectrometer Settings	
Ar Gas flow (L min^{-1})	1
Ar Auxiliary gas flow (L min^{-1})	1.2
Ar Plasma flow (L min^{-1})	18
Cell A gas flow (NH3, mL m^{-1})	0
Cell B gas flow (He, mL m^{-1})	0
Nebulizer gas flow (L min^{-1})	0.95
Mode of operation	Standard
RF power (W)	1600

Table 7.3 Parameters for ICP-MS Method

ICP-MS – Method parameters	
Elements mass	^{185}Re
Dwell time (ms)	100
RPa	0
RPq	0.25
Calibration (µg/L)	1-1000
Replicates per sample	5
LOD (µg/L)	0.03
LOQ (µg/L)	0.1
Internal standard (µg/L)	Tb - 50 µg/L

7.2.3. Pilot Study Results

The raw data provided by the LMF is shown in Table 7.4, whilst the samples codes are identified in Table 7.5, as the codes used for analysis do not clearly reflect those used within this thesis.

Table 7.4 Raw data from ICP-MS Pilot Study recorded on 4/5/21.

Run	Sample	Acquisition time	Re (µg/L)	^{185}Re RSD	Mo (µg/L)	^{95}Mo RSD
1	pre-blank	15:50:45	0.0	5.0	-0.1	5.6
2	Blank	15:55:54	-0.1	7.0	-0.9	6.9
3	Standard 1	16:01:00	0.0	2.2	-0.1	3.8
4	Standard 2	16:06:03	0.1	0.5	0.1	1.8
5	Standard 3	16:11:07	1.0	0.5	1.0	1.0
6	Standard 4	16:16:12	10.0	0.3	10.0	0.4
7	Standard 5	16:21:17	50.0	0.3	50.0	0.4
8	Standard 6	16:26:23	100.0	0.6	100.0	0.6
9	Standard 7	16:31:30	500.0	0.4	500.0	0.4
10	Standard 8	16:36:37	986.7	0.8	997.7	0.8
11	pre-blank	16:41:45	0.0	34.8	0.7	13.7
12	Blank	16:46:53	0.0	38.2	3.4	10.7
13	CRM-TMDW-100	16:52:01	0.0	13.8	88.5	0.5
14	Standard 4	16:57:07	9.8	0.3	10.2	0.3
15	Blank	17:02:14	-0.1	14.4	1.3	9.0
16	R1	17:07:19	4776.6	1.4	0.8	5.3
17	R2	17:12:23	3440.4	1.1	0.6	3.2
18	R3	17:17:26	4795.1	0.9	0.5	2.4
19	P HC1	17:22:30	14.2	0.6	0.4	4.5
20	P HC2	17:27:34	13.9	0.3	0.3	3.1
21	P HC3	17:32:38	9.5	0.5	0.3	1.9
22	P1	17:37:43	48.4	0.5	0.3	3.6
23	P2	17:42:48	51.1	0.4	0.2	5.2
24	P3	17:47:53	40.3	0.5	0.2	3.3
25	R HC1	17:52:59	18.0	0.7	0.1	4.3
26	CRM-TMDW-100	17:58:05	0.0	3.1	87.0	0.5
27	Standard 4	18:03:11	9.7	0.4	9.8	0.7
28	Blank	18:08:18	0.3	8.4	0.4	9.4

29	R HC2	18:13:25	18.9	0.6	0.2	3.3
30	R HC3	18:18:31	27.1	0.9	0.2	3.1
31	ER1	18:23:36	7374.0	0.4	0.9	4.0
32	ER2	18:28:39	7376.7	0.6	0.9	2.2
33	ER3	18:33:42	7206.9	0.6	0.9	3.3
34	EP1	18:38:46	11471.9	0.4	1.1	3.4
35	EP2	18:43:50	11419.3	0.4	1.0	4.1
36	EP3	18:48:54	11727.9	1.0	1.1	2.0
37	H1	18:53:58	2.6	14.1	-0.8	4.7
38	H2	18:59:03	0.9	4.9	-0.8	5.9
39	H3	19:04:08	0.5	0.7	0.3	4.4
40	Digestion blank	19:09:14	0.0	1.2	-0.1	4.1
41	CRM-TMDW-100	19:14:20	0.0	2.3	86.9	0.5
42	Standard 4	19:19:26	9.7	0.3	10.0	0.5
43	Blank	19:24:33	0.2	6.4	0.3	6.3

Standard solutions and blanks are labelled as such and CRM-TMDW-100 is a CRM. R1-3 = cell lysate of HeLa cells exposed to **3.11**, P1-3 = cell lysate of HeLa cells exposed to $Re(CO)_3(H_2O)_3Br$, ER1-3 = exposure solution of **3.11**, EP1= exposure solution of $[Re(CO)_3(H_2O)_3]Br$, R HC1-3 = handling control for **3.11**, P HC1-3 = handling control for $Re(CO)_3(H_2O)_3Br$, H1-3 = untreated HeLa cells. All information is tabulated in **Table 7.5**

Table 7.5 Table for Sample identification for all Pilot Study samples.

Run	Sample Name	Identity
1	pre-blank	-
2	Blank	-
3	Standard 1	Calibrant
4	Standard 2	Calibrant
5	Standard 3	Calibrant
6	Standard 4	Calibrant
7	Standard 5	Calibrant
8	Standard 6	Calibrant
9	Standard 7	Calibrant
10	Standard 8	Calibrant
11	pre-blank	-
12	Blank	-
13	CRM-TMDW-100	CRM
14	Standard 4	Calibrant

15	Blank	-
16	R1	**3.11** lysate
17	R2	**3.11** lysate
18	R3	**3.11** lysate
19	P HC1	$[Re(CO)_3(H_2O)_3Br]$ handling control
20	P HC2	$[Re(CO)_3(H_2O)_3Br]$ handling control
21	P HC3	$[Re(CO)_3(H_2O)_3Br]$ handling control
22	P1	$[Re(CO)_3(H_2O)_3Br]$ lysate
23	P2	$[Re(CO)_3(H_2O)_3Br]$ lysate
24	P3	$[Re(CO)_3(H_2O)_3Br]$ lysate
25	R HC1	**3.11** handling control
26	CRM-TMDW-100	CRM
27	Standard 4	Calibrant
28	Blank	-
29	R HC2	**3.11** handling control
30	R HC3	**3.11** handling control
31	ER1	**3.11** exposure solution
32	ER2	**3.11** exposure solution
33	ER3	**3.11** exposure solution
34	EP1	$[Re(CO)_3(H_2O)_3Br]$ exposure solution
35	EP2	$[Re(CO)_3(H_2O)_3Br]$ exposure solution
36	EP3	$[Re(CO)_3(H_2O)_3Br]$ exposure solution
37	H1	untreated HeLa lysate
38	H2	untreated HeLa lysate
39	H3	untreated HeLa lysate
40	Digestion blank	-
41	CRM-TMDW-100	CRM
42	Standard 4	Calibrant
43	Blank	-

7.2.4. Large Scale ICP-MS Study (Chapter 3, Section 3.4.2.3)

The raw data provided by the LMF for the larger scale ICP-MS uptake study (Chapter 3, Section 3.4.2.3) is shown in Table 7.6, whilst the samples are identified in Table 7.7, as the codes used for analysis do not clearly reflect those used within this thesis.

Table 7.6 Raw data from larger scale ICP-MS study recorded on 2/8/21 and 3/8/21.

Run	Sample	Acquisition time	Re (µg/L)	^{185}Re RSD	Mo (µg/L)	^{95}Mo RSD
1	pre-blank	18:18:24	-0.02	9.10	-0.03	4.60
2	Blank	18:23:08	-0.16	14.60	-0.27	12.70
3	Standard 1	18:27:49	0.00	2.70	-0.02	3.80
4	Standard 2	18:32:27	0.10	1.30	0.10	0.70
5	Standard 3	18:37:07	1.00	0.60	1.00	0.80
6	Standard 4	18:41:47	10.00	0.40	10.00	0.60
7	Standard 5	18:46:27	50.00	1.40	50.00	0.50
8	Standard 6	18:57:09	100.00	2.60	100.00	0.70
9	Standard 7	19:01:51	500.00	1.20	500.00	0.10
10	Standard 8	19:06:33	998.00	0.70	1013.97	0.50
11	pre-blank	19:11:16	0.02	31.00	0.51	14.40
12	Blank	19:15:59	-0.11	18.20	1.87	8.30
13	CRM-TMDW-500	19:20:43	-0.03	9.20	93.01	0.20
14	Standard 4	19:25:24	1.00	0.80	1.10	1.00
15	Blank	19:30:06	-0.15	10.70	0.65	1.70
16	1_Blank handling	19:34:47	-0.15	9.00	1.11	1.10
17	2_124 HC D	19:39:25	11.01	0.50	1.76	2.00
18	3_124 HC D	19:44:04	9.75	0.50	1.04	2.80
19	4_124 HC D	19:48:43	10.00	0.60	0.62	5.50
20	5_PC HC D	19:53:22	12.58	0.70	1.42	1.90
21	6_PC HC D	19:58:02	11.29	0.80	1.36	3.00
22	7_PC HC D	20:02:42	11.39	0.80	1.81	2.10
23	8_17 HC D	20:07:22	13.45	0.40	0.83	2.40
24	9_17 HC D	20:12:02	12.27	0.20	0.61	1.80
25	10_17 HC D	20:16:43	13.25	0.70	0.47	1.80
26	CRM-TMDW-500	20:21:25	-0.03	4.50	91.89	0.60
27	Standard 4	20:26:06	9.68	0.50	9.96	0.30
28	Blank	20:30:48	-0.15	9.70	0.24	3.60
29	11_193 HC D	20:35:31	46.62	0.90	0.97	2.30
30	12_193 HC D	20:40:12	44.44	0.50	0.67	1.40
31	13_193 HC D	20:44:52	42.41	0.50	0.67	3.50
32	14_124 HC M	20:49:30	14.55	0.70	0.76	0.80
33	15_124 HC M	20:54:09	11.50	0.80	0.50	3.10
34	16_124 HC M	20:58:48	14.57	0.60	0.51	2.40
35	17_PC HC M	21:03:27	18.61	0.40	0.53	1.90
36	18_PC HC M	21:08:06	17.14	0.40	0.37	3.20

37	19_PC HC M	21:12:46	17.66	0.50	2.07	1.40
38	20_17 HC M	21:17:26	18.46	0.20	0.29	3.30
39	CRM-TMDW-500	21:22:08	-0.03	5.30	92.04	0.40
40	Standard 4	21:26:50	9.69	0.20	9.93	0.70
41	Blank	21:31:32	-0.15	12.00	0.21	9.80
42	21_17 HC M	21:36:14	16.75	0.40	0.47	2.30
43	22_17 HC M	21:40:54	18.46	0.80	0.41	3.90
44	23_193 HC M	21:45:35	44.69	0.60	0.72	1.80
45	24_193 HC M	21:50:17	51.51	0.80	0.50	2.10
46	25_193 HC M	21:54:57	59.33	0.60	0.40	3.10
47	26_124 H	21:59:35	1653.83	0.40	0.27	2.60
48	27_124 H	22:04:14	1871.47	0.40	0.90	4.20
49	28_124 H	22:08:53	2012.18	0.50	0.22	3.50
50	29_PC H	22:13:32	42.69	0.20	0.26	2.60
51	30_PC H	22:18:11	38.25	0.60	0.34	3.30
52	CRM-TMDW-500	22:22:53	0.05	6.40	91.61	0.40
53	Standard 4	22:27:34	9.54	0.50	9.96	0.50
54	Blank	22:32:16	0.15	6.10	0.21	5.20
55	31_PC H	22:36:58	31.79	0.70	1.80	2.40
56	32_17 H	22:41:38	1107.10	0.50	0.45	2.20
57	33_17 H	22:46:19	1238.14	0.70	0.59	1.20
58	34_17 H	22:50:59	1000.95	0.50	0.26	2.10
59	35_193 H	22:55:40	317.47	0.80	0.89	2.30
60	36_193 H	23:00:22	339.89	0.80	0.48	1.20
61	37_193 H	23:05:02	364.13	0.10	0.97	1.10
62	38_UN H	23:09:41	0.38	5.20	0.33	2.40
63	39_UN H	23:14:19	0.27	2.00	0.37	2.30
64	40_UN H	23:18:58	0.22	1.00	0.35	3.70
65	CRM-TMDW-500	23:23:39	-0.01	4.40	91.40	0.40
66	Standard 4	23:28:21	9.57	0.40	10.02	0.50
67	Blank	23:33:03	-0.06	4.70	0.20	5.00
68	41_124 F	23:37:45	1200.14	0.50	2.37	1.90
69	42_124 F	23:42:24	1181.04	0.40	0.42	1.30
70	43_124 F	23:47:04	1332.37	0.90	0.74	1.10
71	44_PC F	23:51:44	37.27	0.70	0.44	3.10
72	45_PC F	23:56:25	42.38	0.30	0.68	2.80
73	46_PC F	00:01:05	41.85	0.50	1.79	0.50
74	47_17 F	00:05:46	872.05	0.00	0.89	1.70
75	48_17 F	00:10:28	569.13	0.10	0.52	2.20
76	49_17 F	00:15:08	657.90	0.30	0.25	4.30
77	50_193 F	00:19:47	465.61	0.40	0.52	2.70
78	CRM-TMDW-500	00:24:28	0.05	6.70	91.95	0.30
79	Standard 4	00:29:10	9.47	0.40	9.97	0.20
80	Blank	00:33:52	0.17	3.40	0.21	8.50
81	51_193 F	00:38:33	436.22	0.30	1.86	0.90
82	52_193 F	00:43:12	378.96	0.70	0.63	0.60

83	53_UN F	00:47:51	0.28	2.10	0.70	3.50
84	54_UN F	00:52:31	0.20	1.90	0.53	2.00
85	55_UN F	00:57:11	0.16	2.40	0.48	1.50
86	56_124 E	01:01:51	796.20	0.30	0.49	3.10
87	57_124 E	01:06:31	1004.07	0.70	0.67	2.80
88	58_124 E	01:11:12	874.87	0.10	0.34	2.40
89	59_PC E	01:15:53	17.04	0.50	0.40	1.30
90	60_PC E	01:20:34	19.72	0.50	1.29	2.10
91	CRM-TMDW-500	01:25:16	0.03	3.10	91.97	0.80
92	Standard 4	01:29:58	9.48	0.60	9.99	0.80
93	Blank	01:34:40	0.13	1.60	0.21	11.10
94	61_PC E	01:39:21	18.38	0.30	1.10	0.60
95	62_17 E	01:44:01	457.17	0.20	0.41	2.60
96	63_17 E	01:48:40	430.09	0.30	1.04	2.20
97	64_17 E	01:53:19	503.34	0.20	0.28	2.90
98	65_193 E	01:57:59	157.28	0.30	1.25	2.20
99	66_193 E	02:02:38	207.14	0.30	0.41	2.90
100	67_193 E	02:07:18	185.13	0.30	0.23	1.20
101	68_UN E	02:11:58	0.23	2.90	0.40	2.60
102	69_UN E	02:16:38	0.17	3.10	0.41	6.20
103	70_UN E	02:21:19	0.15	1.80	0.30	2.00
104	CRM-TMDW-500	02:26:01	-0.01	1.00	92.77	0.80
105	Standard 4	02:30:43	9.47	0.60	10.06	0.50
106	Blank	02:35:24	-0.08	1.80	0.21	10.30
107	71_P H pink	02:40:07	15743.02	0.40	1.48	1.90
108	72_P H pink	02:44:48	15536.65	0.30	1.49	3.40
109	73_P H pink	02:49:28	15724.20	0.30	3.40	1.50
110	74_17 H pink	02:54:08	4215.19	0.30	1.55	2.90
111	75_17 H pink	02:58:48	3960.50	0.30	1.58	1.60
112	76_17 H pink	03:03:28	4285.85	0.30	1.53	1.70
113	77_93 H pink	03:08:07	3039.32	0.40	1.39	2.30
114	78_93 H pink	03:12:47	3050.63	0.20	3.60	0.80
115	79_93 H pink	03:17:27	3028.63	0.60	1.78	2.40
116	80_124 H pink	03:22:07	7354.64	0.10	6.39	0.60
117	CRM-TMDW-500	03:26:49	0.25	17.20	91.90	0.40
118	Standard 4	03:31:30	9.55	0.80	10.02	1.00
119	Blank	03:36:12	0.28	4.00	0.22	8.80
120	81_124 H pink	03:40:54	7369.57	0.40	6.59	0.90
121	82_124 H pink	03:45:35	7718.25	0.40	6.24	0.60
122	83_P F pink	03:50:16	16609.42	0.30	3.09	1.90
123	84_P F pink	03:54:57	16759.78	0.40	1.51	2.90
124	85_P F pink	03:59:37	16576.81	0.20	1.48	2.30
125	86_17 F pink	04:04:17	4330.98	0.30	1.52	2.20
126	87_17 F pink	04:08:57	3773.39	0.10	1.46	2.50
127	88_17 F pink	04:13:37	3690.56	0.30	1.53	2.00
128	89 _ 93 F pink	04:18:17	2816.55	0.20	2.56	1.00

129	90_ 93 F pink	04:22:57	2805.07	0.30	5.95	1.40
130	CRM-TMDW-500	04:27:39	0.13	9.80	92.83	0.50
131	Standard 4	04:32:20	9.42	0.40	10.16	0.40
132	Blank	04:37:02	0.26	3.60	0.21	11.80
133	91_ 93 F pink	04:41:44	2773.74	0.40	1.39	2.50
134	92_ 124 F pink	04:46:24	7529.81	0.30	4.99	0.90
135	93_ 124 F pink	04:51:05	7483.40	0.30	5.27	0.60
136	94_ 124 F pink	04:55:45	7659.55	0.20	5.12	1.00
137	95_ P E pink	05:00:26	16034.77	0.50	1.57	2.60
138	96_ P E pink	05:05:07	15973.85	0.50	1.58	2.30
139	97_ P E pink	05:09:48	15822.93	0.30	1.57	3.80
140	98_ 17 E pink	05:14:28	4990.07	0.60	1.51	2.60
141	99_ 17 E pink	05:19:09	4243.25	0.60	1.67	3.20
142	100_ 17 E pink	05:23:49	4253.96	0.40	1.71	3.20
143	101_ 93 E pink	05:28:29	3273.73	0.20	1.65	1.60
144	102_ 93 E pink	05:33:09	3224.65	0.20	3.65	0.80
145	103_ 93 E pink	05:37:50	3087.19	0.60	1.93	2.50
146	104_ 124 E pink	05:42:30	7887.05	0.40	7.93	0.60
147	105_ 124 E pink	05:47:10	7519.40	0.30	6.61	1.30
148	106_ 124 E pink	05:51:51	7457.08	0.30	6.91	0.50
149	CRM-TMDW-500	05:56:33	0.34	17.30	94.48	0.60
150	Standard 4	06:01:14	9.46	0.60	10.38	0.30
151	Blank	06:05:56	0.44	2.80	0.23	14.30

Table 7.7 Sample identification table for larger scale ICP-MS study.

Run	Sample	Identification
1	pre-blank	-
2	Blank	-
3	Standard 1	Calibrant
4	Standard 2	Calibrant
5	Standard 3	Calibrant
6	Standard 4	Calibrant
7	Standard 5	Calibrant
8	Standard 6	Calibrant
9	Standard 7	Calibrant
10	Standard 8	Calibrant
11	pre-blank	-
12	Blank	-
13	CRM-TMDW-500	CRM
14	Standard 4	Calibrant
15	Blank	-
16	1_Blank handling	-
17	2_124 HC D	**3.11** DMEM handling control
18	3_124 HC D	**3.11** DMEM handling control

19	4_124 HC D	**3.11** DMEM handling control
20	5_PC HC D	$[Re(CO)_3(H_2O)_3Br]$ DMEM handling control
21	6_PC HC D	$[Re(CO)_3(H_2O)_3Br]$ DMEM handling control
22	7_PC HC D	$[Re(CO)_3(H_2O)_3Br]$ DMEM handling control
23	8_17 HC D	**3.17** DMEM handling control
24	9_17 HC D	**3.17** DMEM handling control
25	10_17 HC D	**3.17** DMEM handling control
26	CRM-TMDW-500	CRM
27	Standard 4	Calibrant
28	Blank	-
29	11_193 HC D	**3.21** DMEM handling control
30	12_193 HC D	**3.21** DMEM handling control
31	13_193 HC D	**3.21** DMEM handling control
32	14_124 HC M	**3.11** MEM handling control
33	15_124 HC M	**3.11** MEM handling control
34	16_124 HC M	**3.11** MEM handling control
35	17_PC HC M	$[Re(CO)_3(H_2O)_3Br]$ MEM handling control
36	18_PC HC M	$[Re(CO)_3(H_2O)_3Br]$ MEM handling control
37	19_PC HC M	$[Re(CO)_3(H_2O)_3Br]$ MEM handling control
38	20_17 HC M	**3.17** MEM handling control
39	CRM-TMDW-500	CRM
40	Standard 4	Calibrant
41	Blank	-
42	21_17 HC M	**3.17** MEM handling control
43	22_17 HC M	**3.17** MEM handling control
44	23_193 HC M	**3.21** MEM handling control
45	24_193 HC M	**3.21** MEM handling control
46	25_193 HC M	**3.21** MEM handling control
47	26_124 H	**3.11** HeLa lysate
48	27_124 H	**3.11** HeLa lysate
49	28_124 H	**3.11** HeLa lysate
50	29_PC H	$[Re(CO)_3(H_2O)_3Br]$ HeLa lysate
51	30_PC H	$[Re(CO)_3(H_2O)_3Br]$ HeLa lysate
52	CRM-TMDW-500	CRM
53	Standard 4	Calibrant
54	Blank	-
55	31_PC H	$[Re(CO)_3(H_2O)_3Br]$ HeLa lysate
56	32_17 H	**3.17** HeLa lysate
57	33_17 H	**3.17** HeLa lysate
58	34_17 H	**3.17** HeLa lysate
59	35_193 H	**3.21** HeLa lysate
60	36_193 H	**3.21** HeLa lysate
61	37_193 H	**3.21** HeLa lysate
62	38_UN H	Untreated HeLa lysate
63	39_UN H	Untreated HeLa lysate
64	40_UN H	Untreated HeLa lysate

65	CRM-TMDW-500	CRM
66	Standard 4	Calibrant
67	Blank	-
68	41_124 F	**3.11** HDF lysate
69	42_124 F	**3.11** HDF lysate
70	43_124 F	**3.11** HDF lysate
71	44_PC F	$[Re(CO)_3(H_2O)_3Br]$ HDF lysate
72	45_PC F	$[Re(CO)_3(H_2O)_3Br]$ HDF lysate
73	46_PC F	$[Re(CO)_3(H_2O)_3Br]$ HDF lysate
74	47_17 F	**3.17** HDF lysate
75	48_17 F	**3.17** HDF lysate
76	49_17 F	**3.17** HDF lysate
77	50_193 F	**3.21** HDF lysate
78	CRM-TMDW-500	CRM
79	Standard 4	Calibrant
80	Blank	-
81	51_193 F	**3.21** HDF lysate
82	52_193 F	**3.21** HDF lysate
83	53_UN F	Untreated HDF lysate
84	54_UN F	Untreated HDF lysate
85	55_UN F	Untreated HDF lysate
86	56_124 E	**3.11** EA.hy926 lysate
87	57_124 E	**3.11** EA.hy926 lysate
88	58_124 E	**3.11** EA.hy926 lysate
89	59_PC E	$[Re(CO)_3(H_2O)_3Br]$ EA.hy926 lysate
90	60_PC E	$[Re(CO)_3(H_2O)_3Br]$ EA.hy926 lysate
91	CRM-TMDW-500	CRM
92	Standard 4	Calibrant
93	Blank	-
94	61_PC E	$[Re(CO)_3(H_2O)_3Br]$ EA.hy926 lysate
95	62_17 E	**3.17** EA.hy926 lysate
96	63_17 E	**3.17** EA.hy926 lysate
97	64_17 E	**3.17** EA.hy926 lysate
98	65_193 E	**3.21** EA.hy926 lysate
99	66_193 E	**3.21** EA.hy926 lysate
100	67_193 E	**3.21** EA.hy926 lysate
101	68_UN E	Untreated EA.hy926 lysate
102	69_UN E	Untreated EA.hy926 lysate
103	70_UN E	Untreated EA.hy926 lysate
104	CRM-TMDW-500	CRM
105	Standard 4	Calibrant
106	Blank	-
107	71_P H pink	$[Re(CO)_3(H_2O)_3Br]$ HeLa exposure solution
108	72_P H pink	$[Re(CO)_3(H_2O)_3Br]$ HeLa exposure solution
109	73_P H pink	$[Re(CO)_3(H_2O)_3Br]$ HeLa exposure solution
110	74_17 H pink	**3.17** HeLa exposure solution

111	75_17 H pink	**3.17** HeLa exposure solution
112	76_17 H pink	**3.17** HeLa exposure solution
113	77_93 H pink	**3.21** HeLa exposure solution
114	78_93 H pink	**3.21** HeLa exposure solution
115	79_93 H pink	**3.21** HeLa exposure solution
116	80_124 H pink	**3.11** HeLa exposure solution
117	CRM-TMDW-500	CRM
118	Standard 4	Calibrant
119	Blank	-
120	81_124 H pink	**3.11** HeLa exposure solution
121	82_124 H pink	**3.11** HeLa exposure solution
122	83_P F pink	$[Re(CO)_3(H_2O)_3Br]$ HDF exposure solution
123	84_P F pink	$[Re(CO)_3(H_2O)_3Br]$ HDF exposure solution
124	85_P F pink	$[Re(CO)_3(H_2O)_3Br]$ HDF exposure solution
125	86_17 F pink	**3.17** HDF exposure solution
126	87_17 F pink	**3.17** HDF exposure solution
127	88_17 F pink	**3.17** HDF exposure solution
128	89 _ 93 F pink	**3.21** HDF exposure solution
129	90_ 93 F pink	**3.21** HDF exposure solution
130	CRM-TMDW-500	CRM
131	Standard 4	Calibrant
132	Blank	-
133	91_ 93 F pink	**3.21** HDF exposure solution
134	92_ 124 F pink	**3.11** HDF exposure solution
135	93_ 124 F pink	**3.11** HDF exposure solution
136	94_ 124 F pink	**3.11** HDF exposure solution
137	95_ P E pink	$[Re(CO)_3(H_2O)_3Br]$ EA.hy926 exposure solution
138	96_ P E pink	$[Re(CO)_3(H_2O)_3Br]$ EA.hy926 exposure solution
139	97_ P E pink	$[Re(CO)_3(H_2O)_3Br]$ EA.hy926 exposure solution
140	98_ 17 E pink	**3.17** EA.hy926 exposure solution
141	99_ 17 E pink	**3.17** EA.hy926 exposure solution
142	100_ 17 E pink	**3.17** EA.hy926 exposure solution
143	101_ 93 E pink	**3.21** EA.hy926 exposure solution
144	102_ 93 E pink	**3.21** EA.hy926 exposure solution
145	103_ 93 E pink	**3.21** EA.hy926 exposure solution
146	104_ 124 E pink	**3.11** EA.hy926 exposure solution
147	105_ 124 E pink	**3.11** EA.hy926 exposure solution
148	106_ 124 E pink	**3.11** EA.hy926 exposure solution
149	CRM-TMDW-500	CRM
150	Standard 4	Calibrant
151	Blank	-

Two handling blanks are reported (DMEM and MEM) as DMEM media was used for HeLa and EA.hy926 cells, MEM media was used for HDF cells.

7.2.5. Example Calculation

The following calculations demonstrate how value of Re (µg/L) was converted into Re (µg) in each sample. Example calculations are shown for **3.11** in HeLa, but all calculations to give the results shown in Chapter 3, Section 3.4.2.3 were performed using the same method. It should be noted that although ICP-MS only analysed 0.3 mL aliquots, the original sample volumes were as follows: cell lysate (1 mL) and exposure solution (3 mL).

For each sample per cell line, there is an exposure solution, a lysate and a handing control, and all work has been done in triplicate. The exposure solution is the original Re sample (3 mL) that was incubated with the cells, the lysate (1 mL) is the cellular sample itself, and the handling control (in DMEM media for HeLa) accounts for any background contamination. Handling controls are given in DMEM and MEM media, as DMEM media was used for HeLa and EA.hy926 cells whilst MEM media was used for HDF cells.

Using the results for **3.11** in HeLa cells, shown in Table 7.8, averages can be calculated and are shown in Table 7.9.

Table 7.8 ICP-MS data relating to the uptake of complex **3.11** in HeLa cells. Uptake studies were performed in triplicate.

Sample	Identity	Re (µg/L)
2_124 HC D	**3.11** DMEM handling control	11.01
3_124 HC D	**3.11** DMEM handling control	9.75
4_124 HC D	**3.11** DMEM handling control	10.00
26_124 H	**3.11** HeLa lysate	1653.83
27_124 H	**3.11** HeLa lysate	1871.47
28_124 H	**3.11** HeLa lysate	2012.18
80_124 H pink	**3.11** HeLa exposure solution	7354.64
81_124 H pink	**3.11** HeLa exposure solution	7369.57
82_124 H pink	**3.11** HeLa exposure solution	7718.25

Table 7.9 Average results from ICP-MS analysis for **3.11** uptake in HeLa.

Identity	Average Re (µg/L)
Average **3.11** DMEM handling control	10.25
Average **3.11** HeLa lysate	1845.82
Average **3.11** HeLa exposure solution	7480.82

The averaged results in Table 7.9 were therefore used for calculating the quantity of Re (in µg) in the HeLa cells that were treated with **3.11**. This value was calculated as shown in Table 7.10.

Table 7.10 Table of calculations performed in order to convert the quantity of Re in **3.11** treated HeLa cells, from a concentration (in µg/L) to a mass (in µg).

Calculation	Formula	Result	Units
Average **3.11** HeLa lysate	-	1845.82	µg/L
Average **3.11** DMEM handling control	-	10.25	µg/L
Corrected **3.11** HeLa lysate in µg/L (aliquot)	$c_{(\mu g/L)}$=lysate-handling control =1845.82-10.25	1835.57	µg/L
Corrected **3.11** HeLa lysate in mol/L (aliquot, 0.3 mL)	$c_{aliquot}=c_{(\mu g/L)}/MW_{Re}$ = (1835.5/186.207)*1x10^{-6}	9.86x10^{-6}	mol/L
Moles of Re in lysate (aliquot, 0.3 mL)	$n_{aliquot}=c_{aliquot}*V_{aliquot}$ =9.86x10^{-}6*0.0003	2.96x10^{-9}	moles
Moles of Re in lysate (original sample, 1 mL)	$n_{original}= n_{aliquot}*(V_{original}/ V_{aliquot})$ = 2.96x10^{-9}*(1/0.3)	9.86x10^{-9}	moles
Mass (g) of Re in lysate (original sample, 1 mL)	$g=n_{original}*MW_{Re}$= 9.86x10^{-9}*186.207	1.836x10^{-6}	g
Mass (µg) of Re in lysate (original sample, 1 mL)	-	1.836	µg

The mass of Re the **3.11** treated HeLa lysate after 2 h was therefore 1.836 µg.

These same calculations were applied to the average **3.11** HeLa exposure solution to determine the mass of Re from **3.11** that was incubated with the cells for 2 h. It is not ecessary to consider a handling control here. The results of these calculations are shown in

Table 7.11.

Table 7.11 Table of calculations performed in order to convert the quantity of Re from **3.11** that was incubated with HeLa cells from a concentration in µg/L to a mass with units of µg.

Calculation	Formula	Result	Units
Average **3.11** HeLa exposure solution in µg/L (aliquot, 0.3 mL)	-	7480.82	µg/L
Average **3.11** HeLa exposure solution in mol/L (aliquot, 0.3 mL)	$c_{aliquot}=c_{(\mu g/L)}/MW_{Re}$ = (7480.82/186.207)*1x10^{-6}	4.02x10^{-5}	mol/L
Moles of Re in exposure solution (aliquot, 0.3 mL)	$n_{aliquot}=c_{aliquot}*V_{aliquot}$ =4.02x10^{-5}*0.0003	1.21x10^{-8}	moles
Moles of Re in exposure solution (original sample, 3 mL)	$n_{original}= n_{aliquot}*(V_{original}/ V_{aliquot})$ =1.21x10^{-8}*(3/0.3)	1.21x10^{-7}	moles
Mass (g) of Re in exposure solution (original sample, 3 mL)	$g=n_{original}*MW_{Re}$= 1.21x10^{-7}*186.207	2.25x10^{-5}	g
Mass (µg) of Re in exposure solution (original sample, 3 mL)	-	22.457	µg

The mass of Re in the **3.11** exposure solution for HeLa cells was therefore 22.457 µg. Consequently, the percentage of Re from complex **3.11** that was transported into HeLa cells after a 2 h incubation was 8.18%.

These same calculations were performed for each of the other samples (**3.17**, **3.21** and $[Re(CO)_3(H2O)_3Br]$) and the other cell lines (HDF and EA.hy926). When performing calculations for samples in HDF cells, MEM handling controls were used (opposed to DMEM handling controls) as HDF studies were performed in MEM media, whilst HeLa and EA.hy926 studied were performed in DMEM media. All other transformations remained the same.

See Chapter 3, Section 3.4.2.2 and 3.4.2.3 for the results of the pilot and larger scale study.